SAVANNA VEGETATION DYNAMICS AND THEIR INFLUENCE ON LANDSCAPE-SCALE C, N, AND P BIOGEOCHEMISTRY

A Dissertation

by

YONG ZHOU

Submitted to the Office of Graduate and Professional Studies of
Texas A&M University
in partial fulfillment of the requirements for the degree of

DOCTOR OF PHILOSOPHY

Chair of Committee,	Thomas W. Boutton
Co-Chair of Committee,	X. Ben Wu
Committee Members,	Jason B. West
	Frank M. Hons
Head of Department,	Kathleen Kavanagh

May 2018

Major Subject: Ecosystem Science and Management

ABSTRACT

Recent global trends of woody encroachment into grass-dominated ecosystems have substantially altered soil biogeochemical cycles. However, previous studies were mostly conducted at the ecosystem level and results were not spatially-explicit. Meanwhile, most of these studies considered only surface soils, and did not assess the extent to which biogeochemical cycles in subsurface soils may be altered by woody encroachment.

In this dissertation, spatially-specific soil samples were taken to a depth of 1.2 m across a 160 m × 100 m subtropical savanna landscape which has undergone the encroachment by *Prosopis glandulosa* and other woody species in southern Texas, USA. Soil samples were analyzed for root biomass, soil organic carbon (SOC), total nitrogen (TN), total phosphorus (TP), soil $\delta^{13}C$, and soil $\delta^{15}N$.

Soil $\delta^{13}C$ values throughout the soil profile indicate that this landscape was once primarily dominated by C_4 grasses, and woody encroachment has occurred within the past century. Subsurface non-argillic inclusions across this landscape favor the establishment and persistence of large woody patches by enabling root penetration deeper into the profile, providing greater access to water and soil nutrients and thereby regulating vegetation distribution.

Woody encroachment increased SOC, TN, and TP throughout the entire 1.2 m soil profile, albeit at different rates. SOC and TN were coupled with respect to increasing magnitudes and spatial patterns following woody encroachment, while TP increased

slower than SOC and TN in surface soils but faster in subsurface soils. Spatial patterns of soil C: P and N: P ratios were similar throughout the soil profile, but differed from those of soil C: N ratio.

Soil $\delta^{15}N$ increased with depth, reached the maximum at an intermediate depth, and then decreased in the deepest portions of the profile. Woody encroachment decreased soil $\delta^{15}N$, creating spatial patterns of soil $\delta^{15}N$ resembling the spatial distribution of woody patches throughout the soil profile.

These results highlight the difference of soil C, N, and P dynamics in response to woody encroachment and the change of mechanistic controls throughout the soil profile, providing valuable insights necessary to developing integrative climate-biogeochemical models that could represent changes in soil biogeochemical cycles following vegetation change.

DEDICATION

To my parents

For their unfailing support

ACKNOWLEDGEMENTS

Special thanks to Thomas Boutton for his generous assistance through this Ph. D. program. Despite the passage of time, I can still vividly remember Tom picked me up from the George Bush Intercontinental Airport when I first came to this land on the 6th of August 2013. On the way back to College Station, we had a really nice conversation from ecosystems in Texas to cultures in America. For the past four years, I cannot thank him enough for making me feel so welcome and included here at Texas A&M. He has spent countless hours helping me through this program and offered me on life advice. Thanks for his patience, encouragement, and belief in me.

I would also like to thank Ben Wu for serving as co-chair and for his encouragement, provision of resources and wisdom, and ongoing motivation. I appreciate Frank Hons (Department of Soil and Crop Sciences) and Jason West for serving on my Ph. D. program committee.

Thanks are extended to my colleagues in the Stable Isotopes for Biosphere Science Laboratory: Ryan Mushinski, Ayumi Hyodo, Yang Zhang, Elizabeth Wilson, Darcy Moreland, Anais Dion, Rachel Adams, Matthew Smith, and Saadat Malghani for their generous help on field/lab work and on my writing and presentations. Thank you to my friends in the Department of Ecosystem Science and Management, to name a few, Michele Clark, Xiangmin Sun, and Cynthia Wright for fun activities and their dependable support.

I am sincerely grateful to David McKown and his wife Stacy for their ongoing hospitality at the Texas A&M AgriLife La Copita Research Area in southern Texas. Thanks for teaching me how to shoot and inviting me to their bay house for fishing. I enjoyed my stay there, even in the face of a damn hot Texan summer.

Finally, thanks to my parents and siblings for their unfailing love and support during my stay at Texas A&M.

CONTRIBUTORS AND FUNDING SOURCES

Contributors

This work was supervised by a dissertation committee consisting of Dr. Thomas W. Boutton (advisor), Dr. X. Ben Wu (co-advisor), and Dr. Jason B. West of the Department of Ecosystem Science and Management and Dr. Frank M. Hons of the Department of Soil and Crop Sciences.

Yong Zhou, Dr. Thomas W. Boutton, and Dr. X. Ben Wu designed this work. Yong Zhou conducted the field work, lab and data analyses, interpreted the data and wrote this dissertation with advice from Dr. Thomas W. Boutton, Dr. X. Ben Wu, Dr. Jason B. West, and Dr. Frank M. Hons.

Funding Sources

Yong Zhou was supported by a Sid Kyle Graduate Merit Assistantship (2013-2017) from the Department of Ecosystem Science and Management and a Tom Slick Graduate Research Fellowship (2017-2018) from the College of Agriculture and Life Sciences, Texas A&M University.

This work was supported by a Doctoral Dissertation Improvement Grant from the U.S. National Science Foundation (DEB/DDIG1600790), USDA/NIFA Hatch Project (1003961), an Exploration Fund Grant from the Explorers Club, a Howard McCarley Student Research Award from the Southwestern Association of Naturalists, and a Graduate Student Research Mini-Grant from Department of Ecosystem Science and Management, Texas A&M University.

TABLE OF CONTENTS

Page

Page

LIST OF FIGURES

Page

Page

Page

Page

LIST OF TABLES

Page

Page

CHAPTER I

INTRODUCTION

Grass-dominated ecosystems in arid and semi-arid regions around the world have experienced increased woody plant abundance during the past century (Van Auken 2000, 2009; Eldridge *et al.* 2011; Stevens *et al.* 2017). This globally extensive phenomenon has been documented in North America, South Africa, South America, Asia, Australia and Europe (Archer *et al.* 1988; Archer 1995; Price & Morgan 2008; Blaser *et al.* 2014; Eldridge & Codina 2014; González-Roglich *et al.* 2014), and has dramatically altered the structure and function of grassland and savanna ecosystems (Eldridge *et al.* 2011), with the potential to profoundly influence grassland biodiversity (Ratajczak *et al.* 2012), hydrology (Huxman *et al.* 2005), biogeochemistry (Boutton 1999; Barger *et al.* 2011) and livestock production (Dalle *et al.* 2006). Since grasslands and savannas occupy more than 40% of the Earth's land surface (Bailey 1996), woody encroachment has long been a concern of land managers and ecologists.

Modification of soil carbon (C) and nitrogen (N) storage and dynamics during woody plant encroachment is particularly noteworthy, especially for ecosystems encroached by N_2-fixing trees and shrubs (e.g. *Prosopis* in North American and *Acacia* in Africa), which have the capability to increase soil N and drive rapid accumulation of C in both vegetation and soil (Sitters *et al.* 2013; Balser *et al.* 2014; Soper *et al.* 2015). However, it is still far from being fully exploited whether and to what extent woody plant encroachment could alter soil C and N storage since results from field studies are often

inconsistent, with studies showing increases (e.g. Liao *et al.* 2006; Liu *et al.* 2011), decreases (e.g. Jackson *et al.* 2002) or no change (e.g. Hughes *et al.* 2006). Meanwhile, plants simultaneously require multiple essential elements, and the supply of one element can interactively affect the cycling of many others (Sterner & Elser 2002). In addition to N, phosphorus (P) is another common limiting element for primary productivity and soil biological processes (Vitousek *et al.* 2010), and its dynamics are poorly studied in water-limited systems (Selmants & Hart 2010). Since ecosystems begin their existence with a fixed amount of P derived from rock weathering (Walker & Syers 1976; Vitousek *et al.* 2010), it remains unclear how soil P affects the accrual of C in encroached systems with substantial addition of atmospheric N by N-fixers.

Stable isotopes of C and N have been utilized to document changes in structure and function of ecosystems where woody plant encroachment has been occurring (Boutton 1999; Bai *et al.* 2009, 2012, and 2013). C_3 and C_4 plants have unique stable carbon isotope ratios ($\delta^{13}C$) caused by biochemical differences between photosynthetic pathways in these plants. These unique plant $\delta^{13}C$ signatures are retained without significant isotope fractionation as litter and dead roots become incorporated into the soil organic carbon pool (Boutton *et al.* 1999). Thus, $\delta^{13}C$ values of soil organic matter record the relative importance of C_3 vs. C_4 inputs to the soil, and are powerful tools for documenting ecosystem processes and vegetation changes involving C_3 and C_4 plants (Boutton *et al.* 1998; Sanaiotti *et al.* 2002; Dumig *et al.* 2008). Many soil N processes cause isotope fractionation ($\delta^{15}N$) (Hobbie & Ouimette 2009), and as a result soil $\delta^{15}N$ can be used to understand soil N dynamics. Soil $\delta^{15}N$ is primarily controlled by N inputs (e.g. deposition

and fixation) vs. outputs (e.g. N leaching, gaseous loss via nitrification and denitrification) (Houlton *et al.* 2007; Hobbie & Ouimette 2009; Bai *et al.* 2013). The dramatic changes in soil N storage and dynamics during the shift of vegetation cover from grassland to woodland, as mentioned above, is expected to leave an imprint on soil $\delta^{15}N$ that encodes information of soil N cycling in response to woody plant encroachment.

As woody plants encroach into grass-dominated ecosystems, spatial heterogeneity of soil properties becomes amplified (Schlesinger *et al.* 1996), making it more difficult to accurately quantify ecosystem properties and processes based on micro-sites and limited sample size (Liu *et al.* 2011). Previous studies have demonstrated the value of quantifying spatial patterns of soil properties and associated spatial variability to study related processes in arid and semi-arid regions with patchy vegetation (Jackson & Caldwell, 1993; Schlesinger *et al.* 1996; Throop & Archer 2008; Liu *et al.* 2011; Bai *et al.* 2013; Mudrak *et al.* 2014), but their results were restricted to the topsoil (0-15 cm). Compared to herbaceous species, trees and shrubs typically have much deeper root systems (Walter 1971; Jackson *et al.* 1996). Therefore, it is reasonable to expect that the invasion of deep rooted woody plants modifies the spatial variability of soil properties and processes not only in the upper 15 cm of the profile, but also in deeper portions of the soil. However, little is known regarding the impacts of woody encroachment on either deep soil properties or their spatial patterns.

The primary objective of this dissertation was to investigate how woody encroachment altered landscape-scale spatial patterns of soil C, N, and P storage and dynamics along a soil profile and to link these spatial patterns to elucidate vegetation

dynamics and soil biogeochemical processes (Fig. 1.1). To this end, spatially-specific soil samples to a depth of 1.2 m were collected across a 160 m × 100 m subtropical savanna landscape where grasslands have been encroached by *Prosopis glandulosa* (a N_2-fixer) and other woody species during the past century in southern Texas, USA.

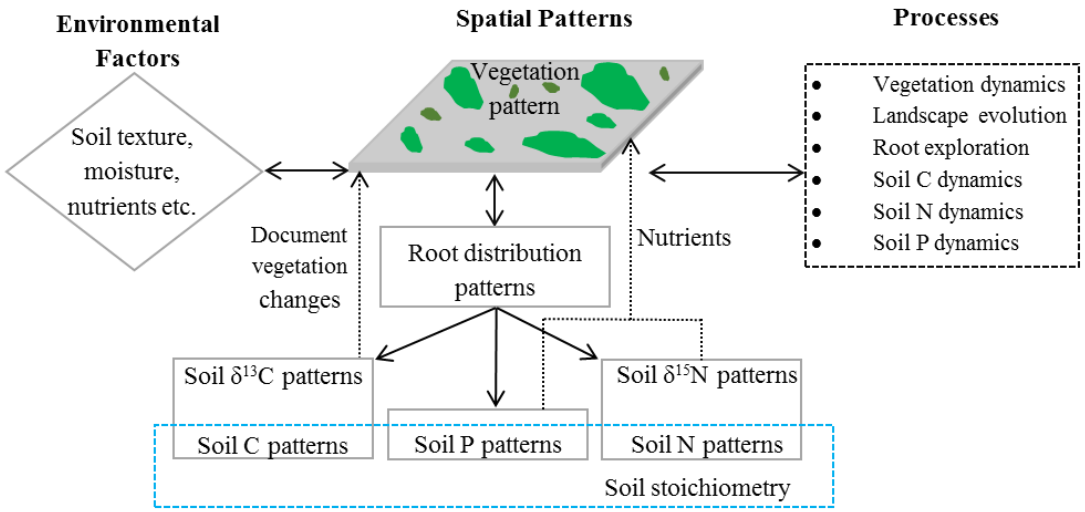

Figure 1.1 Schematic of the dissertation structure.

More specifically, this dissertation addressed the following objectives, each forming a chapter of the dissertation:

(1) Infer vegetation dynamics based on landscape-scale spatial patterns of soil $\delta^{13}C$ throughout the soil profile in conjunction with radiocarbon dating and historical aerial photographs;

(2) Determine the factors controlling landscape-scale spatial distribution of grove vegetation in this subtropical savanna;

(3) Examine the landscape-scale spatial patterns of fine root distribution throughout the soil profile and its role in linking aboveground plant communities to belowground soil biogeochemical dynamics;

(4) Quantify the influence of woody plant encroachment on landscape-scale patterns of spatial heterogeneity of soil organic C storage throughout the soil profile;

(5) Quantify the influence of woody plant encroachment on landscape-scale patterns of spatial heterogeneity of soil total P storage throughout the soil profile;

(6) Test whether soil total P increases proportionally with the accrual of soil organic C and total N following woody plant encroachment across this landscape and throughout the soil profile;

(7) Investigate the impact of woody plant encroachment on landscape-scale patterns of spatial heterogeneity of soil C: N, N: P, and C: P ratios throughout the soil profile;

(8) Apply landscape-scale spatial patterns of soil $\delta^{15}N$ throughout the soil profile to infer soil N dynamics in this legume encroached subtropical savanna.

CHAPTER II

VEGETATION CHANGE AND SOIL CARBON DYNAMICS IN A SUBTROPICAL SAVANNA: A LANDSCAPE-SCALE ASSESSMENT BASED ON SOIL $\delta^{13}C$

SYNOPSIS

Woody plant encroachment into grasslands is a geographically extensive land cover change that can have strong impacts on the structure and function of dryland ecosystems. This vegetation change often modifies soil organic carbon (SOC) storage and dynamics, and appears to be an important yet uncertain component of the C cycle in global drylands. To reduce this uncertainty, sampling is needed at broader spatial scales, at greater depths in the soil profile, and within a chronological context. We quantified spatial patterns of soil $\delta^{13}C$ and SOC across a landscape to a depth of 1.2 m in a subtropical savanna undergoing woody encroachment. Those data were then examined in a chronological context using radiocarbon dating and historical aerial photography and integrated to estimate the timing of this vegetation change and its impacts on SOC dynamics. Results showed that woody encroachment dramatically altered spatial patterns of soil $\delta^{13}C$ throughout the entire soil profile, with soil $\delta^{13}C$ being lowest in the centers of woody patches, increasing towards canopy edges, and reaching highest values within the grassland matrix. Soil $\delta^{13}C$ and radiocarbon dating throughout the soil profile indicated that this landscape was once primarily dominated by C_4 grasses over timescales of hundreds to thousands of years ago. However, a rapid shift in vegetation dominance occurred during the past century, characterized by (1) the increasing abundance of C_3 forbs

within the remnant grassland matrix and (2) the active formation and expansion of woody patches across this landscape. This shift in vegetation dominance has substantially increased the proportion of new soil C originating from C_3 plants into the SOC pool throughout the soil profile. These findings suggest that vegetation dominance in this dryland ecosystem is undergoing an unprecedented change and that increased new C input, driven by such change, has important implications for the C cycle in this system.

INTRODUCTION

Arid and semiarid regions (drylands) cover around 40 % of the Earth's land surface (Bailey 1996), and support the livelihoods of almost 20 % of the world's population (Turner *et al.* 1990). Furthermore, dryland soils store approximately 15.5 % of global soil organic carbon (SOC) and represent an important sink for greenhouse gas emissions (Lal 2004). However, C cycling in dryland ecosystems is particular sensitive to environmental changes (Delgado-Baquerizo *et al.* 2013), and dryland responses to climate change scenarios remain a major source of uncertainty in the global C cycle (Poulter *et al.* 2014).

One of the most significant environmental changes occurring in many dryland ecosystems around the world is woody proliferation in grasslands and savannas (Stevens *et al.* 2017). This global phenomenon appears to be driven by a combination of land use and climatic drivers, such as the intensification of livestock grazing, fire suppression, elevated atmospheric CO_2 concentration, and long-term climate change (Scholes & Archer 1997; Van Auken 2009), and has dramatically altered dryland C cycling across multiple spatial scales (Jackson *et al.* 2003; Barger et al. 2011; Eldridge *et al.* 2011; Zhou *et al.* 2017a). For example, up to 330 million hectares of non-forest land are currently

undergoing woody encroachment in the United States (Pacala *et al*. 2001; Eldridge *et al.* 2011); this conversion represents 20-40 % of the current C sink strength in the United States (Houghton *et al.* 2000; Pacala *et al.* 2001; King *et al.* 2012). However, field studies regarding the effects of woody encroachment on SOC storage yield inconsistent results, showing net increase in some dryland ecosystems (Liao *et al.* 2006; Springsteen *et al.* 2010; Blaser *et al.* 2014; Zhou *et al.* 2017a), but no net change (Hughes *et al.* 2006), or even a decrease in others (Jackson *et al.* 2003). These discrepancies might be ascribed to soil characteristic, climate regimes, and historical land use patterns (Jackson *et al.* 2003; Barger *et al*. 2011; Li *et al.* 2016). Since vegetation dynamics have significant impacts on the C cycle in dryland ecosystems (Schlesinger *et al.* 1996), a better understanding of the legacy effect of vegetation change on SOC dynamics is important to gauge this uncertainty and crucial for making robust predictions of dryland C budgets.

The natural abundance of stable C isotopes in soils has been utilized to study vegetation and SOC dynamics where C_3 plants replace C_4 plants, or vice versa (Dzurec *et al.* 1985; Victoria et al. 1995; Boutton *et al.* 1998). C_3 and C_4 plant species have distinctive $\delta^{13}C$ values in plant litter and residues which are incorporated into soils without significant discrimination during soil organic matter formation (Dzurec *et al.* 1985; Boutton *et al.* 1996; Ehleringer *et al.* 2000). Differences in soil $\delta^{13}C$ have been applied to deduce vegetation dynamics on a timescale of decades with the aid of aerial photography (Bai *et al.* 2009) and on timescales of centuries to millennia in association with radiocarbon dating (Victoria *et al.* 1995; Boutton *et al.* 1998; Biedenbender *et al*. 2004). In addition, where C_3-C_4 vegetation changes have occurred at known points in time, it has been possible to

use the subsequent rate of change in soil $\delta^{13}C$ values to estimate and model SOC dynamics (Liao *et al.* 2006; Freier *et al*. 2010; Puttock *et al.* 2012).

The encroachment of C_3 woody species into C_4 grass-dominated ecosystems provides an ideal platform for the application of stable C isotopic techniques to address changes in soil carbon cycling following vegetation change. As a result, soil $\delta^{13}C$ values have been used to document and quantify woody expansion (Boutton *et al.* 1996; Biedenbender *et al.* 2004; Krull *et al.* 2007), SOC dynamics (Liao *et al.* 2006; Puttock *et al.* 2012), and erosional processes (Turnbull *et al.* 2008; Puttock *et al.* 2012). However, most of these previous studies were conducted at the ecosystem scale, limited to relatively shallow soil sampling, and were not spatially explicit. In dryland ecosystems, patchiness of woody cover is the main characteristic of ecosystem function and service across spatial scales (Pringle *et al.* 2010). In order to cope with this patchiness, there is increasing recognition of the fundamental need to explore ecosystem structure and function at larger spatial scales and in a spatially-specific manner (Ettema & Wardle 2002; Liu *et al.* 2011). A few previous studies demonstrated the merits of integrating quantitative spatial analyses and soil $\delta^{13}C$ values to study vegetation dynamics following vegetation change at landscape scale (van Kessel *et al.* 1994; Biggs *et al.* 2002; Bai *et al.* 2009), but their results were constrained to surface soils. Woody encroachment into grasslands substantially amplifies spatial heterogeneity of soil properties both vertically, through the soil profile, and horizontally, across multiple spatial scales (Zhou *et al*. 2017a). However, little is known about the extent to which spatial patterns of soil $\delta^{13}C$ in deeper portions of the

profile are affected by woody encroachment into grasslands and how this might influence soil C cycling in dryland ecosystems.

The primary purpose of this study was to quantify landscape-scale spatial patterns of soil $\delta^{13}C$ throughout a soil profile and relate these spatial patterns to vegetation change and SOC dynamics. To accomplish this, spatially georeferenced soil samples to a depth of 1.2 m were collected across a 160 m × 100 m landscape in a subtropical savanna which has experienced increased woody plant abundance during the past century (Archer 1995; Boutton *et al.* 1998). Our specific objectives were to: (1) quantify spatial patterns of soil $\delta^{13}C$ across this landscape and throughout the soil profile; (2) use these patterns to reconstruct historical vegetation change for timescales of decades in terms of the formation and expansion of woody patches or of centuries to millennia in terms of the relative proportions of C_3 vs C_4 vegetation; and (3) explore the impact of vegetation change on SOC dynamics with respect to C origins across this landscape and throughout the soil profile.

MATERIALS AND METHODS

Study site

This study was conducted at the Texas A&M AgriLife La Copita Research Area (27˚40′ N, 98˚12′ W) in the Rio Grande Plains of southern Texas, USA. The climate is subtropical, with a mean annual temperature of 22.4 ˚C and mean annual precipitation of 680 mm. Rainfall peaks occur in May and September. Elevation ranges from 75 to 90 m above sea level. Topography consists of nearly level uplands that grade (1-3% slopes) gently into lower-lying drainage woodlands and playas. The site has not burned for at least

the past 30 years, and was grazed by livestock from approximately 1880-2000 (Archer et al. 1988).

Upland soils are sandy loams (Typic and Pachic Argiustolls) with non-argillic inclusions interspersed into a continuous subsurface argillic horizon (*Bt*) (Watts 1993; Archer 1995; Zhou *et al.* 2017b). Upland vegetation is characterized as a two-phase vegetation pattern consisting of woody patches embedded within a remnant grassland matrix. Woody patches include small discrete clusters (< 10 m in diameter) and large groves (> 10 m in diameter). Woody plant proliferation is initiated when grassland is colonized by *Prosopis glandulosa*, a N-fixing tree legume, which then facilitates the recruitment of other understory woody species to form discrete clusters (Archer *et al.* 1988). Where the non-argillic inclusions are present, discrete clusters expand laterally and coalesce to form large groves (Archer 1995; Zhou *et al*. 2017b). Thus, discrete clusters and grasslands occur where the argillic horizon is well-formed, whereas groves occur on soils with non-argillic inclusions. Woody species composition and relative dominance are similar in both groves and discrete clusters, but individual plants are often larger and older in groves than in discrete clusters (Archer 1995; Boutton *et al.* 1998; Liu *et al*. 2011). Species composition can be found in Appendix A.

Field sampling and preparation

On an upland portion of this study site, a 160 m × 100 m landscape was established and subdivided into 10 m x 10 m grid cells in January 2002 (Fig. 2.1) (Bai *et al.* 2009; Liu *et al.* 2011). This area included all of the upland landscape elements: grasslands, clusters, and groves. Each corner of each grid cell was marked with a PVC pole and georeferenced

using a GPS unit (Trimble Pathfinder Pro XRS, Trimble Navigation Limited, Sunnyvale, CA, USA) based on a UTM coordinates system (WGS, 1984). Aerial photographs of this landscape taken in 1930 and 2015 were digitized and areas of each landscape element were calculated in ArcMap 10.1.

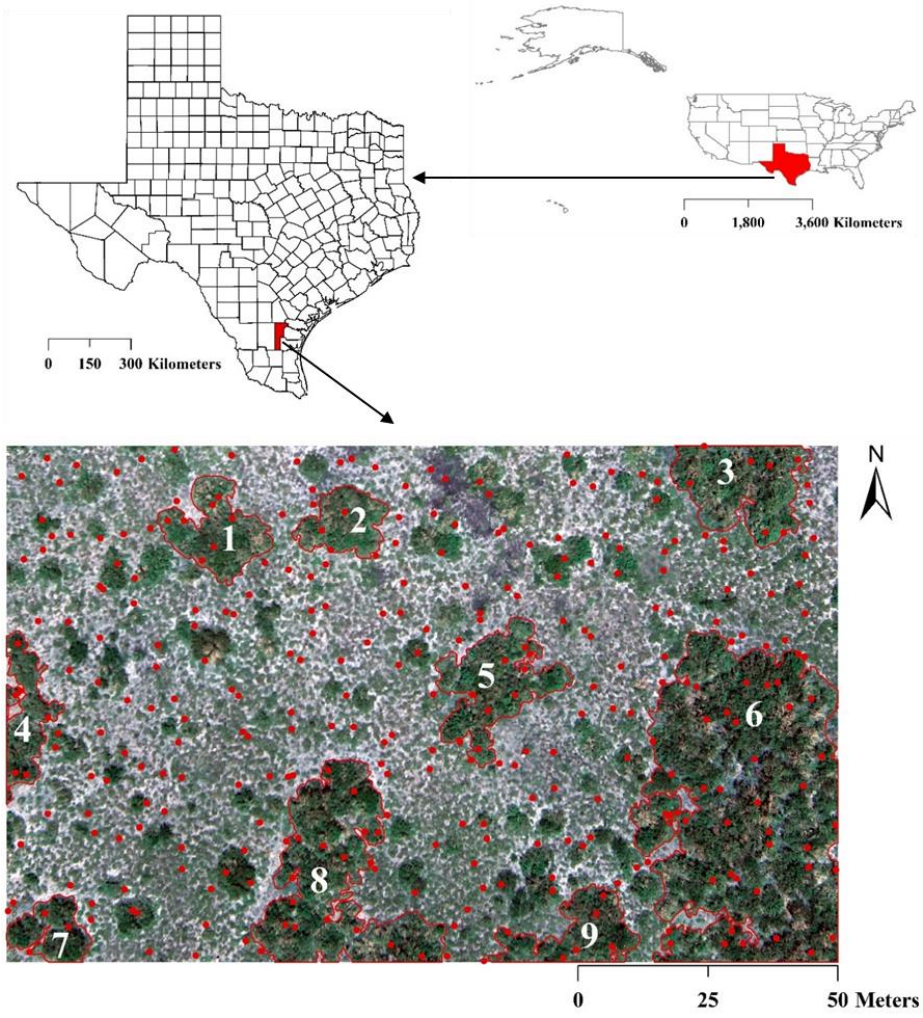

Figure 2.1 Location of Jim Wells County in southern Texas, United States, and aerial photograph of the 160 × 100 m landscape in a subtropical savanna. Red points indicate 320 random soil sampling points. Green patches are woody clusters and groves, while light grey areas indicate open grasslands. Groves are highlighted with red lines and labeled with numbers.

Within each 10 m × 10 m grid cell, two points were randomly selected for soil sampling in July 2014, yielding a total of 320 sampling points across the study area (Fig. 2.1). Vegetation cover at each soil sampling point was categorized as grassland (n = 200), cluster (n = 41) or grove (n = 79) based on vegetation type and the canopy size of woody patches. Distances from each soil sampling point to two unique georeferenced cell corners were recorded. At each soil sampling point, two adjacent soil cores (2.8 cm in diameter and 120 cm in length) were collected with a PN150 JMC Environmentalist's Subsoil Probe (Clements Associates Inc., Newton, IA, USA). Each soil core was subdivided into 6 depth increments (0-5, 5-15, 15-30, 30-50, 50-80, and 80-120 cm). Leaf and fine root (< 2 mm) tissues of each species occurring on this landscape were collected in September 2016 (Appendix A).

Lab analyses

One soil core was oven-dried (105 °C for 48 hours) to determine soil bulk density, then subsequently used to determine fine (< 2 mm) and coarse root (> 2 mm) biomass by washing through sieves. No attempt was made to distinguish between live or dead roots. Roots were dried at 65 °C for 48 hours for biomass. Three composite fine root samples were created for each landscape element by combining fine roots from 10 soil cores for each depth increment. These composite fine roots samples, as well as the leaf and fine root tissues collected from individual plant species, were then pulverized in a centrifugal mill (Angstrom Inc., Belleville, MI, USA), and saved for elemental and isotopic analyses.

The other soil core was air-dried and passed through a 2 mm sieve. An aliquot of sieved soil was dried at 60 °C for 48 hours and pulverized in the centrifugal mill.

Pulverized soil samples were weighed into silver capsules (5 mm × 9 mm), treated with HCl vapor in a desiccator to remove carbonates (Harris *et al.* 2001), and then dried. SOC concentrations (g C kg^{-1} soil) and $\delta^{13}C$ values of acid-treated soil samples were determined using a Costech ECS 4010 elemental combustion system (Costech Analytical Technologies Inc., Valencia, CA, USA) interfaced via a ConFlo IV device with a Delta V Advantage isotope ratio mass spectrometer (Thermo Scientific, Bremen, Germany). The C concentrations and $\delta^{13}C$ values of composited fine root samples, leaf and fine root tissues of each species were determined similarly, but without acid treatment. Carbon isotope ratios are presented in δ notation:

$$\delta = (\frac{R_{Sample} - R_{STD}}{R_{STD}}) \times 10^3$$

where R_{Sample} is the $^{13}C/^{12}C$ ratio of the soil sample and R_{STD} is the $^{13}C/^{12}C$ ratio of the V-PDB standard. Precision of duplicate measurements was 0.1‰ for $\delta^{13}C$.

Estimating sources of soil carbon by mass balance

The proportion of C derived from C_3 vegetation (or percentage of C_3 vegetation vs C_4 vegetation) was calculated using soil $\delta^{13}C$ values in a simple mass balance mixing model (Boutton 1996; Boutton *et al.* 1998):

$$\delta^{13}C_{Soil} = f * \delta^{13}C_3 + (1 - f) * \delta^{13}C_4$$

where $\delta^{13}C_{Soil}$ is the measured $\delta^{13}C$ value of soil samples; $\delta^{13}C_3$ is the averaged $\delta^{13}C$ value of C_3 vegetation; $\delta^{13}C_4$ is the averaged $\delta^{13}C$ value of C_4 vegetation; and *f* is the percentage of C derived from C_3 vegetation (or percentage of C_3 vegetation vs C_4 vegetation). Averaged $\delta^{13}C$ values of contemporary C_3 and C_4 vegetation are usually used as proxies

for past C_3 and C_4 vegetation (Boutton *et al.* 1998). In this study, based on $\delta^{13}C$ values of leaf and fine root tissues, average $\delta^{13}C$ values of -28.2 ‰ (n = 48) and -12.9 ‰ (n = 26) were used as contemporary values for C_3 and C_4 vegetation, respectively. It is worth noting that this simple mass balance mixing model may underestimate the proportion of C with C_3 origins (or percentage of C_3 vegetation) due to the depth-enrichment of $\delta^{13}C$ throughout the soil profile via several proposed mechanisms which are independent from vegetation change (e.g. Boutton *et al.* 1996; Ehleringer *et al.* 2000; Boström *et al.* 2007), including: (1) the decline in the $\delta^{13}C$ value of atmospheric CO_2 due to large-scale burning of ^{13}C-depleted fossil fuels since the beginning of the Industrial Revolution (the Suess effect); (2) microbial discrimination during decomposition; and (3) adsorption of ^{13}C-enriched microbial residues to fine mineral particles. Soil $\delta^{13}C$ enrichment throughout the soil profile is usually between 1-3 ‰ (Ehleringer *et al.* 2000), and larger enrichment is likely the result of changes from C_3 to C_4 vegetation.

As vegetation shifts from grass- to woody plant-domination, new C derived from woody plants is continuously added to the old C pool derived from the original grassland. A simple mass balance mixing model was used to estimate the percentage of new C (f_{new}) to the total SOC pool underneath woody patches for each soil depth increment:

$$f_{new} = \frac{\delta^{13}C_{new} - \delta^{13}C_{old}}{\delta^{13}C_{veg} - \delta^{13}C_{old}} * 100\%$$

where $\delta^{13}C_{new}$ is the $\delta^{13}C$ values of the soil samples from woody patches (cluster or grove); $\delta^{13}C_{old}$ is the averaged $\delta^{13}C$ value of the soil samples from grasslands (n = 200) which is used as paired "control" site; and $\delta^{13}C_{veg}$ is the $\delta^{13}C$ value of composited fine root sample

from clusters or groves. Here, we assume new C derived from woody plants in wooded landscape elements had the same $\delta^{13}C$ values as those of fine roots in each depth increment since roots and root exudates are the main sources of C input into subsoil (Rumpel & Kögel-Knabner 2011). This calculation may underestimate the proportions of new C derived from woody plants as averaged $\delta^{13}C$ values of soil samples from grasslands for each soil depth increment were used as baselines, which are more depleted due to the increasing abundance of C_3 forbs in the contemporary grassland vegetation than the supposed baseline values when woody patches were once established, this is especially true for surface soils (0-15 cm, hereafter).

Data analyses

Datasets that were not normally distributed were log-transformed before variable means of different landscape elements were compared using a mixed model in JMP Pro 12.0 (SAS Institute Inc., Cary, NC, USA). In the mixed model, spatial autocorrelation was considered as a spatial covariance for adjustment (Littell *et al.* 2006). A p value < 0.05 was used as the cutoff for statistical significance. A sample variogram fitted with a variogram model was developed to quantify the spatial structure of soil $\delta^{13}C$ based on soil $\delta^{13}C$ values of 320 random soil sampling points for each depth increment using R statistical software (R Development Core Team 2014). Ordinary kriging based on the best fitted variogram model was used to predict soil $\delta^{13}C$ values at un-sampled locations for each soil depth increment. A kriged map of soil $\delta^{13}C$ for each depth increment was generated in ArcMap 10.2.2 (ESRI, Redlands, CA, USA) using the Spatial Analyst tool.

Kriged maps of percentage (%) of C derived from C_3 vegetation were generated for each soil depth increment in the same way.

RESULTS

Woody plant encroachment altered spatial patterns of soil $\delta^{13}C$ throughout the soil profile

Raster calculations based on aerial photographs taken in 1930 and 2015 showed that total woody plant cover for this 160 m × 100 m landscape increased 16.7 % (2671.8 m^2) during the past 85 years (Table 2.1, Fig. 2.1 and 2.6a). Approximately 10.7 % (1716.3 m^2) of this increase was attributable to groves, while clusters accounted for 6.0 % (955.5 m^2) (Table 2.1). Since C_3 woody plants have markedly lower mean $\delta^{13}C$ values in both leaf (-28.7 ‰ vs -13.0 ‰) and fine root (-27.2 ‰ vs -12.7 ‰) tissues than C_4 grasses (Fig. 2.2), this vegetation change from grass- to woody plant-dominance has dramatically altered soil $\delta^{13}C$ values (Fig. 2.3) and corresponding spatial patterns of soil $\delta^{13}C$ across this landscape and throughout the soil profile (Fig. 2.4).

Table 2.1 Woody plant cover changes from 1930 to 2015 for this 160 m × 100 m landscape assessed from aerial photography.

Time	Grove cover		Cluster cover		Total woody cover	
	m^2	%	m^2	%	m^2	%
1930 †	2659	16.6	693	4.3	3352	20.9
2015	4375	27.3	1649	10.3	6024	37.6
Net change (1930-2015)	+ 1716	+ 10.7	+ 956	+ 6.0	+ 2672	+ 16.7

† See Fig. 2.7 for the woody plant cover in 1930.

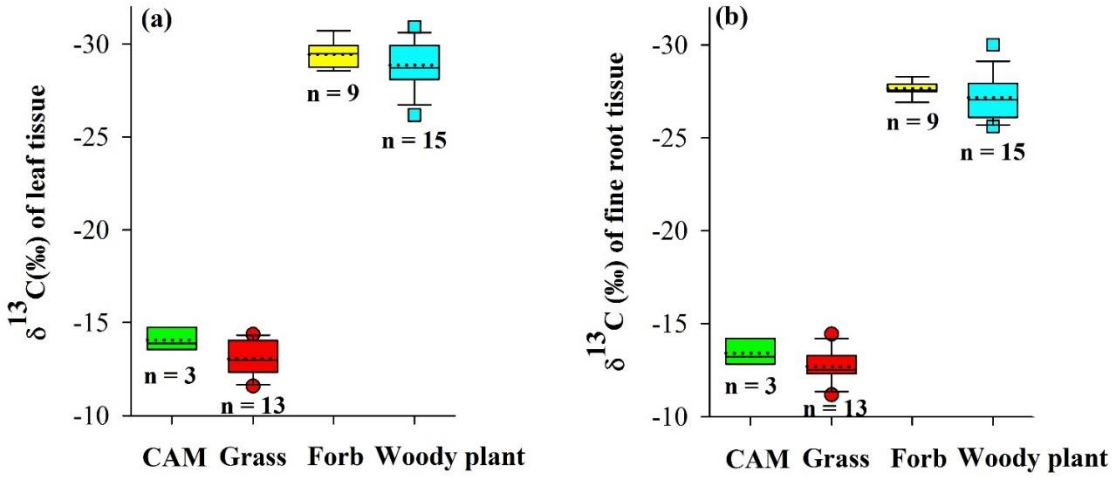

Figure 2.2 $\delta^{13}C$ values (‰) of leaf (a) and fine root (b) tissues for different plant life-forms occurring within the study area. The box plots summarize the distribution of points for each variable within each plant life-form. The central box shows the inter-quartile range, median (horizontal solid line in the box), and mean (horizontal dotted line in the box). Lower and upper error bars indicate 10^{th} and 90^{th} percentiles, and points above and below the error bars are individuals above the 90^{th} or below the 10^{th} percentiles. CAM, crassulacean acid metabolism species. More details see Appendix A.

Soil $\delta^{13}C$ values of woody patches were significantly lower than those of grasslands throughout the soil profile; and groves had significantly lower soil $\delta^{13}C$ values than clusters in the 15-30 and 30-50 cm soil depth increments (Fig. 2.3). Soil $\delta^{13}C$ values increased with soil depth, reaching maximums in the 30-50 cm (grasslands and clusters) and 50-80 cm (groves) soil depth increments, and then decreased slightly in the 80-120 cm depth increment (Fig. 2.3). The kriged maps indicated that soil $\delta^{13}C$ values were lowest in the centers of woody patches, increased towards the edges of woody patches, and reached highest values within the grassland matrix (compare Fig. 2.1 and 2.4). This spatial

pattern of soil $\delta^{13}C$ gradually weakened with soil depth (Fig. 2.4). Statistically, the coefficient of variation (CV) of soil $\delta^{13}C$ across this landscape decreased with depth throughout the soil profile (|CV| = 9.78%, 10.13%, 9.19%, 8.20%, 6.06%, 5.57%, respectively). Collectively, these results indicate the reduced impact of woody encroachment on spatial variability of soil $\delta^{13}C$ in deeper portions of the soil profile.

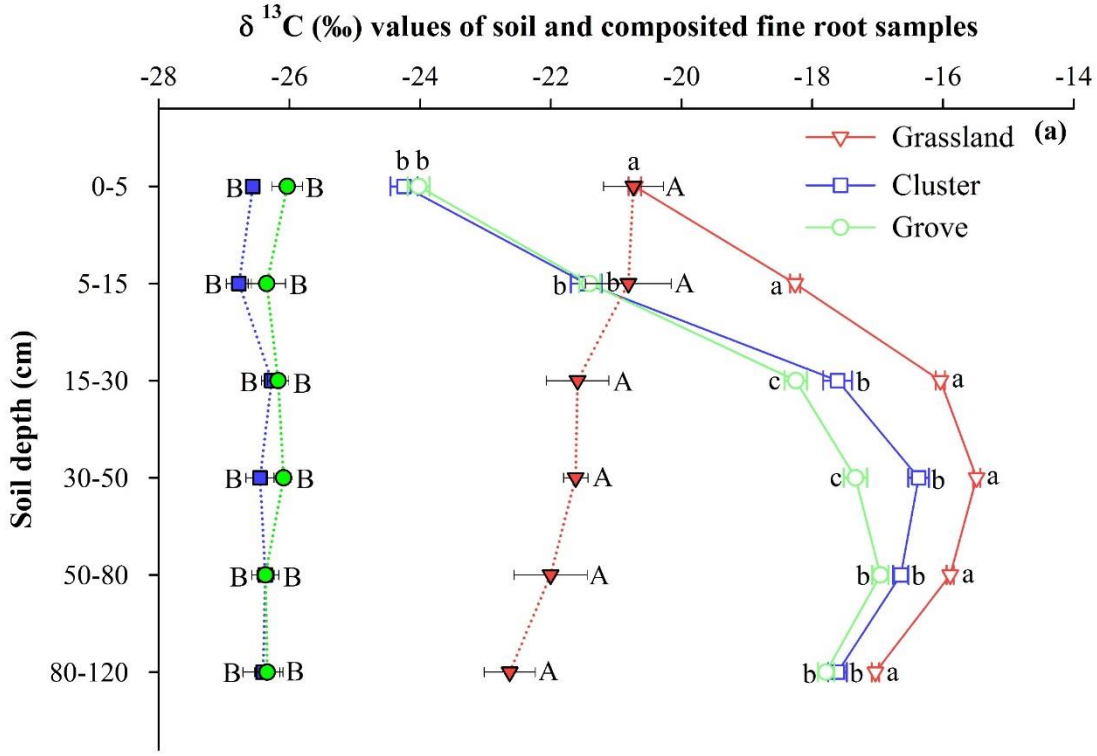

Figure 2.3 $\delta^{13}C$ values (‰) of soil (hollow symbol) and composited fine root (solid symbol) samples for different landscape elements across this 160 m ×100 m landscape throughout the soil profile. Significant difference ($p < 0.05$) between means in landscape elements are indicated with different letters. Number of samples for $\delta^{13}C$ values (‰) of soil samples: grassland = 200, cluster = 41, and grove = 79. $\delta^{13}C$ values (‰) of composited fine root samples for different landscape elements are with three replicates.

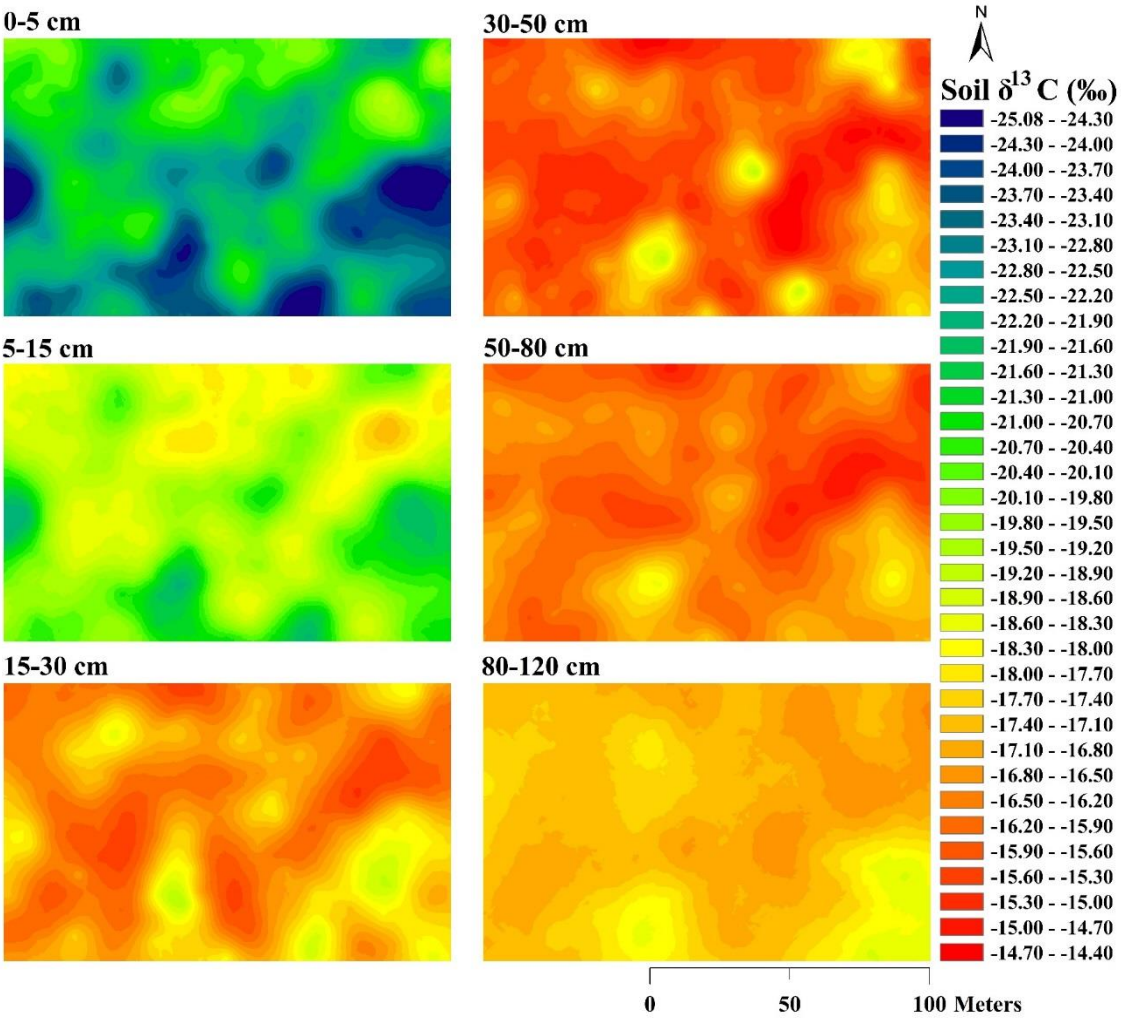

Figure 2.4 Kriged maps of $\delta^{13}C$ (‰) based on 320 randomly located sampling points for this 160 m ×100 m landscape throughout the soil profile.

Vegetation dynamics inferred from the spatial patterns of soil $\delta^{13}C$

Both conventional ^{14}C age and mean residence times (MRTs) of SOC from the remnant grassland increased with depth (Table 2.2). The mass balance mixing model revealed that approximately 75% of the vegetation productivity is of C_4 origin in the 80-120 cm soil depth increment, suggesting vegetation was dominated by C_4 grasses with a small proportion of C_3 vegetation at approximately 1500 yr BP across this landscape (Fig. 2.5). The proportion of C_4 vegetation productivity reached the highest value in the 30-50 cm soil depth increment, suggesting that the vegetation was primarily dominated by C_4 grasses around 700 yr BP (Fig. 2.5). Soil $\delta^{13}C$ values in grasslands became progressively more negative from 30 cm to the surface, consistent with the increased abundance of C_3 forbs known to have occurred within the last century (Fig. 2.3 and 2.5). Current grasslands are co-dominated by C_4 grasses and C_3 forbs (Fig. 2.5), with forbs having average $\delta^{13}C$ values of -29.4 ‰ and -27.7 ‰ in leaf and fine root tissues, respectively (Fig. 2.2).

Table 2.2 Conventional ^{14}C age (yr BP) and model-estimated mean residence time (yr BP, MRT) of soil organic matter in upland grassland throughout the soil profile.

Depth (cm)	^{14}C content (% modern)	^{14}C age	MRT	Reference
0-15	112.20 ± 0.65	Modern †	71 ± 4	Boutton *et al.*,
15-30	100.90 ± 1.10	8 ± 8‡	272 ± 40	1998
30-60	92.70 ± 1.70	610 ± 150	730 ± 30	
60-90	NA ǂ	NA	NA	
90-120	83.15 ± 0.35	1480 ± 35	1480 ± 35	

† Modern denotes that soils contained > 100 % modern carbon, indicating that these soil samples were influenced by the presence of post-1960s bomb carbon, and conventional ages could not be assigned to these samples. ‡ Values are mean ± standard error of 2 replicate soil cores. ǂ NA indicates not available.

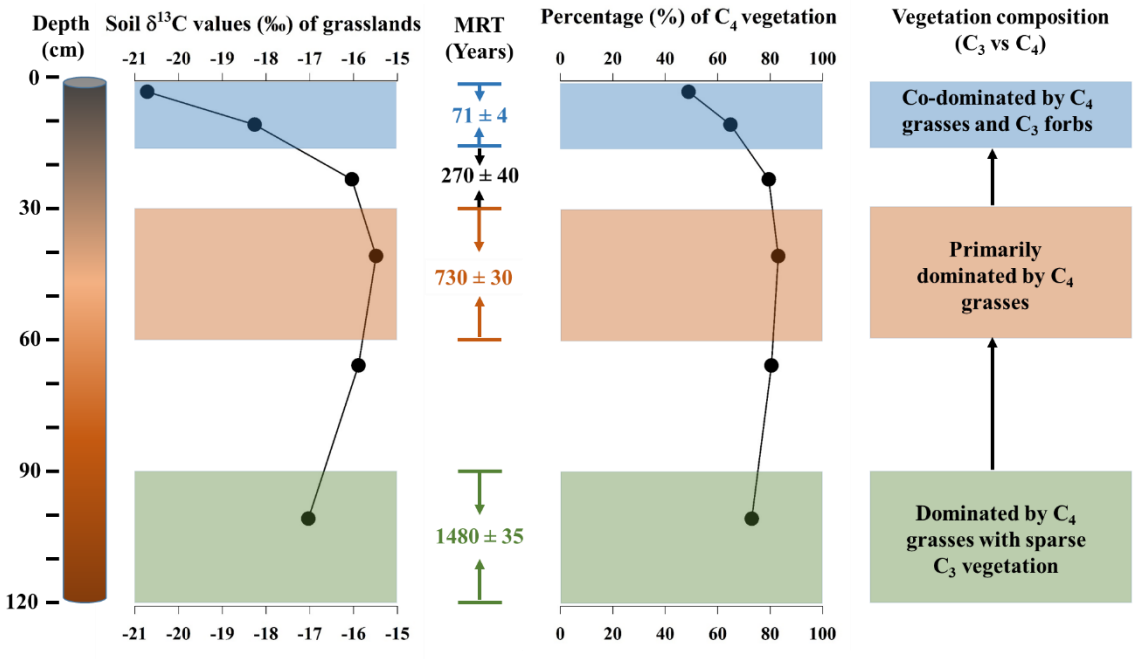

Figure 2.5 Historic vegetation dynamics (C_3 vs C_4) for grasslands based on $\delta^{13}C$ values (‰) and ^{14}C ages (years) of SOC throughout the soil profile.

A contour map generated from the kriged map of soil $\delta^{13}C$ in the 0-5 cm soil depth increment together with aerial photographs taken in 1930 and 2015 provide evidence for the formation and expansion of woody patches across this landscape. Trees/shrubs near the centers of woody patches are generally older than those near the edges of those patches, consistent with soil $\delta^{13}C$ contours that have progressively more depleted values moving from the centers of woody patches out into the surrounding grasslands (Fig. 2.6b). Where groves have recently expanded into grassland, soil $\delta^{13}C$ values decrease gradually, and grove/grassland boundaries with low densities of contour lines represent areas undergoing active woody expansion in recent time (see red arrows, Fig. 2.6b). However, where

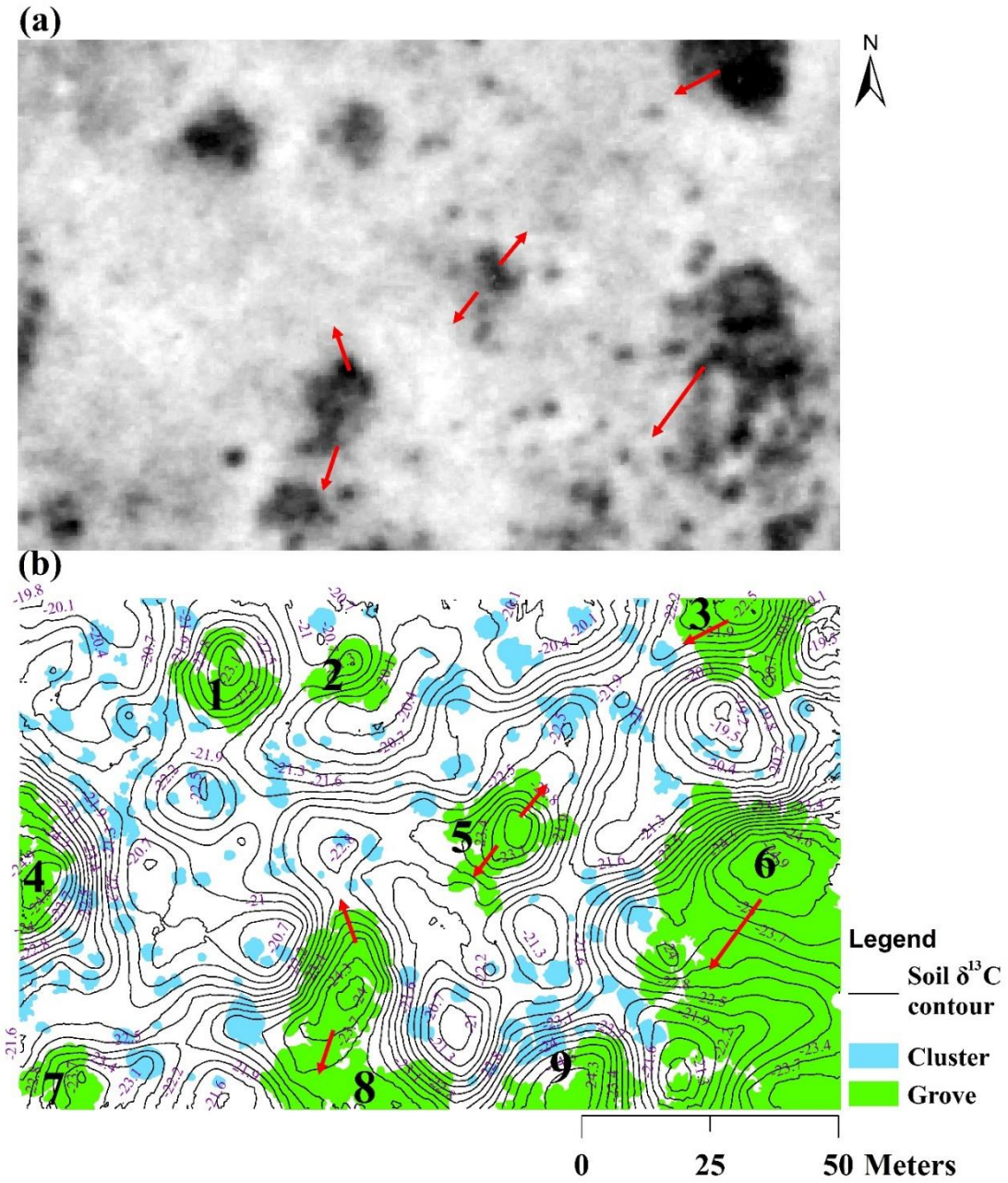

Figure 2.6 Aerial photo taken in 1930 (a) and $\delta^{13}C$ contours (at 0.2 ‰ interval) for the 0-5 cm depth increment superimposed on the digitized vegetation cover derived from a 2015 aerial photograph (b) showing the formation and dynamics of groves during the past century. For the 1930 aerial photo, gray areas are herbaceous vegetation and dark areas are woody vegetation. Red arrows indicate the potential directions of grove expansion inferred from the density of soil $\delta^{13}C$ contours, see the main text for elaboration.

grove/grassland boundaries have remained relatively stationary over time, contour lines are denser and indicate that soil $\delta^{13}C$ values change abruptly at those stable boundaries. For example, the northern areas of grove no. 6 had high density of contour lines, while southwestern areas had low density of contour lines, indicating grove 6 expanded actively towards the southwestern direction (Fig. 2.6b). This inference is supported by visual assessment of aerial photographs taken in 1930 and 2015 (Fig. 2.6). This evidence indicated that these woody patches are actively expanding in different directions, albeit with different rates.

SOC sources inferred from the spatial patterns of soil $\delta^{13}C$

SOC concentrations in woody patches were higher than those in grasslands throughout the entire soil profile (Table 2.3). SOC concentrations were negatively correlated with soil $\delta^{13}C$ values throughout the soil profile. These relationships were exponential in surface soils, but became linear at depths > 15 cm (Fig. 2.7). Soil $\delta^{13}C$ values occupied the range between the mean values of contemporary C_3 and C_4 vegetation (Fig. 2.2 and 2.3), indicating SOC was derived from both C_3 and C_4 sources. Proportions of C derived from C_3 vegetation underneath woody patches were significantly higher than those underneath grasslands throughout the entire soil profile (Table 2.3), and much of this C_3-derived C originated from woody plants, especially in the surface soils (Table 2.3). In grasslands, approximately 50% of the SOC was derived from C_3 forbs in the 0-5 cm depth increment (Table 2.3). Spatial patterns of the proportion of C derived from C_3 vegetation showed higher values inside the woody patches and lower values within the remnant grassland matrix throughout the soil profile (Fig. 2.8).

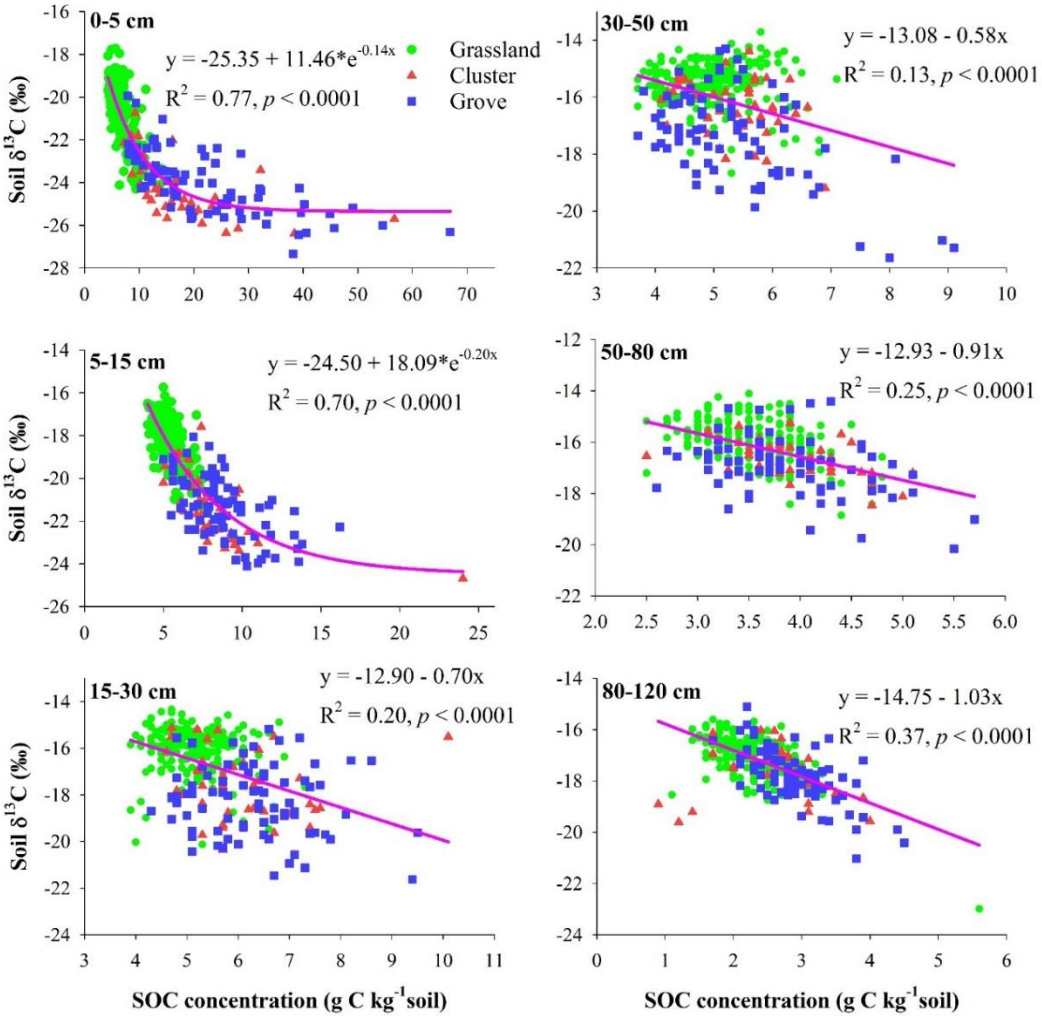

Figure 2.7 Relationships between soil $\delta^{13}C$ (‰) and SOC concentration (g C kg^{-1} soil) throughout the soil profile. Please note that scales are different throughout the soil profile.

Table 2.3 Soil organic carbon (SOC) concentration (g C kg^{-1} soil), percentage (%) of C derived from C_3 plants, and percentage (%) of new C derived from woody plants for different landscape elements across this 160 m × 100 m landscape throughout the soil profile. Significant differences between means in landscape elements are indicated with different superscript letters. Values are mean ± standard errors (SE). Number of samples: grassland = 200, cluster = 41, and grove = 79.

Depth (cm)	SOC concentration (g C kg^{-1} soil)			Percentage (%) of C derived from C_3 plants			Percentage (%) of new C derived from woody plants	
	Grassland	Cluster	Grove	Grassland	Cluster	Grove	Cluster	Grove
0-5	6.7 ± 0.1^{c}	17.0 ± 1.4^{b}	22.1 ± 1.4^{a}	51.1 ± 0.6^{b}	74.2 ± 1.4^{a}	72.7 ± 1.1^{a}	60.5 ± 3.6^{a}	62.3 ± 3.1^{a}
5-15	5.4 ± 0.1^{b}	8.2 ± 0.5^{a}	8.8 ± 0.3^{a}	35.1 ± 0.5^{b}	55.9 ± 1.5^{a}	55.6 ± 1.1^{a}	37.6 ± 2.8^{a}	38.9 ± 2.0^{a}
15-30	5.1 ± 0.0^{b}	6.0 ± 0.2^{a}	6.3 ± 0.1^{a}	20.5 ± 0.5^{c}	30.8 ± 1.5^{b}	35.0 ± 1.1^{a}	15.4 ± 2.2^{b}	21.8 ± 1.7^{a}
30-50	5.0 ± 0.1^{a}	5.3 ± 0.1^{a}	5.3 ± 0.1^{a}	16.9 ± 0.4^{c}	22.7 ± 1.0^{b}	29.0 ± 1.2^{a}	8.0 ± 1.4^{b}	17.4 ± 1.7^{a}
50-80	3.5 ± 0.0^{b}	3.9 ± 0.1^{a}	3.9 ± 0.1^{a}	19.5 ± 0.4^{b}	24.5 ± 0.8^{a}	26.5 ± 0.8^{a}	7.2 ± 1.1^{a}	10.2 ± 1.2^{a}
80-120	2.3 ± 0.0^{b}	2.6 ± 0.1^{a}	2.9 ± 0.1^{a}	27.0 ± 0.4^{b}	30.8 ± 0.9^{a}	32.0 ± 0.8^{a}	6.5 ± 1.5^{a}	8.4 ± 1.3^{a}

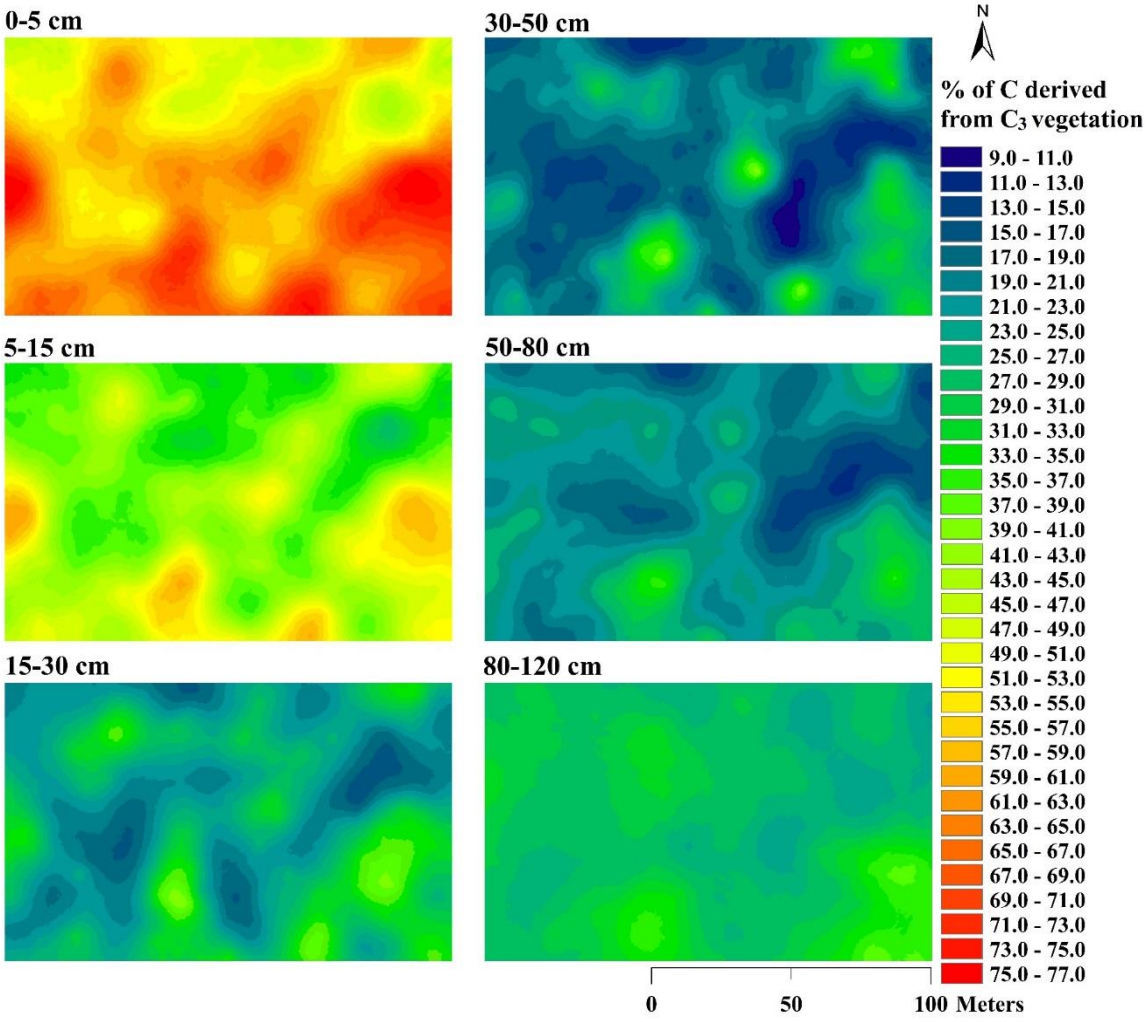

Figure 2.8 Kriged maps of percentage (%) C derived from C_3 plants calculated based on the mixed model for this 160 m × 100 m landscape throughout the soil profile.

DISCUSSION

Overall spatial patterns of soil δ13C throughout the soil profile

The encroachment of C_3 woody plants into the original C_4 grassland delivers ^{13}C deleted plant materials to soils (Fig. 2.2 and 2.3), altering patterns of spatial heterogeneity in soil $\delta^{13}C$ throughout the soil profile. This alteration is especially evident in surface soils

(0-15 cm) where spatial patterns of soil $\delta^{13}C$ across this landscape (Fig. 2.4) showed strong resemblance to the current vegetation cover (Fig. 2.1), especially the spatial distribution of groves. This result is consistent with previous studies showing that changes in the C_3-C_4 dominance of plant communities alter surface soil $\delta^{13}C$ across multiple spatial scales (van Kessel *et al.* 1994; Biggs *et al.* 2002; Bai *et al.* 2009).

More importantly, for the first time, we have demonstrated that changes in spatial patterns of soil $\delta^{13}C$ were substantially observed to a depth of 1.2 m following the conversion from grasslands to woody patches, albeit to a lesser degree in deeper portions of the soil profile (Fig. 2.4). Soil $\delta^{13}C$ was significantly negatively correlated with root density (kg m^{-3}) throughout the soil profile. The gradually dissipating impact of woody encroachment on spatial patterns of soil $\delta^{13}C$ deep in the profile is likely due to the fact that root biomass, as the primary source of SOC (Rasse *et al.* 2005; Rumpel & Kögel-Knabner 2011; Schmidt *et al.* 2011), decreases exponentially with depth as shown in this (Zhou *et al.* 2017a) and other studies (Jackson *et al.* 1996). Despite such dramatic decreases with depth, mean root densities of woody patches were still two time greater than those of grasslands in the 80-120 cm soil depth increment (Zhou *et al.* 2017a), as woody species in dryland ecosystems generally have greater rooting depths than grass species (Schenk & Jackson 2002). The deposition of ^{13}C-depleted organic matter via root turnover of woody species, though in reduced quantity in subsurface soils, has differentiated soil $\delta^{13}C$ between woody patches and grasslands (Fig. 2.3) and amplified patterns of spatial heterogeneity in $\delta^{13}C$ of subsurface soils across this landscape (Fig. 2.4). These findings emphasize the importance of studying biogeochemical properties and

processes in subsurface soils whenever changes in rooting characteristics accompany vegetation changes.

Vegetation dynamics across this landscape

Averaged $\delta^{13}C$ values of subsurface soils in grasslands across this landscape (-17.0 to -15.5 ‰, Fig. 2.3) are comparable to the average value of $\delta^{13}C$ for soils covered by pure C_4 grasses (-16.1 ± 2.2 ‰) throughout the world as summarized by Victoria *et al.* (1995). Our simple mass balance mixing model revealed that the relative productivity of the C_4 grass component was greater than 75% in subsurface soils. All these suggest that this landscape was once primarily dominated by C_4 grass species (Fig. 2.5). However, this landscape has experienced a dramatic vegetation change during the past century, characterized by both a progressive increase of C_3 forbs within the remnant grasslands, as well as the ongoing formation and expansion of woody patches (Table 2.1, Fig. 2.5 and 2.6). Mean soil $\delta^{13}C$ of grasslands in the 0-5 cm soil depth increment was -20.7 ‰ (Fig. 2.3), indicating that about half of the present productivity is derived from C_3 vegetation (Table 2.3, Fig. 2.5). This proportion is unlikely influenced by C_3 woody plants, as root biomass from woody patches declines exponentially with distance from the patch perimeter and is negligible at 2 m beyond the perimeter (Watts 1993). Based on $\delta^{13}C$ values of SOC coupled with the ^{14}C mean residence times of that SOC, this decline in C_4 grass productivity appears to have occurred primarily during the past century (Fig. 2.5). This estimate is coincident with historical accounts that indicate this site has been continuously grazed by cattle since the late 1800s (Archer *et al.* 1988; Archer 1995). This prior history of livestock grazing resulted in an increased proportion of forb biomass, and

a corresponding decrease in C_4 grass productivity (Archer & Smeins 1991; Boutton *et al.* 1998; Augustine *et al.* 2017).

The dramatic increase in soil $\delta^{13}C$ from the 0-5 to 15-30 cm soil depth increment under woody patches (Fig. 2.3) and the fact that most of the new C derived from C_3 woody plants is concentrated in surface soils (Table 2.3) suggests that woody patches are recent components of this landscape. This inference is well-supported by tree-ring analyses which indicate the maximum ages of dominant trees (i.e. *P. glandulosa*) found in groves and clusters are < 130 yrs (Stoker 1997; Boutton *et al.* 1998; Liao *et al.* 2006). Raster calculations based on aerial photos and soil $\delta^{13}C$ contour analysis indicate that these woody patches, especially groves, are actively expanding, though in different directions and rates (Table 2.1 and Fig. 2.6). Previous studies on the upland portion of this site proposed that rates and directions of woody patch expansion are regulated by rainfall, subsurface soil texture (i.e. non-argillic inclusion), and topography (Archer 1995; Wu & Archer 2005; Zhou *et al.* 2017b). Though the exact rate of woody patch expansion is still unclear, simulations based on transition probabilities (Archer 1995) and spatial analyses of subsurface soil texture (Zhou *et al.* 2017b) suggest that the current landscape is an intermediate stage in the conversion of grasslands to closed-canopy woodlands. Studies in Africa also suggest that, when mean annual precipitation is above 650 mm (our site is 680 mm), savannas are unstable and have a tendency for woody canopy closure (Bond *et al.* 2003; Sankaran *et al*. 2005).

It should be noted that interpretations of vegetation change based on soil radiocarbon and $\delta^{13}C$ values can be problematic, and may be affected by: (1) the gradual

enrichment of soil $\delta^{13}C$ with increasing soil depth due to organic matter decay (Boutton *et al*. 1996; Ehleringer *et al.* 2000; Boström *et al.* 2007); (2) the possibility that some C_3 forbs in the contemporary vegetation might be deep-rooted and capable of depositing ^{13}C depleted soil organic matter in subsurface soils (Fig. 2.3); and (3) the difficulty of obtaining accurate estimates of soil ages (Wang *et al.* 1996). However, these results provide a record of vegetation change that is broadly consistent with historical records, aerial photos from the 1930's to the present, and the ages of the trees that currently dominate wooded areas.

Impact of vegetation change on SOC dynamics

Our data has demonstrated that this change from C_4 grassland to C_3 vegetation during the past century has significant impacts on SOC dynamics in this subtropical savanna. The increasing abundance of both forbs and woody plants has increased the proportion of C derived from C_3 vegetation (Table 2.3) and altered spatial patterns of C with C_3 origins across this landscape and throughout the soil profile (Fig. 2.8). Though the inherent behavioral difference between C_3 and C_4 derived C in soil C cycling is still unclear, C derived from C_3 vegetation tends to be decomposed slower than its C_4 counterpart in mixed C_3/C_4 soils due mainly to differences in lignin content and/or mean size of particulate organic matter (Wynn & Bird 2007; Saiz *et al.* 2015). Previous studies at this site also revealed that grassland to woodland conversion increased the proportions of biochemically recalcitrant lignin and aliphatic structures present in SOC (Liao *et al.* 2006; Filley *et al.* 2008; Creamer *et al*. 2013). Thus, SOC sequestration potential per unit of organic matter input might be higher for C_3 vegetation compared to C_4 grasslands.

In order to interpret the observed increases in SOC concentration under woody patches, we separated the SOC pool into proportions of new C derived from woody plants vs. old C with herbaceous origins using a mass balance approach. Though substantial proportions of C derived from woody plants were observed throughout the soil profile, new C derived from woody plants was concentrated in surface soils (Table 2.3). Previous studies using a chronosequence approach with an age series of woody patches at this study site found a linear increase in SOC concentration over periods of time exceeding 100 yr in surface soils (Liao *et al.* 2006; Kantola 2012); and dynamic simulation models predict that it may take ca. 400 yr after woody encroachment for SOC saturation in surface soils (Hibbard *et al.* 2003). No evidence for SOC saturation in surface soils following woody proliferation has also been reported in other ecosystems (Throop & Archer, 2008; Blaser *et al.* 2014). Thus, it is possible that more new C derived from woody plants will be continuously accumulated in surface soils as woody patches are actively expanding. The exponential relationships between soil $\delta^{13}C$ and SOC concentration in surface soils also indicate that many soil cores from woody patches have not yet reached the maximum for SOC or the minimum for $\delta^{13}C$ (Fig. 2.7). In contrast, soil $\delta^{13}C$ and SOC concentration in subsurface soils were linearly related (Fig. 2.7) and new C derived from woody plants only contributed less than 20 % of the SOC pool (Table 2.3), implicating that subsurface soils have a great potential for the accumulation of new C derived from woody plants (Zhou *et al.* 2017a). Collectively, these results suggest that woody encroachment into grasslands in dryland ecosystems may represent an even larger C sink for atmospheric CO_2 than previously thought as most previous studies have focused on surface soils only

(Liao *et al.* 2006; Springsteen *et al.* 2010; Blaser *et al.* 2014; Barger *et al.* 2011; Li *et al.* 2016).

CONCLUSIONS

Shifts in vegetation dominance across this landscape, especially the encroachment of C_3 woody plants into the remnant grassland matrix, creates a heterogeneous vegetation structure and coincident spatial variability in soil $\delta^{13}C$ throughout the soil profile. Results from this subtropical savanna, which may be analogous with other dryland ecosystems in southwestern U.S., Africa, and Australia, showed that vegetation across this landscape is experiencing a dramatic change. Such change is characterized by a significant increase in abundance of both C_3 woody plants and forbs in a system that was once primarily dominated by C_4 grasses. While there are discrepancies over the role of woody encroachment on SOC storage, we did observe that woody encroachment has substantially added new C to the old C pool originated from grasslands throughout the entire soil profile and therefore increased SOC concentrations under woody patches across this landscape. Given the extent of woody encroachment at the global scale, we suggest that this vegetation change has important implications for predicting and modeling soil overall C dynamics in dryland regions.

CHAPTER III

SPATIAL HETEROGENEITY OF SUBSURFACE SOIL TEXTURE DRIVES LANDSCAPE-SCALE PATTERNS OF WOODY PATCHES IN A SUBTROPICAL SAVANNA*

SYNOPSIS

In the Rio Grande Plains of southern Texas, subtropical savanna vegetation is characterized by a two-phase pattern consisting of discrete woody patches embedded within a C_4 grassland matrix. Prior trench transect studies have suggested that, on upland portions of the landscape, large woody patches (groves) occur on non-argillic inclusions, while small woody patches (clusters) are dispersed among herbaceous vegetation where the argillic horizon is present. To test whether spatial heterogeneity of subsurface soil texture drives the landscape-scale pattern of woody patches in this subtropical savanna, landscape-scale spatial patterns of soil texture were quantified by taking spatially-specific soil samples to a depth of 1.2 m in a 160 m × 100 m plot. Kriged maps of soil texture were developed, and the locations of non-argillic inclusions were mapped. Visual comparison of kriged maps of soil texture to a high resolution aerial photograph of the study area revealed that groves were present exclusively where the non-argillic inclusions were

* Originally published as: Zhou, Y., Boutton, T.W., Wu, X.B., & Yang, C. (2017) Spatial heterogeneity of subsurface soil texture drives landscape-scale patterns of woody patches in a subtropical savanna. *Landscape Ecology*, **32**, 915-929. The publication is available at https://link.springer.com/article/10.1007/s10980-017-0496-9.

present. This clear visual relationship was further supported by positive correlations between soil sand concentration in the lower soil layers and total fine root biomass which mapped the locations of groves. Subsurface non-argillic inclusions may favor the establishment and persistence of groves by enabling root penetration deeper into the profile, providing greater access to water and nutrients that are less accessible on those portions of the landscape where the argillic horizon is present, thereby regulating the distribution of grove vegetation and structuring the evolution of this landscape.

INTRODUCTION

Savannas are comprised of two divergent growth forms, trees and grasses, and are globally important ecosystems that sustain the livelihoods of a large proportion of the world's human population (Scholes & Archer 1997; Sankaran *et al.* 2005). In these biomes, patchiness of woody cover is a chief characteristic and determinant of ecosystem services (Pringle *et al.* 2010). The abundance and distribution of woody patches has the potential to profoundly influence species diversity (Ratajczak *et al.* 2012), plant and livestock production (Anadón *et al.* 2014), as well as many other aspects of ecosystem function, including hydrological and biogeochemical cycles (i.e. "island of fertility", Schlesinger *et al.* 1996). Since savannas represent an intermediate/dynamic physiognomy between closed-canopy woodlands and open grasslands, many efforts are underway to assess the factors that determine the relative abundances of woody vs. herbaceous components, and to clarify the mechanisms that permit trees and grasses to coexist without the exclusion of one growth form by the other (e.g. Scholes & Archer 1997; Sankaran *et al.* 2004; Sankaran *et al.* 2005; Buitenwerf *et al.* 2012). However, the mechanisms that

regulate the distribution of woody patches in savannas remain uncertain. Because savannas are experiencing increased woody plant abundance globally (Van Auken 2000) and are potentially susceptible to future climate change (Buitenwerf *et al.* 2012; Volder *et al.* 2013; Scheiter *et al.* 2015), an improved understanding of factors that structure the spatial patterns of woody patches in savannas is necessary to better represent this phenomenon in integrated climate-biogeochemical models (Liu *et al.* 2012), and to improve land management efforts in these regions (Sankaran *et al.* 2005).

The distribution of woody patches in savannas could be controlled by climate, soils, disturbance regimes (e.g. herbivory and fire), and/or interactions between those factors (Higgins *et al.* 2000; Zou *et al.* 2005; Sileshi *et al.* 2010; Sankaran *et al.* 2013). Besides climate, which is important at larger scales, subtle spatial heterogeneity in soil properties at the landscape-scale can produce corresponding patchiness in the distribution of woody vegetation in savannas (McAuliffe 1994; Sileshi *et al.* 2010). This spatial heterogeneity in soils can be a consequence of either pedogenic or biotic processes. For example, in many arid and semiarid savanna ecosystems, termite activities could produce vegetation patterns at different spatial scales by altering soil properties to impart substrate heterogeneity (Arshad 1982; Sileshi *et al.* 2010; Bonachela *et al.* 2015). Discontinuity of subsurface soil horizons formed pedogenically is a common feature of soil development in arid and semi-arid regions. Spatial heterogeneity of subsurface soil texture caused by discontinuous soil horizons could affect the abundance and distribution of roots (Watts 1993; Schenk & Jackson 2005) and the movement and availability of soil water and nutrients (McAuliffe 1994; Hamerlynck *et al.* 2000; Zou *et al.* 2005), thereby affecting

the distribution of woody plants in savannas. For example, coarser-textured subsoils permit root penetration deeper into the soil profile through reduced resistance (Schenk & Jackson 2005) and enable greater infiltration and deeper percolation of water (Brown & Archer 1990), in turn favoring the establishment and persistence of deeply rooted woody plants capable of exploiting soil moisture at greater depths.

In the subtropical Rio Grande Plains of southern Texas, woody plants have markedly increased during the past century (Archer *et al.* 1988; Boutton *et al.* 1998; Archer *et al.* 2001), and upland portions of the landscape display strong patchiness in the distribution of woody vegetation (Archer *et al.* 1988; Archer 1995). In this region, small discrete woody clusters (generally < 100 m^2 in canopy area) comprised of multiple shrub species organized around a central honey mesquite (*Prosopis glandulosa*) tree, and large groves (generally > 100 m^2) that coalesced from several clusters are embedded in a C_4 grassland matrix (Archer 1995; Bai *et al*. 2012). Previous studies in which trenches were excavated along transects from open grassland into the centers of groves showed that subsurface soil horizons were not laterally continuous, with non-argillic (or sandy) inclusions interspersed within a well-developed clay-rich argillic horizon (*Bt*) (Fig. 3.1) (Loomis 1989; Watts 1993). In addition, grove vegetation occurred almost entirely within areas where the argillic horizon was absent (Fig. 3.1). This suggests that there might be strong spatial associations between these coarse-textured non-argillic inclusions and grove vegetation in this region. However, it has been difficult to generalize this relationship to larger spatial scales based on spatially limited sampling. Even if this relationship that grove vegetation is present on non-argillic inclusions is true, it raises questions concerning

cause and effect. Did the presence of grove vegetation disrupt the well-developed argillic horizon to form coarser-textured inclusions? For example, the modification of subsurface soil texture beneath woody patches as a result of belowground faunal activity (e.g. termites) has been well-documented in other savanna ecosystems (Konaté *et al.* 1999; Turner *et al.* 2006; Sileshi *et al.* 2010). Or, alternatively, did non-argillic inclusions form pedogenically (i.e., fluvial or aeolian depositional processes) before the current biota, favoring the establishment of grove vegetation and structuring the distribution of woody patches in this subtropical savanna?

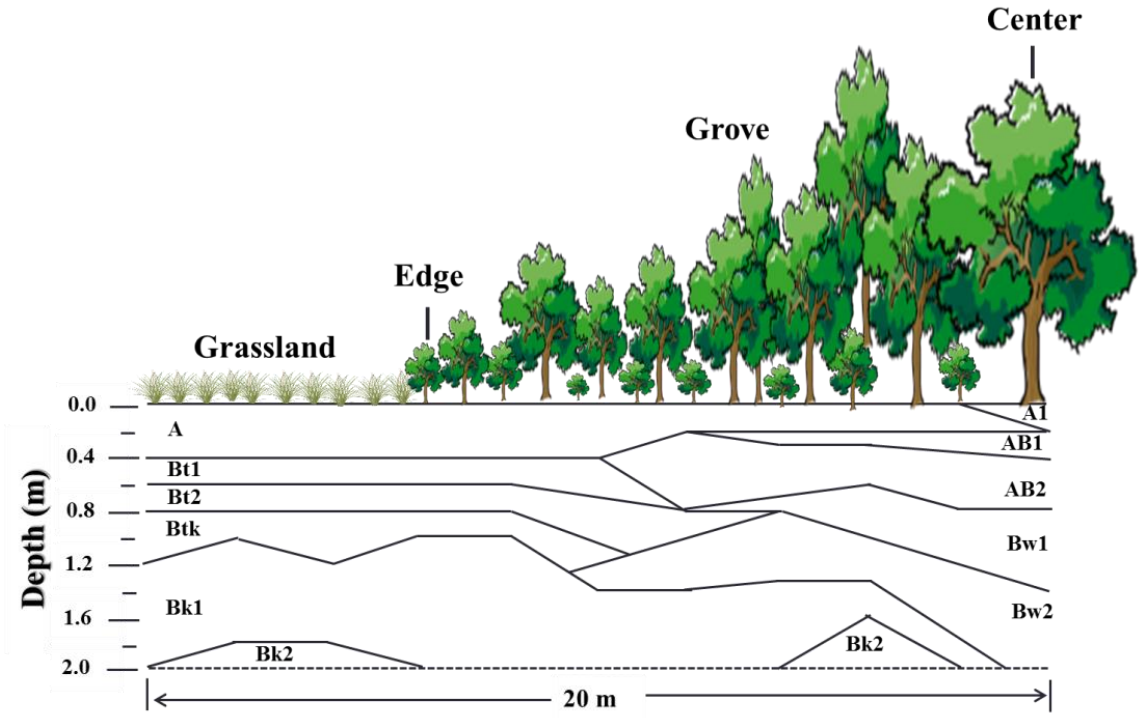

Figure 3.1 Map of soil horizons to a depth of 2 m in a subtropical savanna ecosystem in southern Texas. The map was developed from a transect running from open grassland to the center of a grove, and shows that the grove vegetation is largely confined to areas where the argillic horizon (B_t) is absent (adapted from Watts 1993).

The primary objective of this study was to quantify the landscape-scale distribution of soil texture throughout an entire soil profile to map the locations of non-argillic inclusions, and spatially associate them with the current distribution of grove vegetation. Specific objectives were to (1) map the locations of non-argillic inclusions across this landscape; (2) spatially associate non-argillic inclusions with the current distribution of grove vegetation to infer cause-effect relationships; and (3) assess the potential for new grove development and future landscape evolution. We hypothesize that spatial heterogeneity of subsurface soil texture drives the distribution of grove vegetation and structures the spatial pattern of woody patches in this subtropical savanna, rather than the alternative that current grove vegetation induced the discontinuous subsurface argillic horizon. If this is true, current grove vegetation should be located exclusively on non-argillic inclusions, but some non-argillic inclusions might not yet be colonized by grove vegetation. These unoccupied non-argillic inclusions then have the potential to develop grove vegetation and shape the future landscape evolution. To test this hypothesis, we took 320 spatially georeferenced soil cores to a depth of 1.2 m across a 160 m × 100 m landscape and measured soil texture within multiple depth increments. These measurements enabled us to model the spatial structure of soil texture using variogram analysis, and to map the distribution of non-argillic inclusions across this landscape using spatial interpolation (i.e. ordinary kriging).

MATERIALS AND METHODS

Study area

This study was conducted at the Texas A&M AgriLife La Copita Research Area (27˚40′ N, 98˚12′ W), approximately 65 km west of Corpus Christi, Texas. Climate is subtropical, with a mean annual temperature of 22.4 ˚C and an average annual precipitation of 680 mm distributed mostly in May and September. Elevation ranges from 75 to 90 m above sea level. The landscape consists of fairly gentle slopes (1-3%), and is comprised of nearly level uplands, lower-lying drainage woodlands, and playas.

This study was confined to upland portions of the landscape. Upland soils are sandy loam (Typic and Pachic Argiustolls) (Boutton *et al.* 1998). The vegetation is characterized as subtropical savanna parkland, consisting of a continuous C_4 grassland matrix, with discrete woody patches interspersed within that matrix. Woody patches are categorized into smaller shrub clusters and large groves. Clusters, usually with diameters < 10 m, are comprised of a single honey mesquite tree with up to 15 understory shrub/tree species. Groves, usually with diameters > 10 m, are comprised of several clusters that have fused together (Archer 1995; Bai *et al.* 2012). Species composition of this landscape can be found in Appendix A.

Field sampling

A 160 m × 100 m plot consisting of 10 m × 10 m grid cells was established in 2002 on an upland portion of the study site (Fig. 3.2), which included all of the upland landscape elements: grasslands, clusters and groves (Bai *et al.* 2009; Liu *et al*. 2011). Each corner of each 10 m × 10 m grid cell was marked with a PVC pole and georeferenced using a

GPS unit (Trimble Pathfinder Pro XRS, Trimble Navigation Limited, Sunnyvale, CA, USA) based on a UTM projection (WGS, 1984).

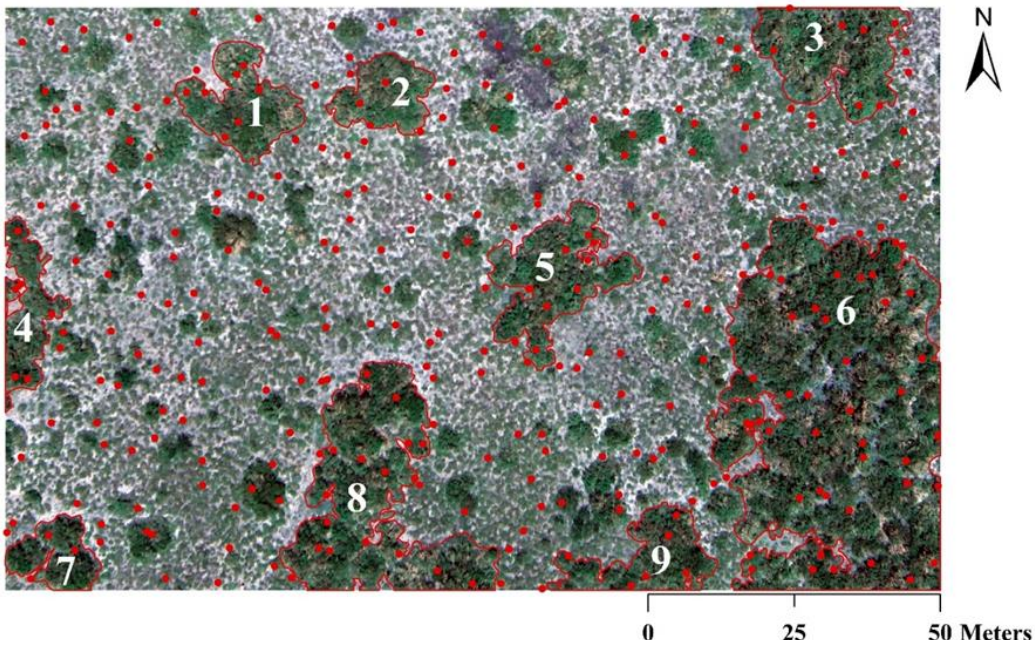

Figure 3.2 Aerial photograph of the 160 m × 100 m study area. Red dots indicate 320 random soil sampling points. Green patches are woody clusters and groves, while light grey areas indicate open grasslands. Groves are highlighted with red lines and labeled with numbers.

Two points within each 10 m × 10 m cell were randomly selected for sampling soil (320 points, Fig. 3.2) in July 2014. Landscape elements for each soil sampling point were categorized as grassland, cluster, or grove. Distances from each soil sampling point to two georefenced cell corners were measured. At each soil sampling point, two adjacent soil cores (2.8 cm in diameter × 120 cm in depth) were collected with a PN150 JMC Environmentalist's Subsoil Probe (Clements Associates Inc., Newton, IA, USA). Each soil

core was subdivided into 6 depth increments (0-5, 5-15, 15-30, 30-50, 50-80, and 80-120 cm). One soil core was oven-dried (105 ˚C for 48 hours) to determine soil bulk density. Depth increments from the other core were passed through a 2-mm sieve to remove large organic fragments, then dried at 60 ˚C for analysis of soil texture and other soil physicochemical parameters. An additional adjacent soil core (10 cm in diameter × 15 cm in depth) was collected to meet the mass requirement of soil texture analysis for 0-5 and 5-15 cm soil depth increments.

A color infrared aerial photograph was acquired in July 2015. To facilitate georeferencing of the photo, 14 evenly distributed cell corners with 30 cm × 30 cm white surfaces fastened on the top of the PVC poles were used as ground control points.

Lab analyses

Soil texture was analyzed by the hydrometer method according to Sheldrick & Wang (1993). Briefly, 80.0 ± 1.0 g oven-dried soil were mixed with 2.0 g sodium hexametaphosphate, placed into a soil dispersing cup, and soaked with deionized water. The cup was then attached to a mixer for 10 minutes to disrupt soil aggregates. The soil suspension was transferred to a graduated cylinder and filled with deionized water to the 1000-ml mark. A calibrated hydrometer was placed carefully into the soil suspension after the suspension was well mixed with a plunger. After 40 seconds, the hydrometer reading was recorded, and this process was repeated once to obtain an average. The hydrometer was removed from the soil suspension and temperature was recorded. After 2-hours, hydrometer and temperature readings were repeated on each soil suspension. Sand, silt, and clay concentrations were calculated according to Sheldrick & Wang (1993).

Roots were separated from oven-dried soil samples after determining soil bulk density through washing with sieves, and sorted into fine roots (< 2 mm in diameter) and coarse roots (> 2 mm). All roots samples were then oven-dried (65 ˚C) to constant weight for biomass.

Statistical analyses

Mantel tests were used to test spatial autocorrelation of soil variables using PASSaGE 2 (Rosenberg & Anderson 2011). Significance (two-tailed) of Mantel tests was determined by permutation (1000 randomizations). The mixed model was used to compare soil variables in different landscape elements within each soil depth increment using JMP Pro 12 (SAS Institute Inc., Cary, NC, USA). Spatial autocorrelation of variable was considered as a spatial covariance component for adjustment in the mixed model (Littell *et al.* 2006). *Post-hoc* comparisons of these variables in different landscape elements were conducted using the Tukey-Kramer method which adjusts for unequal sample sizes. Pearson correlation coefficients were determined between total fine root biomass to a depth of 1.2 m and soil sand, silt and clay concentrations for each soil layer using R statistical software (R Development Core Team 2014). A modified t-test (Dutilleul 1993) which accounts for the effects of spatial autocorrelation was used to determine the significance levels of these correlation coefficients. For all these statistical analyses, a cutoff of $p = 0.05$ was used to indicate significant differences.

Color-infrared aerial photography (6 cm × 6 cm in resolution) was processed and georeferenced using ERDAS Imagine 9.2 (ERDAS, Inc., Atlanta, GA, USA). Edges of woody patches (clusters and groves) were manually delineated using ArcGIS 10.1 (ESRI,

Redlands, CA, USA). The centroid (X and Y coordinates) of each woody patch was calculated using Calculate Geometry in ArcGIS 10.1. Ordinary kriging was used in Spatial Analyst Tools of ArcGIS 10.1 for spatial interpolation of values at unsampled locations based on 320 random sampling points and their spatial structure determined by using variogram analysis. Soil clay concentration contours (at 2% intervals) for the 80-120 cm soil layer were generated using Spatial Analyst Tools in ArcGIS 10.1.

The spatial pattern of clusters was examined with Ripley's *K*-function, a second-order statistic for quantifying spatial patterns (Ripley 1981), based on the calculated centroid of each cluster. The sample statistic $K(d)$ is calculated separately for a range of distance d, to examine the distribution pattern of clusters as a function of scale. A weighting approach was used to correct for edge effects (Haase 1995). For an easier interpretation, the result of the spatial pattern analysis was plotted as $\sqrt{K[(d)/\pi]}-d$ against d. The statistic $\sqrt{K[(d)/\pi]}-d$ was tested with 1000 randomizations at a 99% confidence interval. If the sample statistic stays within the confidence interval, the null hypothesis of complete spatial randomness is true, values above the confidence interval indicate aggregation, while values below the confidence interval indicate a regular or uniform distribution.

RESULTS

Landscape-scale patterns of soil texture throughout the soil profile

Results of the Mantel test indicated that soil sand, silt, and clay concentrations for all examined soil layers were spatially autocorrelated ($p < 0.05$, Table 3.1). Soil sand concentration decreased, while soil silt and clay concentrations increased with soil depth

across this landscape (Table 3.2, Fig. 3.3). On average, soil sand concentration decreased 25.6% from the upper 0-5 cm soil layer to the lower 80-120 cm soil layer, while soil silt and clay concentrations increased 26.2% and 127.2%, respectively. Soil sand concentration beneath groves was comparable with that beneath grasslands for 0-5, 5-15, and 15-30 cm soil layers, but was significantly higher in the 50-80 and 80-120 cm soil layers (Table 3.2). No significant differences were found among landscape elements for soil clay concentration for the upper 0-30 cm soil layers, while soil clay concentration beneath groves was significantly lower than that beneath grasslands for the lower 30-120 cm soil layers (Table 3.2).

Table 3.1 Results of Mantel tests (*r* and *p*) for spatial autocorrelations of soil sand, silt, clay concentration and fine root biomass throughout the soil profile.

Soil layers (cm)	Sand		Silt		Clay		Fine root biomass	
	r	*p*	*r*	*p*	*r*	*p*	*r*	*p*
0-5	0.265	0.001	0.233	0.001	0.208	0.001	0.090	0.001
5-15	0.292	0.001	0.220	0.001	0.245	0.001	0.086	0.001
15-30	0.236	0.001	0.263	0.001	0.170	0.001	0.061	0.002
30-50	0.110	0.001	0.250	0.001	0.073	0.002	0.042	0.036
50-80	0.074	0.002	0.077	0.001	0.081	0.001	0.035	ns
80-120	0.071	0.003	0.052	0.038	0.088	0.001	0.038	ns

Significance (*p*, two tailed) of Mantel tests was determined by permutation (1000 randomizations), ns indicates not significant ($p > 0.05$).

Ordinary kriging based on the data for 320 sampling points and variogram analysis provided an interpolation tool to estimate the values of unsampled locations, and to develop maps of soil sand, silt and clay concentrations across this landscape and

throughout the soil profile (Fig. 3.3). Spatial distributions of soil sand, silt and clay concentrations for the upper 0-30 cm soil layers were directional across this landscape (Fig. 3.3). Soil sand concentration was higher in the northern portion of this landscape and decreased gradually toward the southeast corner (Fig. 3.3). In contrast, soil silt and clay concentrations were concentrated at the southeast corner and lower values were found in north and northwest directions (Fig. 3.3). For example, soil clay concentration in the 0-5 cm soil layer doubled from the north towards the southeast. In addition, the spatial distribution of soil sand, silt and clay concentrations revealed the presence of non-argillic inclusions dispersed within a matrix of relatively higher clay concentration at depths > 30 cm (Fig. 3.3). This spatial pattern was especially prominent within the 80 -120 cm soil layer (Fig. 3.3), where the clay concentration at the center of these non-argillic inclusions was half less than the values in adjacent soil with a clayey argillic horizon. When aerial photography is compared visually to the kriged map of either soil clay or sand concentration at the 80-120 soil layers, it is obvious that all of the groves are located on these non-argillic inclusions.

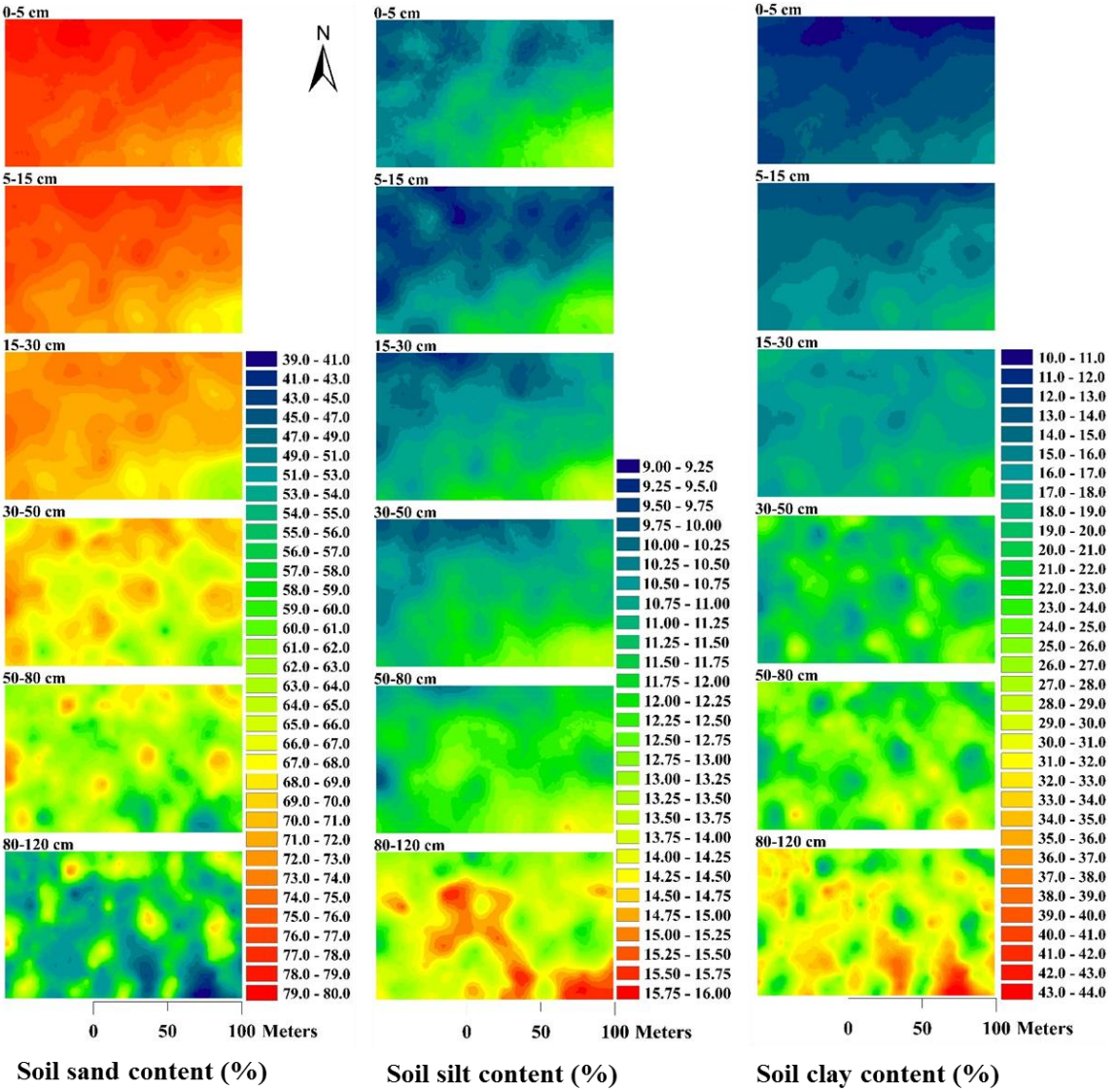

Figure 3.3 Kriged maps of soil sand, silt and clay concentrations throughout the soil profile based on 320 random sampling points across this landscape in a subtropical savanna.

Table 3.2 Mean and standard error (SE) of soil sand, silt, and clay concentrations, and fine root biomass in contrasting landscape elements throughout the soil profile in a subtropical savanna.

Parameters	Soil layers (cm)					
	0-5	5-15	15-30	30-50	50-80	80-120
Sand (%)						
Grassland	76.42 ± 0.15^{a}	74.49 ± 0.15^{a}	71.50 ± 0.14^{a}	67.21 ± 0.20^{b}	62.85 ± 0.21^{b}	55.75 ± 0.33^{b}
Cluster	75.42 ± 0.43^{a}	74.13 ± 0.43^{ab}	71.39 ± 0.39^{ab}	67.80 ± 0.58^{ab}	62.99 ± 0.78^{b}	55.40 ± 0.86^{b}
Grove	74.99 ± 0.40^{b}	73.32 ± 0.43^{b}	70.44 ± 0.46^{b}	68.11 ± 0.50^{a}	64.90 ± 0.56^{a}	58.96 ± 0.86^{a}
Silt (%)						
Grassland	10.75 ± 0.07^{b}	10.13 ± 0.06^{a}	10.69 ± 0.06^{a}	11.11 ± 0.07^{a}	12.18 ± 0.07^{a}	14.12 ± 0.07^{a}
Cluster	11.11 ± 0.21^{a}	10.69 ± 0.17^{a}	11.10 ± 0.15^{a}	11.34 ± 0.15^{a}	12.15 ± 0.16^{a}	13.97 ± 0.18^{a}
Grove	11.78 ± 0.18^{a}	11.16 ± 0.16^{a}	11.65 ± 0.14^{a}	11.88 ± 0.14^{a}	12.20 ± 0.14^{a}	13.46 ± 0.16^{b}
Clay (%)						
Grassland	12.83 ± 0.11^{a}	15.38 ± 0.11^{a}	17.81 ± 0.11^{a}	21.68 ± 0.19^{a}	24.97 ± 0.18^{a}	30.12 ± 0.28^{a}
Cluster	13.46 ± 0.30^{a}	15.18 ± 0.31^{a}	17.51 ± 0.30^{a}	20.85 ± 0.55^{b}	24.86 ± 0.70^{a}	30.63 ± 0.71^{a}
Grove	13.23 ± 0.25^{a}	15.52 ± 0.30^{a}	17.91 ± 0.35^{a}	20.00 ± 0.40^{c}	22.89 ± 0.48^{b}	27.57 ± 0.73^{b}
Fine root biomass (g m^{-2})						
Grassland	173.69 ± 5.41^{b}	216.90 ± 5.81^{b}	208.31 ± 5.15^{b}	202.83 ± 4.77^{b}	154.86 ± 4.17^{c}	118.79 ± 4.72^{c}
Cluster	506.07 ± 34.66^{a}	535.91 ± 30.66^{a}	411.69 ± 24.29^{a}	353.10 ± 16.18^{a}	264.04 ± 18.13^{b}	221.03 ± 15.63^{b}
Grove	509.99 ± 22.04^{a}	573.78 ± 21.93^{a}	461.66 ± 16.62^{a}	381.62 ± 17.16^{a}	328.16 ± 13.64^{a}	307.31 ± 14.52^{a}

Different letters indicated significant different ($p < 0.05$) between means in landscape elements based on mixed models. Number of samples: grassland = 200, cluster = 41, grove = 79.

Spatial correlations between fine root biomass and soil texture

Results of the Mantel test indicated that fine root biomass in soil layers above 50 cm was spatially autocorrelated ($p < 0.05$, Table 3.1). Total fine root biomass to a depth of 120 cm beneath woody patches (clusters: 2291 ± 97.44 g m^{-2}, n = 41; groves: 2562.52 ± 74.08 g m^{-2}, n = 79) was significantly higher than that for grassland (1075.38 ± 18.79 g m^{-2}, n = 200). This pattern was true for each individual soil depth increment along the profile (Table 3.2). Interestingly, fine root biomass beneath groves was significantly higher than that beneath clusters for the 50-80 and 80-120 cm soil layers (Table 3.2). A kriged map of total fine root biomass to a depth of 120 cm based on 320 random sampling points indicated that fine root biomass was highest at the center of woody patches (clusters and groves), decreased towards the canopy edges of woody patches and reached the lowest values within the grassland matrix (Fig. 3.4). The kriged map of total fine root biomass displayed a spatial pattern similar to that of vegetation cover, especially the distribution of grove vegetation (Fig. 3.2 and 3.4). Thus, total fine root biomass was used as an indicator of vegetation cover to correlate with soil texture. Quantitatively, there were no significant correlations either between total fine root biomass and soil sand concentration or between total fine root biomass and soil clay concentration for soil layers above 30 cm (Table 3.3). However, below 30 cm where the non-argillic inclusions begin, total fine root biomass was significantly and positively correlated with soil sand concentration, while significantly and negatively correlated with soil clay concentration (Table 3.3).

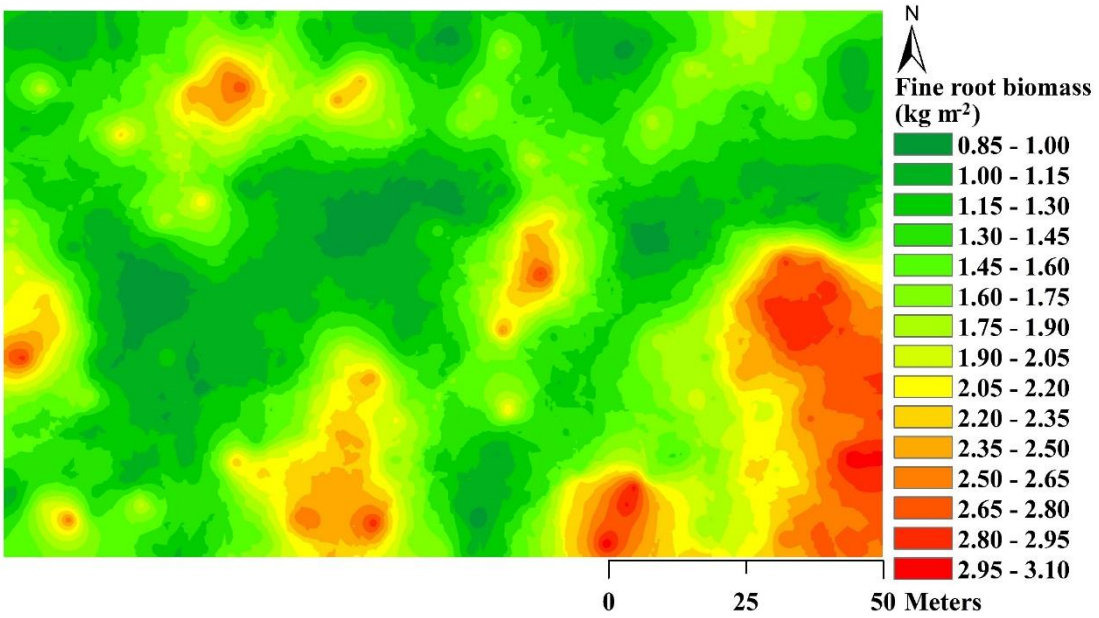

Figure 3.4 Kriged map of total fine root biomass (kg m^{-2}) to a depth of 120 cm based on 320 random sampling points across this landscape in a subtropical savanna.

Table 3.3 Pearson correlation coefficients (*r*) for the relationships between total fine root biomass, soil clay, silt, and sand concentrations throughout the soil profile.

Depth (cm)	Total fine root biomass					
	Sand		Silt		Clay	
	r	*p*	*r*	*p*	*r*	*p*
0-5	-0.181	ns	0.245	0.022	0.098	ns
5-15	-0.111	ns	0.315	0.004	-0.026	ns
15-30	-0.068	ns	0.283	0.011	-0.049	ns
30-50	0.180	0.046	0.201	ns	-0.271	< 0.0001
50-80	0.239	0.005	-0.032	ns	-0.266	< 0.0001
80-120	0.228	0.004	-0.243	0.002	-0.210	0.008

Statistical significance (*p*) of correlation coefficients was calculated based on a modified *t*-test (Dutilleul 1993) which takes the effect of spatial autocorrelation into account within data sets; ns indicates not significant ($p > 0.05$).

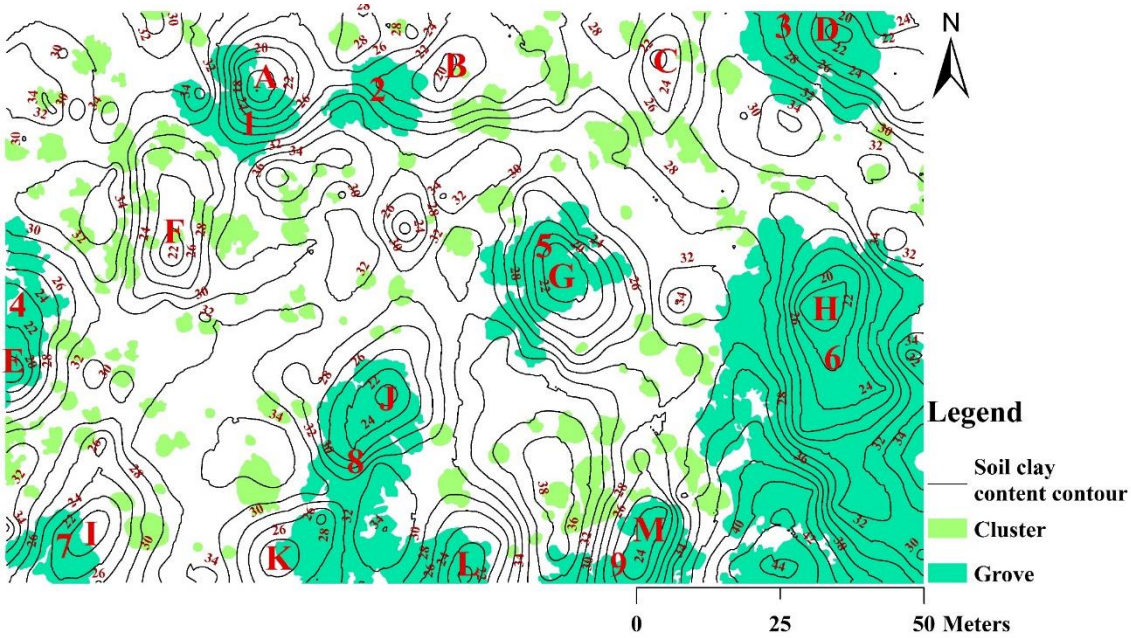

Figure 3.5 Soil clay concentration contours (at 2% intervals) for the 80-120 cm soil layer superimposed on the categorized landscape elements for this 160 m × 100 m landscape in a subtropical savanna. Capital letters indicate locations of non-argillic inclusions.

Spatial distribution of grove vegetation associated with subsurface soil texture

Based on the kriged map of soil clay concentration for the 80-120 cm soil layer, a contour map with 2% intervals was developed to reveal the locations of non-argillic inclusions which were labeled with capitalized letters (Fig. 3.5). This depth was selected because it most clearly delineates the positions of the non-argillic inclusions. Categorized landscape elements were superimposed on the contour map to show the positions of groves in relation to non-argillic inclusions. Generally, each grove exclusively occupied one of these non-argillic inclusions, except grove no. 8 which occupied three coarse-textured inclusions (J, K and L), and may have coalesced from three individual groves (Table 3.4,

Fig. 3.5). No grove was found beyond a non-argillic inclusion (Fig. 3.5). Non-argillic inclusions C and F are still not occupied by groves (Fig. 3.5).

Table 3.4 The status of non-argillic inclusions occupied by groves, and the potential expanding direction of groves.

Sandy inclusions	Corresponding Groves	Status occupied by groves	Potential expanding direction†
A	1	Partially	Northeast; May coalesce with grove No. 2.
B	2	Partially	Northeast ; May coalesce with grove No.1 and other three adjacent large clusters
D	3	Partially	Southeast
E	4	Partially	East or Southeast; May coalesce with several adjacent clusters
G	5	Partially	Southeast
H	6	Completely	Slowly all directions; May coalesce with grove no. 9
I	7	Partially	Northeast
K, J, L	8	Extensively	Slowly all directions
M	9	Extensively	Slowly all directions; may coalesce with several adjacent clusters or grove no.6
C, F	NA	Not occupied	Have the potential to form groves

†Potential expanding direction is developed based on the hypothesis that non-argillic inclusions are susceptible to the establishment /expansion of grove vegetation.

Exact positional correspondences, unoccupied non-argillic inclusions, and spatial correlations between total fine root biomass and soil texture mentioned above all support the hypothesis that spatial heterogeneity of subsurface soil texture drives the distribution of grove vegetation. It appears unlikely that groves modified subsurface soil to form these non-argillic inclusions. If the hypothesis holds true, it implies that non-argillic inclusions

favor the formation of grove vegetation, and the future expansion of grove vegetation may be predictable (Table 3.4). Groves no. 1, 2, 3, 4, 5, and 7 only occupied portions of non-argillic inclusions, and may eventually expand to fill unoccupied portions of these inclusions. Non-argillic inclusions C and F have the potential to form grove vegetation in the future (Fig. 3.5).

Conceptual model of landscape evolution

Second order point pattern analysis showed that the spatial distribution of clusters was random at most detected scales, with marginally aggregated patterns at certain scales (Fig. 3.6a). This marginal aggregation might be ascribed to the exclusion of groves when performing the analysis. If each grove was considered to be formed from one cluster, the spatial pattern of clusters was completely random (Fig. 3.6b). Based on the random distribution of clusters and the spatial association between grove vegetation and non-argillic inclusions, a conceptual model of landscape evolution is proposed (Fig. 3.7). Woody plants, mainly honey mesquite, encroached into grasslands that were once exclusively dominated by C_4 grasses, serving as nurse plants for other woody plants and initiating a process of autogenic succession to form clusters (Fig. 3.7) (Archer 1988). This phase of cluster formation was a completely random and ongoing process. If clusters coincidentally occupied pre-existing non-argillic inclusions, they eventually expanded and coalesced with adjacent clusters that occupied the same inclusion to form groves, and became prominent and persistent features of the landscape (Fig. 3.7). Clusters developing where the argillic horizon was present would ultimately undergo a process of self-thinning and senescence, or become stable landscape elements (Fig. 3.7). Groves, together with

stable clusters, developed within the grassland matrix to form the current landscape (Fig. 3.7). This phase of landscape development was structured by the spatial heterogeneity of subsurface soil texture.

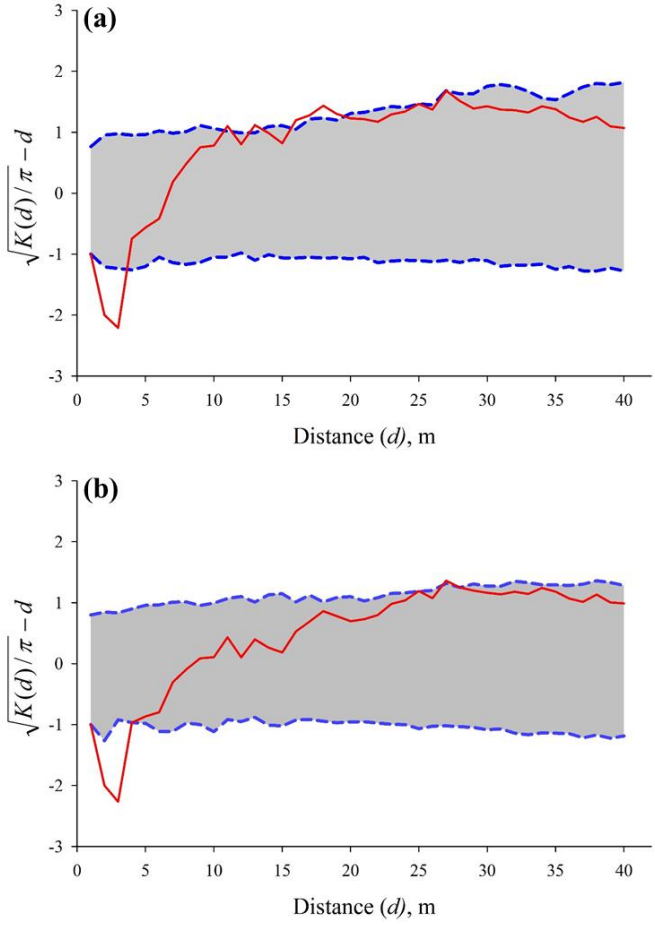

Figure 3.6 Plot of the sample statistic $\sqrt{K}[(d)/\pi]-d$ against distance d reveals the spatial pattern of clusters (a) and woody patches (include clusters and groves) (b) at various scales. The sample statistic was tested based on 1000 randomizations of actual data. Dotted lines show 99% confidence intervals. Values staying within the confidence intervals indicate complete spatial randomness; values above confidence intervals indicate aggregation, while values below signify regularity.

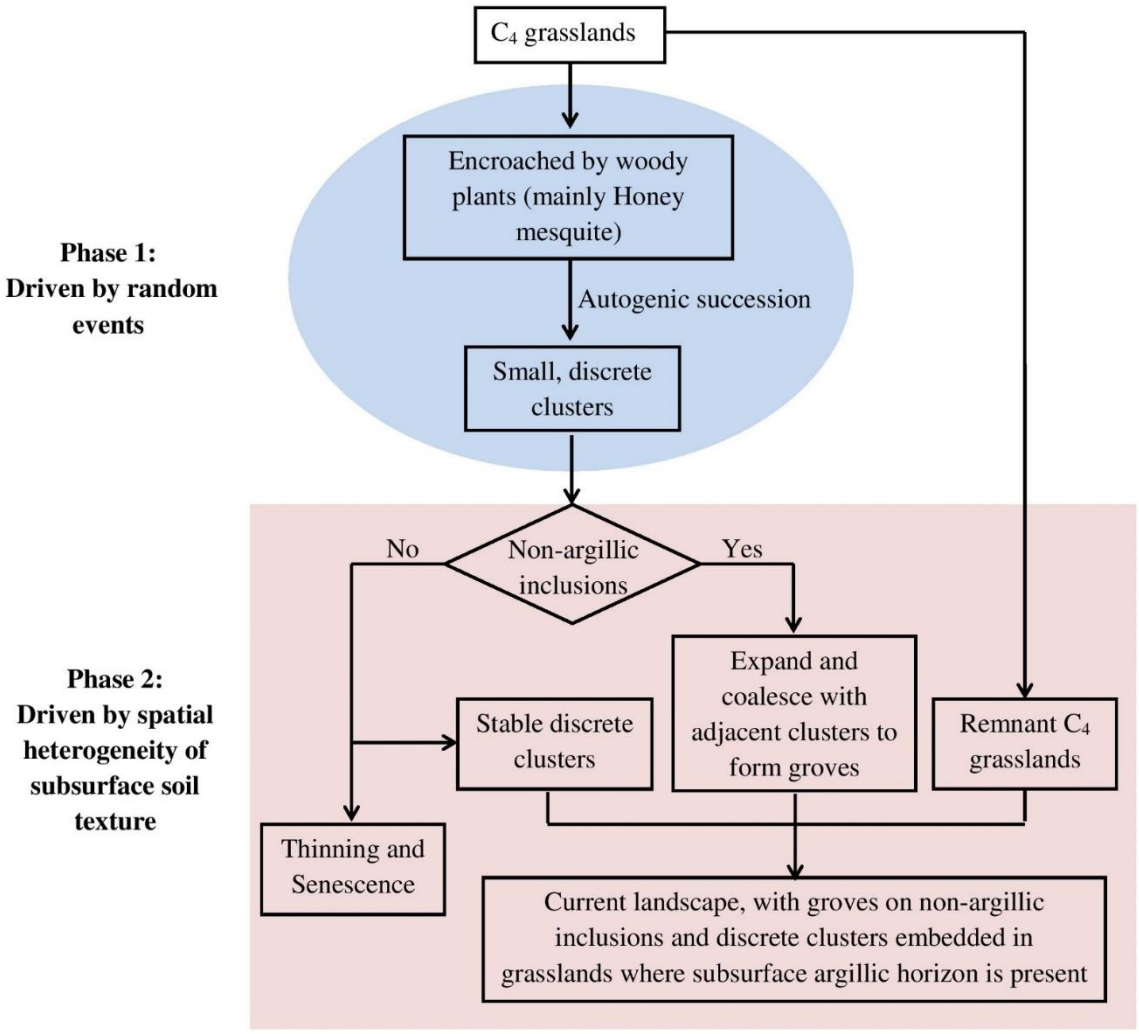

Figure 3.7 A conceptual model of landscape evolution in an upland subtropical savanna ecosystem in southern Texas, USA.

DISCUSSION

Landscape-scale spatial patterns of soil texture throughout the soil profile

Spatial patterns of soil texture in the upper 30 cm of the soil profile were directional, with sand concentration decreasing and silt and clay concentrations increasing

from the north towards the southeastern corner of this landscape (Fig. 3.3). These spatial patterns were consistent with a previous study in the same plot in which soil texture in the upper 15 cm soil layer was examined (Bai *et al.* 2009). The anisotropic distribution of soil texture in the upper portion of the soil profile is likely related to landscape processes that are influenced by elevation, such as runoff and erosion.

Patches that lacked an argillic horizon and had a higher sand concentration were interspersed in a laterally extensive subsurface argillic horizon, particular at depth > 50 cm (Fig. 3.3). The spatial association between grove vegetation and these non-argillic inclusions presented in this study (Fig. 3.5) raised an additional cause-effect question. Did grove vegetation contribute to the formation of non-argillic inclusions? Since the modification of subsurface soil texture by woody plants associated below-ground faunal activities has been reported in other savanna ecosystems (Lobry de Bruyn & Conacher 1990; Konaté *et al.* 1999; Turner *et al.* 2006), it's reasonable to hypothesize that extensively observed rodent (pack rat, *Neotoma micropus*) and leaf-cutter ant (*Atta texensis*) burrowing and excavating activities confined to grove vegetation in this study area (Loomis 1989; Archer 1995; Liu *et al.* 2011) could have the potential to disrupt and obliterate a once continuous argillic soil horizon to form these non-argillic inclusions. If this assumption is correct, (1) soil clay concentration beneath grove vegetation in the upper soil layers should be significantly higher than non-grove soils due to faunal uplift-translocating activities, and (2) total clay concentration, when summed across the soil profile, should be comparable between grove and non-grove soils. However, no significant differences were detected in soil clay concentration between grove and non-grove soils in

the upper 30 cm of soils (Table 3.2). Furthermore, soil cores at the center of groves were coarser-textured throughout the entire profile, and total clay concentration to a depth of 1.2 meters was significantly lower than in soil cores beyond grove boundaries (data not shown). These lines of evidence suggest the hypothesis that grove vegetation is responsible for the formation of non-argillic inclusions is not tenable.

Alternatively, non-argillic inclusions are pre-existing and intrinsic features of this landscape. If this is true, there should be non-argillic inclusions which, by chance, have not yet been occupied by grove vegetation. In fact, across this landscape, two such inclusions have been mapped (labelled as C and F, Fig. 3.5), and stable carbon isotopic analysis excluded the possibility that these two inclusions have ever been occupied by C_3 woody plants. Therefore, it seems likely that the spatial heterogeneity of subsurface soil texture was generated pedogenically (i.e. fluvial or aeolian depositional processes, Loomis 1989) prior to the recent vegetation changes that have transformed this landscape.

Spatial heterogeneity of subsurface soil texture drives the distribution of grove vegetation

Previous results from space-for time substitution models (Archer 1995), modelling studies of vegetation structure (Stokes 1999) and spatial patterns of soil $\delta^{13}C$ (Bai *et al.* 2012) indicated that as new clusters were initiated by the encroachment of honey mesquite trees and existing clusters expanded, coalescence would occur to form groves where the argillic horizon was absent. Although the role of the non-argillic inclusions in grove formation has been recognized and documented (Loomis 1989; Watts

1993; Archer 1995), the distribution and abundance of these non-argillic inclusions has not been quantified at the landscape scale.

The landscape-scale 3-dimensional distribution of soil texture developed in this study provides additional direct evidence for the essential role that pre-existing non-argillic inclusions play in regulating the distribution of grove vegetation. In this study, we found that groves occurred only within non-argillic inclusions (Fig. 3.5). Based on the results of this study and previous findings (Archer 1988; Loomis 1989; Watts 1993; Archer 1995; Stokes 1999; Bai *et al.* 2012), we presented a conceptual model that recognized the spatial heterogeneity of subsurface soil texture as a factor in vegetation change at the landscape scale (Fig. 3.7). The spatial distribution of existing clusters across this landscape was random, suggesting that the formation of clusters is entirely determined by the dispersion of honey mesquite seeds via animals, and their germination and establishment can occur on a wide range of soil conditions across this landscape, regardless of the subtle spatial heterogeneity of subsurface soil texture. However, clusters that coincidently developed on non-argillic inclusions likely experienced more favorable growth conditions on these coarser-textured soils, and expanded laterally and ultimately fused with other clusters to form groves. In this study, we found that fine root biomass of woody plants beneath groves was significantly higher than beneath clusters in the 50 - 80 and 80 - 120 cm depth increments (Table 3.2), and total fine root biomass was significantly and positively correlated with soil sand concentration in the 30-50, 50-80, and 80-120 cm depth increments (Table 3.3). This suggests that coarse-textured subsoils may benefit the growth of woody plants by enabling root penetration deeper into the profile, providing

them greater access to water and nutrients that are less accessible on those portions of the landscape where the argillic horizon is present. As woody plants communities develop within the non-argillic inclusions, they may also trigger a positive feedback loop by increasing soil nutrient pool sizes and turnover rates (i.e. islands of fertility), which could further stimulate growth, recruitment, and survival of woody species (Schlesinger *et al.* 1996; Scholes & Archer, 1997; Boutton *et al*. 1999; McCulley *et al*. 2004a and 2004b). In fact, honey mesquite trees on non-argillic inclusions were larger and older than their counterparts growing on subsoils with an argillic horizon (Archer 1995; Boutton *et al.* 1998), and total tree and shrub basal areas were 2.5 times more in groves than in clusters (Liu *et al.* 2010), reflecting enhanced woody plant growth and production on coarser-textured subsoils. In contrast, clusters that occur on soils with an argillic horizon are constrained in their expansion rates (Fig. 3.5). In this study, 121 clusters were observed, with an average size of 13.4 m^2, and 80% of them are less than 20 m^2. This may suggest that clusters, compared to groves, are unable to expand beyond a certain size across this landscape. As such, the current landscape is comprised of groves on non-argillic inclusions as large and relatively long-lived features, and comparatively transient and size-constrained clusters dispersed among the remnant C_4 grasslands where the argillic horizon is present (Fig. 3.7).

Although spatial heterogeneity of subsurface soil texture appears to function as a key determinant for the distribution of grove vegetation across this landscape, other factors, including plant-soil interactions and topography, should be considered in the expansion of grove vegetation. Once groves extensively or even completely occupy these

easily colonized non-argillic inclusions and encounter resistance from the argillic soils that surround them, their expansion rates may be reduced. However, these groves may continue to play an active role in recruitment of woody plants around their canopy edges (even where the argillic horizon is present) by altering surficial soils and microclimate in ways that enhance the survival probability of these woody recruits. Areas at (or even beyond) canopy edges of groves may experience some degree of soil nutrient enrichment through leaf litter deposition, horizontal root extension (Watts 1993; Boutton *et al.* 2009; Bai *et al.* 2012), and/or potential transfer of N fixed by honey mesquite (Soper *et al.* 2015; Zhang *et al.* 2016). In addition, improved water regimes through water uptake and redistribution (Zou *et al.* 2005; Miller *et al.* 2010), and reduced light levels and temperature extremes (Archer 1995; Scholes & Archer 1997) likely characterize the edges of groves. These environmental modifications near grove edges may collectively override the limitations of the argillic horizon and facilitate the recruitment of woody plants. An example of such a case is grove no. 8. Apparently, grove no. 8 coalesced from three individual groves that once occupied each of these non-argillic inclusions (J, K, and L), and expanded beyond these inclusions (Fig. 3.2 and 3.5).

Implications for future landscape evolution

Mapped non-argillic inclusions across this landscape and the fact that subsurface coarse-textured soils favor the development of grove vegetation may provide a glimpse of the future landscape evolution. Some of the current groves occupy only a portion of the non-argillic inclusions on which they occur, and therefore have the potential to expand into unoccupied portions of these inclusions. As these groves expand, they have the

potential to coalesce with adjacent groves or stable clusters (Table 3.4). For example, grove 2 and three adjacent large clusters will likely expand towards the center of the sandy inclusion B, and coalesce to form an even larger grove (Fig. 3.5). Groves 1 and 2 are both actively expanding towards the northeast to colonize the remainder of their sandy inclusions, and will likely coalesce (Fig. 3.5). This prediction is consistent with a previous study in which spatial patterns of soil $\delta^{13}C$ and chronosequences of aerial photographs were used to infer vegetation dynamics in the same plot (Bai *et al.* 2009). Several large clusters have been established around unoccupied non-argillic inclusions C and F (Fig. 3.5); with time, they may expand and eventually coalesce to form grove vegetation. Groves that have extensively or even completely occupied entire non-argillic inclusions are still active in expansion due to the positive feedbacks from plant-soil interactions as mentioned above. However, more accurate predictions of the future rate and direction of grove expansion for this landscape will require detailed information about the subsurface soil texture-rainfall-topography relationships and plant-soil interactions (Wu & Archer 2005).

Based on forward simulation using transition probabilities, Archer (1995) concluded that the present vegetation configuration in this subtropical savanna is an intermediate stage in the conversion of grassland to closed-canopy woodland, and this conversion will be completed within the next 180 years. Our study also suggests that the present landscape still has the capacity for further woody plant expansion. Without major disturbances (i.e. fire, drought, and insect outbreak), current coverage of grove vegetation (27.3%) may be doubled through the expansion of existing groves and the formation of

new groves on unoccupied portions of these non-argillic inclusions. Furthermore, based on historical aerial photographs, cluster coverage for this study plot increased from 4.3 % in 1930 to current coverage of 10.3%, indicating that cluster formation is an ongoing process. Taken together, these patterns suggest the present landscape is likely to evolve to a closed-canopy woodland configuration in the future.

CONCLUSIONS

In savanna ecosystems, vegetation patchiness is a key regulator of ecosystem functions and services. However, the mechanisms responsible for the distribution of woody patches in savanna landscapes remain unclear. In this study, landscape-scale kriged maps of soil texture derived from spatially-specific soil samples taken to a depth of 1.2 m allowed us to reveal the spatial heterogeneity in subsurface soil texture (particularly the presence and location of non-argillic inclusions) as an intrinsic feature of this landscape. Exact positional correspondences between mapped non-argillic inclusions and the distribution of grove vegetation, and spatially correlated relationships between total fine root biomass and soil texture, collectively suggest that the spatial heterogeneity in subsurface soil texture functioned as a dominant factor driving the formation and distribution of grove vegetation. Based on inferences from previous studies and this study, a conceptual model was proposed to explain the evolution of current landscape. The establishment of clusters is a random ongoing process which largely depends on the seedling recruitment of woody plants, while the formation of groves appears to be strongly regulated by the spatial heterogeneity of subsurface soil texture. Since coarser-textured non-argillic inclusions enable the formation of grove vegetation, future landscape

development is predicted based on kriged maps of soil texture. Without major disturbances, current woody cover may double as these mapped non-argillic inclusions are completely occupied by grove vegetation, and this landscape may have the potential to develop into canopy-closed woodlands in the future. We suggest that spatial heterogeneity of subsurface soil properties (i.e. soil texture, water regimes, and nutrient status) should be considered in the study of savanna ecology since these heterogeneities could shape the spatial patterns of woody vegetation which strongly determine savanna ecosystem services and function.

CHAPTER IV

ROOTING STRATEGIES IN A SUBTROPICAL SAVANNA: A LANDSCAPE-SCALE THREE-DIMENSIONAL ASSESSMENT*

SYNOPSIS

In resource-limited savannas, the distribution and abundance of fine roots play an important role in acquiring essential resources and structuring vegetation patterns and dynamics. However, little is known regarding the three-dimensional distribution of fine roots in savanna ecosystems at the landscape scale. We quantified spatial patterns of fine root density to a depth of 1.2 m in a subtropical savanna landscape using spatially specific sampling. Kriged maps revealed that fine root density was highest at the centers of woody patches, decreased towards the canopy edges, and reached lowest values within the grassland matrix throughout the entire soil profile. Lacunarity analyses indicated that spatial heterogeneities of fine root density decreased continuously to a depth of 50 cm and then increased in deeper portions of the soil profile across this landscape. This vertical pattern might be related to inherent differences in root distribution between trees/shrubs and herbaceous species, and the presence/absence of an argillic horizon across this landscape. The greater density of fine roots beneath woody patches in both upper and lower portions of the soil profile suggests an ability to acquire disproportionately more

---

* Originally published as: Zhou, Y., Boutton, T.W., Wu, X.B., Wright, C.L. & Dion, A.L. (2018) Rooting strategies in a subtropical savanna: A landscape-scale three-dimensional assessment. *Oecologia*, doi: org/10.1007/s00442-018-4083-9. In press. The publication is available at: https://link.springer.com/article/10.1007%2Fs00442-018-4083-9.

resources than herbaceous species, which may facilitate the development and persistence of woody patches across this landscape.

INTRODUCTION

Savanna ecologists have long been interested in root distribution patterns, and have invoked niche partitioning to explain the mechanisms that permit co-existence of growth-form divergent trees and grasses (Walter 1971). It is well recognized that the characterization of root distribution in savannas is relevant not only for explaining species co-existence and community dynamics (Walter 1971; February & Higgins 2010; Holdo 2013; Kambatuku *et al.* 2013), but also for understanding the hydrology and biogeochemistry of these ecosystems (Oliveira *et al.* 2005; Boutton *et al.* 2009b), and anticipating the responses of savannas to potential changes in rainfall regimes associated with climate change (Kulmatiski & Beard 2013). Previous studies leave little doubt that the size and shape of root systems differ between woody and herbaceous species in savanna ecosystems (Jackson *et al.* 1996; Schenk 2006). Compared to grasses that have comparatively shallow and laterally constrained root systems, trees/shrubs generally have deeper root systems with significant lateral extent (Schenk 2006). This difference in size and structure could potentially enable trees/shrubs to acquire disproportionately more resources, conferring a competitive advantage relative to grasses (Schwinning & Weiner 1998; Rajaniemi 2003; Schenk 2006; DeMalach *et al.* 2016), and facilitating their development and persistence. However, the question remains whether and to what extent this size-asymmetric advantage might change throughout the soil profile.

Fine roots (< 2 mm) are extremely important functional components of plants, as they not only acquire essential resources from highly heterogeneous soils (Pregitzer 2002), but also provide a pathway for carbon and energy transfer from plants to soils (Matamala *et al.* 2003). Exceptionally high spatial heterogeneity in soil resources is an intrinsic feature of arid and semiarid ecosystems (including many savannas, Schlesinger *et al.* 1996) that can structure and constrain the growth and elongation of fine roots (Caldwell *et al.* 1996; Hodge 2004; Loiola *et al.* 2016), making it more difficult to quantitatively assess fine root distribution based on non-spatial sampling approaches. Therefore, quantifying fine root distribution in a spatially specific manner in savannas could provide critical insights towards understanding plant functional strategies for soil resource acquisition and also soil biogeochemical processes that are related to fine root turnover. Despite this, most empirical and modeling studies on root distribution patterns in savannas have been confined to the individual tree or woody patch scale (e.g. Hipondoka & Versfeld 2006; Koteen *et al.* 2015; O'Donnell *et al.* 2015), and have not been spatially explicit at the landscape scale. There is increasing recognition of the fundamental need for the application of landscape-scale quantitative spatial analyses to enhance our understanding of community and ecosystem processes in savannas (Jackson & Caldwell 1993; Bai *et al.* 2009; Liu *et al*. 2011; Mudrak *et al.* 2014; Zhou *et al.* 2017a). Landscape scale topoedaphic drivers could interact with the size, species composition, and distribution of woody patches to affect patterns of spatial heterogeneity of fine root distribution throughout the soil profile in savannas, though this has not been explicitly investigated.

To address this, we quantified landscape-scale three-dimensional fine root distribution patterns in a subtropical savanna by spatially-explicit soil sampling to a depth of 1.2 meters across a 160 m × 100 m landscape. This landscape, consisting of different sizes of woody patches interspersed within a grassland matrix, is uniform with respect to topographic features (e.g. slope, aspect, elevation, and exposure) and land use history, but varies with respect to subsurface soil texture with non-argillic inclusions embedded within an otherwise continuous argillic horizon (Archer 1995; Zhou *et al.* 2018). Therefore, in this study, we examined how landscape scale patterns of spatial heterogeneity in fine root density change throughout the soil profile. We hypothesized that landscape scale fine root distribution would be primarily controlled by (i) the spatial distribution of woody vs herbaceous vegetation, and (ii) edaphic heterogeneity related to the presence/absence of a subsurface argillic horizon.

MATERIALS AND METHODS

Study site

Research was conducted at the Texas A&M AgriLife La Copita Research Area (27˚40′ N, 98˚12′ W) in the Rio Grande Plains, Texas, USA. Climate is subtropical, with a mean annual temperature of 22.4 ˚C and mean annual precipitation of 680 mm. Although rainfall generally peaks in May and September, there are no distinct dry and wet seasons in this study site. In 2014, the cumulative rainfall from January to June prior to the sampling time (i.e. July) was 48% less than the 30-year average due to a dry winter. However, at the beginning of the growing season in May 2014, the study site received approximately 47% more rainfall than the 30-year average. Topography consists of gently

sloping (1- 3%) uplands, surrounded by lower-lying ephemeral drainages and playas. Elevation ranges from 75 to 90 m above sea level across the entire research station. This site was continuously grazed by cattle from the late 1800s until it became a research area in 1984 (Scifres & Koerth 1987). The portion of the La Copita Research Area where our research was conducted has not been grazed since 2000.

This study was conducted on an upland portion of the landscape where soils are sandy loams (Typic and Pachic Argiustolls) derived from the Goliad formation (NRCS 1979) and characterized by a nearly continuous argillic (Bt) horizon with non-argillic inclusions distributed randomly across the landscape (Zhou *et al*. 2017b). Multiple lines of evidence (i.e. tree ring analysis, historical aerial photographs, and coupled $\delta^{13}C$-^{14}C analyses of soil organic matter) show that uplands were once almost exclusively dominated by C_4 grasses, and woody encroachment into grasslands has occurred during the past century (Archer *et al*. 1988; Archer 1995; Boutton *et al.* 1999). Woody encroachment is initiated by the colonization of N_2-fixing honey mesquite (*Prosopis glandulosa*) trees, which serve as nurse plants that facilitate the establishment of other understory tree/shrub species to form discrete woody clusters (< 100 m^2) (Archer *et al.* 1988). Discrete clusters occupying non-argillic inclusions expand laterally and often coalesce to form large groves (> 100 m^2) (Archer 1995; Bai *et al.* 2012; Zhou *et al*. 2017b). Current vegetation structure on uplands of this study site has a two-phase pattern (Whittaker *et al.* 1979), with discrete woody clusters and groves embedded within a nearly continuous grassland matrix. Common understory shrub/tree species in clusters and groves include *Zanthoxylum fagara*, *Schaefferia cuneifolia*, *Celtis pallida,* and *Zizyphus*

obtusifolia. In the herbaceous matrix, dominant C_4 grasses include *Paspalum setaceum*, *Setaria geniculata*, *Bouteloua rigidiseta* and *Chloris cucullata*, and dominant C_3 forbs include *Croton texensis*, *Wedelia texana*, *Ambrosia confertiflora*, and *Parthenium hysterophorus* (Boutton *et al.* 1998).

Field sampling & lab analyses

A 160 m × 100 m landscape consisting of three landscape elements (grasslands, clusters, and groves) was established on an upland in January 2002 (Fig. 4.1a) (Bai *et al.* 2009; Liu *et al.* 2011). Elevations within this sample area were measured directly by terrain surveying, GIS, and kriging interpolation (Bai *et al.* 2009). The highest elevation within plot is the northeast corner (90.67 m) and the lowest is the southwest corner (87.93 m), resulting in a gentle northeast to southwest slope of 1.4%. A color-infrared aerial photograph (6 cm x 6 cm resolution) of this landscape was acquired in July 2015.

The 160 m × 100 m landscape was subdivided into 10 m × 10 m grid cells, and the corners of each grid cell were georeferenced based on UTM coordinates system (14 North, WGS 1984). Within each grid cell, two randomly located sampling points were selected in July 2014 (320 points in total) (Fig. 4.1a). The distances from each sampling point to two georeferenced cell corners were recorded to calculate the exact location of each sampling point. The landscape element present at each sampling point was classified as grassland, cluster, or grove. Clusters were distinguished from groves based on their canopy area, as described above. At each sampling point, two adjacent soil cores (2.8 cm in diameter × 120 cm in length) were collected using a PN150 JMC Environmentalist's Subsoil Probe (Clements Associates Inc., Newton, IA, USA).

Immediately after sampling, each soil core was subdivided into six depth increments (0-5, 5-15, 5-30, 30-50, 50-80, and 80-120 cm). One soil core was oven-dried (105 ˚C for 48 hours) to determine soil bulk density, and the other was air-dried and passed a 2 mm sieve prior to subsequent analysis of soil texture by the hydrometer method. To estimate root biomass, the oven-dried soil samples were soaked in water and gently washed via low-pressure spray through two sieves: a 0.5 mm mesh followed by a 0.25 mm mesh. Roots extracted on the 0.5 mm mesh were picked out manually and sorted into fine roots (< 2mm) and coarse roots (> 2 mm). Soils and roots that passed the 0.5 mm mesh but were retained on the 0.25 mm mesh were transferred to a shallow tray, and water was run cautiously to separate the remaining roots from soils by flotation. Roots retrieved by flotation were added to fine root category. No attempt was made to distinguish between live or dead roots. All roots samples were oven-dried (65 ˚C) to constant weight for biomass determination.

Data analysis

To facilitate comparisons between the unequal sampling depth intervals, fine root density was expressed in units of kg m^{-3}. The Normalized Difference Vegetation Index (NDVI) was calculated as (NIR-RED)/(NIR+RED), in which NIR and RED represent the spectral reflectance measurements from the near-infrared and the red regions, respectively, of the aerial photograph. Areas covered by woody plants have significantly higher NDVI values compared to grassland/bare soil areas. Pearson correlation coefficients between fine root density, NDVI, soil bulk density, soil sand, silt and clay content within each depth increment were determined using R statistical software (R Development Core Team

2014). A modified t-test (Dutilleul 1993) which accounts for the effects of spatial autocorrelation was used to determine the significance levels of these correlation coefficients. For all these statistical analyses, p value < 0.05 was used as a cutoff for statistical significance.

Ordinary kriging was used for spatial interpolation based on values of 320 random sampling points within each depth increment and their spatial structure determined by fitting variogram models. Kriged maps of fine root density for each depth increment with a 0.5 m × 0.5 m resolution were generated in ArcGIS 10.2.2 (ESRI, Redlands, CA, USA). Lacunarity analysis, a scale-dependent measurement of spatial heterogeneity or the "gappiness" of a landscape structure (Plotnick *et al.* 1996), was used to assess changes in spatial heterogeneity of fine root density throughout the soil profile. Briefly, a gliding box algorithm at seven different spatial scales with corresponding box sizes (side length of the gliding box, r) of 0.5, 1, 2, 4, 8, 16, and 32 m was used to determine the lacunarity value of each kriged map. The gliding box of a given size (r) was first placed at one corner of the kriged map, and the "box mass" S(r), the sum of fine root density of the pixels within the box, was determined. Then the box was systematically moved through the map one pixel at a time and the box mass was recorded at each location. The lacunarity was calculated according to:

$$\Lambda(r) = \frac{Var\left(S(r)\right)}{E^2\left(S(r)\right)} + 1$$

where E(S(r)) is the mean and Var(S(r)) is the variance of the box mass S(r) for given box size r. All calculations were performed using R statistical software (R Development Core Team 2014). The lacunarity curve, natural log-transformed lacunarity $\Lambda(r)$ against box size

(r), was plotted to quantify the spatial heterogeneity of fine root distribution at different scales throughout the soil prolife, with a higher value of lacunarity indicating a more heterogeneous distribution pattern.

To more clearly evaluate and describe variation in root densities within woody patches vs. grasslands, edges of woody patches were delineated in the aerial photograph using ArcGIS 10.2.2. The distance from each sampling point to the nearest woody patch edge was calculated. Sampling points located within woody patches were assigned positive values; hence, large values indicated that sampling points were away from woody patch edges and near the centers of woody patches. In contrast, sampling points within the grassland matrix were assigned negative values. Thus, more negative values indicate sampling points were farther away from woody patch edges.

RESULTS

Since woody patches (both clusters and groves) had significantly higher fine root densities than grasslands throughout the entire soil profile (Table 4.1), spatial patterns of fine root density for each depth increment displayed a strong resemblance to that of vegetation pattern, especially the distribution of grove vegetation (Fig. 4.1). Fine root density was highest at the centers of woody patches, decreased towards the canopy edges, and reached lowest values in the grassland matrix (Fig. 4.1). This spatial trend was statistically supported by the significantly positive correlations between fine root density and distance from each sampling point to the nearest woody patch edge throughout the soil profile (Fig. 4.2).

Quantitatively, lacunarity analysis indicated that spatial heterogeneities of fine root density were significantly higher in the upper and lower soil depth increments (i.e. 0-5, 5-15, and 80-120 cm) than in the intermediate depth increments (i.e. 15-30, 30-50, and 50-80 cm) (Fig. 4.3). The variabilities of fine root density based on coefficient of variation (CV) across this landscape decreased with soil depth and then increased in the two deepest increments (CVs from top to bottom throughout the soil profile = 71.34%, 62.8%, 53.27%, 48.48%, 54.26%, and 68.26%). The ratios of fine root densities between woody patch and grassland were also higher in the upper and lower soil depth increments than in the intermediate depth increments (ratios throughout the soil profile from top to bottom = 2.93, 2.56, 2.09, 1.81, 1.89, and 2.23) (Fig. 4.4, Table 4.1).

Table 4.1 Mean and standard error (SE) of fine root density (kg m^{-3}) in contrasting landscape elements (cluster, grove, and grassland), and fine root density ratios of woody patch to grassland throughout the soil profile in a subtropical savanna landscape.

Soil depth (cm)	Cluster		Grove		Grassland		Ratio
	Mean	SE	Mean	SE	Mean	SE	Woody patch: Grassland
0-5	10.12^{a}	0.43	10.20^{a}	0.31	3.47^{b}	0.20	2.93
5-15	5.36^{a}	0.21	5.74^{a}	0.15	2.17^{b}	0.10	2.56
15-30	2.74^{a}	0.11	3.08^{a}	0.08	1.39^{c}	0.05	2.09
30-50	1.76^{a}	0.08	1.90^{a}	0.06	1.01^{b}	0.04	1.81
50-80	0.88^{b}	0.05	1.09^{a}	0.03	0.52^{c}	0.02	1.89
80-120	0.56^{b}	0.04	0.78^{a}	0.03	0.30^{c}	0.02	2.23

Significant differences ($p < 0.05$) between means in landscape elements are indicated with different superscript letters. Number of samples: cluster = 41, grove = 79, grassland = 200.

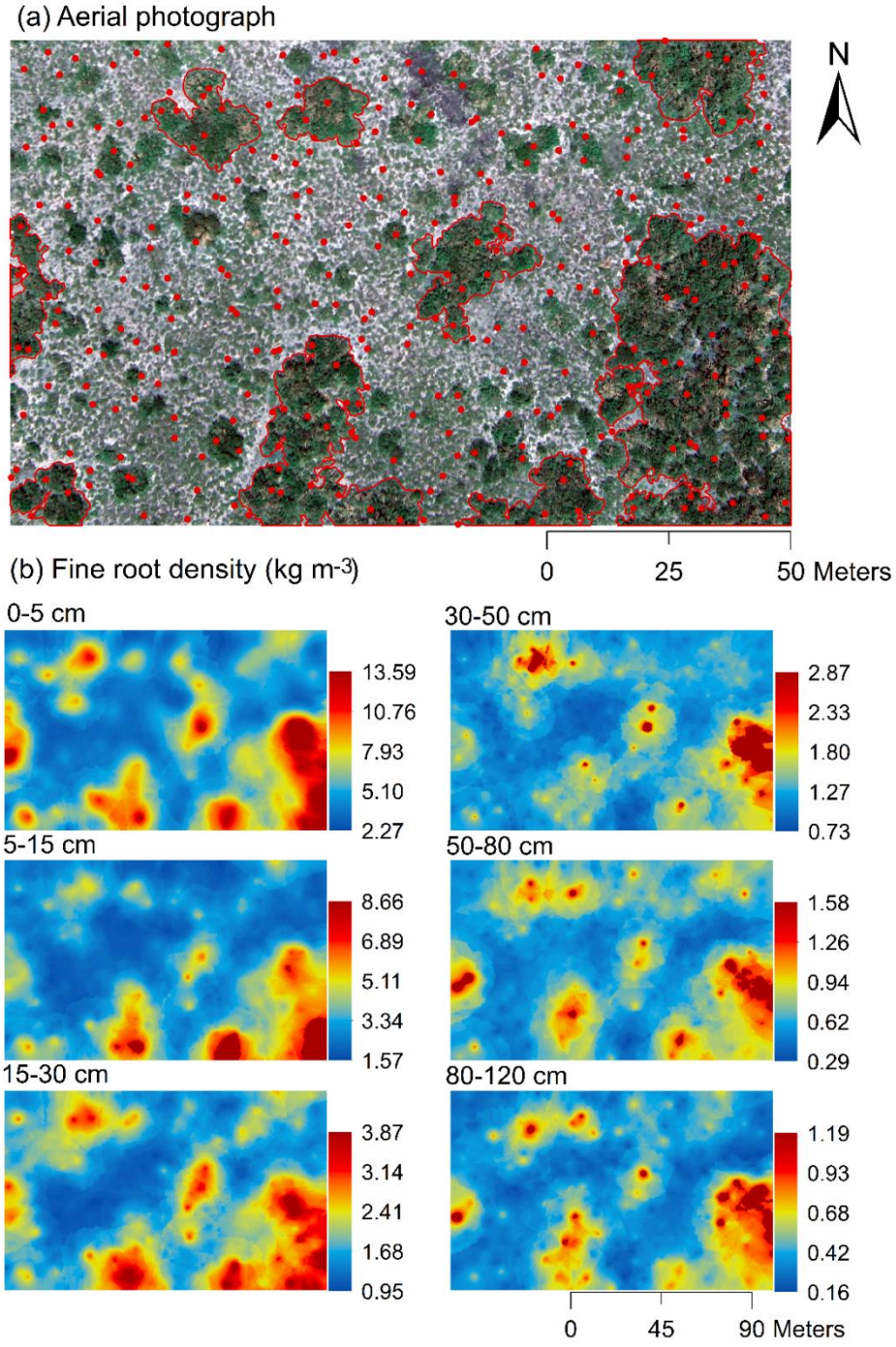

Figure 4.1 (a) Aerial photograph of the 160 m × 100 m study area. Red dots indicate 320 random soil sampling points and red lines indicate the edge of groves. Dark green patches are shrub clusters and groves, while light grey color indicates open grassland. (b) Kriged maps of fine root density (kg m^{-3}) throughout the soil profile based on 320 random soil sampling points.

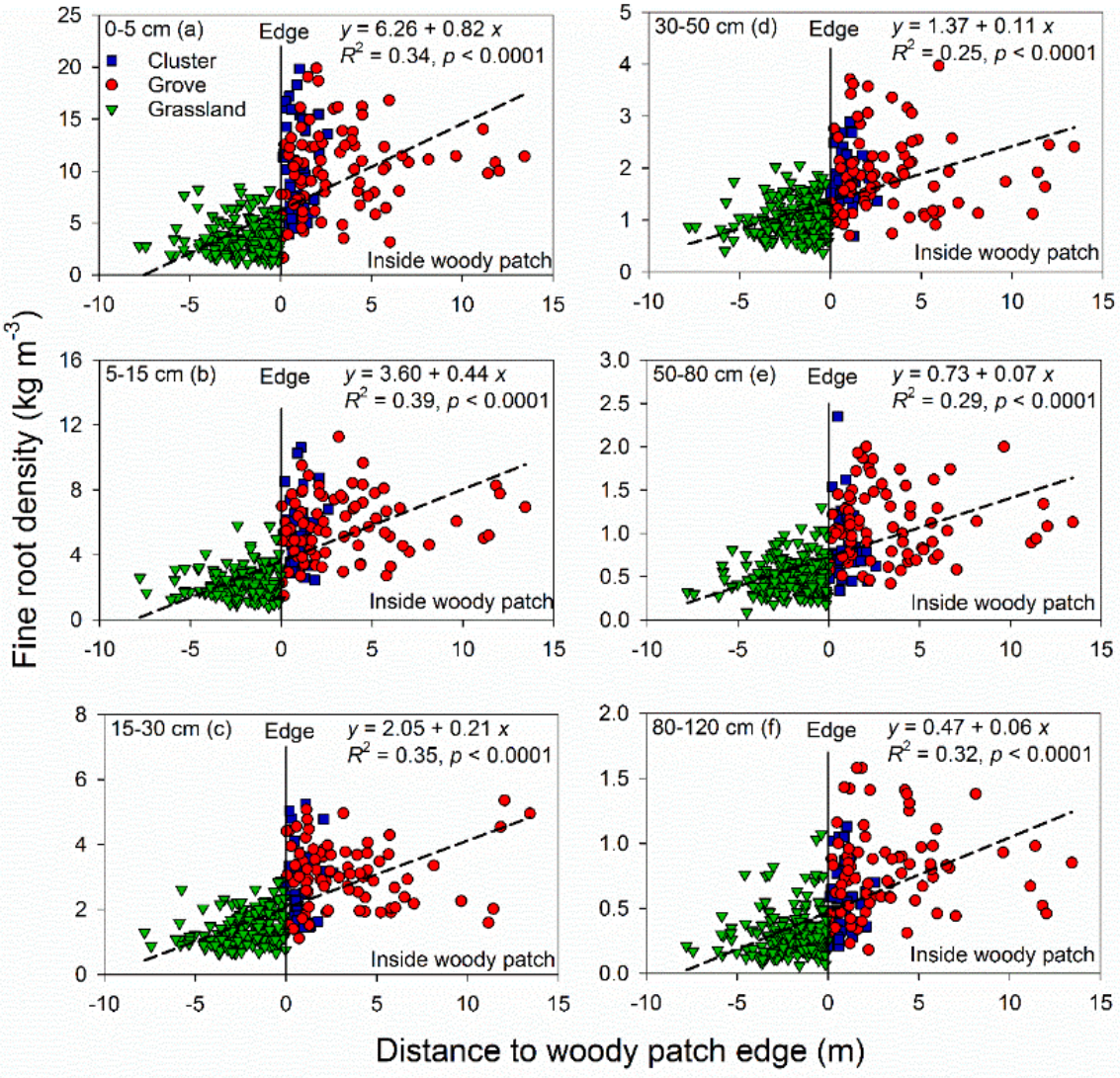

Figure 4.2 Relationships between fine root density (kg m^{-3}) and distance of each sampling point to the nearest woody patch edge (m) for 0–5, 5–15, 15–30, 30–50, 50–80, and 80–120 cm throughout the soil profile. Positive distances indicate that sampling points are within woody patches, whereas negative distances indicate that sampling points are within the grassland matrix. Please note that the scale on y-axis is different throughout the soil profile. Number of samples: grassland = 200 (triangles), grove = 79 (circles), and cluster = 41 (squares).

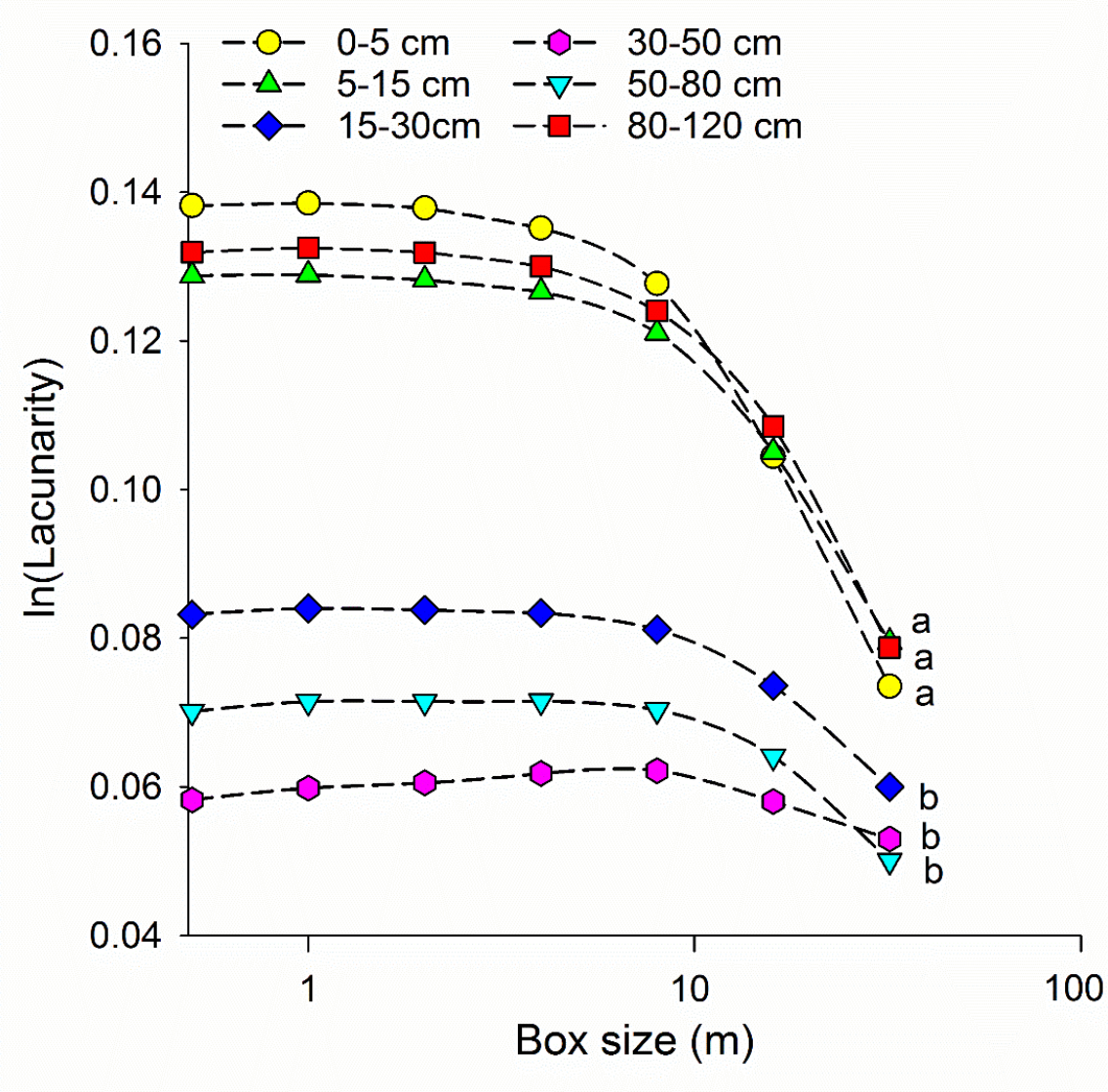

Figure 4.3 Lacunarity curves calculated based on kriged maps of fine root density throughout the soil profile. Significant differences ($p < 0.05$) were detected based on a paired Student's t test and indicated with different letters.

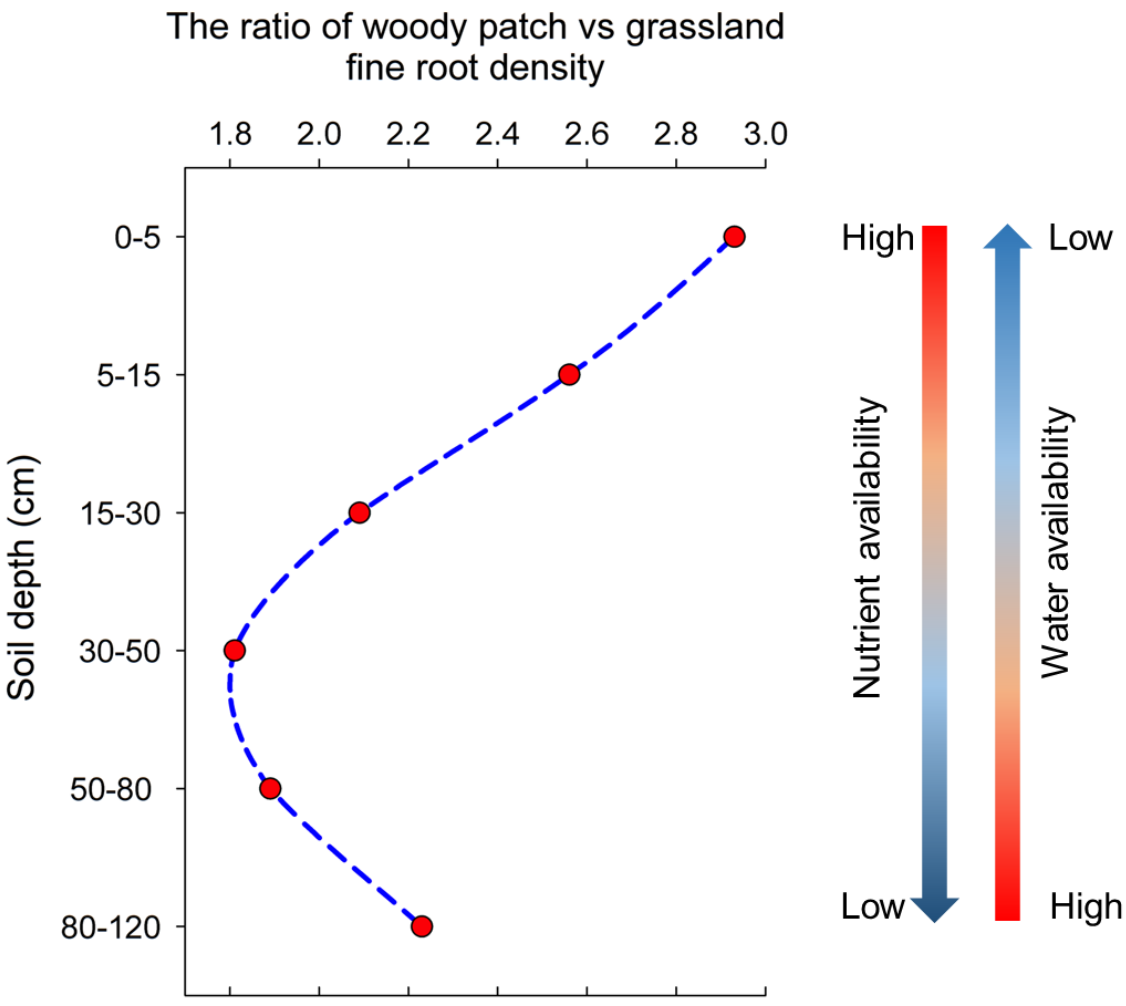

Figure 4.4 Changes in the ratio of woody patch vs. grassland fine root density throughout the soil profile.

Fine root density was significantly and positively correlated with NDVI throughout the entire soil profile (Table 4.2). In addition, fine root density was significantly and positively correlated with soil sand content and negatively correlated with clay content, but only at depths > 30 cm below the soil surface where the argillic horizon starts to form across this landscape (Table 4.2).

Table 4.2 Pearson correlation coefficients (*r*) for fine root density (kg m^{-3}) to NDVI, soil bulk density (g cm^{-3}) (SBD), soil sand (%), silt (%), and clay (%) contents throughout the soil profile.

Depth (cm)	NDVI	SBD	Sand	Silt	Clay
0-5	0.41^{***}	-0.66^{***}	-0.14^{ns}	0.19^{ns}	0.08^{ns}
5-15	0.41^{***}	-0.59^{***}	-0.22^{ns}	0.38^{**}	0.08^{ns}
15-30	0.36^{***}	-0.15^{*}	-0.11^{ns}	0.25^{*}	0.02^{ns}
30-50	0.36^{***}	-0.02^{ns}	0.19^{**}	0.04^{ns}	-0.23^{***}
50-80	0.36^{***}	-0.25^{***}	0.31^{***}	-0.07^{ns}	-0.34^{***}
80-120	0.34^{***}	-0.26^{***}	0.20^{**}	-0.18^{*}	-0.19^{**}

Statistical significance of correlation coefficients was calculated based on a modified *t*-test (Dutilleul, 1993) which takes the effect of spatial autocorrelation into account within data sets. $^{*} = p < 0.05$, $^{**} = p < 0.01$, $^{***} = p < 0.001$, $^{ns} = p > 0.05$.

DISCUSSION

The three-dimensional spatial patterns of fine root distribution and the factors that determine them have the potential to influence plant water and nutrient acquisition, pool sizes and turnover rates of key limiting nutrients (e.g., N, P), and, ultimately, the spatial structure of aboveground vegetation. As expected, fine root densities were significantly higher beneath woody patches than beneath grasslands throughout the entire profile (Table 4.1, Fig. 4.1). This is consistent with prior studies at this site (e.g. Boutton *et al.* 1999),

and with comprehensive literature reviews on root distribution patterns (Jackson *et al.* 1996; Schenk 2006). The resemblance between spatial patterns of fine root density and the spatial distribution of woody patches, and positive correlations between fine root density and NDVI throughout the entire soil profile, suggest that vegetation patterns were the primary factor driving fine root distribution across this landscape (Fig. 4.1 and Table 4.2). Fine root densities within each depth increment throughout the profile were highest near the centers of woody patches, especially for grove vegetation, decreased towards canopy edges, and reached the lowest in the grassland matrix (Fig. 4.1 and 4.2). In a California oak savanna, Koteen *et al.* (2015) also reported this center-to-edge spatial variability in fine root biomass, and such variability was more pronounced with large trees or woody patches.

Although fine root density was significantly higher beneath small woody clusters compared to grasslands throughout the 1.2 m profile (Table 4.1), these differences were generally not evident in the kriged maps. The size of woody clusters across this landscape ranged from 1.3 to 78.7 m^2, with an average of 13.4 m^2 (n =121) (Zhou *et al.* 2017b). In contrast, two randomly sampling points were selected in each 10 m × 10 m grid cell. Therefore, this inability to clearly resolve cluster vs. grassland differences in the kriged maps is attributable to our sampling intensity that could not detect this finer-scale spatial variability in this complex landscape (Liu *et al.* 2011).

Lacunarity analyses indicated that landscape-scale patterns of spatial heterogeneity in fine root density was relatively high in the surface soil (0-5 and 5-15 cm), decreased in the middle of the profile (15-80 cm), but then increased again in deeper

portions (80-120 cm) of the soil profile (Fig. 4.3). These depth distribution patterns may be related to: (1) inherent differences in rooting depth between trees/shrubs and herbaceous species, as trees/shrubs in arid and semiarid ecosystems generally have deeper rooting systems than grasses/forbs (Jackson *et al.* 1996; Schenk 2006); and (2) the presence of non-argillic inclusions across this landscape. Several previous studies have reported a negative correlation between root density and soil clay content, and suggested that higher clay content would reduce soil porosity and hydraulic conductivity and increase soil resistance, thereby inhibiting root growth and elongation (Strong & Roi 1985; Ludovici 2004; Macinnis-Ng *et al.* 2010; Plante *et al.* 2014). For this reason, the presence of a clay-accumulated subsurface soil horizon (i.e. argillic horizon) has been shown to affect vertical root distribution (Sudmeyer *et al.* 2004; Macinnis-Ng *et al*. 2010). For example, Sudmeyer *et al.* (2004) found that, in duplex soils, tree root densities were highest in the upper sandy portion of the profile, but then decreased sharply in subsurface clayey soils. Across this landscape, grove vegetation exclusively occupies those portions of the landscape with coarse-textured non-argillic inclusions, while grasslands occur on portions of the landscape where the argillic horizon is present at approximately 30-50 cm in the profile (Archer 1995; Zhou *et al.* 2017b). This subsurface clay-rich argillic horizon may significantly impede the vertical distribution of fine roots beneath grasslands, while subsurface coarse-textured non-argillic inclusions beneath groves offer less resistance to fine root penetration. Therefore, we have observed significant negative correlations between fine root density and soil clay content at the 30-50, 50-80, and 80-120 cm depth increments (Table 4.2).

Size differences between plants (both above- and belowground) may potentially confer a competitive advantage for a larger individual to acquire disproportionately more resources over a smaller individual (Schwinning & Weiner 1998; Rajaniemi *et al.* 2003; Schenk 2006; DeMalach *et al.* 2016). Fine roots are the primary functional components of root systems that enable plants to acquire water and nutrients from the highly heterogeneous soil environment (Pregitzer 2002). Although Walter's two-layered niche differentiation hypothesis has long been proposed as an explanation for the coexistence of grasses and trees in savannas (Walter 1971), emerging studies have shown that trees and grasses actually occupy overlapping rooting niches (Hipondoka & Versfeld 2006; February & Higgins 2010; Holdo 2013; Kambatuku *et al.* 2013). Our results show that fine root densities beneath woody patches were always 2 to 3 times more abundant than grasslands in both upper and lower soil depth increments (Fig. 4.4, Table 4.1), consistent with other studies at this site (Midwood *et al*. 1998; Boutton *et al.* 1998). Greater abundance of fine root density in upper soil depth increments where soils generally have higher nutrient availability (Schlesinger *et al.* 1996; Jobbágy & Jackson 2001), and in lower soil depth increments where soils typically have higher water availability (Boutton *et al.* 1999), suggest that woody species may be able to acquire disproportionately more resources than herbaceous species (Fig. 4.4), thereby facilitating their development, persistence, and encroachment across this landscape.

Overall, landscape scale spatial patterns of fine root density throughout the soil profile in this subtropical savanna were primarily controlled by the spatial distribution of woody patches in the horizontal plane, and by edaphic factors (presence/absence of argillic

horizon, soil clay content) in the vertical plane, supporting both of our original hypotheses. These results have important implications for understanding belowground biogeochemical cycles and representing them in modeling studies. Characterized by fast turnover rates (Gill & Jackson 2000) and high decomposability (Silver & Miya 2001), fine roots represent a major pathway transferring carbon, nutrients, and energy from plants to soils (Matamala *et al.* 2003), especially to the subsurface soils (Rasse *et al*. 2005; Schmidt *et al.* 2011). At the individual tree or woody patch scale, spatial patterns of soil carbon storage closely mirror those of fine root biomass (Koteen *et al*. 2015), and the total amount of sub-canopy soil carbon storage generally increases linearly with the size of tree or woody patch (Throop & Archer 2008; Boutton *et al.* 2009; Koteen *et al*. 2015). Thus, we may expect that landscape scale spatial patterns of soil carbon storage would be tightly linked to the size and spatial distribution of root systems. However, soil characteristics that can affect the stabilization of organic carbon derived from fine root turnover (e.g., soil texture, organomineral interactions) may vary with depth and contribute to landscape scale heterogeneity in soil carbon storage in the vertical dimension. Therefore, it remains uncertain how this alteration of root distribution at the landscape scale following a shift from grass to woody plant dominance will affect the spatial patterns of soil biogeochemical properties and processes. Current models linking root traits and morphology to ecosystem function likely oversimplify the true complexity of belowground interactions (Nippert & Holdo 2015). Our results indicate that landscape-scale spatial heterogeneity of fine root distribution changes not only in response to vegetation cover, but also in response to soil textural variation with depth in the profile.

The characterization of root biomass by soil depth, however, is absent in most terrestrial biosphere models and the ability to account for horizontal and vertical root spatial patterns could improve the predictive capabilities of these models (Warren *et al.* 2015). We suggest that root distribution patterns and soil processes in deeper portions of the soil profile, especially at the landscape scale, deserve greater attention in savanna ecology.

CONCLUSIONS

Overall, we found that woody patches had significantly higher fine root density than grasslands throughout the entire 1.2 m soil profile, creating spatial patterns of fine root density that were similar to the spatial distribution of woody patches. However, spatial heterogeneity of fine root density decreased with soil depth and increased in the last two depth increment, suggesting that woody patches have an ability to acquire disproportionately more resources than herbaceous species which may facilitate the development and persistence of woody patches across this landscape.

CHAPTER V

SOIL CARBON RESPONSE TO WOODY PLANT ENCROACHMENT: IMPORTANCE OF SPATIAL HETEROGENEITY AND DEEP SOIL STORAGE*

SYNOPSIS

Recent global trends of increasing woody plant abundance in grass-dominated ecosystems may substantially enhance soil organic carbon (SOC) storage and could represent a strong carbon (C) sink in the terrestrial environment. However, few studies have quantitatively addressed the influence of spatial heterogeneity of vegetation and soil properties on SOC storage at the landscape scale. In addition, most studies assessing SOC response to woody encroachment consider only surface soils, and have not explicitly assessed the extent to which deeper portions of the soil profile may be sequestering C. We quantified the direction, magnitude, and pattern of spatial heterogeneity of SOC in the upper 1.2 m of the profile following woody encroachment via spatially-specific intensive soil sampling across a landscape in a subtropical savanna in the Rio Grande Plains, USA, that has undergone woody proliferation during the past century. Increased SOC accumulation following woody encroachment was observed to considerable depth, albeit at reduced magnitudes in deeper portions of the profile. Overall, woody clusters and

* Originally published as: Zhou, Y., Boutton, T.W., & Wu, X.B. (2017) Soil carbon response to woody plant encroachment: Importance of spatial heterogeneity and deep soil storage. *Journal of Ecology*, **105**, 1738-1749. The publication is available at http://onlinelibrary.wiley.com/doi/10.1111/1365-2745.12770/full.

groves accumulated 12.87 and 18.67 Mg C ha^{-1} more SOC compared to grasslands to a depth of 1.2 m. Woody encroachment significantly altered the pattern of spatial heterogeneity of SOC to a depth of 5 cm, with marginal effect at 5-15 cm, and no significant impact on soils below 15 cm. Fine root density explained greater variability of SOC in the upper 15 cm, while a combination of fine root density and soil clay content accounted for more of the variation in SOC in soils below 15 cm across this landscape. Substantial SOC sequestration can occur in deeper portions of the soil profile following woody encroachment. Furthermore, vegetation patterns and soil properties influenced the spatial heterogeneity and uncertainty of SOC in this landscape, highlighting the need for spatially specific sampling that can characterize this variability and enable scaling and modeling. Given the geographic extent of woody encroachment on a global scale, this undocumented deep soil C sequestration suggests this vegetation change may play a more significant role in regional and global C sequestration than previously thought.

INTRODUCTION

Grass-dominated ecosystems in arid and semi-arid regions around the world have experienced increased woody plant abundance during the past century (Van Auken 2000, 2009; Eldridge *et al.* 2011; Stevens *et al.* 2017). This globally widespread phenomenon has dramatically altered the structure and function of grassland and savanna ecosystems (Maestre *et al.* 2009; Eldridge *et al.* 2011), with the potential to profoundly influence grassland biodiversity (Ratajczak *et al.* 2012), hydrology (Huxman *et al.* 2005), biogeochemistry (Boutton *et al.* 1999; Hibbard *et al.* 2003; Chiti *et al.* 2017) and livestock production (Dalle *et al.* 2006). Since arid and semi-arid systems occupy more than 40%

of Earth's land surface (Bailey 1996), a shift from grass dominated to woody dominated ecosystems could potentially influence the global carbon (C) cycle and the climate system via the impacts on soil organic carbon (SOC) stocks and dynamics.

Land cover change is often associated with a change in C stocks (Guo & Gifford 2002; Don *et al.* 2011; Pellegrini *et al.* 2014). The encroachment of woody plants into grasslands/savannas has been considered to be a potentially large C sink at regional and global scales due to the accumulation of C in both biomass and soils (Pacala *et al.* 2001; King *et al.* 2007; Dean *et al.* 2015). However, at the ecosystem level, the effects of woody encroachment on SOC stocks are often equivocal, with studies showing increased SOC stocks in some ecosystems (Schlesinger *et al.* 1996; Maestre *et al.* 2009; Liu *et al.* 2011; Blaser *et al.* 2014), no net change (Hughes *et al.* 2006) and reductions in others (Jackson *et al.* 2002; Oelofse *et al.* 2016). Reasons for these inconsistences still remain unknown, but may be ascribed to soil characteristics and historical land use patterns (Jackson *et al.* 2002; Barger *et al.* 2011; Li *et al.* 2016), or the lack of appropriate methodology for estimating SOC stocks in encroached systems with complex vegetation patterns (Throop & Archer 2008; Liu *et al.* 2011). In addition, most of these studies have evaluated the impact of woody encroachment only on surficial SOC stocks (down to 30 cm at most, IPCC recommended sampling depth [IPCC, 2006]) (e.g. Hughes *et al.* 2006; Maestre *et al.* 2009; Liu *et al.* 2011; Blaser *et al.* 2014), and few studies have examined SOC accumulation in deeper soil layers (below 30 cm) (Boutton *et al.* 1999; Jackson *et al.* 2002; Chiti *et al.* 2017). Compared to herbaceous species, trees/shrubs typically have much deeper rooting systems (Jackson *et al.* 1996; Schenk 2006; Yang *et al.* 2016b). The

allocation of C to deep roots by encroaching woody plants, as the major source of C input in subsoil (Rumpel & Kögel-Knabner 2011), may be expected to increase SOC accumulation in deeper soil layers. On the other hand, deep roots may prime the decomposition of otherwise stable subsurface SOC through the addition of labile root C (e. g. Fontaine *et al.* 2007; Mobley *et al.* 2015). Therefore, the direction and magnitude of SOC stocks response to woody encroachment in deeper portions of the soil profile remain largely unknown, and study of deep soil is crucial for understanding SOC dynamics and for making robust predictions of terrestrial C budgets following vegetation cover change.

Woody encroachment into grass-dominated ecosystems may also increase the spatial heterogeneity of soil properties (e.g. islands of fertility, Schlesinger *et al.* 1996), making it more difficult to accurately quantify ecosystem properties and processes based on micro-sites and limited sample size (Throop & Archer 2008; Liu *et al.* 2011). Previous studies have demonstrated the value of quantifying spatial patterns of soil properties and associated variability to study related processes in arid and semi-arid regions with patchy vegetation (Schlesinger *et al.* 1996; Throop & Archer 2008; Bai *et al.* 2009; Liu *et al.* 2011; Daryanto *et al.* 2013b), but their results were restricted to the topsoil (0-20 cm). Woody encroachment has been confirmed to substantially alter the spatial pattern and variability of SOC in topsoil at the individual woody patch scale from bole to the perimeter (Throop & Archer 2008) and at the landscape scale where the landscape comprises different sizes of woody patches (Liu *et al.* 2011). To our knowledge, however, no study has explicitly assessed the extent to which woody encroachment alters the spatial pattern of SOC in deeper portions of the soil profile. Non-spatial soil core studies suggest that

deeper SOC pool size may be modified following woody encroachment (Boutton *et al.* 1998; Jackson *et al.* 2002; Chiti *et al.* 2017). This implies that potentially strong spatial gradients of SOC may exist throughout the soil profile at the landscape scale, because organic matter inputs from litterfall and root turnover will be more concentrated in topsoil compared to deeper portions of the profile. Given the fact that most studies on spatial patterns of SOC following woody encroachment have been conducted on surface soils, and that substantial SOC is stored in subsurface soils, this represents a major knowledge gap concerning the effects of vegetation cover change on the pattern of spatial heterogeneity in SOC throughout the soil profile.

The primary purpose of this study was to determine how woody encroachment into grassland affects the direction, magnitude and pattern of spatial heterogeneity in SOC throughout the soil profile. To accomplish this, spatially-specific soil samples to a depth of 1.2 m were collected across a landscape in a subtropical savanna ecosystem where woody plants have been encroaching into grasslands for the past century (Archer *et al.* 1988; Boutton *et al.* 1998). Our specific objectives were to: (1) estimate SOC stocks following woody encroachment and the proportion of these stocks derived from woody plants based on $\delta^{13}C$ values of SOC throughout the soil profile; (2) quantify the pattern of spatial heterogeneity in SOC across this landscape and throughout the soil profile; and (3) elucidate factors responsible for the variances in SOC across this landscape and throughout the soil profile. We hypothesized that woody encroachment into this grasslands would substantially: (1) increase SOC sequestrations to considerable depth, albeit at

reduced magnitudes in deeper portions of the soil profile; and (2) alter the pattern of spatial heterogeneity in SOC throughout the soil profile.

MATERIALS AND METHODS

Study site

This study was conducted in the Rio Grande Plains region at the Texas A&M AgriLife La Copita Research Area (27˚40' N, 98˚12' W) in Jim Wells County, 65 km west of Corpus Christi, Texas, USA. The climate is subtropical, with a mean annual temperature of 22.4 ˚C and mean annual precipitation of 680 mm. Rainfall peaks occur in May and September. Elevation ranges from 75 to 90 m above sea level. Topography is relatively flat, with 1-3% slopes where uplands transition to lower-lying portions of the landscape.

This study was confined to upland portions of the landscape where soils are primarily sandy loam Typic Argiustolls with a laterally continuous subsurface argillic horizon (*Bt*); however, some portions of the upland landscape have patches where the *Bt* horizon is absent (i.e. non-argillic inclusions), and these soils classify as Typic Haplustepts (Loomis 1989; Archer 1995; Zhou *et al.* 2017b). The vegetation is characterized as subtropical savanna parkland, consisting of an herbaceous matrix comprised of C_4 grasses and C_3 forbs, with discrete woody patches interspersed throughout the herbaceous matrix. Woody patches are categorized into small shrub clusters and large groves. Clusters with diameters of < 10 m are comprised of a single N-fixing *Prosopis glandulosa* tree with up to 15 understorey shrub/tree species. Groves with diameters of > 10 m occur exclusively on non-argillic inclusions, and are comprised of several clusters that have fused together

(Archer 1995; Bai *et al.* 2012; Zhou *et al.* 2017b). Species composition can be found in Appendix A.

Field sampling

A 160 m × 100 m landscape divided into 10 m × 10 m grid cells was established on an upland portion of this study site in January 2002 (Bai *et al.* 2009; Liu *et al.* 2011) that included all three of the major upland landscape elements: grassland, cluster and grove (Fig. 5.1). The corners of each cell were georeferenced based on the UTM coordinates system (14 North, WGS 1984) using a GPS unit (Trimble Pathfinder Pro XRS, Trimble Navigation Limited, Sunnyvale, CA, USA). In July 2014, two randomly located points were selected within each 10 m × 10 m grid cell, yielding a total of 320 sample points within this 160 m × 100 m plot (Fig. 5.1). Landscape element types for each sample point were categorized as grassland, cluster or grove based on the size of canopy area. The distances from each sample point to two georeferenced cell corners were recorded. At each of the two sample points in each cell, two adjacent soil cores (28 mm in diameter ×120 cm in length) were collected using the PN150 JMC Environmentalist's Subsoil Probe (Clements Associates Inc., Newton, IA, USA). Each soil core was subdivided into six depth increments (0-5, 5-15, 15-30, 30-50, 50-80, and 80-120 cm). One soil core was oven-dried (105 ˚C for 48 hours) to determine soil bulk density; the other core was air-dried prior to subsequent analyses. A color-infrared aerial photograph (6 cm x 6 cm resolution) of this 160 m × 100 m landscape was acquired in July 2015, and used to compute the Normalized Difference Vegetation Index (NDVI = [NIR-RED]/

[NIR+RED], in which NIR and RED represent the spectral reflectance measurements from the near-infrared and the red regions of the aerial photograph, respectively).

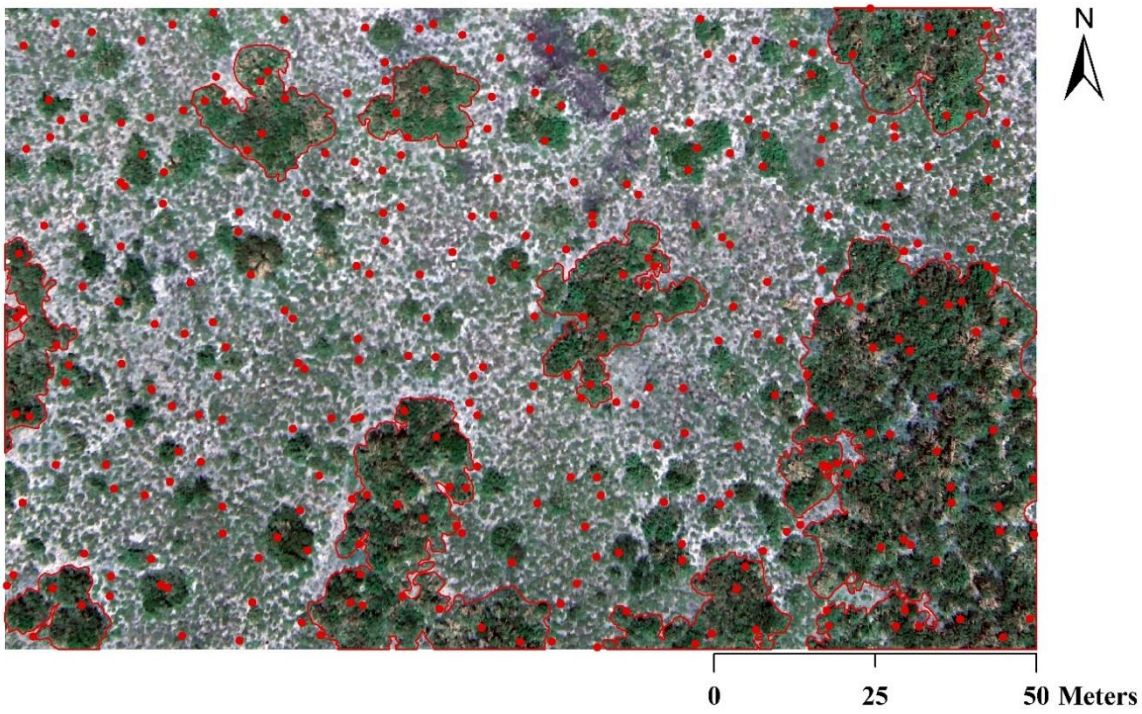

Figure 5.1 Aerial photograph of the 160 m × 100 m study area and locations of 320 random soil samples (red points). Green patches are shrub clusters and groves (highlighted with red lines) and light grey color indicates open grassland.

Lab analyses

Soils used to determine bulk density were subsequently used to estimate fine (< 2 mm) and coarse (> 2 mm) root biomass by washing through sieves. No attempt was made to distinguish between live or dead roots. Roots were dried at 65 ˚C and weighed to

determine root biomass. For elemental and isotopic analyses, three composite fine root samples were created for each landscape element by combining fine roots from 10 cores for each depth increment. Composite fine roots were homogenized and pulverized in a Mixer Mill MM 400 (Retsch GmbH, Haan, Germany).

Air-dried soil samples were passed through a 2 mm sieve to remove coarse organic fragments. No gravel was present in these soils. An aliquot of sieved soil was used to determine soil texture by the hydrometer method (Sheldrick & Wang 1993). Soil *p*H was determined on a 1:2 (soil: 0.01 mol/L $CaCl_2$) mixture using a glass electrode. An aliquot of sieved soil was dried at 60 ˚C for 48 hours and pulverized in a centrifugal mill (Angstrom, Inc., Belleville, MI, USA). Pulverized soil samples were weighed into silver capsules (5 mm × 7 mm), treated with HCl vapor in a desiccator to remove carbonates for 8 hours (Harris *et al.* 2001), and then dried.

Carbon concentrations and the $\delta^{13}C$ values of acid-treated and dried soils and fine roots were determined using a Costech ECS 4010 elemental combustion system (Costech Analytical Technologies Inc., Valencia, CA, USA) interfaced via a ConFlo IV device with a Delta V Advantage isotope ratio mass spectrometer (Thermo Scientific, Bremen, Germany). Carbon isotope ratios are presented in δ notation (Equation 1):

$$\delta = \left(\frac{R_{Sample} - R_{STD}}{R_{STD}}\right) \times 10^3 \quad (1)$$

where R_{Sample} is the $^{13}C/^{12}C$ ratio of the soil sample and R_{STD} is the $^{13}C/^{12}C$ ratio of the V-PDB standard. Precision of duplicate measurements was 0.1‰ for $\delta^{13}C$ for both soil and fine root samples.

Data analyses

SOC stocks (Mg C ha^{-1}) were calculated based on the following equation:

$$Mg\ C\ ha^{-1} = \left(\frac{C_c}{1000}\right) \times SBD \times D \times 10^2 \quad (2)$$

Where C_c is SOC concentration (g C kg^{-1} soil), *SBD* is soil bulk density (g cm^{-3}) and *D* is the depth interval (or thickness) in cm for each depth increment. To facilitate comparisons between the unequal sampling depth intervals, we conducted our analyses on SOC density (kg C m^{-3}), amount of C per unit volume of soil, which was calculated using the following equation:

$$kg\ C\ m^{-3} = \left(\frac{C_c}{1000}\right) \times SBD \times 10^3 \quad (3)$$

An identical soil sampling regime (i.e. 2 randomly located sampling points per 10 m × 10 m grid cell) was used to collect surface soils (0-15 cm) when this 160 m × 100 m landscape was established in 2002 (see Liu *et al.* 2011 for more details), and we used this previous data set in conjunction with our new measurements to estimate SOC accumulation rates in surface soils for each landscape element during the past 12 years (2002-2014). To accomplish this, we combined our SOC stocks in the 0-5 and 5-15 cm depth increments obtained in 2014, and then compared them with stocks obtained in 2002.

Datasets that were not normally distributed were log-transformed before variable means of different landscape elements for each soil depth increment were compared using mixed models. Spatial autocorrelation of variables was taken into account as a spatial covariance for adjustment in mixed models (Littell *et al.* 2006). In mixed models, spherical, exponential, and Gaussian structures were tested, and the best fitting model for

each variable in each soil depth increment was selected based on Akaike Information Criterion (AIC). *Post hoc* comparisons of these variables in different landscape elements were also conducted using the mixed models with Tukey's correction. A cutoff value of $p < 0.05$ was used to indicate significant differences. Mixed models were performed using JMP pro 12.0 (SAS Institute Inc., Cary, NC, USA).

The relative proportions of SOC derived from woody plants (*F*) for each depth increment under woody patches (hereafter, clusters and groves) were calculated using a mass balance (Equation 4):

$$F = \frac{\delta_{WS} - \delta_{GS}}{\delta_{WR} - \delta_{GS}} \quad (4)$$

where δ_{WS} is the $\delta^{13}C$ value of SOC in woody patches for each depth increment; δ_{GS} is the average $\delta^{13}C$ value of SOC in remnant grassland soils (n = 200) for each depth increment; δ_{WR} is the average $\delta^{13}C$ value of fine roots in woody patches for each depth increments. Here, we assumed that (1) prior to woody encroachment, the $\delta^{13}C$ of SOC in grasslands was relatively homogeneous across this landscape and the average values for each depth increment were used as baselines; (2) SOC derived from woody plants in wooded landscape elements had the same $\delta^{13}C$ values as those of fine roots in each depth increment since roots and root exudates are the main sources of C input into subsoil (Rumpel & Kögel-Knabner 2011), and, even in topsoil, root-derived C is retained in soils much more efficiently than C derived from aboveground litterfall (Rasse *et al.* 2005; Schmidt *et al.* 2011; Clemmensen *et al.* 2013).

A sample variogram fitted with a variogram model was developed to quantify the spatial structure of SOC density based on values of 320 random sample points for each depth increment using R statistical software (R Development Core Team 2014). Ordinary kriging based on the best fitted variogram model was used to predict SOC densities at unsampled locations for each soil depth increment. Kriged maps of SOC density for each depth increment with a 0.5 m × 0.5 m resolution were generated in ArcMap 10.2.2 (ESRI, Redlands, CA, USA) using the Spatial Analyst tool.

Lacunarity was used to assess the spatial heterogeneity of SOC density for each depth increment across this landscape. Lacunarity is a scale-dependent measurement of spatial heterogeneity or the "gappiness" of a landscape structure (Plotnick *et al.* 1996). Lacunarity was calculated based on each kriged map of SOC density using R statistical software (R Development Core Team 20114). The lacunarity curve, natural log transformation of lacunarity values $\Lambda(r)$ against box size (r), was plotted to quantify the spatial heterogeneity of SOC density at different scales for each soil depth increment, with a higher value of lacunarity indicating a more heterogeneous distribution pattern across the landscape.

A spatial generalized least squares (GLS) model that incorporates spatial structure in the error term of the regression model (Beale *et al.* 2010) was used to analyze the relationships among the explanatory variables and SOC density within each soil depth increment and across this landscape. Explanatory variables included vegetation factors (NDVI and fine root biomass) and soil physical factors (soil bulk density, soil clay and silt contents, and soil pH). We excluded soil sand content as explanatory variable because

of its high correlation with soil clay content. We initially explored the spatial autocorrelation in both the explanatory variables and response variable for each soil depth increment, then we tested different models with spatial structure (assuming linear, spherical, exponential, and Gaussian structure) and non-spatial structure. The best fitting model for each soil depth increment was selected using the Akaike Information Criterion (AIC). Parameters were estimated based on restricted maximum likelihood (REML). *t*-values for explanatory variables were used to indicate their relative importance in explanation of response variable (Diniz-Filho *et al.* 2003). Analyses were performed using R statistical software (R Development Core Team 2014).

RESULTS

Vegetation and soil characteristics

Overall, grasslands, clusters and groves covered 62.4%, 10.3%, and 27.3 % of this 160 m × 100 m landscape, respectively. Clusters (0.36 ± 0.02, n = 41) and groves (0.31 ± 0.02, n = 79) exhibited significantly higher NDVI values than grasslands (0.20 ± 0.00, n = 200). Soil bulk densities of woody patches were significantly lower than those of grasslands throughout the entire soil profile (Table 5.1). Due to the presence of non-argillic inclusions interspersed within a laterally continuous subsurface argillic horizon, and the fact that groves occurred only on these non-argillic inclusions (Zhou *et al.* 2017b), groves had significantly lower clay content than grasslands in the 30-50, 50-80 and 80-120 cm depth increments (Table 5.1). Woody patches had higher *p*H values than grasslands throughout the entire soil profile (Table 5.1).

Table 5.1 Mean and standard error (SE) of soil bulk density (g cm^{-3}), soil sand, silt and clay content (%), and soil *p*H in different landscape elements across this 160 m × 100 m landscape throughout the soil profile.

Variables	Vegetation type	Soil Depth (cm)					
		0-5	5-15	15-30	30-50	50-80	80-120
Soil bulk density	Grassland	1.34 ± 0.01^{a}	1.44 ± 0.00^{a}	1.41 ± 0.01^{a}	1.46 ± 0.00^{a}	1.52 ± 0.00^{a}	1.62 ± 0.00^{a}
	Cluster	1.10 ± 0.02^{b}	1.29 ± 0.01^{b}	1.36 ± 0.01^{b}	1.43 ± 0.01^{b}	1.49 ± 0.01^{b}	1.59 ± 0.01^{b}
	Grove	1.06 ± 0.01^{b}	1.31 ± 0.01^{b}	1.37 ± 0.01^{b}	1.43 ± 0.01^{b}	1.47 ± 0.01^{b}	1.59 ± 0.01^{b}
Soil sand content	Grassland	76.4 ± 0.2^{a}	74.5 ± 0.2^{a}	71.5 ± 0.1^{a}	67.2 ± 0.2^{b}	62.9 ± 0.2^{b}	$55.8(0.3)^{b}$
	Cluster	75.4 ± 0.4^{a}	74.1 ± 0.4^{ab}	71.4 ± 0.4^{ab}	67.8 ± 0.6^{ab}	63.0 ± 0.8^{b}	$55.4(0.9)^{b}$
	Grove	75.0 ± 0.4^{b}	73.3 ± 0.4^{b}	70.4 ± 0.5^{b}	68.1 ± 0.5^{a}	64.9 ± 0.6^{a}	$59.0(0.9)^{a}$
Soil silt content	Grassland	10.8 ± 0.1^{b}	10.1 ± 0.1^{a}	10.7 ± 0.1^{a}	11.1 ± 0.1^{a}	12.2 ± 0.1^{a}	$14.1(0.1)^{a}$
	Cluster	11.1 ± 0.2^{a}	10.7 ± 0.2^{a}	11.1 ± 0.2^{a}	11.3 ± 0.2^{a}	12.2 ± 0.2^{a}	$14.0(0.2)^{a}$
	Grove	11.8 ± 0.2^{a}	11.2 ± 0.2^{a}	11.7 ± 0.1^{a}	11.9 ± 0.1^{a}	12.2 ± 0.1^{a}	$13.5(0.2)^{b}$
Soil clay content	Grassland	12.8 ± 0.1^{a}	15.4 ± 0.1^{a}	17.8 ± 0.1^{a}	21.7 ± 0.2^{a}	25.0 ± 0.2^{a}	30.1 ± 0.3^{a}
	Cluster	13.5 ± 0.3^{a}	15.2 ± 0.3^{a}	17.5 ± 0.3^{a}	20.9 ± 0.6^{b}	24.9 ± 0.7^{a}	30.6 ± 0.7^{a}
	Grove	13.2 ± 0.3^{a}	15.5 ± 0.3^{a}	17.9 ± 0.3^{a}	20.0 ± 0.4^{c}	22.9 ± 0.5^{b}	27.6 ± 0.7^{b}
pH	Grassland	7.34 ± 0.02^{a}	7.21 ± 0.03^{b}	7.17 ± 0.03^{b}	7.30 ± 0.02^{b}	7.54 ± 0.02^{b}	7.74 ± 0.01^{b}
	Cluster	7.34 ± 0.04^{a}	7.34 ± 0.04^{a}	7.35 ± 0.06^{a}	7.46 ± 0.05^{a}	7.65 ± 0.03^{a}	7.79 ± 0.02^{a}
	Grove	7.39 ± 0.04^{a}	7.48 ± 0.03^{a}	7.54 ± 0.04^{a}	7.64 ± 0.04^{a}	7.74 ± 0.03^{a}	7.82 ± 0.01^{a}

Number of samples: grassland = 200, cluster = 41, and grove = 79. Significant differences ($p < 0.05$) between means for landscape elements are indicated with different superscript letters.

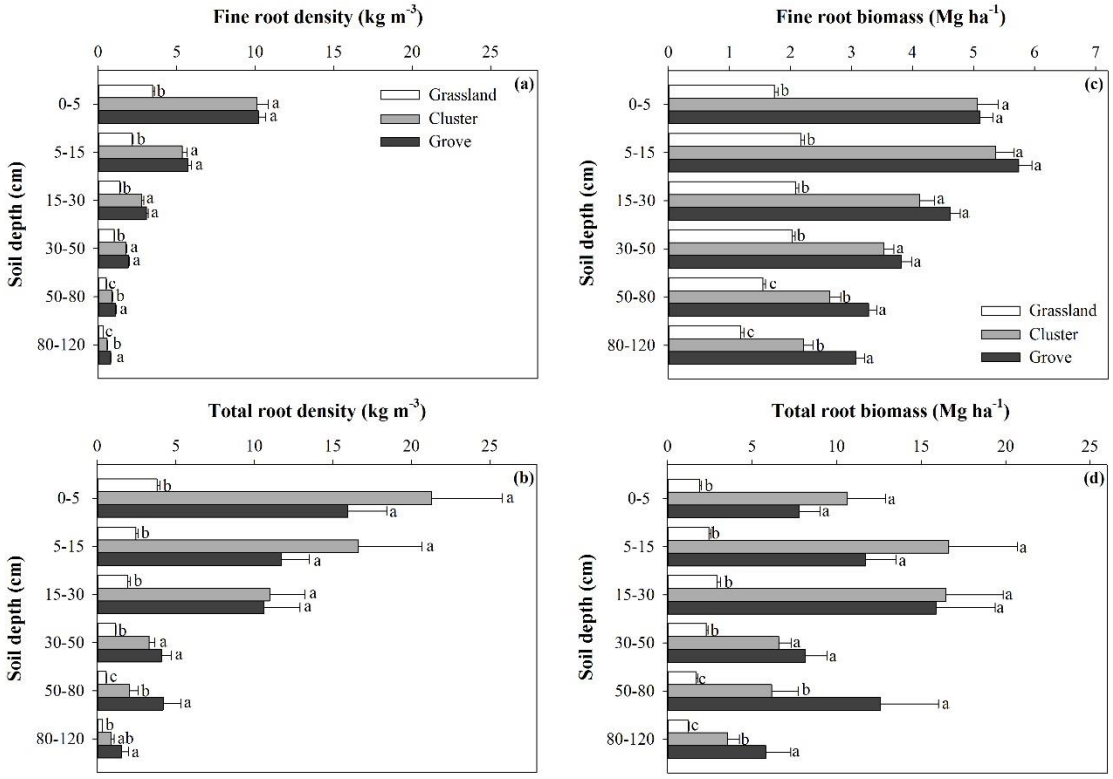

Figure 5.2 Fine and total root density (kg m^{-3}) (a, b) and biomass (Mg ha^{-1}) (c, d) for different landscape elements across this 160 m × 100 m landscape throughout the soil profile. Significant differences ($p < 0.05$) between means for landscape elements are indicated with different letters. Number of samples: grassland = 200, cluster = 41, and grove = 79.

Woody patches had significantly higher root densities (kg m^{-3}) than grasslands throughout the entire soil profile (Fig. 5.2a and b). For example, in the 0-5 cm depth increment, average fine root densities of clusters (10.12 ± 0.69 kg m^{-3}) and groves (10.20 ± 0.44 kg m^{-3}) were almost three times higher than those of grasslands (3.47 ± 0.11 kg m^{-3}). Fine and total root density decreased dramatically throughout the soil profile (Fig. 2a, b). However, the absolute magnitudes of root biomass stock (Mg ha^{-1}) in deeper soil

increments were still remarkable (Fig. 5.2c and d). For example, in the 80-120 cm depth increment, mean fine root biomass stocks of grasslands, clusters and groves were 1.19 ± 0.05, 2.21 ± 0.16, and 3.07 ± 0.15 Mg ha^{-1}, respectively (Fig. 5.2c and d).

Woody patches had significantly higher root densities (kg m^{-3}) than grasslands throughout the entire soil profile (Fig. 5.2a and b). For example, in the 0-5 cm depth increment, average fine root densities of clusters (10.12 ± 0.69 kg m^{-3}) and groves (10.20 ± 0.44 kg m^{-3}) were almost three times higher than those of grasslands (3.47 ± 0.11 kg m^{-3}). Fine and total root density decreased dramatically throughout the soil profile (Fig. 2a, b). However, the absolute magnitudes of root biomass stock (Mg ha^{-1}) in deeper soil increments were still remarkable (Fig. 5.2c and d). For example, in the 80-120 cm depth increment, mean fine root biomass stocks of grasslands, clusters and groves were 1.19 ± 0.05, 2.21 ± 0.16, and 3.07 ± 0.15 Mg ha^{-1}, respectively (Fig. 5.2c and d).

SOC storage and $\delta^{13}C$ values throughout the soil profile

Woody patches had significantly higher SOC densities (kg C m^{-3}) than those of grasslands for all depth increments, except at 30-50 cm (Fig. 5.3a). SOC densities decreased throughout the soil profile (Fig. 5.3a), while cumulative SOC stock (Mg C ha^{-1}) increased with depth (Table 5.2). Woody patches had higher SOC stocks than grasslands for each depth increment (Table 5.2). Overall, to a depth of 120 cm, cumulative SOC stocks for grasslands, clusters and groves were: 68.30 ± 0.45, 81.17 ± 1.82, and 86.97 ± 1.40 Mg C ha^{-1}, respectively (Table 5.2). SOC sequestration following woody encroachment was observed in the full 120 cm soil profile, albeit at reduced magnitudes in deeper portions of the profile; clusters and groves accumulated 12.87 and 18.67 Mg C

ha^{-1} more SOC than grasslands, respectively (Fig. 5.3b). Estimated SOC accumulation rates for groves and clusters in the 0-15 cm depth increment during the past 12 years (2002-2014) were 41.5 and 38.8 g C m^{-2} yr^{-1}, respectively (Fig. 5.4).

Table 5.2 Mean and standard error (SE) of SOC stock (Mg C ha^{-1}) (a) and cumulative SOC stock (Mg C ha-1) (b) for different landscape elements across this 160 m × 100 m landscape throughout the soil profile.

Soil depth (cm)	Grassland	Cluster	Grove
(a) SOC stock (Mg C ha^{-1})			
0-5	4.44 ± 0.08^{c}	9.18 ± 0.77^{b}	11.91 ± 0.72^{a}
5-15	7.79 ± 0.07^{b}	10.48 ± 0.47^{a}	11.39 ± 0.30^{a}
15-30	10.83 ± 0.10^{b}	12.29 ± 0.32^{a}	12.90 ± 0.25^{a}
30-50	14.50 ± 0.14^{a}	15.16 ± 0.30^{a}	15.27 ± 0.36^{a}
50-80	16.00 ± 0.13^{b}	17.51 ± 0.39^{a}	17.05 ± 0.30^{a}
80-120	14.73 ± 0.20^{c}	16.55 ± 0.59^{b}	18.45 ± 0.38^{a}
(b) Cumulative SOC stock (Mg C ha^{-1})			
Surface to 5 cm	4.44 ± 0.08^{c} (6.5)	9.18 ± 0.77^{b} (11.0)	11.91 ± 0.72^{a} (13.3)
Surface to 15 cm	12.23 ± 0.13^{c} (17. 9)	19.66 ± 1.16^{b} (23.8)	23.30 ± 0.91^{a} (26.4)
Surface to 30 cm	**23.07 ± 0.19^{c} (33. 8)**	**31.95 ± 1.37^{b}(39.0)**	**36.21 ± 1.01^{a} (41.3)**
Surface to 50 cm	37.57 ± 0.27^{c} (55.1)	47.12 ± 1.51^{b} (58.0)	51.48 ± 1.13^{a} (58.9)
Surface to 80 cm	53.58 ± 0.36^{c} (78.5)	64.62 ± 1.63^{b} (79.6)	68.52 ± 1.21^{a} (78.7)
Surface to 120 cm	68.30 ± 0.45^{c}(100.0)	81.17 ± 1.92(100.0)	86.97 ± 1.40^{a}(100.0)

Numbers in the parentheses are percentages of cumulative SOC stock from the surface to the specified depth divided by the cumulative SOC stock to a depth of 120 cm. Row with text in bold indicates the IPCC recommended sampling depth (30 cm). Number of samples: grassland = 200, cluster = 41, and grove = 79. Significant differences ($p < 0.05$) between means for landscape elements are indicated with different superscript letters.

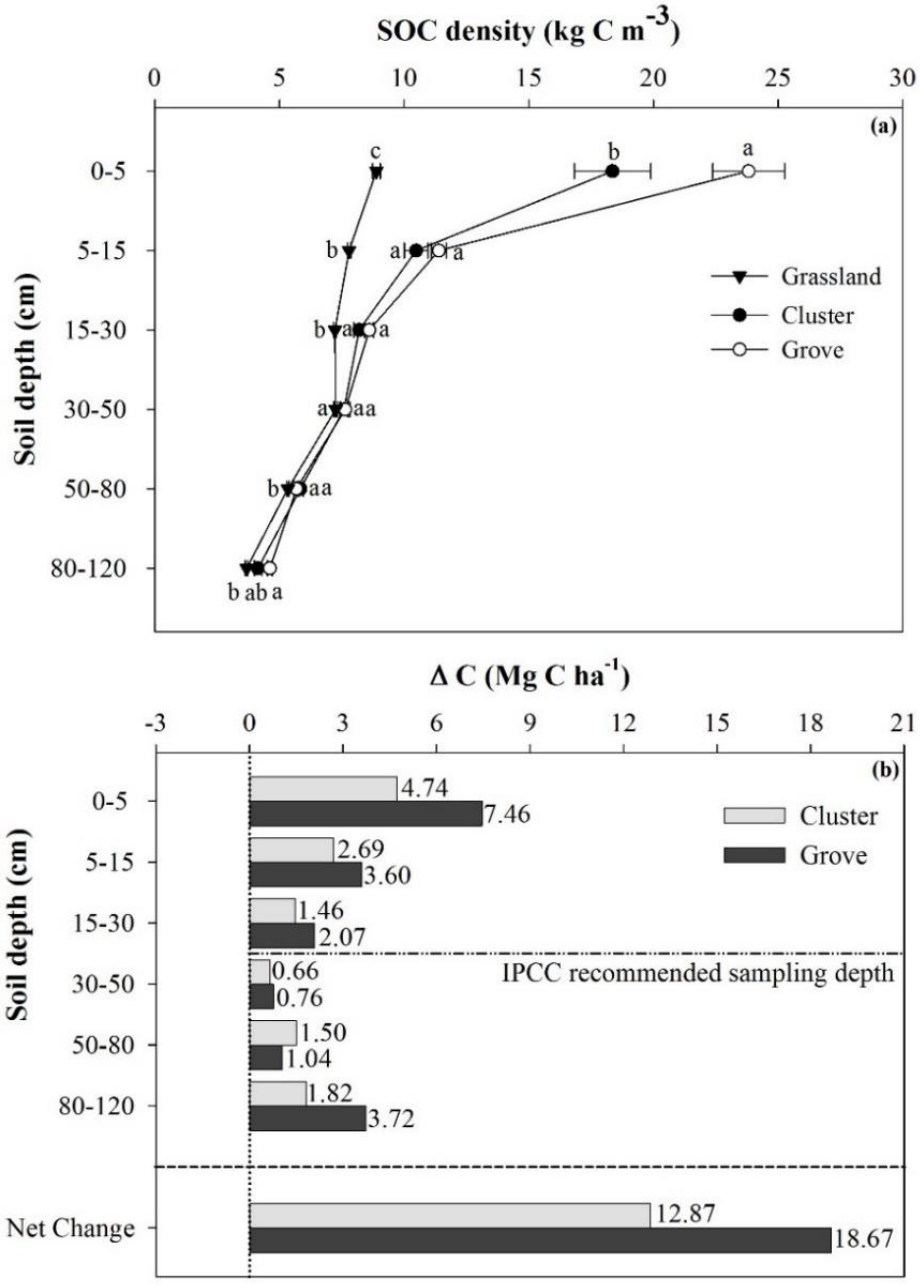

Figure 5.3 SOC density (kg C m^{-3}) for different landscape elements throughout the soil profile (a) and averaged changes in SOC stock for clusters and groves compared to grasslands for each depth increment and in the full 0-120 cm profile (b) across this 160 m × 100 m landscape. Significant differences ($p < 0.05$) between means for landscape elements are indicated with different letters. Number of samples: grassland = 200, cluster = 41, and grove = 79.

Table 5.3 Mean and standard error (SE) of $\delta^{13}C$ values (‰ vs. V-PDB) of SOC and fine roots, and percentage (%) of SOC derived from woody plants in clusters and groves across this 160 m × 100 m landscape throughout the soil profile.

Soil depths (cm)	SOC $\delta^{13}C$ (‰)$^{\alpha}$			Fine root $\delta^{13}C$ (‰)$^{\beta}$		Estimates (%) of SOC derived from woody plants $^{\gamma}$	
	Grassland	Cluster	Grove	Cluster	Grove	Cluster	Grove
0-5	-20.7 ± 0.1^{a}	-24.3 ± 0.2^{b}	-24.0 ± 0.2^{b}	-26.6 ± 0.1	-26.0 ± 0.2	60.5 ± 3.6^{a}	62.3 ± 3.1^{a}
5-15	-18.3 ± 0.1^{a}	-21.5 ± 0.2^{b}	-21.4 ± 0.2^{b}	-26.8 ± 0.2	-26.4 ± 0.3	37.6 ± 2.8^{a}	38.9 ± 2.0^{a}
15-30	-16.4 ± 0.1^{a}	-17.6 ± 0.2^{b}	-18.3 ± 0.2^{c}	-26.3 ± 0.2	-26.2 ± 0.2	15.4 ± 2.2^{b}	21.8 ± 1.7^{a}
30-50	-15.9 ± 0.1^{a}	-16.4 ± 0.2^{b}	-17.3 ± 0.2^{c}	-26.5 ± 0.2	-26.1 ± 0.1	8.0 ± 1.4^{b}	17.4 ± 1.7^{a}
50-80	-15. 9 ± 0.1^{a}	-16.7 ± 0.1^{b}	-17.0 ± 0.1^{b}	-26.4 ± 0.2	-26.4 ± 0.1	7.2 ± 1.1^{a}	10.2 ± 1.2^{a}
80-120	-17.0 ± 0.1^{a}	-17.6 ± 0.1^{b}	-17.8 ± 0.1^{b}	-26.4 ± 0.3	-26.3 ± 0.2	6.5 ± 1.5^{a}	8.4 ± 1.3^{a}

α: number of samples: grassland = 200, cluster = 41, and grove = 79.
β: number of replicates: cluster = 3, and grove = 3.
γ: significance was based on unpaired t test.
Significant differences ($p < 0.05$) between means for landscape elements are indicated with different superscript letters.

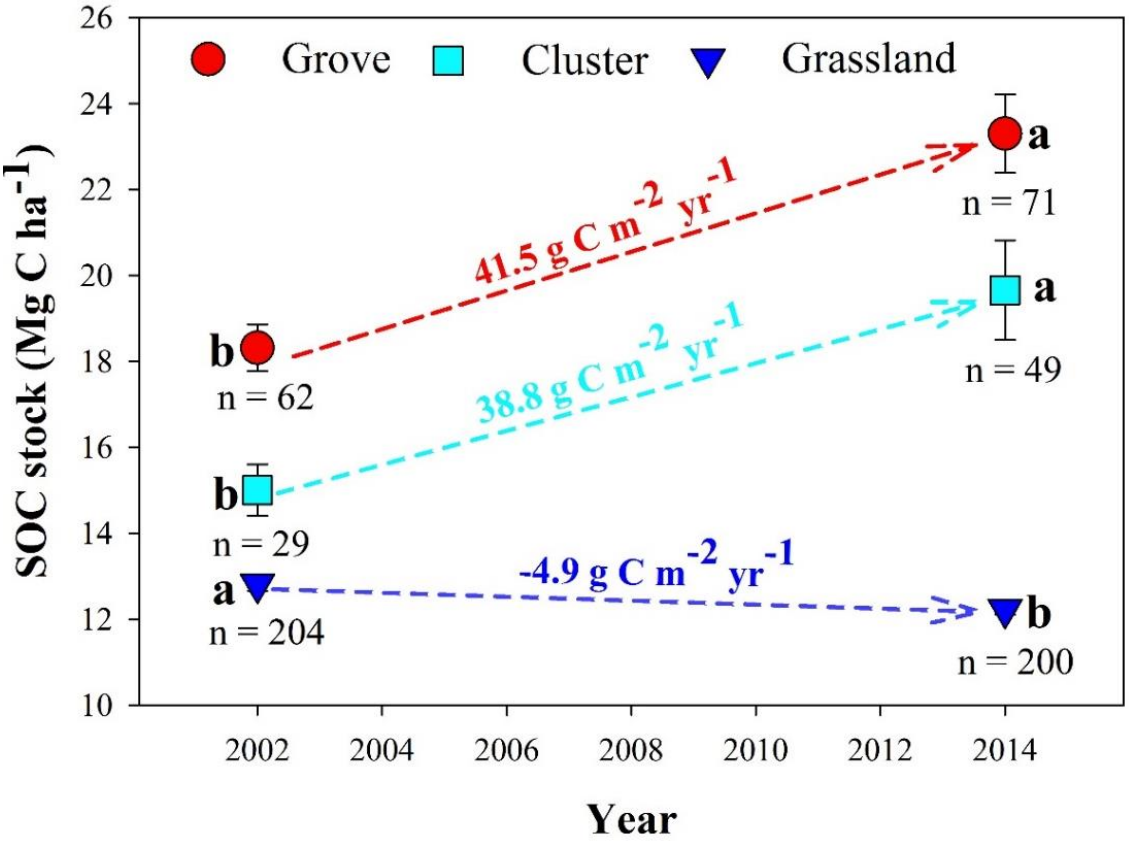

Figure 5.4 SOC accumulation rates at the 0-15 cm depth increment for different landscape elements from 2002 to 2014 for this 160 m × 100 m landscape. SOC stocks (Mg C ha-1) for 2002 were reported in Liu et al., 2011. Significant differences ($p < 0.05$) between means for landscape elements are indicated with different letters based on unpaired t test.

Mean soil $\delta^{13}C$ values beneath grasslands range from -20.7 ‰ near the soil surface to -15.9 ‰ deeper in the profile (Table 5.3), reflecting the mixed C_4 grass/C_3 forb composition of the grassland. Mean soil $\delta^{13}C$ values beneath woody patches (-24.3 to -16.4 ‰) were significantly lower than those beneath grasslands throughout the entire soil profile, but higher than those of woody fine roots (-26.6 to -26.0 ‰) (Table 5.3), indicating

current SOC beneath woody patches was comprised of both C derived from woody plants during the recent shift of vegetation cover as well as legacy C derived from the original grasslands that once dominated this region. Mass balance calculation revealed that 60.5% and 62.3% of soil C beneath clusters and groves were derived from woody plants in the 0-5 cm depth increment, respectively (Table 5.3). The proportions of SOC derived from woody plants beneath woody patches decreased throughout the soil profile (Table 5.3); however, even in the 80-120 cm depth increment, 6.52% and 8.44 % of SOC was derived from woody plants in clusters and groves, respectively (Table 5.3).

Pattern of spatial heterogeneity in SOC density throughout the soil profile

Visual comparison of the kriged map of SOC density in the 0-5 cm depth increment (Fig. 5.5) with aerial photography of this landscape (Fig. 5.1) reveals a strong resemblance of the spatial pattern of SOC density to that of vegetation cover. SOC densities were highest at the centers of woody patches, decreased towards the canopy edges of woody patches, and reached lowest values within the grassland matrix (Fig. 5.1 and 5.5). However, this strong pattern became weaker in the 5-15 cm depth increment, and grew less distinct with increasing depth throughout the soil profile (Fig. 5.1 and 5.5). In fact, SOC density in the 0-5 cm depth increment ranged from 5.35 to 73.90 kg C m^{-3}, and had a higher variability (coefficient of variation (CV) = 71.61%) than other depth increments (CVs range from 13.75% ~ 27.54%). Lacunarity analysis based on kriged maps also indicated that the 0-5 cm depth increment had significantly higher lacunarity values than other depth increments (Fig. 5.6), indicating that the 0-5 cm depth increment had a spatially more heterogeneous distribution of SOC density across this landscape.

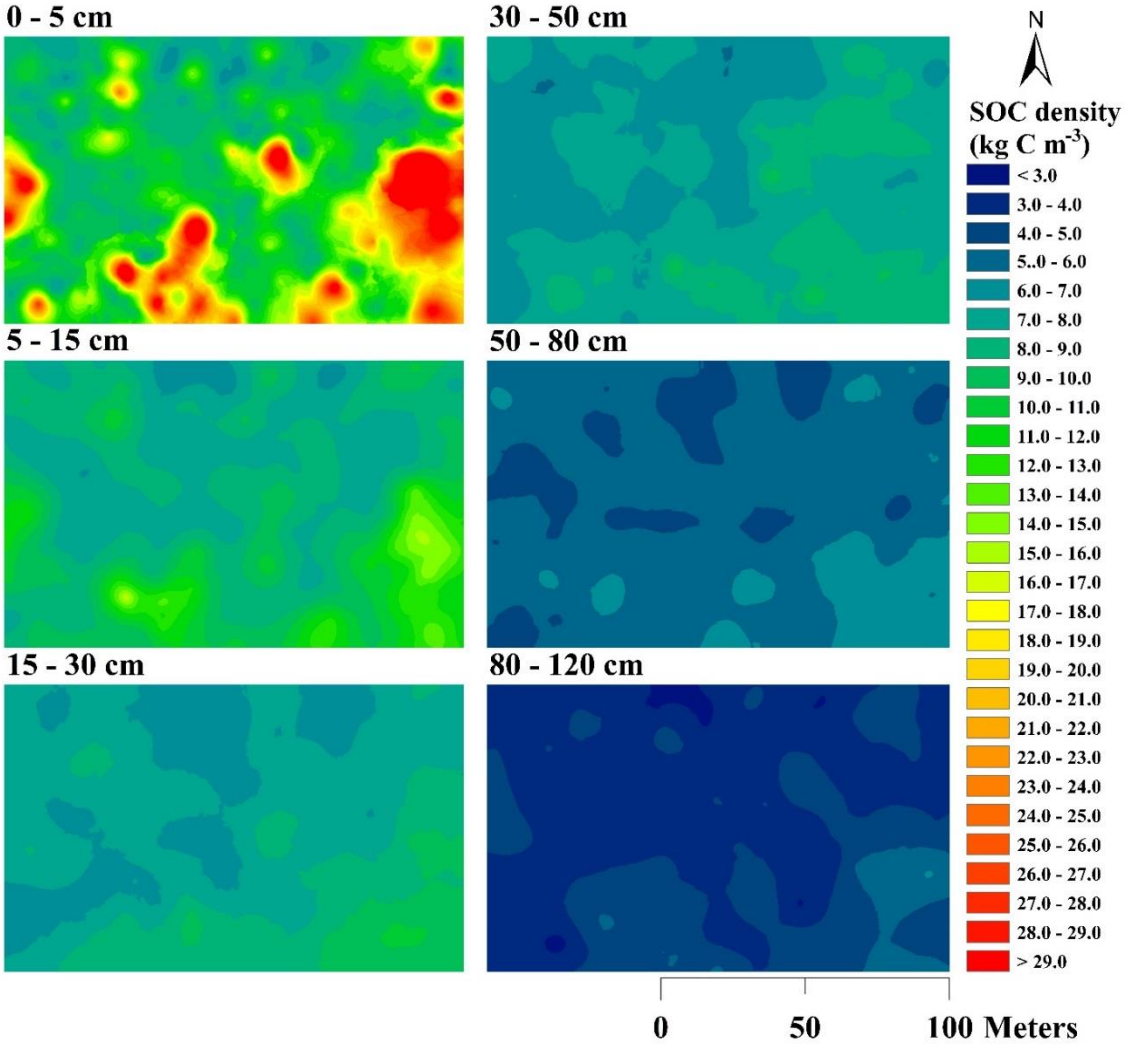

Figure 5.5 Kriged maps of SOC density (kg C m^{-3}) based on 320 randomly located sampling points for this 160 m × 100 m landscape throughout the soil profile.

Spatial generalized least squares models revealed that vegetation factors (i.e. NDVI and fine root density), especially fine root density, were the most important explanatory variables for variation in SOC density in the 0-5 and 5-15 cm depth increments (Table 5.4). However, from 15 to 120 cm in the soil profile, a combination of vegetation factors and soil physical factors, especially soil clay content, were responsible for the variation in SOC density across this landscape (Table 5.4).

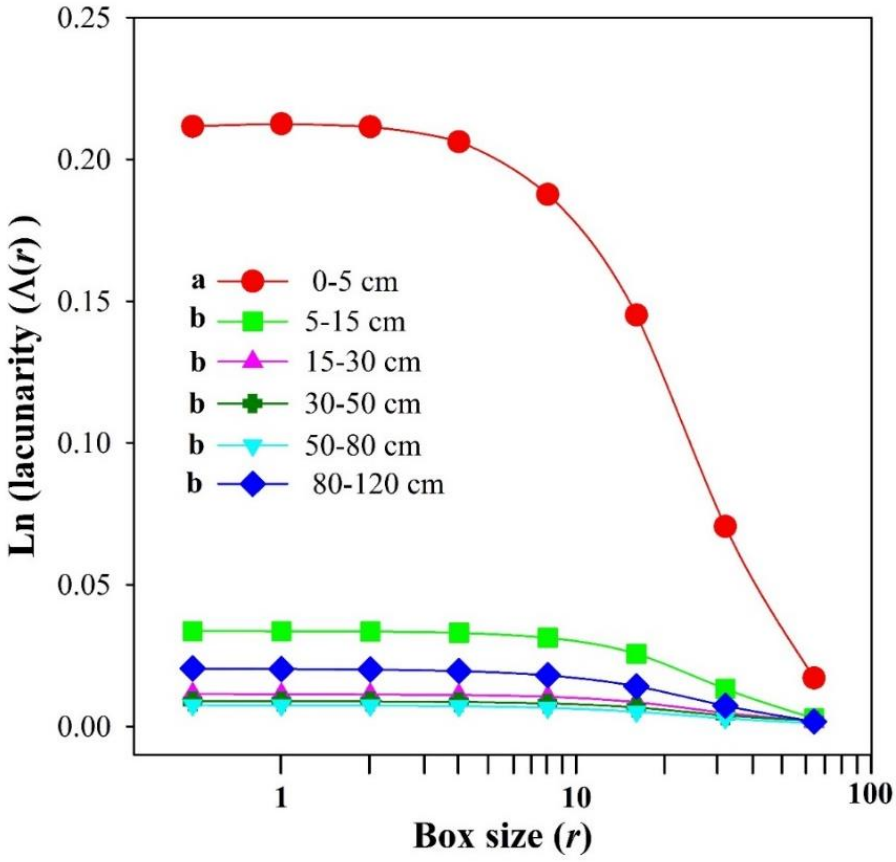

Figure 5.6 Lacunarity curves throughout the soil profile derived from kriged maps of SOC density. Significant differences ($p < 0.05$) between different soil depth increments were detected based on one-way ANOVA (student's t-test) and indicated with different letters.

Table 5.4 Best fit regressions for SOC density (kg C m^{-3}) as the response variable explained by explanatory variables according to spatial generalized least squares (GLS) models. Explanatory variables are vegetation variables including NDVI, fine root density (kg m^{-3}) (FRD), and soil physical variables including soil bulk density (g cm-3) (SBD), soil clay (%) and silt (%) contents, and soil pH.

Depth (cm)	Parameters	Vegetation variables		Soil physical variables			
		NDVI	FRB	SBD	Clay	Silt	pH
0-5	Coefficients	**8.03**	**1.28**	-0.38	-0.22	0.70	-1.48
	t	**2.48**	**10.06**	-0.11	-0.80	1.80	-1.06
	p	**0.01**	**<0.0001**	0.91	0.42	0.07	0.29
5-15	Coefficients	**2.16**	**0.57**	-2.04	0.09	0.20	**0.66**
	t	**2.65**	**9.22**	-1.69	1.50	1.74	**2.11**
	p	**0.008**	**<0.0001**	0.09	0.13	0.08	**0.03**
15-30	Coefficients	**1.29**	**0.57**	**4.28**	**0.17**	0.13	**0.35**
	t	**2.94**	**9.78**	**5.45**	**5.70**	1.84	**2.10**
	p	**0.004**	**<0.0001**	**<0.0001**	**<0.0001**	0.07	**0.04**
30-50	Coefficients	**1.71**	**0.50**	**5.15**	**0.19**	**0.26**	**-0.34**
	t	**3.96**	**5.64**	**5.63**	**10.38**	**4.54**	**-1.90**
	p	**0.0001**	**<0.0001**	**<0.0001**	**<0.0001**	**<0.0001**	**<0.0001**
50-80	Coefficients	0.54	**0.25**	0.91	**0.06**	**0.12**	0.02
	t	1.86	**2.18**	1.41	**4.15**	**2.82**	0.11
	p	0.06	**0.03**	0.16	**<0.0001**	**0.01**	0.91
80-120	Coefficients	0.56	**0.46**	-0.90	**0.03**	0.04	**1.41**
	t	1.89	**3.10**	-0.98	**2.24**	0.89	**3.55**
	p	0.06	**0.002**	0.33	**0.03**	0.38	**0.0004**

Bold text indicates significant variables ($p < 0.05$)

DISCUSSION

Increased SOC sequestration throughout the profile

Overall, our results indicate grassland-to-woodland conversion substantially increased SOC sequestration which is consistent with other studies in South America (e.g.

González-Roglich *et al.* 2014), Australia (e.g. Daryanto *et al.* 2013a), South Africa (e.g. Blaser *et al.* 2014; Chiti *et al.* 2017), and Europe (e.g. Maestre *et al.* 2009). More importantly, we observed that SOC sequestration following woody encroachment occurred at considerable soil depth, albeit to a lesser degree in deeper portions of the soil profile. Thus, these results support our first hypothesis.

Although the 0-15 cm depth increment stored only around 20% of the cumulative SOC stock in the full 120 cm soil profile (Table 5.2), it accounted for more than half (57.75 % and 59.23 % for clusters and groves, respectively, Fig. 5.3b) of all the SOC sequestered following woody encroachment. Strong changes in topsoil C stock with increasing woody plant abundance have been observed in many grassland/savanna ecosystems around the world (see Barger *et al.* 2011; Eldridge *et al.* 2011; Blaser *et al.* 2014; Li *et al.* 2016 for reviews), with C accretion rates ranging from negative up to > 100 g C m^{-2} $year^{-1}$ depending on the encroaching species, stand age, land management practice, mean annual precipitation, and soil sampling depth. Our estimated accumulation rates for both groves (41.5 g C m^{-2} $year^{-1}$) and clusters (38.8 g C m^{-2} $year^{-1}$) (Fig. 5.4) are higher than those estimated using a chronosequence approach spanning the past 120 years for this area (10-30 g C m^{-2} $year^{-1}$ to 15 cm depth, Liao *et al.* 2006), but are within the range of values reported in reviews (Barger *et al.* 2011; Blaser *et al.* 2014). However, any attempts to account for relatively small temporal changes in SOC within such large soil volumes are subject to errors from amplified spatial variations in SOC in encroached ecosystems (Throop & Archer 2008; Liu *et al.* 2011) and climatic variations during the sampling time period.

The results from this study also reveal that substantial SOC sequestration occurs in deeper portions of the soil profile following woody encroachment (Fig. 5.3b). Apart from dissolved organic C and soil faunal bioturbation, plant roots and root exudates are the primary sources of C input in subsoil (Jobbágy & Jackson 2000; Rumpel & Kögel-Knabner 2011). Plant growth forms differ in their rooting patterns, with trees/shrubs having root systems that are larger and deeper than grasses (Jackson *et al.* 1996; Schenk 2006). Thus, grassland to woodland conversions are expected to alter the depth and distribution of plant roots, and influence SOC stocks. In this study, we found significantly higher fine and total root densities beneath woody patches than beneath grasslands throughout the entire soil profile (Fig. 5.2). Even in the 80-120 cm depth increment, mean fine root densities of woody patches were still more than 2 times higher than those of grasslands (Fig. 5.2a). Considering the relatively rapid turnover rate of fine roots (Gill & Jackson 2000), this implies strong potential for the formation of SOC in subsoil. Lower $\delta^{13}C$ values of SOC in woody patches compared to grasslands confirm that C_3 woody plant roots are indeed contributing to SOC stocks, even at considerable soil depth (Table 5.3). However, SOC accumulation is regulated by processes influencing the balance between C inputs and losses (Six *et al.* 2002; Schmidt *et al.* 2011). In a long-term study of reforestation, subsoil losses of soil C were reported due to enhanced microbial activity and soil organic matter decomposition following vegetation cover change (Mobley *et al.* 2015). Thus, the future trajectory of SOC sequestration observed following woody encroachment in deeper portions of the soil profile remains an open question. Will the amount of SOC sequestered in subsoil be counterbalanced by the enhanced microbial

decomposition (i.e. priming) following labile C input from woody plant roots (e.g. Fontaine *et al.* 2007)? Or, will the subsoil continue to accumulate C that is derived from deep roots since organic matter protection mechanisms in the subsoil may not yet be saturated?

Amplified pattern of spatial heterogeneity in SOC in surface soil

Several studies have quantified spatial heterogeneity of soil properties after woody encroachment (e.g. Throop & Archer 2008; Bai *et al.* 2009; Liu *et al.* 2011; Daryanto *et al.* 2013b); however, none has explored the extent to which woody encroachment modifies the pattern of spatial heterogeneity in SOC in deeper soil layers. Our analyses revealed that woody encroachment significantly amplified the pattern of spatial heterogeneity in SOC in the 0-5 cm depth increment, had a smaller impact on 5-15 cm depth increment, but had no distinct influence on soils below 15 cm across this landscape. These minimal impacts at depths > 15 cm cause us to reject our second hypothesis that woody encroachment would substantially alter the pattern of spatial heterogeneity in SOC throughout the soil profile.

The spatial patterns of SOC in the 0-5 cm depth increment indicated that SOC values were highest near the centres of woody patches, decreased towards the canopy edges, and reached lowest values in grasslands (Fig. 5.5). Previous studies show that SOC accumulation is initiated once woody patches/plants establish in grasslands (Schlesinger *et al.* 1996; Maestre *et al.* 2009; Daryanto *et al.* 2013a), and that this SOC accumulation is positively correlated with the size or age of woody patches/plants (Liao *et al.* 2006; McClaran *et al.* 2008; Blaser *et al.* 2014). Therefore, our observed SOC spatial gradient

from the centre-to-edge of the woody patches likely reflects the size and/or age of the woody patch, and the rate at which it expands laterally into the grassland (Throop & Archer 2008; Bai *et al.* 2012). Based on historical accounts, tree rings, and soil $\delta^{13}C$ analyses, it is well established that the conversion of grasslands to the current landscape began in the mid to late 1800s in this area (Archer 1995; Boutton *et al.* 1998; Bai *et al.* 2009). Because the woody vegetation near the centres of clusters and groves is older (> 100 yrs.) than near the periphery of those woody patches (Bai *et al.* 2012), there has been more time for SOC to accumulate near the central portions of these woody patches compared to their peripheral areas near the boundary with grassland. Consequently, the strong SOC gradients within woody patches coupled with dramatic differences in SOC between woody patches and open grasslands creates strong pattern of spatial heterogeneity across this landscape (Fig. 5.6).

Contrary to our hypothesis, we did not observe substantial impacts of woody encroachment on the pattern of spatial heterogeneity in SOC below the 15 cm depth. However, we did find root density, the primary sources of C inputs into subsoil (Rumpel & Kögel-Knabner 2011), was significantly higher under woody patches than under grasslands (Fig. 5.2); and spatial patterns of root distribution for each depth increment strongly resembled vegetation patterns (unpublished data). In addition, the spatial patterns of soil $\delta^{13}C$ also strongly resembled vegetation pattern throughout the soil profile (unpublished data). This raises the issue of why spatial patterns of roots and soil $\delta^{13}C$ values resembled those of vegetation cover (even below 15 cm depth) while those of SOC did not. There are two possible explanations for this discrepancy.

Firstly, results from this study are a response to woody patches that are relatively young (ca. 100 years, Archer 1995; Bai *et al.* 2009) from a SOC stabilization perspective. Dynamic simulation models indicate that it may take ca. 200 years to reach plant C stabilization after woody encroachment, with SOC stabilization in the topsoil (0-20 cm) not occurring until ca. 400 after woody encroachment in this area (Hibbard *et al.* 2003). Since carbon input declines with soil depth, subsoil (below 20 cm) may need more time to reach SOC stabilization/saturation. Therefore, we predict that, without any disturbances (i.e. fire, brush management), woody encroachment into this landscape will continue to alter the spatial heterogeneity of SOC in subsoil for at least the next 400 years.

Secondly, many mechanisms have been identified to account for the accumulation/stabilization of organic matter in soils (Six *et al.* 2002; Rumpel & Kögel-Knabner 2011; Schmidt *et al.* 2011), and C dynamics in topsoil and in subsoil may be controlled by different mechanisms (Salomé *et al.* 2010). In this study, we suggest that both biological and soil physical mechanisms contribute to the reduced influence of woody encroachment on spatial patterns and heterogeneity of SOC in deeper soil layers. This suggestion is supported by spatial generalized least squares models which revealed that a combination of fine root density and soil clay content predicted more of the variability of SOC in soils below 15 cm depth (Table 5.4). These results suggest that physical protection, the intimate association of organic matter with soil minerals (i.e. clay particles) (Six *et al.* 2002), may have played an important role in SOC stabilization in subsoil across this landscape. Subsurface soils across this landscape are characterized by an argillic horizon which begins at ca. 30 cm (Loomis 1989). However, non-argillic inclusions with coarse-

textured subsoils are also present across this landscape and are usually covered by woody groves (Archer 1995; Zhou *et al.* 2017b). Thus, higher C inputs from roots beneath groves may be offset by reduced physical protection due to coarse-textured subsoils. In contrast, lower C inputs under grasslands may be more effectively protected from decay by physical protection in the clayey argillic horizon. The net outcome is a great similarity in SOC density between woody patches and grasslands in deeper soil layers. This inference is supported by our results which showed no significant difference in SOC density between woody patches and grasslands (Fig. 5.3a), and reduced SOC accumulation (Table 5.2, Fig. 5.3b) in the 30-50 cm depth increment. These smaller discrepancies in SOC between woody patches and grasslands in deep portions of the profile may reduce spatial heterogeneity at deeper soil depths.

Implications for SOC estimates following vegetation cover change

Our findings emphasize the importance of deep soil sampling to assess SOC inventories following woody encroachment, as highlighted in other land cover change studies (Don *et al.* 2011; Mobley *et al.* 2015). For example, our results showed that ca. 60% of the total SOC stock to 120 cm depth across this landscape was found in soils below 30 cm depth (the IPCC recommended sampling depth) (Table 5.2). This is consistent with global estimates which show a 50-50 split in SOC stocks between 0-30 cm and 30-100 cm depth (Batjes 1996; Jobbágy & Jackson 2000). More important, in terms of SOC sequestration, 30% of total sequestered SOC to 120 cm depth across this landscape was stored below 30 cm depth following woody encroachment (Fig. 5.3b). This implies that current terrestrial C budgets likely underestimate the potential magnitude of C

sequestration following woody encroachment due to the overlooked subsoil. Given the geographic extent of woody encroachment into grass-dominated ecosystems around the world (Eldridge *et al.* 2011; Stevens *et al.* 2017), taking deep SOC into account is critical to evaluate dryland ecosystem services in terms of climate change mitigation through C sequestration (Pacala *et al.* 2001; King *et al.* 2007; Dean *et al.* 2015). This recommendation of deep sampling to improve accurate soil C inventories also applies to studies of soil C dynamics following vegetation cover change in other ecosystem types. Since SOC accumulation/stabilization in topsoil and subsoil is controlled by different regulatory mechanism according to this and others studies (Salomé *et al.* 2010; Rumpel & Kögel-Knabner 2011; Mobley *et al.* 2015), a better understanding of these mechanisms is essential to predict the vulnerability of deep SOC to vegetation cover change. Meanwhile, the amplified pattern of spatial heterogeneity in SOC density in the 0-5 cm depth increment following woody encroachment emphasizes that the majority of soil C studies working on surface soils should consider appropriate sample distribution and intensity to account for spatial heterogeneity and uncertainty of SOC in landscapes where complex vegetation cover exist. Limited sample sizes or inappropriate sample regimes that fail to capture the spatial gradient from centre to canopy edge of patchy vegetation (Throop & Archer 2008; Liu *et al.* 2011) may subsequently overestimate or underestimate the impact of vegetation cover change on SOC stocks and dynamics.

CONCLUSIONS

We found that woody encroachment into this landscape increased SOC storage throughout the upper 1.2 m of the soil profile, and 30% of the C sequestered following

encroachment was stored below 30 cm. This highlights the merit and necessity of deep soil sampling to quantify SOC stocks and dynamics, which are not accounted for in the majority of soil C inventories following land cover/ land use change (Don *et al.* 2011). In addition, we found that woody encroachment into this landscape significantly altered the pattern of spatial heterogeneity in SOC in topsoil. However, spatial heterogeneity in subsoil SOC was less distinct and not related to vegetation distribution, perhaps due to variation in subsoil texture across the landscape, and/or inadequate time for deep soil carbon pools to respond to the relatively recent (ca. 100 years) woody plant encroachment. Given the global extent of land cover change, these findings have important implications for current terrestrial C inventories/models and future management of SOC stock to mitigate climate change.

CHAPTER VI

WOODY PLANT ENCROACHMENT AMPLIFIES SPATIAL HETEROGENEITY OF SOIL PHOSPHORUS TO CONSIDERABLE DEPTH*

SYNOPSIS

The geographically extensive phenomenon of woody plant encroachment into grass-dominated ecosystems has strong potential to influence biogeochemical cycles at ecosystem to global scales. Previous research has focused almost exclusively on quantifying pool sizes and flux rates of soil carbon and nitrogen (N), while few studies have examined the impact of woody encroachment on soil phosphorus (P) cycling. Moreover, little is known regarding the impact of woody encroachment on the depth distribution of soil total P at the landscape scale. We quantified patterns of spatial heterogeneity in soil total P throughout a soil profile by taking spatially-explicit soil cores to a depth of 120 cm across a subtropical savanna landscape that has undergone encroachment by *Prosopis glandulosa* (an N_2-fixer) and other tree/shrub species during the past century. Soil total P increased significantly following woody encroachment throughout the entire 120 cm soil profile. Large groves (> 100 m^2) and small discrete clusters (< 100 m^2) accumulated 53 and 10 g P m^{-2} more soil P, respectively, compared to grasslands. This P accumulation in soils beneath woody patches is most likely attributable

* Originally published as: Zhou, Y., Boutton, T.W., & Wu, X.B. (2018) Woody plant encroachment amplifies spatial heterogeneity of soil phosphorus to considerable depth. *Ecology*, **99**, 136-147. The publication is available at http://onlinelibrary.wiley.com/doi/10.1002/ecy.2051/full.

to P uplift by roots located deep in the soil profile (> 120 cm) and transfer to upper portions of the profile via litterfall and root turnover. Woody encroachment also altered patterns of spatial heterogeneity in soil total P in the horizontal plane, with highest values at the centers of woody patches, decreasing towards the edges, and reaching lowest values in the surrounding grassland matrix. These spatial patterns were evident throughout the upper 1.2 m of the soil profile, albeit at reduced magnitude deeper in the soil profile. Spatial generalized least squares models indicated that fine root biomass explained a significant proportion of the variation in soil total P both across the landscape and throughout the profile. Our findings suggest that transfer of P from deeper soil layers enlarges the P pool in upper soil layers where it is more actively cycled may be a potential strategy for encroaching woody species to satisfy their P demands.

INTRODUCTION

In terrestrial ecosystems, nitrogen (N) and phosphorus (P) are generally the most limiting nutrients for primary production and other major biological processes (Vitousek et al. 2010). Although P stocks and dynamics are relatively well studied in humid ecosystems (i.e. Walker & Syers 1976; Hobbie & Vitousek 2000; Cleveland *et al.* 2002; Vitousek 2004), the P cycle in more water-limited arid and semiarid ecosystems remains poorly understood (Selmants & Hart 2010), particularly with respect to responses to anthropogenic disturbances such as woody encroachment and climate change. Given that drylands cover about 41% of Earth's land surface (Reynolds *et al.* 2007) and play a major role in global biogeochemical cycles (Poulter *et al.* 2014), a more thorough understanding of P distribution patterns and dynamics in these ecosystems is essential for the

development of integrated climate-biogeochemical models that incorporate P cycle properties and processes (Yang *et al.* 2013; Reed *et al.* 2015; Achat *et al.* 2016; Sun *et al.* 2017).

Arid and semiarid ecosystems around the world have experienced woody plant proliferation during the past 100 years due to overgrazing, fire suppression, rising atmospheric CO_2 concentrations, and/or long-term climate change (Van Auken 2009; Eldridge *et al.* 2011; Stevens *et al.* 2017). In these ecosystems, vegetation patchiness serves as a key regulator of P redistribution during soil and ecosystem development, often resulting in islands of fertility beneath tree/shrub canopies (Schlesinger *et al.* 1996). This is especially true for ecosystems dominated or encroached by symbiotic N_2-fixing trees or shrubs with high canopy area (e.g., *Prosopis* in North America and *Acacia* in Africa) which generally have a high P requirement and accumulate significant amounts of P in their biomass (Vitousek *et al.* 2002; Houlton *et al.* 2008). Unlike N, which accumulates rapidly from the atmosphere via biological N_2-fixation, P in terrestrial ecosystems is derived ultimately from weathering of parent material (Walker & Syers 1976; Vitousek 2004; Schlesinger & Bernhardt 2013). Since ecosystems begin their existence with a fixed amount of P from soil parent materials (Walker & Syers 1976) and new atmospheric inputs are relatively low (Mahowald *et al.* 2008), significant accumulation of P in plant biomass could lead to depletion of P within the soil.

More recently, some field studies have shown that N_2-fixing woody plants encroaching into grasslands actually increase P storage in topsoil beneath their canopies (e.g. Kantola 2012; Sitters *et al.* 2013; Blaser *et al.* 2014). This increase in surface soil is

likely a consequence of P acquisition from root activity in deeper portions of the soil profile (Kantola 2012; Sitters *et al.* 2013; Blaser *et al.* 2014), or from lateral roots in the surface soil that spread beyond the woody canopy (Scholes & Archer 1997). Sitters *et al.* (2013) and Blaser *et al.* (2014) found no evidence of depletion of either total or extractable P in topsoil beyond the boundaries of woody patches in grasslands, suggesting P accrual in the topsoil underneath woody patches is almost certainly derived from P acquisition by roots located deep in the soil profile. Since trees/shrubs typically have much deeper rooting systems than herbaceous species (Jackson *et al.* 1996; Schenk 2006), it is reasonable to presume that amplified P dynamics are occurring not only in topsoil, but also deeper in the soil profile following shifts in plant functional composition. However, with most studies focused solely on topsoil ($\leq$ 15 cm), there is a knowledge gap regarding the potential for changes in soil P stocks in deeper portions of the soil profile following grassland to woodland transitions in drylands around the world.

Woody encroachment into grass-dominated ecosystems has been shown to alter patterns of spatial heterogeneity in surface soil C and N storage at scales ranging from the patch to the landscape (Jackson & Caldwell 1993; Schlesinger *et al.* 1996; Throop & Archer 2008; Liu *et al.* 2011; Zhou *et al.* 2017a). The fact that the biogeochemical cycles of C, N and P are interlinked by their strong stoichiometric relationships (Finzi *et al.* 2011; Reed *et al.* 2015), together with observed accrual of topsoil total P underneath woody patches (e.g. Kantola 2012; Sitters e*t al.* 2013; Blaser *et al.* 2014), suggests that spatial patterns of total P in surface soil are likely altered by woody plant encroachment into grasslands, though this has not been explicitly investigated. Deep soil cores at the

ecosystem level (e.g. forestland, grassland, and cropland) have shown that soil total P decreases gradually with soil depth (McCulley *et al.* 2004b; Yang *et al.* 2012; Li *et al.* 2016b), implying that potentially strong spatial gradients of soil total P may exist throughout the soil profile at the landscape scale in complex ecosystems with different plant life forms. However, no study has assessed the extent to which woody encroachment into grasslands alters the spatial pattern of soil total P in deeper portions of the profile at the landscape scale.

The primary purpose of this study was to assess how woody encroachment into grasslands alters the direction, magnitude, and patterns of spatial heterogeneity in soil total P across the landscape and throughout the soil profile. To this end, we collected spatially explicit soil cores to a depth on of 120 cm and analyzed them for total P across a 100 m × 160 m subtropical savanna landscape which has undergone encroachment by *Prosopis glandulosa* (an N_2-fixer) and other trees/shrubs during the past century. Our specific objectives were to: (1) estimate changes in direction and magnitude of soil total P throughout the soil profile after woody encroachment; (2) quantify patterns of spatial heterogeneity in soil total P across this landscape and throughout the soil profile; and (3) elucidate factors responsible for the variance in soil total P across this landscape and throughout the soil profile. We hypothesized that woody plant encroachment would (i) increase soil total P only in surface soils, with no changes or even a decrease in deeper portions of the soil profile; and, correspondingly (ii) alter spatial patterns of soil total P only in surface soils, with marginal to no effects in subsurface soils.

MATERIALS AND METHODS

Study site

This study was conducted at the Texas A&M AgriLife La Copita Research Area (27˚40′N, 98˚12′W), 65 km west of Corpus Christi, Texas, USA. The climate is subtropical (mean annual temperature is 22.4 ˚C; mean annual precipitation is 680 mm), and rainfall peaks occur in May and September. Topography is relatively flat, with gentle slopes (< 3%) where well-drained uplands transition to lower-lying drainage woodlands. Elevation ranges from 75 to 90 m a.s.l.

Upland soils are sandy loams with non-argillic inclusions embedded within a laterally continuous subsurface argillic horizon (Bt) (Loomis 1989; Watts 1993; Archer 1995; Zhou *et al.* 2017b). Vegetation is characterized by a two-phase pattern consisting of woody patches interspersed within a matrix of remnant C_4 grasslands. Studies using historical aerial photos, tree rings, coupled $\delta^{13}C$ and natural ^{14}C measurements on soil organic carbon, and simulation models have all indicated that woody plant encroachment into these grasslands, which were once almost exclusively dominated by C_4 grasses, occurred over the past 100 years (Archer 1995; Boutton *et al.* 1998 and 1999; Bai *et al.* 2009). Woody encroachment is initiated when grasslands are colonized by *Prosopis glandulosa* (honey mesquite), an N_2-fixing tree legume. As mesquite trees grow, they serve as nurse plants, facilitating the recruitment and establishment of other woody plant species in their understory to form discrete clusters (generally < 100 m^2) (Archer *et al.* 1988; Archer 1995; Bai *et al.* 2012). If discrete clusters occur on non-argillic inclusions, they expand laterally and ultimately fuse to form large groves (generally > 100 m^2)

(Archer 1995; Bai *et al.* 2012; Zhou *et al.* 2017b). Clusters occurring where the argillic horizon is present remain as small isolated patches and do not fuse with other clusters to form groves. Though large groves are restricted to non-argillic inclusions, they also expand their canopies laterally beyond these inclusions to soils with subsurface argillic horizon (Archer 1995; Zhou *et al*. 2017b). Species composition can be found in Appendix A.

Field sampling

On an upland portion of this study site, a 100 m × 160 m landscape consisting of 10 m × 10 m grid cells was established in January 2002 (Bai *et al.* 2009; Liu *et al.* 2011), and included all three of the upland landscape elements: grasslands, clusters and groves (Fig. 6.1). The corners of each 10 m × 10 m grid cell were georeferenced (UTM 14 N, WGS 1984) using a GPS unit (Trimble Pathfinder Pro XRS, Trimble Navigation limited, Sunnyvale, CA). A color-infrared aerial photograph (6 cm x 6 cm resolution) was acquired for this landscape in July 2015, and used to create a classified vegetation map for the site.

In July 2014, two points were selected randomly within each 10 m × 10 m grid cell, yielding a total of 320 sample points (Fig. 6.1). The distance from each sample point to two georeferenced cell corners were recorded. At each sample point, the landscape element was classified as grassland, cluster or grove based on the vegetation type and size of woody canopy area, and two adjacent soil cores (2.8 cm in diameter ×120 cm in length) were collected using the PN150 JMC Environmentalist's Subsoil Probe (Clements Associates Inc., Newton, IA). Each soil core was subdivided into six depth increments (0-5, 5-15, 15-30, 30-50, 50-80, and 80-120 cm). One soil core was oven-dried (105 ˚C for

48 hours) to determine soil bulk density. The other core was air-dried prior to subsequent analyses. In September 2015, fine roots from each plant species occurring on this landscape were collected by careful soil excavations that confirmed linkages to identified plant species.

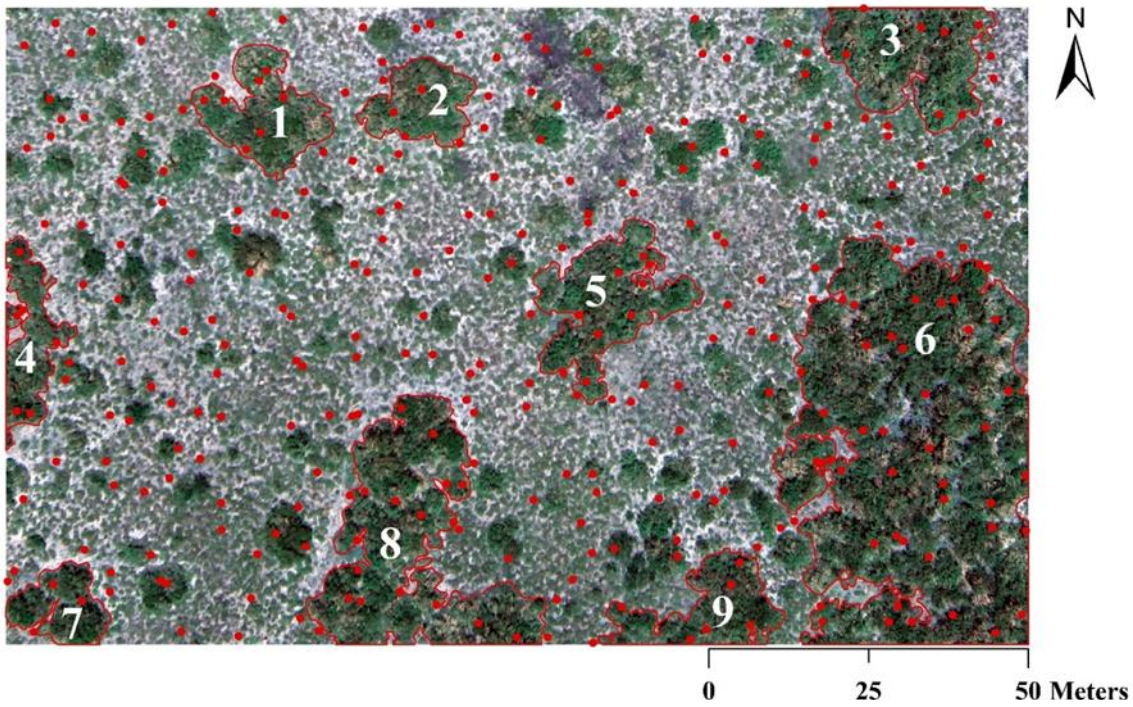

Figure 6.1 Aerial photograph of the 160 m × 100 m study area. Red dots indicate 320 random soil sampling points. Green patches are woody clusters and groves, while light grey areas indicate open grasslands. Groves are highlighted with red lines and labeled with numbers.

Lab analyses

Soils used to determine bulk density were subsequently used to estimate fine (< 2 mm) and coarse (> 2mm) root biomass by washing through sieves. Soils from the air-dried

cores were passed through a 2 mm sieve; roots and other coarse organic fragments not passing throught the sieve were discarded. No soils contained rock or gravel-sized particles. Soil pH was determined on a 1: 2 (10 g soil: 20 mL 0.01 mol/L $CaCl_2$) mixture using a glass electrode. Soil texture was determined by the hydrometer method (Sheldrick & Wang 1993). An aliquot of air-dried, sieved soil was dried at 60 ˚C for 48 hours and pulverized in a centrifugal mill (Angstrom, Inc., Belleville, MI) in preparation for subsequent chemical analyses. Fine roots from each species were washed carefully to remove soil particles, dried, and pulverized.

Total P concentrations in pulverized soils and fine roots were determined using the lithium fusion method (Lajtha *et al.* 1999). Briefly, 0.25 g of pulverized soil or root tissue was mixed with 0.75 g of pure lithium metaborate ($LiBO_2$) (Spex Sample Prep, Metuchen, NJ) in precombusted graphite crucibles, and heated to 1050 ºC in a muffle furnace. The molten flux was poured into a 150 mL beaker containing a magnetic spin bar and 50 mL of 10 % HNO_3, placed on a stir plate, and a watch glass was placed over the beaker while the flux was stirred and completely dissolved. The dissolved solution was filtered (Whatman 42 ashless filters), transferred to a volumetric flask, and made up to 100 mL with Type 1 water. Then, 30 mL of the solution was pipetted into a 50 mL volumetric flask and its *p*H was adjusted by adding 4 mol L^{-1} NaOH. The P concentration of the solution was determined by the molybdenum blue colorimetry method (Murphy and Riley 1962). The concentration of P was measured on a Spectronic $20D^+$ spectrophotometer (Thermo Fisher Scientific, Inc., Waltham, MA, USA) and referenced with a standard curve of potassium phosphate solution (KH_2PO_4 at 0, 0.125, 0.25, 0.375, 0.5, and 0.625

μg P ml^{-1}). To control the quality of soil total P concentration analysis, one method blank was included within each batch of samples (1 blank + 11 samples). A NIST-certified standard reference material (San Joaquin soil, NIST SRM 2709a with certified total P concentration = 688 mg P kg^{-1}) was analyzed periodically to check the accuracy of this method (mean = 678.71 mg P kg^{-1}, SE = 1.57 mg P kg^{-1}, n = 25). In addition, we developed an internal lab soil standard that was analyzed with each batch of 11 samples to verify the repeatability of this method (Mean = 103.10 mg P kg^{-1}, SE = 0.14 mg P kg^{-1}, maximum = 108.39 mg P kg^{-1}, minimum = 98.20 mg P kg^{-1}, n = 151).

Data analyses

Since P is derived primarily from weathering of parent material, soil development exerts strong control over the status of P in an ecosystem. Pedogenic formation of non-argillic inclusions embedded into the laterally continuous subsurface argillic horizon across this landscape may leave a legacy effect on the distribution pattern of total P in soil prior to the encroachment of woody plants. At this site, groves occur exclusively on non-argillic inclusions and expand laterally to soils with a subsurface argillic horizon; however, some non-argillic inclusions in the remnant grassland matrix are still not occupied by groves across this landscape (Zhou *et al.* 2017b). Thus, we subdivided soil cores from grasslands into those on non-argillic inclusions and those on argillic horizons to address potential differences in soil total P that might be inherited from soil development. Across this study site, clay illuviation generally starts at approximately 30 cm below the surface soil (Archer 1995). According to horizons and characteristics diagnostic for the higher catergories in USDA Soil Taxonomy (Soil Survey Staff, 1999),

we used the following modified criteria to test whether there is clay illuviation (or argillic horizon) in the 30-50 cm depth increment: (1) if the clay content in the prior depth increment (i.e. 15-30 cm) is less than 15%, the 30-50 cm depth increment must contain at least 3% (absolute) more clay; or (2) if the clay content in the prior depth increment (i.e. 15-30 cm) is between 15-40%, the 30-50 cm depth increment must have at least 1.2 times more clay. These criteria were also used to test the 50-80 and 80-120 cm depth increments. If one or more of these three depth increments from a soil core have clay illuviation, then we considered the argillic horizon to be present at that point. Where the argillic horizon was present, it generally began within the 30-50 cm depth increment; in a few cases, it did not begin until the 50-80 cm increment.

Mixed models were used to compare total P concentrations (g P kg^{-1} soil), stocks (g P m^{-2}), cumulative stocks, and fine root biomass (g m^{-2}) in different landscape elements within each depth increment. In mixed models, spatial autocorrelation of a variable was considered as a spatial covariance component for adjustment. *Post hoc* comparisons of these variables in different landscape elements were conducted with Tukey's test. An unpaired t-test was performed to compare total P concentration in grasslands occurring on argillic vs. non-argillic soils within each depth increment. A cutoff value of $p < 0.05$ was used to indicate significant differences. All these statistics were performed using JMP pro 12.0 (SAS Institute Inc., Cary, NC, USA).

A sample variogram fitted with a variogram model was constructed to quantify the spatial structure of soil total P stocks based on 320 random samples for each soil depth increment using R statistical software (R Development Core Team 2014). Ordinary

kriging was used to predict soil total P stocks at unsampled locations based on the best fitting variogram model using ArcMap 10.2.2 (ESRI, Redlands, CA, USA), and kriged maps of soil total P stocks with a 0.5 m × 0.5 m resolution were generated for each soil depth increment. Lacunarity was used to assess the spatial heterogeneity of soil total P concentration across this landscape and throughout the soil profile. Lacunarity is a scale-dependent measurement of spatial heterogeneity or the "gappiness" of a landscape structure (Plotnick *et al.* 1996), with a higher value indicating a more heterogeneous distribution pattern across the landscape. Lacunarity was calculated using R statistical software (R Development Core Team 2014).

Within each soil depth increment, a spatial generalized least squares (GLS) model that incorporated spatial structure in the error term of the regression model (Beale et al. 2010) was used to analyze the relationships between soil total P concentration and explanatory variables, including fine root biomass, soil bulk density, soil clay and silt contents, and soil pH. Values for these explanatory variables have been presented elsewhere (Table 5.1). Different models of spatial structure (i.e. linear, spherical, exponential, Gaussian structure) and non-spatial structure were tested, and the best fitting model was selected using the Akaike Information Criterion (AIC). Parameters were estimated based on restricted maximum likelihood (REML). In each full regression model for each soil depth increment, *t*-values for explanatory variables were used to indicate their relative importance in explaining the response variable (Diniz-Filho *et al.* 2003). Analyses were performed using R statistical software (R Development Core Team 2014).

RESULTS

Phosphorus concentrations in fine roots were 65% higher in woody species (447.4 ± 31.7 mg P kg^{-1}, n =15) than in herbaceous species (270.5 ± 26.0 mg P kg^{-1}, n = 22) (Fig. 6.2a). It is worth noting that the dominant woody species, *P. glandulosa*, had the highest fine root P concentration (640.1 mg P kg^{-1}) among all species collected across this landscape (Fig. 6.2a and Appendix A).

Fine root biomass in soils beneath woody patches (both groves and clusters, hereafter) ranged from > 500 g m^{-2} in upper portions of the profile to approximately 220 g m^{-2} in the deepest portions (Fig. 6.2b). In contrast, fine root biomass in grassland soils ranged from approximately 200 g m^{-2} in the upper profile to 120 g m^{-2} in deeper portions of the profile (Fig. 6.2b).

Both woody patch types had remarkably higher soil total P concentrations than those of grasslands for all soil depth increments, and groves had significantly higher soil total P concentrations than those of clusters throughout the soil profile (Fig. 6.3a). Soil total P concentrations of grasslands on non-argillic inclusions were not significantly different from those on argillic horizon throughout the soil profile (Fig. 6.3b). Soil total P concentrations decreased with depth throughout the soil profile for all landscape elements, and showed slight enrichment in the 30-50 cm soil depth increment where the argillic horizon begins (Fig. 6.3a). Woody patches had higher soil total P stocks (g P m^{-2}) than those of grasslands throughout the soil profile (Table 6.1a), with groves and clusters accumulating 52.88 and 9.59 g m^{-2} more P, respectively, than grasslands in the full 120 cm soil profile (Table 6.1b).

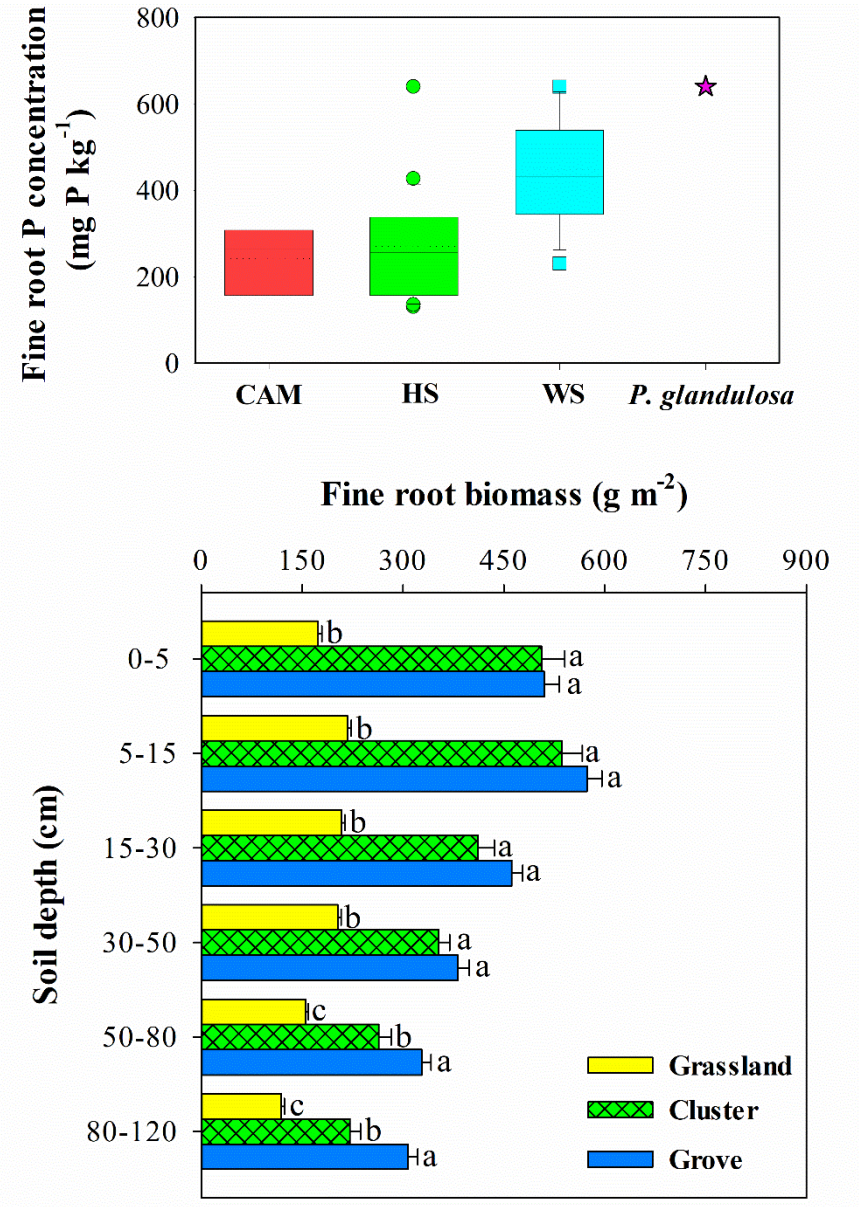

Figure 6.2 Phosphorus concentrations of fine roots from different plant functional group and *Prosopis glandulosa* (a). The central box shows the inter-quartile range, and the horizontal line within the box is the median. Lower and upper error bars indicate 10th and 90th percentiles, and points above and below the error bars are individuals above the 90th or below the 10th percentiles. CAM, crassulacean acid metabolism species, n = 3; HS, herbaceous species (forbs and grasses), n = 21; WS, woody species (including P. glandulosa), n = 15. (b) Fine root biomass (mean and SE) for different landscape elements throughout the soil profile. Significant differences ($P < 0.05$) between means for landscape elements are indicated with different letters. Number of samples: grassland, 200; cluster, 41; grove, 79.

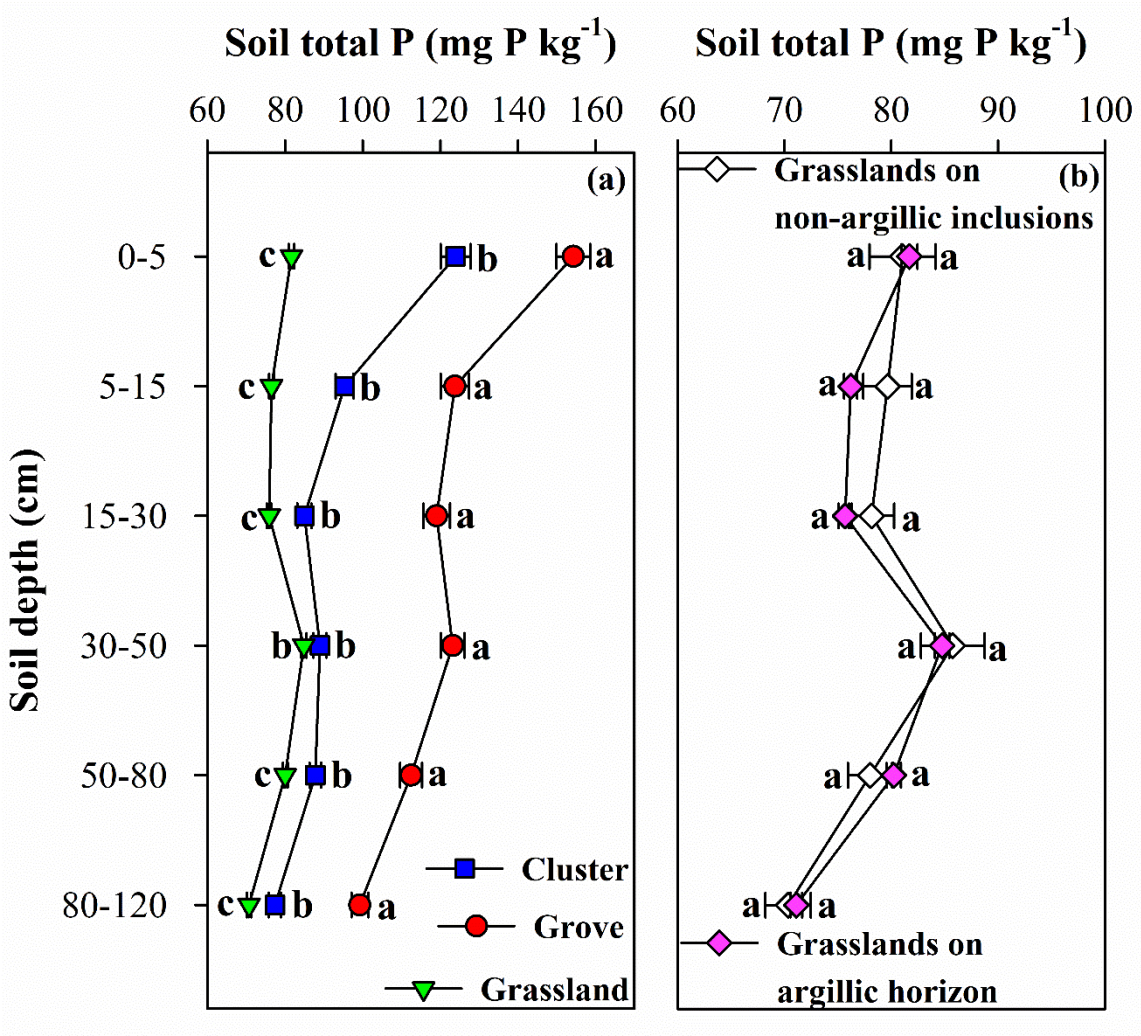

Figure 6.3 Soil total P concentrations (mean ± SE) for different landscape elements throughout the soil profile (a) and for grasslands on non-argillic inclusions and on argillic horizon (b). Significant differences ($P < 0.05$) between means for landscape elements are indicated with different letters. Number of samples: grassland, 200; cluster, 41; grove, 79; grasslands on non-argillic inclusions, 17; grasslands on argillic horizon, 183.

Table 6.1 Soil total P stocks within each depth increment (a), and cumulative soil total P stock (b) in different landscape elements across this subtropical savanna

Soil depth (cm)	Grassland	Cluster	Grove
(a) *Soil total P stock (g P m^{-2})*			
0-5	5.44 ± 0.05^{c}	6.74 ± 0.19^{b}	8.36 ± 0.23^{a}
5-15	10.97 ± 0.08^{c}	12.21 ± 0.23^{b}	16.14 ± 0.48^{a}
15-30	16.09 ± 0.13^{b}	17.33 ± 0.35^{b}	24.45 ± 0.73^{a}
30-50	24.79 ± 0.19^{b}	25.39 ± 0.46^{b}	35.19 ± 0.87^{a}
50-80	36.53 ± 0.27^{c}	39.13 ± 0.62^{b}	49.54 ± 1.17^{a}
80-120	45.99 ± 0.33^{c}	49.16 ± 0.89^{b}	63.12 ± 1.34^{a}
(b) *Cumulative soil total stock (g P m^{-2})*			
Surface to 5 cm	5.44 ± 0.05^{c}	6.74 ± 0.19^{b}	8.36 ± 0.23^{a}
Surface to 15 cm	16.41 ± 0.11^{c}	18.95 ± 0.37^{b}	24.50 ± 0.65^{a}
Surface to 30 cm	32.50 ± 0.21^{c}	36.28 ± 0.63^{b}	48.95 ± 1.32^{a}
Surface to 50 cm	57.28 ± 0.36^{c}	61.67 ± 0.95^{b}	84.14 ± 2.13^{a}
Surface to 80 cm	93.81 ± 0.58^{c}	100.80 ± 1.44^{b}	133.68 ± 3.21^{a}
Surface to 120 cm	130.34 ± 0.83^{c}	139.93 ± 2.00^{b}	183.22 ± 4.34^{a}

Notes: Vales are mean ± SE. Number of samples: grassland = 200, cluster = 41, and grove = 79. Significant differences ($P < 0.05$) between means for landscape elements are indicated with different superscript letters.

The spatial patterns of soil total P stocks revealed in the kriged maps for each soil depth displayed strong resemblance to aboveground vegetation spatial patterns readily discernable in the classified vegetation map derived from the aerial photograph of this landscape (Fig. 6.4). This coincidence of vegetation and soil P spatial patterns is particularly strong where groves occur. Soil total P stocks were highest at the centers of woody patches, decreased towards the canopy edges of woody patches, and reached lowest values within grassland matrix. Though this pattern was clearly evident in each depth increment throughout the entire 1.2 m profile (Fig. 6.4), lacunarity analysis indicated that spatial heterogeneity of soil total P across this landscape decreased with soil depth, with

topsoil (0-30 cm) having higher spatial heterogeneities than those of subsoil (30-120 cm) (Fig. 6.5). Spatial GLS models revealed that fine root biomass explained a significant portion of the variation in soil total P concentrations across this landscape and throughout the soil profile, especially for the 0-5 cm and 5-15 cm depth increments (Table 6.2). In addition, soil *p*H also emerged as an important factor explaining variation in soil total P across this landscape at soil depths > 15 cm (Table 6.2). Soil bulk density was negatively correlated with soil total P throughout the profile, reflecting the fact that woody patches had lower bulk densities than grasslands (Table 5.1), whereas soil silt and clay concentrations were not consistently related to soil total P (Table 6.2).

Table 6.2 Best fit regression models for prediction of soil total P concentration (mg P/kg, log10-transformed) by vegetation and soil variables using spatial generalized least squares (GLS) models with Akaike information criterion (AIC) as model selection for each depth increment. Explanatory variables are fine root biomass (g m^{-2}) and soil physical variables, including soil bulk density (g cm^{-3}) (SBD), soil clay (%) and silt (%) content, and soil pH.

Depth (cm)	Parameters	Fine root biomass	Soil physical variables			
			SBD	Clay	Silt	pH
0-5	Coefficients	0.20	-0.23	0.003	0.017	0.005
	t	10.98***	-6.70***	0.089	4.04***	0.35
5-15	Coefficients	0.09	-0.17	0.002	0.0059	0.003
	t	5.77***	-5.17***	0.64	1.54	3.41***
15-30	Coefficients	0.045	-0.081	0.002	0.005	0.051
	t	3.15**	-2.18*	1.23	1.21	6.17***
30-50	Coefficients	0.04	-0.10	0.005	0.009	0.11
	t	2.63**	-2.54*	4.11***	2.58*	11.95***
50-80	Coefficients	0.28	-0.10	-0.005	0.001	0.099
	t	2.49*	-2.68**	-4.29***	0.19	9.17***
80-120	Coefficients	0.04	-0.17	-0.0019	0.007	0.13
	t	3.79***	-2.72**	-2.07*	2.11*	4.79***

* $P < 0.05$; ** $P < 0.01$; *** $P < 0.001$.

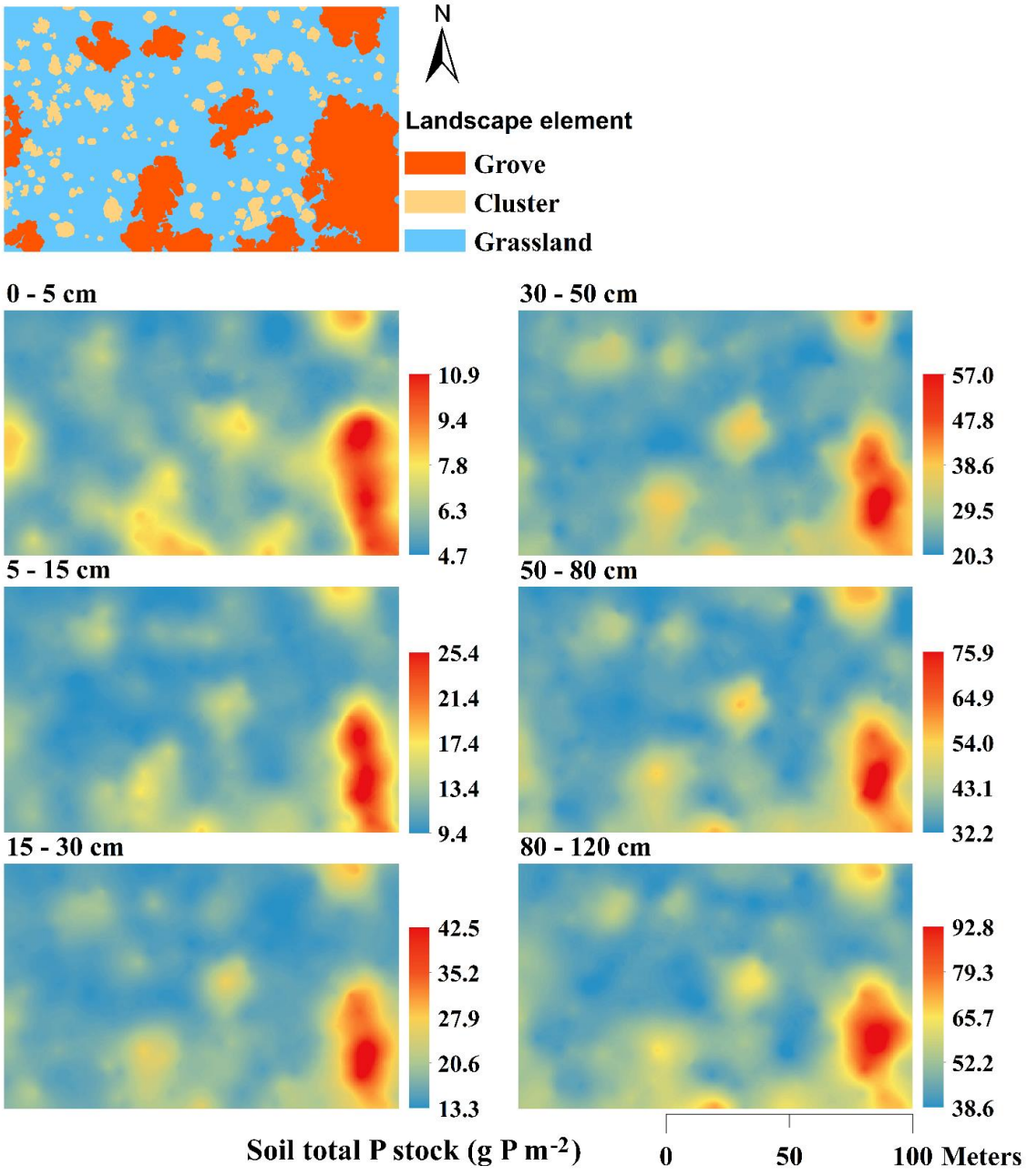

Figure 6.4 Classified vegetation map derived from aerial photo and kriged maps of soil total P stock (g P m^{-2}) throughout the soil profile for this 100 × 160 m landscape in a subtropical savanna based on 320 randomly located sampling points.

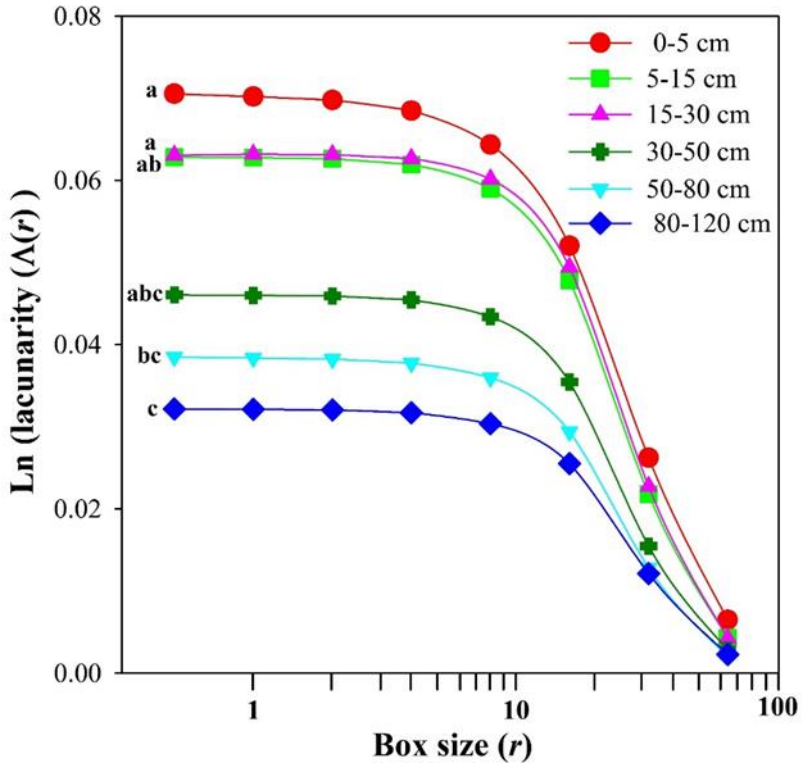

Figure 6.5 Lacunarity curves throughout the soil profile derived from spatial patterns of soil total P concentrations (mg P kg^{-1}). Significant differences ($P < 0.05$) between different soil depth increments were detected based on one-way ANOVA (Student's *t* test) and indicated with different letters.

DISCUSSION

Increases in total P throughout the soil profile

The lack of significant differences in soil total P concentrations between grasslands on non-argillic inclusions and those on argillic horizons (Fig. 6.3b) excludes the possibility of spatially non-homogeneous distribution of soil P due to pedogenic processes, suggesting that observed accumulation of P in soils beneath woody patches (both clusters and groves) results from woody plant encroachment into areas that were once grassland.

More importantly, this accumulation of soil P underneath woody patches is occurring throughout the upper 1.2 m of the soil profile (Figs. 6.3a and 6.4, and Table 6.1). Thus, our first hypothesis that increases in soil total P would occur only in surface soils was rejected.

Since there is no gaseous component of the P cycle (Walker & Syers 1976; Schlesinger & Bernhardt 2013), the accumulation of P in soils beneath woody patches must be derived from the addition or redistribution of P from other potential sources including: (1) atmospheric deposition, (2) faunal activities (e.g., large animals, termites, ants), (3) horizontal transfer from adjacent soils beyond the woody canopy, and/or (4) uplift by roots located deeper than 1.2 m. Atmospheric P deposition rates in this study area located in south-central USA range from 0.5 to 1.0 mg P m^{-2} yr^{-1} (Mahowald *et al.* 2008), which is a small fraction of the soil P accumulation rate (~ 100 mg P m^{-2} yr^{-1} in the 0 - 10 cm soil depth increment) under woody patches estimated for this ecosystem using a chronosequence approach (Kantola 2012). Livestock grazing has been excluded from this study area for at least the past 30 years (Liu *et al.* 2011) and is probably not responsible for the soil P patterns described here. Although desert termites (*Gnathamitermes perplexus*) are present across this landscape, their activities are confined to grassland areas, they feed only on grasses and forbs, and they are absent from wooded portions of the landscape. Thus, faunal activity is an unlikely determinant of P spatial patterns. Soil total P concentrations in grasslands are similar regardless of their proximity to woody patches, suggesting that the woody plants are not using lateral roots to mine P from the surrounding grasslands. These results are consistent with other studies reporting no

depletion of either total or extractable P in grassland soils adjacent to woody patches (Kantola 2012; Sitters *et al.* 2013; Blaser *et al*. 2014).

Given that atmospheric deposition, faunal activity, and lateral mining of P from surrounding grasslands by woody plant roots are unlikely scenarios, we propose that P increases in the upper 1.2 m of the soil profile beneath woody patches are due to translocation of deep soil P via root uptake, and, to a lesser extent, from hydraulic redistribution of dissolved P. Considerable potential for nutrient acquisition from deeper soil layers by deep-rooting plants has been reported in a variety of ecosystems (Scholes & Archer 1997; Jobbágy & Jackson 2001; McCulley *et al*. 2004; Kautz *et al.* 2013; Sardans & Peñuelas 2014). For example, McCulley *et al*. (2004) used $^{87}Sr/^{86}Sr$ isotope ratios of soils and plant tissues to show that roots were able to acquire and translocate Sr from deep in the profile to aboveground plant parts in five semi-arid and arid sites across the southwestern USA, demonstrating strong potential for the acquisition of nutrients by deep roots. Similarly, at our study site, δ^2H values of plant and soil water have shown that woody species are able to acquire water located 2 - 4 m below the soil surface, whereas herbaceous species utilize water exclusively from the upper soil layers (< 1.2 m) (Midwood *et al.* 1998; Boutton *et al.* 1999). Thus, woody plant roots at this site have demonstrated potential to access and acquire P located in deeper portions of the soil profile that are inaccessible to herbaceous species that dominate the grassland portions of the landscape. This additional P derived from deep soils by woody species is initially incorporated in plant tissues and ultimately delivered to upper portions of the soil profile via root turnover and aboveground litterfall. Since fine root biomass is the primary source

of soil organic matter input (Rasse *et al.* 2005) and is significantly higher underneath woody patches than grasslands throughout the entire 1.2 m soil profile (Fig. 6.2b), more P should accumulate underneath woody patches via root turnover. In addition, *P. glandulosa* trees at this study site have been shown to transfer deep soil water upwards into drier portions of the soil profile by hydraulic redistribution (Zou *et al.* 2005). This could create favorable moisture conditions in the surface soil for organic matter decay and subsequent biogeochemical processes that mineralize plant nutrients (including P) and enable plant uptake (Sardans & Penuelas 2014). Alternatively, when deeper portions of the soil profile are dry but surface layers are relatively moist, downward siphoning (the opposite of hydraulic redistribution) via roots may translocate water from surface soils into deep soils, solubilizing P in the soil matrix and facilitating its uptake by deep roots (McCulley *et al.* 2004; Lambers *et al.* 2006; Sardans & Penuelas 2014).

In addition, groves accumulated significantly more soil total P than clusters even though they are composed of the same woody species (Fig. 6.3a, Table 6.1). This is probably due to the fact that clusters in this landscape are constrained in size (mean canopy area = 13.4 m^2, n = 121, Zhou *et al.* 2017b) and are relatively young compared to groves (cluster mean age = 22 years, grove mean age = 48 years; Boutton *et al.* 1998). Since P and other nutrients in soils accumulate linearly with age or size of woody patches (e.g. Liao *et al.* 2006; Throop & Archer 2008; McClaran *et al*. 2008; Kantola 2012; Blaser *et al*. 2014), the generally younger and size-constrained clusters have accrued less soil P than the older and larger groves. Although the formation of discrete clusters is initiated by the colonization of N_2-fixing *P. glandulosa* trees (Archer *et al.* 1988; Archer 1995; Bai *et al.*

2012), many of these mesquite trees in clusters have died (Archer 1995; Boutton *et al.* 1998). Since the process of N_2-fixation requires a substantial supply of P (Treseder & Vitousek 2001; Vitousek *et al.* 2002; Houlton *et al.* 2008), the death of *P. glandulosa* in discrete clusters may significantly reduce P demand and its rate of accumulation in cluster soils as other woody species have lower P concentrations in their tissues (433.6 ± 30.7 mg P kg^{-1}, n = 14) than *P. glandulosa* (640.1 mg P kg^{-1}) (Fig. 6.2a).

Could the increase in soil P in woody patches be influenced by the fact that *P. glandulosa* is an N_2-fixer? As mentioned above, fast growing N_2-fixers have a high P demand (Treseder & Vitousek 2001; Vitousek *et al.* 2002; Houlton *et al.* 2008), and this demand be fulfilled via deep acquisition. Alternatively, N_2-fixing species maintain higher root phosphatase activity than non-N_2 fixers (Houlton *et al*. 2008; Boutton *et al.* 2009a; Blaser *et al.* 2014) which may influence their ability to acquire P and concentrate it within the rooting zone. At our site, acid phosphatase activity is 4 to 8 times greater in soils beneath woody patches with *P. glandulosa* than in grassland soils (Boutton *et al.* 2009a). This difference in enzyme activity results in plant-available P pools (i.e., resin-extractable P) of 3.4 mg P kg^{-1} in grasslands vs. 9.0 to 14.6 mg P kg^{-1} in clusters and groves (Kantola 2012). This is consistent with the hypothesis of Houlton *et al.* (2008), that symbiotic N-fixation may be a mechanism for plants to acquire additional N for investment in the production of N-rich root phosphatase enzymes that can increase the P availability in P-limited environments. If correct, this may be another important mechanism that leads to P accumulation where N_2-fixing woody plants are encroaching into grassland. Regardless of the exact mechanism by which P accumulates following woody encroachment, our

findings suggest that transfer of P from deeper soil layers enlarges the P pool in upper soil layers where it is more actively cycled may be a potential strategy for encroaching woody species to satisfy their P demands and enable their ongoing encroachment into areas that were once grass-dominated.

Patterns of spatial heterogeneity in soil total P

Kriged maps revealed that woody encroachment into grasslands altered patterns of spatial heterogeneity in soil total P throughout the upper 1.2 m of the soil, albeit at reduced magnitude in deeper portions of the profile (Figs. 6.4 and 6.5). Therefore, we reject our second hypothesis that spatial patterns of total P would be altered only in surface soils. Although spatial patterns of soil total P displayed strong resemblance to the distribution of grove vegetation, the same was not true for the smaller woody clusters (Fig. 6.4). One possible reason for this is that clusters accumulated less P due to their smaller sizes and younger ages, as discussed above. However, the more likely reason is that our sampling intensity may not have been sufficient to capture the spatial heterogeneity of soil total P beneath clusters (Liu *et al.* 2011). Approximately 80% of clusters are less than 20 m^2 (Zhou *et al.* 2017b), while only two soil samples were collected randomly within each 100 m^2 grid cell. Kriged maps also revealed that soil total P decreases gradually from the centers of groves to the edges (Fig. 6.4). These strong within-grove spatial gradients illustrate that the accumulation of soil P is time dependent. Woody plants near the centers of groves are generally older (> 100 years) than those closer to the grove/grassland interface (Bai *et al.* 2012), and have had more time to concentrate P in soils beneath their canopies.

The influence of woody encroachment on patterns of spatial heterogeneity in soil total P diminishes gradually with soil depth across this landscape (Fig. 6.5). Root distribution plays an important role in shaping vertical patterns of soil total P (Jobbágy & Jackson 2001) since much of the P in the soil profile is derived from root turnover, although surface soils also receive additional inputs from litterfall. As shown in this study (Figs. 6.2b) and many others (e.g. Jackson *et al.* 1996; Arora & Boer 2003; Laio *et al.* 2006), root distribution generally decreases exponentially with soil depth. Coupled with the fact that deeper roots have greater longevity and slower turnover than roots near the surface (e.g. Hendrick & Pregitzer 1996; Joslin *et al.* 2006), this suggests that the rate of P accrual will be slower and less pronounced in deeper portions of the soil profile. In terms of spatial arrangement, reduced discrepancies in soil total P between groves and other landscape elements in lower soil layers results in diminished spatial heterogeneity (Figs. 6.3a and 6.5). Spatial GLS models also revealed that fine root biomass explained large proportions of the variation in soil total P throughout the soil profile (Table 6.2); however, the strength of this relationship decreased with depth. In deeper portions of the profile, soil *p*H was strongly correlated with total P (Table 6.2), suggesting P dynamics in topsoil and in subsoil may be controlled by different regulatory mechanisms. In this study site, $CaCO_3$ concentrations in subsurface soils beneath groves are higher than those beneath grasslands by up to one order of magnitude (unpublished data). This, taken together with the fact that subsurface soils of this study site have higher pH values (Zhou *et al.* 2017a), may lead to P accumulation by favoring its fixation into insoluble calcium phosphates

(Schlesinger & Bernhardt 2013). Additional experiments are needed to explore the mechanisms leading to P accrual and storage in upper vs. lower portions of the soil profile.

CONCLUSIONS

In this subtropical savanna ecosystem, soil total P in the upper 1.2 m of the soil profile increases dramatically as N_2-fixing *P. glandulosa* trees and associated woody species encroach into the grassland matrix. The accumulation of P underneath woody patches is most likely driven by translocation of deep soil P via root uptake. Substantial accrual of soil total P underneath woody patches alters patterns of spatial heterogeneity in soil P to considerable depth, albeit at reduced magnitude deeper in the profile. We speculate that the transfer of P from deeper to shallower portions of the soil profile may foster a positive feedback that enables the persistence and ongoing encroachment of woody species which have relatively high tissue P concentrations compared to the grasses and forbs that once dominated this region.

Since P functions as a limiting nutrient and its availability can impose strong controls on plant and soil C and N cycles (Vitousek *et al.* 2010), it is critical to parameterize and represent the P cycle and its interactions with C and N cycles in earth system models (Reed *et al.* 2015; Yang *et al.* 2016a; Sun *et al.* 2017). Considering the vast geographical extent of woody encroachment in arid and semiarid regions throughout the world (Eldridge *et al.* 2011; Stevens *et al.* 2017), our results suggest that further efforts to characterize spatial variability in P storage and dynamics in horizontal and vertical soil space in response to this vegetation change would lead to improved efforts to model the interactions between vegetation change, biogeochemistry, and the climate system.

CHAPTER VII

SOIL PHOSPHORUS DOES NOT KEEP PACE WITH SOIL CARBON AND NITROGEN ACCUMULATION FOLLOWING WOODY ENCROACHMENT*

SYNOPSIS

Soil carbon, nitrogen, and phosphorus cycles are strongly interlinked and controlled through biological processes, and the phosphorus cycle is further controlled through geochemical processes. In dryland ecosystems, woody encroachment often modifies soil carbon, nitrogen, and phosphorus stores, although it remains unknown if these three elements change proportionally in response to this vegetation change. We evaluated proportional changes and spatial patterns of soil organic carbon (SOC), total nitrogen (TN), and total phosphorus (TP) concentrations following woody encroachment by taking spatially-explicit soil cores to a depth of 1.2 m across a subtropical savanna landscape which has undergone encroachment by *Prosopis glandulosa* (an N_2-fixer) and other woody species during the past century in southern Texas, USA. SOC and TN were coupled with respect to increasing magnitudes and spatial patterns throughout the soil profile following woody encroachment, while TP increased slower than SOC and TN in topmost surface soils but faster in subsurface soils. Spatial patterns of TP strongly resembled those of vegetation cover throughout the soil profile, but differed from those of

* Originally published as: Zhou, Y., Boutton, T. W., & Wu, X. B. (2018). Soil phosphorus does not keep pace with soil carbon and nitrogen accumulation following woody encroachment. *Global Change Biology*, doi: 10.1111/gcb.14048. In press. The publication is available at: http://onlinelibrary.wiley.com/doi/10.1111/gcb.14048/full.

SOC and TN, especially in subsurface soils. The encroachment of woody species dominated by N_2-fixing trees into this P-limited ecosystem resulted in the accumulation of proportionally less soil P compared to C and N in surface soils; however, proportionally more P accrued in deeper portions of the soil profile beneath woody patches where alkaline soil pH and high carbonate concentrations would favor precipitation of P as relatively insoluble calcium phosphates. This imbalanced relationship highlights that the relative importance of biotic vs. abiotic mechanisms controlling C and N vs. P accumulation following vegetation change may vary with depth. Our findings suggest that efforts to incorporate effects of land cover changes into coupled climate-biogeochemical models should attempt to represent C-N-P imbalances that may arise following vegetation change.

INTRODUCTION

Globally constrained ratios of carbon (C), nitrogen (N), and phosphorus (P) in marine (Redfield 1958) and terrestrial ecosystems (McGroddy *et al.* 2004; Cleveland & Liptzin 2007) suggest that the cycles of C, N and P are strongly coupled by biological processes. Nevertheless, recent studies indicate that the dramatic shift in the bioavailability of essential elements resulting from anthropogenic perturbations (e.g. atmospheric deposition, N and P fertilizers, land use changes), together with continuously rising atmospheric CO_2 and climate changes, can provoke imbalance between C, N and P in a variety of systems (Elser & Bennett 2011; Peñuelas *et al.* 2012; Sistla & Schimel 2012; Delgado-Baquerizo *et al.* 2013; Jiao *et al.* 2016). As a case in point, human activities (e.g. overgrazing, fire suppression, and increased atmospheric CO_2, Scholes & Archer 1997) have induced woody plant encroachment into grass-dominated dryland ecosystems.

This geographically widespread vegetation change has resulted in profound effects on soil biogeochemical cycles at ecosystem to regional and global scales (Houghton *et al*. 1999; Pacala *et al.* 2001; Liu *et al.* 2011). These changes may have the potential to change the elemental balance of C, N and P in soils, though this has not been explicitly investigated.

Plant species have unique strategies to acquire essential elements, and the supply of one element can interactively affect the cycles of others within plants or soils (Sterner & Elser 2002). Different species generally have distinctive stoichiometries, such that changes in species composition can substantially alter the stoichiometric composition and elemental balance of an ecosystem (Elser *et al.* 2010; Sistla & Schimel 2012). Following vegetation shift from grass to woody plant dominance, numerous studies have demonstrated net increases in soil organic C (SOC), with accumulation rates depending on climate, soil properties, and identity of encroaching woody species (Barger *et al.* 2011; Eldridge *et al.* 2011; Li *et al.* 2016). N and P commonly limit key ecosystem functions (e.g. primary production, Vitousek *et al.* 2010) and services (e.g. C sequestration, Hessen *et al.* 2004), but their supply is fulfilled in different ways. In many dryland ecosystems, woody encroachment is often facilitated by the colonization of N_2-fixing tree legumes (e.g. *Prosopis* in North America and *Acacia* in South Africa), which have the potential to add N to the system to overcome possible N limitation and enable rapid accumulation of C in vegetation and soils (Boutton & Liao 2010; Blaser *et al.* 2014; Soper & Sparks 2017). Unlike N, P is derived mainly from weathering of parent materials (Walker & Syers 1976), and thus ecosystems begin their existence with a fixed amount of P (Vitousek *et al.* 2010). Since woody proliferation can result in woody patches with aboveground biomass and

primary productivity orders of magnitude greater than those of grasslands they replaced (Hibbard *et al.* 2003; Hughes *et al.* 2006), a significant amount of P may become tied up in plant biomass, potentially leading to smaller pools of soil P. However, some field studies have shown that woody encroachment actually increases total P in surface soils beneath woody patches (Kantola 2012; Sitters *et al.* 2013; Blaser *et al.* 2014). The underlying mechanisms remain unknown, but may be related to the deep rooting habits of encroaching woody species, enabling the transfer of deep soil P to surface soils through litterfall and root turnover (Kantola 2012; Blaser *et al.* 2014). Despite dramatic influences of woody encroachment on soil C, N and P cycles, few studies have simultaneously assessed the responses of these three elements and their accumulations at depths below the uppermost portions of the soil profile. Therefore, it remains largely unknown whether concentrations of soil C, N and P change proportionally following woody encroachment into grasslands, especially in the largely overlooked subsurface soils.

Although soil C, N and P cycles are strongly interlinked and controlled through biological processes (e.g. soil organic matter (SOM) input and subsequent microbial decomposition), the P cycle is further controlled through geochemical processes (e.g. dissolution and precipitation reactions) (Schlesinger & Bernhardt, 2013). Woody encroachment into grasslands and subsequent changes in biotic and abiotic factors throughout the soil profile could exert different degrees of control on these biological and geochemical processes, and potentially lead to disproportionate changes in soil C, N and P. Roots and root exudates are the primary sources of organic matter input throughout the soil profile (Rumpel & Kögel-Knabner 2011; Schmidt *et al.* 2011), although aboveground

litterfall contributes significantly to surface soils. Compared to herbaceous species, trees/shrubs in dryland areas typically have enlarged rhizospheres in both horizontal and vertical dimensions (Jackson *et al.* 1996; Schenk & Jackson 2002), resulting in amplified SOM input throughout the soil profile following woody encroachment. Meanwhile, accumulations of soil organic C, N and P are also determined by abiotic factors, such as physicochemical binding between SOM and soil minerals (i.e. clay and silt particles) (Six *et al.* 2002; Schmidt *et al.* 2011) that affect microbial decomposition of SOM and favor the accumulation of soil C, N, and P. In addition, soil pH has been shown to affect the chemical form and solubility of inorganic P, and alkaline soils in dryland areas would generally favor the precipitation of dissolved inorganic P leached from surface soils as calcium phosphates (Carreira *et al.* 2006; Ippolito *et al.* 2010; Schlesinger & Bernhardt 2013). While there is a rich literature reporting the effects of these biotic/abiotic factors on net changes in soil C, N and/or P following woody encroachment, individually or in combination, no studies have simultaneously tested the relative importance of these factors on all three elements. This question is especially relevant throughout the soil profile since these biotic and abiotic factors change significantly with soil depth.

Here, we assessed changes in the pool sizes and spatial patterns of SOC, TN, and TP following woody encroachment, and the relative importance of biotic and abiotic factors in influencing these changes at the landscape scale throughout the soil profile. We hypothesized that landscape-scale accumulations of SOC, TN and TP following woody encroachment into grasslands would be interlinked and their relative changes would be proportional throughout the soil profile. In addition, our previous studies have

demonstrated that woody encroachment has dramatically increased root biomass throughout the entire soil profile (Boutton *et al.* 1998; Zhou *et al.* 2017a) and potentially delivers more plant residues that drive the accrual of more SOC, TN, and TP compared to the grasslands being replaced. Therefore, we also hypothesized that landscape-scale accumulations of SOC, TN, and TP throughout the soil profile would be explained predominantly by root density, and, to a lesser degree, by abiotic factors, such as soil texture and pH.

MATERIALS AND METHODS

Study site

Research was conducted at the Texas A&M AgriLife La Copita Research Area (27˚40' N, 98˚12' W; elevation 75-90 m a.s.l.) in the eastern Rio Grande Plains, Texas, USA. The climate is subtropical (mean annual temperature 22.4 ˚C; mean annual precipitation 680 mm). Topography at this site gently grades (1-3% slopes) from well-drained uplands to lower-lying drainage woodlands. Soils on upland portions of the landscape are sandy loams with a continuous argillic horizon (*Bt*); however, non-argillic inclusions also occur within the upland (Archer 1995; Zhou *et al.* 2017b).

Uplands of this site were once almost exclusively dominated by C_4 grasses, and woody encroachment over the past century has been well documented by historical aerial photographs, tree rings, and $\delta^{13}C$ values of SOC (Archer *et al*. 1988; Archer 1995; Boutton *et al.* 1998; Bai *et al.* 2012). Currently, upland landscapes consist of three landscape elements: grasslands, clusters (woody patches < 100 m^2), and groves (> 100 m^2) (Fig. 7.1). The formation of clusters is initiated by the colonization of honey mesquite (*Prosopis*

glandulosa) (an N_2-fixing tree legume, Zitzer *et al.* 1996; Soper *et al.* 2015) in grasslands. Established honey mesquite trees then serve as nurse plants and facilitate the recruitment of numerous other woody species beneath their canopy (Archer *et al.* 1988). If clusters occur on non-argillic inclusions, they expand and coalesce to form large groves (Archer 1995; Bai *et al.* 2012; Zhou *et al.* 2017b). Groves are dominated by honey mesquite with an understory consisting of approximately 15 other subordinate woody species. Although clusters are composed of the same woody species as groves, honey mesquite in clusters are usually significantly younger and smaller than those in groves (Boutton *et al.* 1998; Liu *et al.* 2010), and some were already dead (Archer 1995; Zhou *et al.* 2017b). The remnant grassland matrix is dominated by C_4 grasses, but also includes a significant proportion of forbs (C_3 plants) and a smaller proportion of cacti (crassulacean acid metabolism or CAM plants). Species composition within our upland landscape study area is provided in Appendix A.

Field sampling

In order to quantify patterns of spatial heterogeneity in soil C, N, and P that have been altered by woody plant encroachment, a 160 m × 100 m upland landscape which included all three landscape elements (i.e. grasslands, clusters, and groves) was established and subdivided into 10 m × 10 m grid cells in January 2002 (Fig. 7.1) (Liu *et al.* 2011). The X, Y coordinates of the corners of each grid cell were determined using a GPS unit based on UTM coordinates system (14 North, WGS 1984). A color-infrared aerial photograph of this landscape was acquired in July 2015. Edges of woody patches

(clusters and groves) were manually delineated in the aerial photo using ArcGIS 10.2.2 (ESRI, Redlands, CA, USA) in order to create a classified vegetation map.

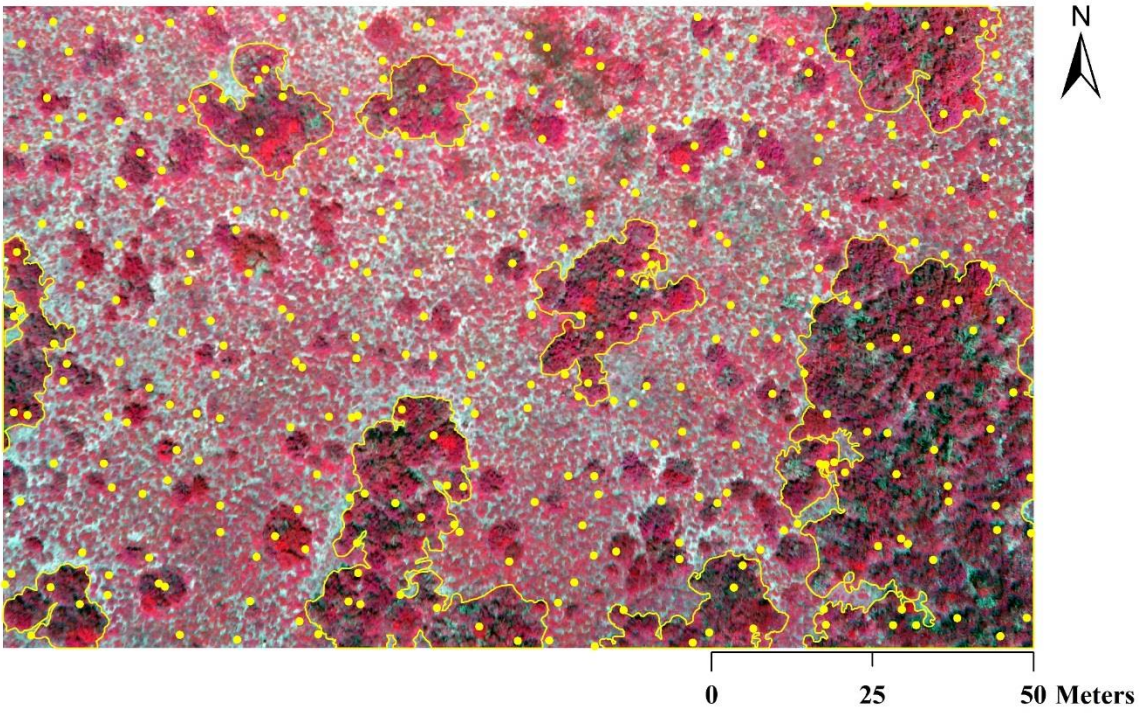

Figure 7.1 Color-infrared aerial view of this 160 m ×100 m landscape showing locations of 320 random soil samples (yellow points). Red areas are woody clusters and groves, and light gray areas indicate open grasslands. Groves are highlighted with yellow lines.

In July 2014, two sample points were selected randomly within each 10 m × 10 m grid cell (320 points in total) (Fig. 7.1). The landscape element present at each sample point was classified as grassland (n = 200), cluster (n = 41) or grove (n = 79) based on woody canopy area and vegetation type. The distances from each sample point to two georeferenced grid cell corners were recorded. At each sample point, two adjacent soil

cores (2.8 cm in diameter and 120 cm in length) were collected using the PN150 JMC Environmentalist's Subsoil Probe (Clements Associates Inc., Newton, IA, USA). This random sampling scheme, stratified within the systematic 10 m x 10 m grid cells, has been shown to effectively capture the overall spatial pattern of SOC on this landscape comprised of multiple vegetation elements (Liu *et al.* 2011).

Lab analyses

Each soil core was subdivided into six depth increments (i.e. 0-5, 5-15, 15-30, 30-50, 50-80, and 80-120 cm). The depth increments between 0-30 cm span the A-horizon, while increments between 30-120 cm span the B-horizon (Boutton *et al.* 1998). One soil core was used to estimate fine (< 2 mm in diameter) and coarse (> 2 mm in diameter) root biomass by washing through sieves. No attempt was made to distinguish between live or dead roots. Retrieved roots were washed carefully to remove soil particles, and dried (65 ˚C for 48 hours) for biomass determination.

The other soil core was air-dried and then passed through a 2 mm sieve to remove coarse organic fragments. An aliquot of sieved soils was used to determine soil pH on a 1: 2 (10 g soil: 20 mL 0.01 mol/L $CaCl_2$) mixture using a glass electrode, and soil texture by the hydrometer method (Sheldrick & Wang 1993). A separate soil aliquot was dried at 65 ˚C for 48 hours, pulverized in a centrifugal mill, and used for analyses of SOC, TN, and TP. Soil TN was quantified by combustion/gas chromatography using a Costech ECS 4010 elemental analyzer (Costech Analytical Technologies Inc., Valencia, CA, USA). Soil organic C concentrations were determined using the same method, but soils were pre-treated with HCl vapor in a desiccator for 8 hours to remove carbonates (Harris *et al.*

2001), and then dried. Soil TP was extracted using the lithium fusion method (Lajtha *et al.* 1999), and P concentrations in extracted solutions were determined by the molybdenum blue colorimetry method (Murphy & Riley 1962) using a Spectronic $20D^{+}$ spectrophotometer (Thermo Fisher Scientific, Inc., Waltham, MA, USA).

Leaf and fine root tissues of each major species occurring on this landscape were collected in September 2016 (Appendix A). Fine root tissues were collected by soil excavation that unequivocally confirmed linkages to identified plant species. These tissues were washed carefully, dried, and pulverized. Plant tissue C and N concentrations were determined by combustion/gas chromatography, and P concentrations by lithium fusion, as described above.

Data analyses

Variable means of SOC, TN, and TP within each depth increment for soil cores from different landscape elements were compared using mixed models in JMP pro 12.0 (SAS Institute Inc., Cary, NC, USA). In mixed models, spatial autocorrelation of each variable was considered as a spatial covariance for adjustment (Littell *et al.* 2006). An alpha level of 0.05 was used to determine statistical significance. Variogram analyses were performed to quantify the spatial structures of SOC, TN, and TP for each depth increment based on 320 random samples across this landscape using the "gstat" package in R statistical software (R Development Core Team 2014). Ordinary kriging was used for spatial interpolation based on parameters obtained from variogram analyses, and kriged maps of SOC, TN, and TP within each depth increment were generated using ArcMap 10.2.2 (ESRI, Redlands, CA, USA).

A scaling approach was used to test the proportional changes between SOC, TN, and TP following woody encroachment into grasslands. We plotted $\log_{10}$-transformed soil TN or TP (mg N or P kg^{-1} soil) on the y-axis and $\log_{10}$-transformed SOC (mg C kg^{-1} soil) on the x-axis to test whether soil TN and TP changed systematically with SOC accumulation. If soil TN and TP accumulate in proportion to accrual of SOC, we would expect that slopes of the N-C and P-C stoichiometric relationships would not be significantly different from 1.0 (i.e. the 95% confidence intervals of the scaling slope included 1.0). If there were directional increases in proportion of soil TN and TP with increasing SOC, we would expect scaling slopes greater than 1.0; in contrast, if there were directional decreases in the proportion of soil TN and TP with increasing SOC, we would expect scaling slopes less than 1.0. Scaling slopes of N-C and P-C stoichiometric relationships were determined by reduced major axis regression (i.e. type II regression) (Reich *et al.* 1997; McGroddy *et al.* 2004; Niklas & Cobb 2005; Cleveland & Liptzin 2007; Yang & Luo 2011) using the "lmodel2" package in R statistical software.

To assess the relative importance of fine roots and soil physicochemical properties on accumulations of SOC, TN, and TP within each depth increment throughout the soil profile, we used structural equation models (SEM), which are based on *a priori* information regarding the relationships among the explanatory and response variables of interest. Compared to other statistical analyses, such as multiple regressions, SEM can assign directions to several relationships resulting in multiple explanatory as well as multiple response variables in a single model (Grace, 2006). Based on current ecological knowledge, we constructed our conceptual *a priori* SEM (Fig. 7.2). In our conceptual

model, we chose soil clay and silt content to be the only exogenous variable as spatial heterogeneity of subsurface soil texture is an intrinsic feature of this landscape (Archer 1995; Zhou *et al.* 2017b). By regulating the distribution of grove vegetation which occurs on non-argillic inclusions (Zhou *et al.* 2017b), soil clay and silt content could affect the size and depth distribution of fine roots (Fig. 7.2). We accounted for the fact that roots are the primary sources of organic matter input in soil by including them in our conceptual model (Fig. 7.2). We also related soil clay and silt content to SOC, TN, and TP because it has been shown that intimate associations between organic matter and fine soil particles (i.e. clay and silt) is an important mechanism for the accumulation/stabilization of organic matter in soils (Fig. 7.2). Soil pH was linked with soil TP because the fixation of soluble P with soil minerals to form insoluble compounds is affected by soil pH (Fig. 7.2). Descriptive statistics (i.e. mean and standard error) for fine root density, soil texture, and soil pH can be presented elsewhere. Meanwhile, our conceptual model included correlations between SOC, TN, and TP in order to detect changes in their stoichiometric relationships throughout the soil profile.

To evaluate the fit of the SEM models, we used χ^2 goodness-of-fit test and the root mean squared error of approximation (RMSEA) according to Grace (2006). The χ^2 test assesses the magnitude of difference between the observed and expected covariance matrix of the SEM. Therefore, if the value of χ^2 is close to zero, it indicates small differences and thus a good fit. RMSEA assesses the magnitude of the approximation error per degree of freedom, and a value of RMSEA close to zero indicates a good fit (Grace 2006). In order to facilitate comparisons between different depth increments, we did not

simplify our *a priori* model by excluding non-significant paths. Dataset were log_{10}-transformed to improve the normality prior to constructing SEMs using AMOS 24.0 (Amos Development Co., Armonk, NY, USA).

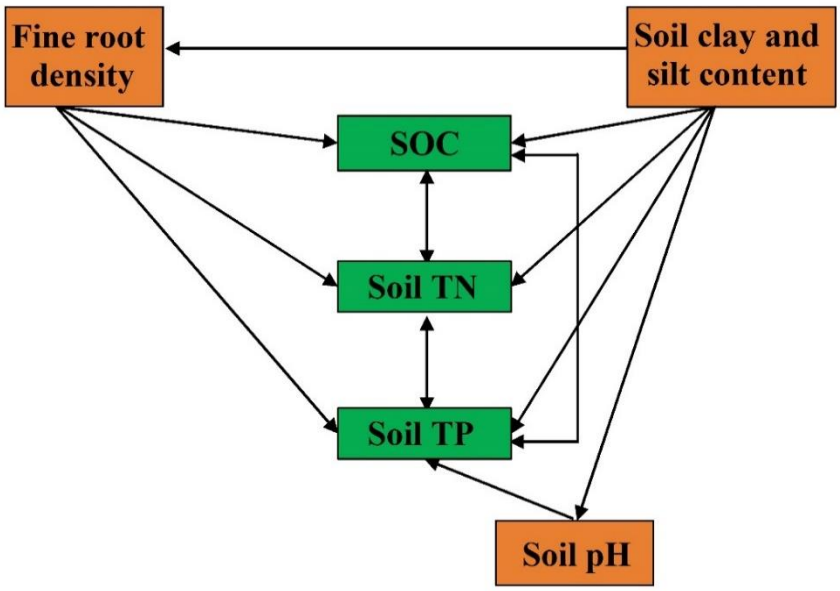

Figure 7.2 A *priori* conceptual structural equation model depicting pathways by which fine root density, soil clay and silt content and soil pH may influence the accumulation of soil organic carbon (SOC), total nitrogen (TN) and total phosphorus (TP) throughout the soil profile following woody encroachment. Single-headed arrows represent hypothesized causal relationships of one variable upon the other. Double-headed arrows signify correlations between two variables, but no direction is specified.

RESULTS

Stoichiometric composition of different plant life-forms

Overall, leaves had higher mean C, N and P concentrations than fine roots (Fig. 7.3). Although not all significant, woody species (both non N_2-fixers and N_2-fixers) had higher

mean C, N and P concentrations than grasses in both leaf and fine root tissues (Fig. 7.3). N_2-fixing woody species had highest mean C, N and P concentrations in both leaves and fine roots (Fig. 7.3). In addition, it is worth noting that N concentrations in leaf and fine root tissues of N_2-fixing woody species were 1.9 and 3.3 times higher, respectively, than those of grasses; in contrast, P concentrations in leaves and fine roots were only 1.4 and 2.3 times higher in N_2-fixing woody plants vs. grasses, respectively (Fig. 7.3).

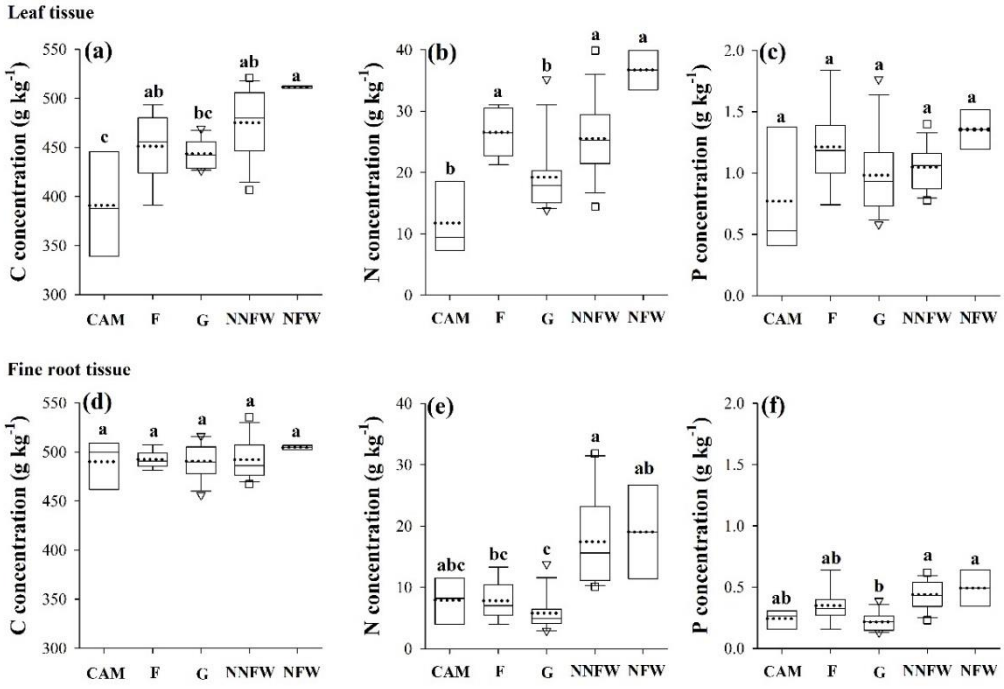

Figure 7.3 Carbon (C), nitrogen (N) and phosphorus (P) concentrations (g kg^{-1}) of leaf and fine root tissues for different plant life-forms occurring on this landscape. The box plots summarize the distribution of points for each variable within each plant life-form. The central box shows the inter-quartile range, median (horizontal solid line in the box), and mean (horizontal dotted line in the box). Lower and upper error bars indicate 10^{th} and 90^{th} percentiles, and points above and below the error bars are individuals in the lower 10^{th} percentiles. CAM, crassulacean acid metabolism species, n = 3; F, forbs, n = 9; G, grasses, n = 13; NNFW, non N_2-fixing woody species, n =13; NFW, N_2-fixing woody species, n = 2.

Table 7.1 Mean and standard error (SE) of soil organic carbon (SOC) (a), total nitrogen (TN) (b), and total phosphorus (TP) (c) in contrasting landscape elements, and also % increases in those values from grassland to cluster or grove along the soil profile in a subtropical savanna.

Depth (cm)	Landscape element			% increases	
	Grassland	Cluster	Grove	Grassland to Cluster	Grassland to Grove
(a) SOC (g C kg^{-1} soil)					
0-5	6.68 ± 0.12^{c}	16.95 ± 1.44^{b}	22.14 ± 1.36^{a}	153.7	231.4
5-15	5.44 ± 0.05^{b}	8.23 ± 0.45^{a}	8.78 ± 0.26^{a}	51.3	61.4
15-30	5.11 ± 0.04^{b}	6.02 ± 0.16^{a}	6.29 ± 0.12^{a}	17.8	23.1
30-50	4.96 ± 0.05^{a}	5.32 ± 0.11^{a}	5.34 ± 0.12^{a}	7.3	7.7
50-80	3.51 ± 0.03^{b}	3.93 ± 0.09^{a}	3.86 ± 0.07^{a}	12.0	10.0
80-120	2.28 ± 0.03^{b}	2.61 ± 0.10^{a}	2.90 ± 0.06^{a}	14.5	27.2
(b) Soil TN (g N kg^{-1} soil)					
0-5	0.65 ± 0.01^{c}	1.57 ± 0.12^{b}	2.09 ± 0.12^{a}	141.5	221.5
5-15	0.56 ± 0.01^{b}	0.83 ± 0.04^{a}	0.88 ± 0.02^{a}	48.2	57.1
15-30	0.51 ± 0.00^{a}	0.59 ± 0.02^{a}	0.62 ± 0.01^{a}	15.7	21.6
30-50	0.52 ± 0.01^{a}	0.54 ± 0.01^{a}	0.53 ± 0.01^{a}	3.8	1.9
50-80	0.41 ± 0.00^{b}	0.44 ± 0.01^{a}	0.42 ± 0.01^{a}	7.3	2.4
80-120	0.28 ± 0.00^{b}	0.31 ± 0.01^{a}	0.34 ± 0.01^{a}	10.7	21.4
(c) Soil TP (mg P kg^{-1} soil)					
0-5	81.7 ± 0.7^{c}	124.0 ± 3.9^{b}	154.2 ± 4.3^{a}	51.8	88.7
5-15	76.5 ± 0.6^{c}	95.3 ± 2.3^{b}	123.7 ± 3.6^{a}	24.6	61.7
15-30	75.9 ± 0.6^{c}	85.0 ± 1.8^{b}	119.1 ± 3.4^{a}	12.0	56.9
30-50	84.8 ± 0.7^{b}	89.0 ± 1.7^{b}	123.2 ± 3.1^{a}	5.0	45.3
50-80	80.0 ± 0.6^{c}	87.8 ± 1.5^{b}	112.5 ± 2.8^{a}	9.8	40.6
80-120	71.0 ± 0.5^{c}	77.4 ± 1.6^{b}	99.3 ± 2.1^{a}	9.0	39.9

Significant difference between means in landscape elements are indicated with different superscript letters. Number of samples: grassland = 200, cluster = 41, and grove = 79. Please note that units for soil TP (mg P kg^{-1} soil) are different than those for SOC (g C kg^{-1} soil) and soil TN (g N kg^{-1} soil).

Table 7.2 Summary of reduced major axis (RMA) regression analyses for the $\log_{10}$-transformed N-C (a) and P-C (b) stoichiometric relationships across this landscape and throughout the soil profile. Numbers in parentheses are 95% confidence intervals for the slopes of N-C and P-C stoichiometric relationships. If the 95% confidence intervals of the slope include 1.0, it indicates that the slope of N-C or P-C stoichiometric relationship is not significantly different from 1.0.

Depth (cm)	Grassland		Cluster		Grove	
	Slope	r^2	Slope	r^2	Slope	r^2
(a) N-C stoichiometric relationships						
0-5	0.93 (0.90, 0.96)	0.96	0.92 (0.86, 0.97)	0.97	0.96 (0.94, 0.98)	0.99
5-15	0.94 (0.89, 0.99)	0.84	0.91 (0.85, 0.97)	0.96	0.96 (0.91, 1.01)	0.95
15-30	0.87 (0.80, 0.94)	0.68	0.92 (0.78, 1.08)	0.75	0.93 (0.84, 1.03)	0.81
30-50	0.98 (0.93, 1.04)	0.85	1.10 (0.96, 1.26)	0.82	0.94 (0.86, 1.02)	0.86
50-80	0.91 (0.85, 0.96)	0.83	0.96 (0.85, 1.07)	0.88	1.11 (1.02, 1.20)	0.86
80-120	0.79 (0.74, 0.84)	0.83	0.76 (0.69, 0.85)	0.89	0.84 (0.78, 0.93)	0.85
(b) P-C stoichiometric relationships						
0-5	0.52 (0.48, 0.56)	0.66	0.43 (0.37, 0.51)	0.76	0.50 (0.44, 0.56)	0.71
5-15	0.75 (0.58, 0.84)	0.42	0.58 (0.48, 0.70)	0.64	1.00 (0.85, 1.18)	0.47
15-30	0.88 (0.77, 1.01)	0.07	0.86 (0.64, 1.15)	0.16	1.46 (1.20, 1.78)	0.23
30-50	0.77 (0.67, 0.89)	0.02	0.86 (0.63, 1.18)	0.02	1.17 (0.94, 1.45)	0.08
50-80	0.87 (0.77, 0.98)	0.23	0.73 (0.54, 0.98)	0.12	1.32 (1.08, 1.60)	0.23
80-120	0.54 (0.50, 0.59)	0.62	0.46 (0.36, 0.58)	0.48	0.98 (0.82, 1.18)	0.35

Number of samples: overall = 320, grassland = 200, cluster = 41, and grove = 79.

Imbalanced soil P with respect to C and N along the soil profile

Overall, woody encroachment into grassland increased SOC, TN, and TP concentrations across this landscape and throughout the entire 120 cm soil profile, albeit in different magnitudes (Table 7.1). SOC and TN were strongly coupled as their proportional increases following woody encroachment were similar within each soil depth increment (Table 7.1). This strong coupled relationship is validated by multiple lines of evidence. Firstly, strong positive correlations between soil P: N vs P: C ratios throughout the soil profile were observed (Fig. 7.4). Secondly, slopes for N-C stoichiometric relationship throughout the soil profiles were consistently near 1.0 across this landscape (Table 7.2) and slopes for clusters and groves were much similar to those for grasslands (Table 7.2). Thirdly, spatial patterns of SOC and TN were identical to each other for each depth increment (Fig. 7.5). Last but not least, SOC and TN were highly correlated to each other ($r > 0.80$) as shown in SEMs (Fig. 7.6).

However, TP was uncoupled from SOC and TN, especially for grove vegetation which is the dominant feature creating spatial heterogeneity in this landscape. In the 0-5 cm depth increment, the % increases in SOC and TN were 2.5 times greater than for TP under groves compared to grasslands (Table 7.1). This proportionally smaller increase in soil TP has resulted in (1) soil samples from groves were scattered below those of grasslands in the plots of soil N: C vs. P: C ratios (Fig. 7.4); and (2) slopes of the P-C stoichiometric relationship for groves in the 0-5 cm depth increment were much less than 1.0 (Table 7.2). In the 5-15 cm depth increment, the % increase in soil TP under groves was comparable to that of SOC and TN (Table 7.1), thus the slope of the P-C

stoichiometric relationship for groves was not different from 1.0 (Table 7.2). In contrast, % increases in TP under groves in the 15-30, 30-50, and 50-80 cm depth increments were several to more than ten times higher than those of SOC and TN at those same depths (Table 7.1). Correspondingly, (1) soil samples from groves were scattered above those of grasslands in these depth increments (Fig. 7.4); and (2) slopes for groves were > 1.0 in these depth increments (Table 7.2). The % increases in soil TP under clusters were less than those for SOC and TN in the 0-5, 5-15, 50-80, and 80-120 cm depth increments, but comparable in the 15-30 and 30-50 cm depth increments (Table 7.1 and 7.2). Due to the substantial increase of TP under groves throughout the soil profiles (Table 7.1), spatial patterns of soil TP for every depth increment displayed strong resemblance to that of vegetation cover (Fig. 7.5). Spatial patterns of TP were distinctive from those of SOC and TN, especially in subsurface soils (> 15 cm) (Fig. 7.5). These decoupled responses of soil TP from those of SOC and TN throughout the soil profile resulted in correlations between soil P: C and N: C ratios and between SOC and TN that were not strong, especially for these intermediate depth increments (Fig. 7.4 and 7.6).

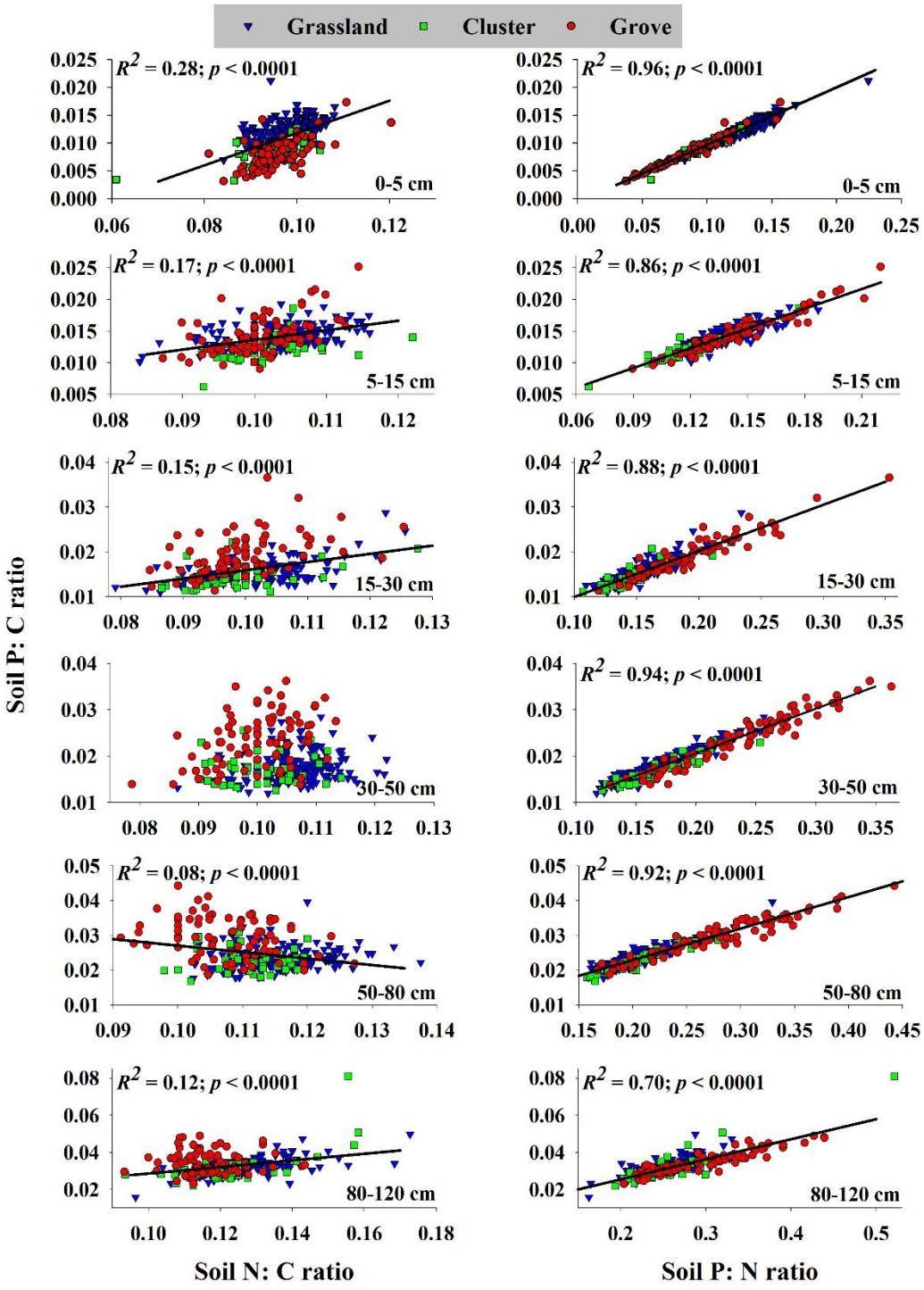

Figure 7.4 Element ratios plotted against each other for all 320 sampling points across this landscape and throughout the soil profile. Grassland = 200, cluster = 41, and grove = 79.

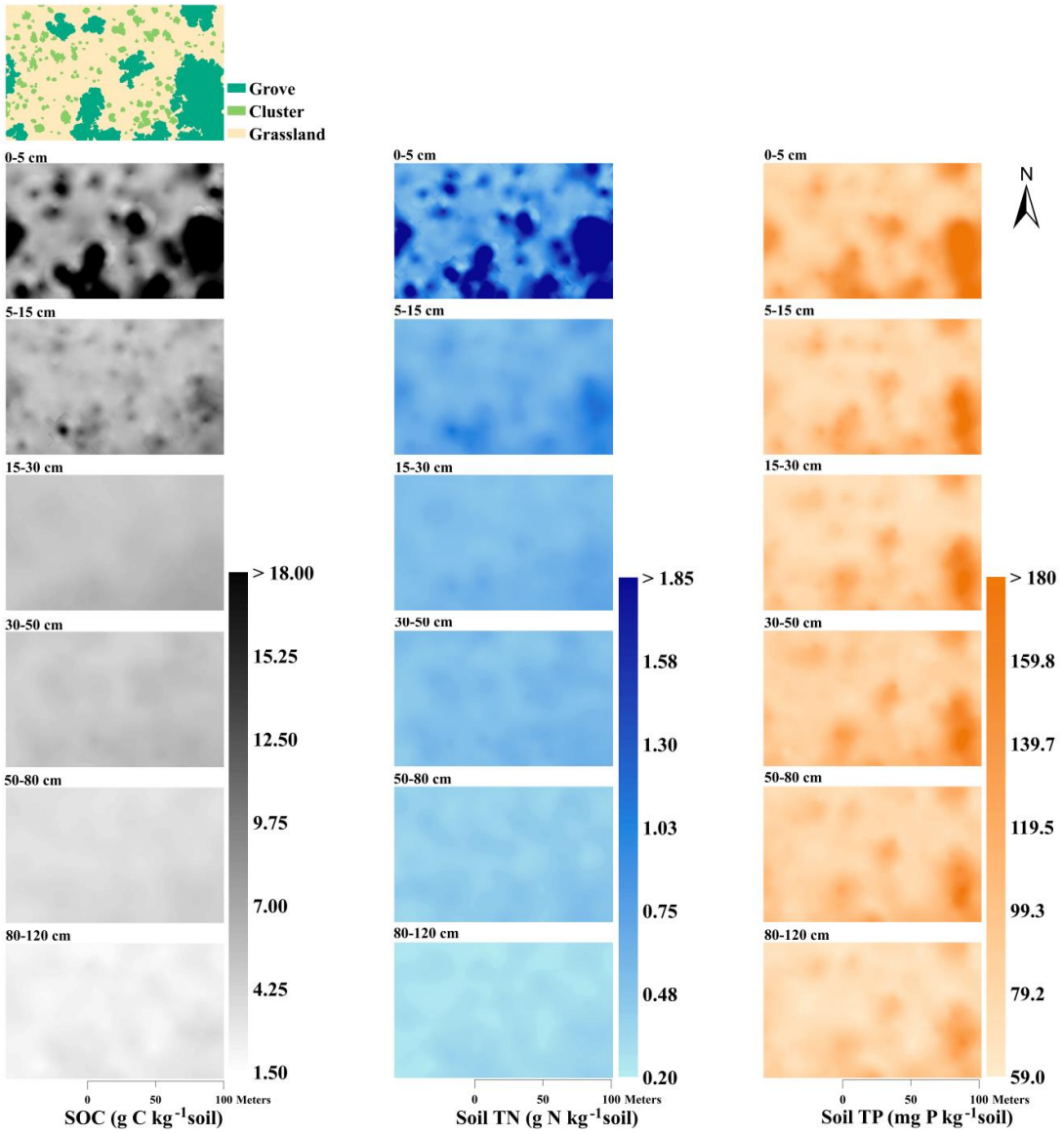

Figure 7.5 Kriged maps of soil organic carbon (SOC), total nitrogen (TN) and total phosphorus (TP) along the soil profile for this 160 m × 100 m landscape based on 320 randomly located sampling points. Please note that soil TP unit (mg P kg^{-1} soil) is different from SOC (g C kg^{-1} soil) and TN (g N kg^{-1} soil).

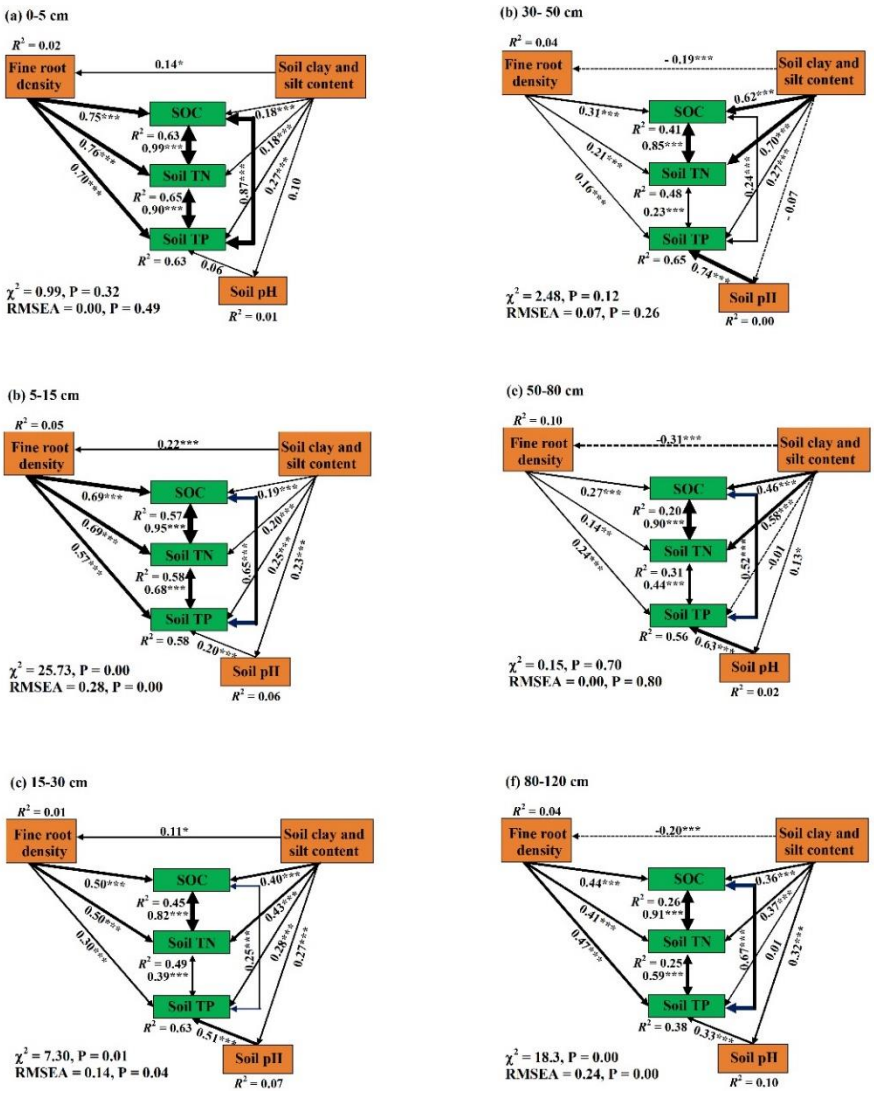

Figure 7.6 Structural equation models showing influences of fine root density, soil clay and silt content, and soil pH on the accumulation of soil organic carbon (SOC), total nitrogen (TN) and total phosphorus (TP) throughout the soil profile following woody plant encroachment, and also correlations between SOC, TN, and TP throughout the soil profile. All variables are observed variables. Single-headed arrows point in the direction of causality, and double-headed arrows indicate correlations between variables. Numbers adjacent to arrows are standardized path coefficients. Continuous and dashed arrows represent positive and negative relationships, respectively, and arrow width is proportional to the strength of the standardized path coefficients. The proportion of variance explained (R^2) is shown alongside each response variable. See the *a-priori* conceptual structural equation model in Figure 2. Models for each soil depth were developed based on the combined data for grasslands, clusters, and groves (N = 320 samples/depth).

Variables associated with this imbalanced accumulation along the soil profile

Goodness of fit tests for SEMs indicated that the data from the 0-5, 15-30, 30-50, and 50-80 cm depth increments fitted the *a priori* model well, as both χ^2 and RMSEA were close to zero (Fig. 7.6). Thus, our SEMs can be accepted as potential explanations for the observed variance in SOC, TN, and TP throughout the soil profile. Overall, the powers of explanation for the variance in SOC, TN, and TP decreased with soil depth (Fig. 7.6). For example, in the 0-5 cm depth increment, the model explained 63%, 65%, 63% of the variance in SOC, TN, and TP, respectively, whereas these values were 26%, 25%, 38% in the 80-120 cm depth increment (Fig. 7.6). Fine root density, soil clay and silt content, and soil pH showed positive relationships with SOC, TN, and TP throughout the soil profile (Fig. 7.6).

The effects of fine root density, soil clay and silt content, and soil pH on SOC, TN, and TP changed with soil depth (Fig. 7.7). For example, in the 0-5 cm depth increment, fine root density, as a biotic factor, explained the greatest proportion of the variance in SOC, TN, and TP, with minor contributions from soil clay and silt content (Fig. 7.7). However, the relative importance of fine root density decreased throughout the soil profile; instead, soil clay and silt content explained a significant proportion of the variance in SOC and TN, while soil pH accounted for an important portion of the variance in soil TP (Fig. 7.7). This is especially true for the 30-50 cm depth increment where clay and carbonate C start to accumulate.

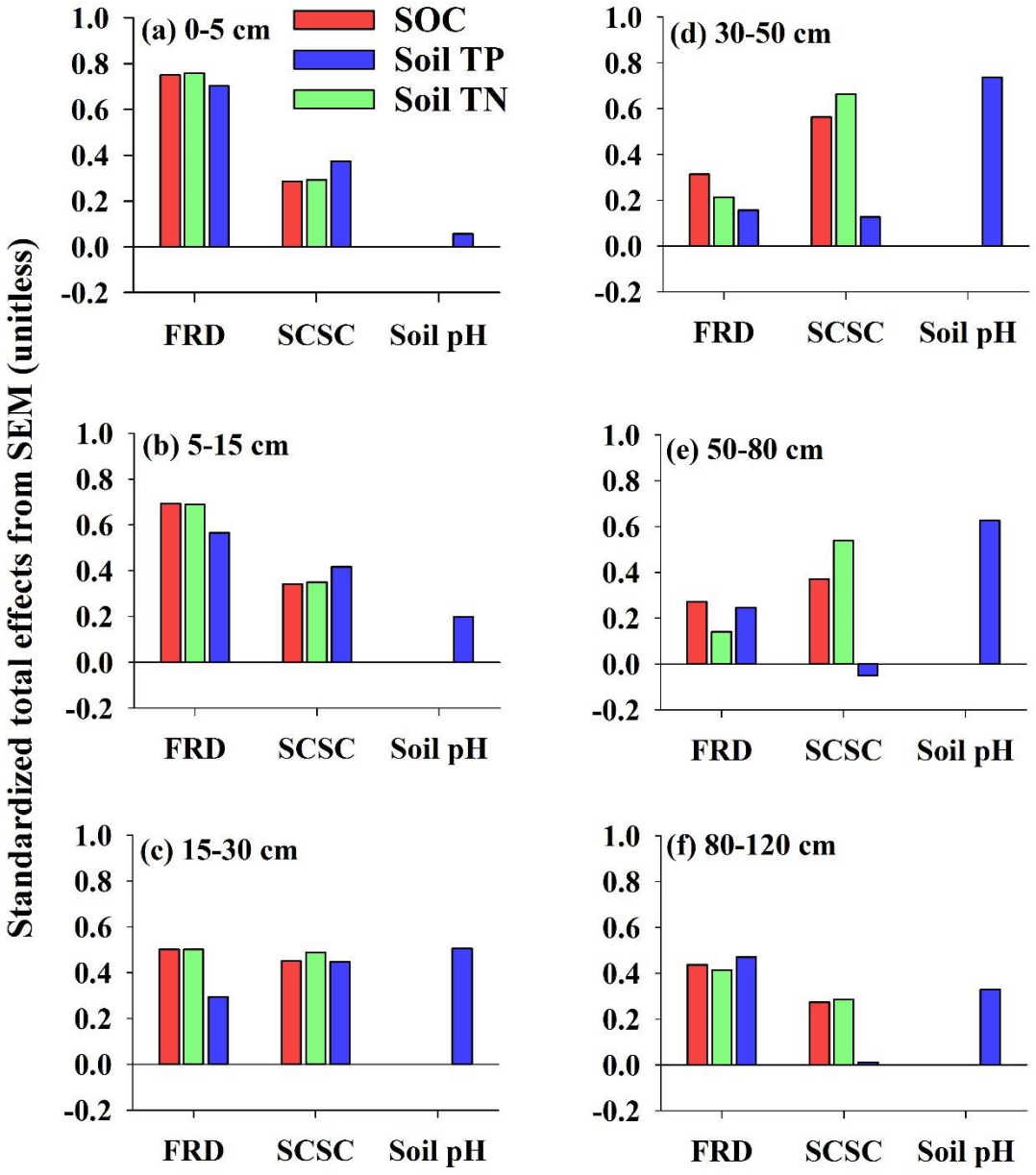

Figure 7.7 Standardized total effects (direct plus indirect effects) derived from the structural equation models. These include the effects of fine root density (FRD), soil clay and silt content (SCSC), and soil pH on the accumulation of soil organic carbon (SOC), total nitrogen (TN), and total phosphorus (TP) throughout the soil profile following woody encroachment. See Figure 2 for a description of the *a priori* model, and Figure 5 for the full graphical representation of the six structural equation models developed for each depth increment throughout the soil profile.

DISCUSSION

Our findings showed that concentrations of SOC, TN, and TP increased following woody encroachment into grasslands in this subtropical savanna, consistent with other studies around the world (Maestre *et al.* 2009; Barger *et al.* 2011; Eldridge *et al.* 2011; Kantola 2012; Sitters *et al.* 2013; Blaser *et al.* 2014; Chiti *et al.* 2017). Contrary to our first hypothesis that landscape-scale accumulation of SOC, TN, and TP would be interlinked and their relative changes would be proportional throughout the soil profile following woody encroachment, only SOC and TN were interlinked throughout the soil profile, with both increasing in similar proportions and yielding comparable spatial patterns following woody encroachment. Soil TP was uncoupled from SOC and TN, increasing more slowly than SOC and TN in surface soils (0-5 cm, hereafter) but faster in subsurface soils (15-120 cm, hereafter). This imbalanced soil C-N-P relationship was likely a consequence of changes in the relative importance of biotic and abiotic factors throughout the soil profile. Since abiotic factors, such as soil clay and silt content and soil pH, were much more important than biotic factors (i.e. fine root density) in explaining variation in SOC, TN, and TP in subsurface soils, we also reject our second hypothesis that landscape-scale accumulations of SOC, TN, and TP throughout the soil profile would be explained predominantly by root density.

Soil C-N-P imbalance in surface soils following woody encroachment

Woody proliferation is often accompanied by significant increases in primary productivity (Hibbard *et al.* 2003; Hughes *et al.* 2006; Barger *et al*. 2011), and rapidly growing trees/shrubs require the coupled use of N- and P- resources to meet the high

demands for C accumulation (Sterner & Elser 2002). In this subtropical savanna, woody encroachment is facilitated by the colonization of N_2-fixing honey mesquite trees, which drives N accumulation in this system (Boutton & Liao 2010; Soper & Sparks 2017). Nitrogen concentrations in leaf and root tissues of honey mesquite trees were 2 times and 5 times greater, respectively, than those of grass leaves and fine roots (Fig. 7.3, Appendix A). This additional N may trigger a positive feedback through a combination of less conservative N-use efficiency, increased deposition of N-rich litter, and faster microbial N-mineralization, thereby creating an N-enriched soil environment that may benefit other woody species under or near honey mesquite trees (McCulley *et al.* 2004; Bai *et al.* 2008; Soper & Sparks 2017).

Results from the scaling approach showed that the slopes of P-C stoichiometric relationships for grasslands were consistent smaller than 1 (Table 7.2). This indicates that, prior to woody plant encroachment, grassland soils contained disproportionately less P than C, and are potentially P-limited. Despite this, encroaching woody plant species across this landscape had higher P concentrations in leaf and fine root tissues than grasses, especially in fine root tissues of N_2-fixing woody species (Fig. 7.3, Appendix A), indicating that they have strategies to overcome P limitation. For example, woody species have more extensive and intensive root systems compared to grasses, especially in the vertical dimension (Jackson *et al.* 1996; Schenk & Jackson 2002), enabling them to mine P (i.e., deep acquisition) located below the depth of grass root systems (Scholes & Archer 1997; Kantola 2012; Sitters *et al.* 2013; Blaser *et al.* 2014). In addition, N_2-fixing woody species generally maintain a high root phosphatase activity enabling them to acquire soil

P present in organic form (Houlton *et al.* 2008; Olde Venterink 2011, Blaser *et al.* 2014). However, percent increases of P concentrations in leaf and fine root tissues from grasses and woody species were substantially lower than those of N (Fig. 7.3, Appendix A), and leaf N: P ratios of woody species (24.5 and 27.2 for non N_2-fixers and N_2-fixers, respectively) were markedly higher than 16.0 (leaf N: P ratios > 16.0 frequently signify P limitations, Koerselman & Meuleman 1996; Aerts & Chapin 1999). Therefore, encroaching woody species appear to be more limited by P rather than N.

Without considering the relative abundance of each plant species (Sterner & Elser 2002) and resorption processes during organ senescence (Reed *et al.* 2012), results emerging from the leaf and fine root analyses discussed above may not represent the resource stoichiometry of detritus inputs into the soil. However, C-N-P stoichiometry of leaf and fine root tissues could still provide clues about the potential mechanisms underlying the observed C-N-P imbalance in surface soils. The dynamics of soil C, N and P in surface soils are predominately regulated by biotic factors (e.g. plant residues in the form of leaf litter and dead roots, and the structure and function of microbial communities) (Zechmeister-Boltenstern *et al.* 2015), and may mimic the changes in plant stoichiometric composition following vegetation change (Sistla & Schimel 2012). Our SEM analyses also showed that fine root density as a biotic factor explained much of the variation in SOC, TN, and TP in the 0-5 cm depth increment across this landscape (Fig. 7.6a and 7.7a). Thus, the proportionally lower accumulation of soil TP compared to SOC and TN in surface soils might be linked to the fact that this system is limited by P, which in turn causes (1) lower deposition of P to surface soils from woody plant residues compared to

N (Fig. 7.3) and (2) more efficient use of P through the active cycling of soil organic P pools (Cleveland & Liptzin 2007; Boutton *et al.* 2009). This result was consistent with a global review (Cleveland & Liptzin 2007) which synthesized 186 observations from surface soils (0-10 cm) and suggested that soil C and N concentrations become increasingly decoupled from soil P concentrations when organic matter accumulates in an ecosystem.

Soil C-N-P imbalance in subsurface soils following woody encroachment

Soil physicochemical properties gradually surpassed the impact of biotic factors on the accumulations of SOC, TN, and TP with increasing soil depth (Fig. 7.6 and 7.7), especially in the 30-50 cm depth increment where clay and carbonate C start to accumulate (Appendix S1; Zhou *et al.* 2017b), leading to relatively greater increases in TP compared to SOC and TN in subsurface soils (Table 7.1 and 7.2) and correspondingly distinctive spatial patterns of TP (Fig. 7.5). Soil organic C and N dynamics tend to be strongly coupled and linked primarily through biological processes such as primary production and subsequent microbial mineralization (Delgado-Baquerizo *et al.* 2013); thus, net accumulations of SOC and TN reflect the balance of SOM inputs and losses (Six *et al.* 2002). As the main source of SOM input in subsoil (Rumpel & Kögel-Knabner 2011), root biomass generally decreases exponentially with depth (Jackson *et al.* 1996). Within this general trend, however, fine root biomass underneath groves was still two times higher than that of grasslands in subsurface soils (Zhou *et al*. 2017a).

Surprisingly, SOC and TN in groves did not appear to be substantially higher than grasslands in subsurface soils (Table 7.1). One explanation for this discrepancy may be

ascribed to the physical accessibility of SOM (Six *et al.* 2002; Salomé *et al.* 2010; Dungait *et al.* 2012). Across this landscape, groves occupy non-argillic inclusions whereas grasslands are present on subsurface soils with an argillic horizon (Archer 1995; Zhou *et al.* 2017b). Although organic matter inputs via root turnover in subsurface soils of grasslands are low, they may be more effectively physically protected from microbial decomposition by association with fine mineral particles (i.e. clay and silt) that are abundant in subsoils. In contrast, while organic matter inputs in subsurface soils of groves are high, this may be counterbalanced by less physical protection from decomposers due to coarse-textured subsoils. The net outcome is reduced differences in subsoil SOC and TN between groves and grasslands (Table 7.1). This explanation for the role of fine mineral particles in regulating the accumulation of SOC and TN may be supported by SEMs, showing that clay and silt content emerged as the main factor explaining the variances of SOC and TN in subsurface soils (Fig. 7.6 and 7.7). These smaller discrepancies lead to lower level of spatial heterogeneity in SOC and TN across this landscape (Zhou *et al.* 2017a), resulting in spatial patterns of SOC and TN in subsurface soils that bear little resemblance to vegetation cover (Fig. 7.5).

While soil organic P is stabilized together with organic C and N and subsequently mineralized through biological processes, the unique geochemical attributes of P cycling allow the fate of mineralized P to differ from C and N (Schlesinger & Bernhardt 2013). Coarse-textured subsurface soils underneath groves could favor the mineralization of organic matter as discussed above. Mineralized C and N, ultimately, leave the soil profile via gas emissions (e.g. CO_2, N_2, and nitrogen oxides), plant uptake (e.g. NO_3^- and NH_4^+),

and leaching. In contrast, mineralized P underneath groves may be immobilized not only by biological uptake, but also via the formation of calcium phosphates in basic subsurface soils, as suggested in other studies in dryland environments (Carreira *et al.* 2006; Ippolito *et al.* 2010). This interpretation is supported by our findings that (1) soil pH is the dominant factor explaining the variance of TP in subsurface soils (Fig. 7.6 and 7.7), and (2) carbonate C in subsurface soils beneath groves is higher than that beneath grasslands by up to one order of magnitude and is positively correlated with soil TP (data not shown). This potential P retention in the form of calcium phosphates may lead to a relatively greater increase in TP compared to SOC and TN in subsurface soils (Table 7.1 and 7.2), and substantial increases of TP under groves throughout the soil profile that creates spatial patterns of TP that resemble vegetation pattern across this landscape (Fig. 7.5).

Implications for soil biogeochemistry following vegetation change

Given the geographic extent of woody encroachment on a global scale (Archer 2010; Eldridge *et al.* 2011; Stevens *et al.* 2017), imbalanced relationships between soil C, N, and P can have important implications for regional and global biogeochemistry and climate. Previous estimates suggest that woody encroachment results in C sequestration (Barger *et al.* 2011), and represents 20%-40% of the U.S. C sink strength (Houghton *et al.* 2000; Pacala *et al.* 2001; King *et al.* 2007). In addition, recent studies have reported that significant C accumulation following woody encroachment occurs in deeper portions of the soil profile, suggesting previous estimates may substantially underestimate the role this vegetation change plays in regional and global C sequestration (Chiti *et al.* 2017; Zhou *et al.* 2017a). However, will the C storage potential of dryland ecosystems that are

experiencing woody encroachment be ultimately constrained by nutrient limitation, particularly by the key nutrients N and P?

In areas where the encroaching woody plants are capable of symbiotic N-fixation, N accrual may be able to increase proportionally with SOC, as observed in this study. Where encroaching woody species are incapable of N-fixation, the rate of SOC accrual may become proportionally greater than that of N if plant-available soil N becomes limiting. Given that soil P is generally present in limiting quantities in dryland ecosystems, this may limit the productivity of encroaching woody species, thereby constraining the strength of the carbon sink associated with woody encroachment. In addition, P is a key element in the N-fixation process, and reduced P availability could limit nodulation and reduce fixation rates (Israel 1987). Thus, the carbon sink strength associated with woody plant encroachment may be tightly linked to concomitant changes in the storage and availability of soil N and P.

Land cover/land use changes often perturb soil biogeochemistry and are considered essential components of coupled biogeochemistry and climate models. Recent studies have recognized the importance of incorporating P cycling into coupled climate-carbon cycling models (Reed *et al.* 2015) and C-N-P interactions into ecosystem models (Achat *et al.* 2016). Our findings suggest that modelers should be aware of the fact that the biogeochemical controls over C and N vs P cycling following vegetation change may be different, and decoupling of P cycling from C and N cycling may lead to differential responses to future perturbations and changes, as shown in this study and others (Delgado-Baquerizo *et al.* 2013; Jiao *et al.* 2016). Specific drivers and mechanisms of P cycling

should be captured in model development (Reed *et al.* 2015; Achat *et al.* 2016), especially when subsurface soils are considered.

CONCLUSIONS

We found that SOC and TN were coupled with respect to increasing magnitudes and spatial patterns throughout the soil profile following woody encroachment, whereas TP increased slower than SOC and TN in surface soils but faster in subsurface soils. This imbalanced relationship is likely due to differences in the biotic/abiotic mechanisms that control C and N vs. P accumulation, and to variation in the relative importance of these mechanisms with depth in the soil profile. Simple SEM models showed that C, N, and P concentrations in surface soils were most strongly related to fine root density, whereas in deeper portions of the soil profile the concentrations of those elements were more strongly related to soil texture and pH. Our study highlights the complex response of soil C, N, and P to vegetation change and has far reaching implication for empirical and modeling studies related to the biogeochemistry of dryland ecosystems which are particularly fragile with respect to anticipated global changes.

CHAPTER VIII

SOIL C-N-P STOICHIOMETRY IN RESPONSE TO WOODY PLANT ENCROACHMENT INTO GRASSLANDS

SYNOPSIS

Woody encroachment has been a major land cover change in dryland ecosystems during the past century. While numerous studies have demonstrated strong effects of woody encroachment on soil carbon (C), nitrogen (N), and phosphorus (P) storage, far less is known about the plasticity of soil C: N: P stoichiometry in response to woody encroachment. We assessed landscape-scale patterns of spatial heterogeneity in soil C: N : P ratios throughout a 1.2 m soil profile in a region where grassland is being replaced by a diverse assemblage of subtropical woody plants dominated by *Prosopis glandulosa*, an N_2-fixing tree. Woody species had leaf and fine root C: N: P ratios significantly different from grasses. Variation in soil C: N ratios in both horizontal and vertical planes was remarkably smaller than that of soil N: P and C: P ratios. Spatial patterns of soil C: N ratio throughout the profile were not strongly related to vegetation cover. In contrast, spatial patterns of soil N: P and C: P ratios displayed a strong resemblance to that of vegetation cover throughout the soil profile. Within the uppermost soil layer (0-5 cm), soil N: P and C: P ratios were higher underneath woody patches while lower within the grassland; however, this pattern was reversed in subsurface soils (15-120 cm). These results indicate a complex response of soil stoichiometry to vegetation change, which should be

considered in empirical and modelling studies aiming at characterizing soil C, N, and P interactions across multiple spatial scales in dryland ecosystems.

INTRODUCTION

The consistent C: N: P stoichiometry in the ocean (Redfield ratio, Redfield 1958) has prompted decades of research in ecological stoichiometry that addresses the balance of C, N, and P between organisms and substrates in ecological interactions, and now serves as a powerful tool for understand the cycling of these elements in terrestrial ecosystems (Sterner & Elser 2002). Despite relatively constrained C: N: P ratios in soils, soil microbial biomass, forest foliage and litter at the global scale (McGroddy *et al.* 2004; Cleveland & Liptzin 2007), C: N: P stoichiometric variability frequently occurs at smaller spatial scales, especially in response to changes in species composition and/or dominance (Sardans *et al.* 2012; Sistla & Schimel 2012), nutrient additions (Güsewell 2004; Sardans *et al.* 2012; Xiao *et al.* 2015), and climate change (Elser *et al.* 2010; Dijkstra *et al.* 2012; Yue *et al.* 2017).

A notable example of species dominance shift is the globally widespread woody plant encroachment into grasslands, savannas, and other arid and semiarid ecosystems (Stevens *et al.* 2017). Although the exact cause remains unclear, livestock grazing, fire suppression, rising atmospheric CO_2 concentration, and/or climate change are likely drivers of this extensive land cover change (Scholes & Archer 1997; Morgan *et al.* 2007; Van Auken 2009; Wigley *et al.* 2010; Brunelle *et al.* 2014; Devine *et al.* 2017). Though grassland to woodland conversions dramatically alter ecosystem structure and function (Eldridge *et al.* 2011) and often modify soil C, N, and P storage and dynamics (Hibbard

et al. 2001; Barger *et al.* 2011; Sitters *et al.* 2013, Li *et al.* 2016), little is known about the plasticity of soil C: N: P stoichiometry in response to woody encroachment. Furthermore, it is unclear how C: N: P responses to woody encroachment might evolve at the landscape scale and throughout entire soil profiles.

Plant C: N: P stoichiometry varies among life-forms (Reich & Oleksyn 2004). Compared to grasses, many of the tree species encroaching into grasslands around the world (e.g. *Prosopis* and *Acacia*) are capable of symbiotic N-fixation, thereby adding N to the ecosystem (Boutton & Liao 2010; Sitters *et al.* 2013; Soper *et al.* 2015). Woody species also have deep rooting systems (Jackson *et al.* 1996; Schenk & Jackson 2002) which enable them to acquire P from subsurface soils that are inaccessible to the more shallow-rooted grasses (Kantola 2012; Sitters *et al.* 2013; Blaser *et al.* 2014). Since there is growing evidence that plant functional traits serve as important drivers of soil biological processes (Bardgett & Wardle 2010), the alteration of plant C: N: P stoichiometry during vegetation change from grass to woody plant dominance is expected to have corresponding effects on soil C: N: P stoichiometry (Zechmeister-Boltenstern *et al.* 2015). However, previous studies assessing the consequences of woody plant encroachment on soil biogeochemical cycling have focused almost exclusively on pool sizes and flux rates of soil C and N (Hibbard *et al.* 2001; Wheeler *et al.* 2007; Boutton & Liao 2010), and few studies have characterized effects on soil P cycling (Kantola 2012; Sitters *et al.* 2013; Blaser *et al.* 2014). Among the studies which have reported soil C: N ratio as a soil characteristic, some have shown no net change following woody encroachment (Hibbard *et al.* 2001; Liao *et al.* 2006; Wheeler *et al.* 2007), some have reported a reduction

(Geesing *et al.* 2000; McCulley & Jackson 2012), while others have reported an increase (Springsteen *et al.* 2010; Creamer *et al.* 2011; Kantola 2012). Additionally, Kantola (2012) found that soil N: P and C: P ratios increased linearly with stand age of woody patches in a subtropical savanna encroached by *Prosopis glandulosa*, while no significant changes in soil N: P and C: P ratios were reported in other studies (Sitters *et al.* 2013; Blaser *et al.* 2014). Reasons for these discrepancies still remain unclear. It is worth noting that the aforementioned studies examined only surface soils (top 15 cm). Given that recent studies have shown that woody encroachment can have a significant impact on subsurface soil C, N and P storage (Jackson *et al.* 2002; McCulley & Jackson 2012; Chiti *et al.* 2017; Zhou *et al.* 2017a), this represents a potential knowledge gap regarding the response of C: N: P stoichiometry in subsurface soils following woody plant encroachment.

There is increasing recognition of the need for application of quantitative spatial methods for the study of ecosystem processes (Ettema & Wardle 2002), especially for soil biogeochemical processes in dryland ecosystems where patchiness of vegetation may favor the development of islands of fertility (Schlesinger *et al.* 1996). Previous studies have demonstrated that woody encroachment into grasslands has dramatically increased spatial variability and uncertainty of soil attributes (Throop & Archer 2008; Bai *et al.* 2009; Liu *et al.* 2011; Zhou *et al.* 2017a and 2018), making it difficult to generalize results from the ecosystem to the landscape scale (Zhou *et al.* 2017b). Despite this, most empirical studies on soil C: N: P stoichiometry have exclusively focused on the ecosystem scale, and far less is known about landscape-scale patterns of spatial heterogeneity in soil C: N, N: P, and C: P ratios in arid and semiarid ecosystems, especially those undergoing

vegetation change from grassland to woodland. This lack of understanding of spatial patterns of soil C: N: P stoichiometry may limit our ability to identify and quantify the biotic and abiotic factors by which they are driven.

The primary objective of this study is to assess the responses of landscapes-scale spatial patterns of soil C: N: P stoichiometry throughout the soil profile to woody encroachment. To accomplish this, we took spatially-explicit soil cores to a depth of 120 cm throughout a 160 m × 100 m subtropical savanna landscape which has undergone encroachment by *Prosopis glandulosa* and other woody species during the past century in southern Texas, USA. Our specific objectives were to (1) investigate changes in plant leaf and root C: N, N: P, and C: P ratios during vegetation change from grassland to woodland; (2) quantify patterns of spatial heterogeneity in soil C: N, N: P, and C: P ratios across this landscape and throughout the soil profile; and (3) identify biotic and abiotic factors responsible for the variation in soil C: N, N: P, and C: P ratios in 3-dimensional soil space.

MATERIALS AND METHODS

Study site

This study was conducted at the Texas A&M AgriLife La Copita Research Area (27˚40′ N, 98˚12′ W) located in the eastern Rio Grande Plains, Texas, USA. Climate is subtropical with mean annual temperature and precipitation of 22.4˚C and 680 mm, respectively. Rainfall peaks generally occur in May and September. Elevation ranges from 75 m to 90 m above sea level. The landscape consists of nearly level uplands that grade gently (1-3 % slope) to lower-lying drainage woodlands and playas. Upland soils are sandy loam with a continuous subsurface argillic horizon (*Typic Argiustolls*); however, non-

argillic inclusions (*Typic Haplustepts*) are also present sporadically (Archer 1995; Zhou *et al.* 2017b).

It has been well documented that upland vegetation at this site was once primary dominated by C_4 grasses, and that woody encroachment has occurred over the past century in response to livestock grazing and fire suppression (Archer 1995; Boutton *et al.* 1998). The increasing abundance of woody plants is initiated by the colonization of *Prosopis glandulosa*, an N_2-fixing tree legume. Once established, these *P. glandulosa* trees then serve as nurse plants to facilitate the recruitment and establishment of other woody species beneath their canopies to form discrete clusters (generally < 100 m^2) (Archer 1995; Bai *et al.* 2012). If discrete clusters occur on soils with non-argillic inclusions, they expand laterally and eventually coalesce to form large groves (generally > 100 m^2) (Archer 1995; Bai *et al.* 2012; Zhou *et al.* 2017b). Current vegetation on upland portions of this study site is characterized as a two-phase pattern of woody patches scattered throughout a grassland matrix (Whittaker *et al.* 1979), with discrete clusters and remnant grasslands occurring where the argillic horizon is well developed, and groves occurring on soils with non-argillic inclusions (Zhou *et al.* 2017b). Species composition for woody patches and remnant grasslands can be found in Appendix A.

Field sampling and lab analyses

On an upland portion of this study site, a 160 m × 100 m landscape was established and subdivided into 10 m × 10 m grid cells in January 2002 (Fig. 8.1) (Bai *et al.* 2009; Liu *et al.* 2011). X, Y coordinates of each corner of each grid cell were assigned using a GPS unit (Pathfinder Pro XRS, Trimble Navigation Ltd., Sunnyvale, CA, USA) based on the

UTM coordinate system (14 North, WGS 1984). Two sampling points were randomly selected within each 10 m × 10 m grid cell in July 2014, yielding a total of 320 sampling points across this landscape (Fig. 8.1). Distances from each sampling point to two georeferenced corners were recorded. The landscape element present at each sample point was categorized as grassland (n = 200), cluster (n = 41) or grove (n = 79) based on vegetation type and the canopy size of woody patches. At each sampling point, two adjacent soil cores (2.8 cm in diameter and 120 cm in length) were collected using the PN150 JMC Environmentalist's Subsoil Probe (Clements Associates Inc., Newton, IA, USA). Soil cores were subsequently divided into 6 depth increments (i.e. 0-5, 5-15, 15-30, 30-50, 50-80, and 80-120 cm). A color-infrared aerial photograph (6 cm x 6 cm resolution) of this landscape was acquired and georeferenced with ground control points in July 2015, and then digitized to produce a classified vegetation map. Leaf and fine root tissues of each plant species occurring on this landscape were collected in September 2016 (Appendix A).

One soil core was used to estimate fine (2 < mm) and coarse (> 2 mm) root biomass by washing through sieves. Retrieved roots were oven-dried (65 ˚C for 48 hours) for biomass determination. The other soil core was air-dried and subsequently passed through a 2 mm sieve to remove coarse organic fragments. No gravel was present in soil samples. Sieved soil samples were used to determine soil *p*H on a 1: 2 (10 g soil: 20 mL 0.01 mol/L $CaCl_2$) mixture using a glass electrode, and soil texture using the hydrometer method.

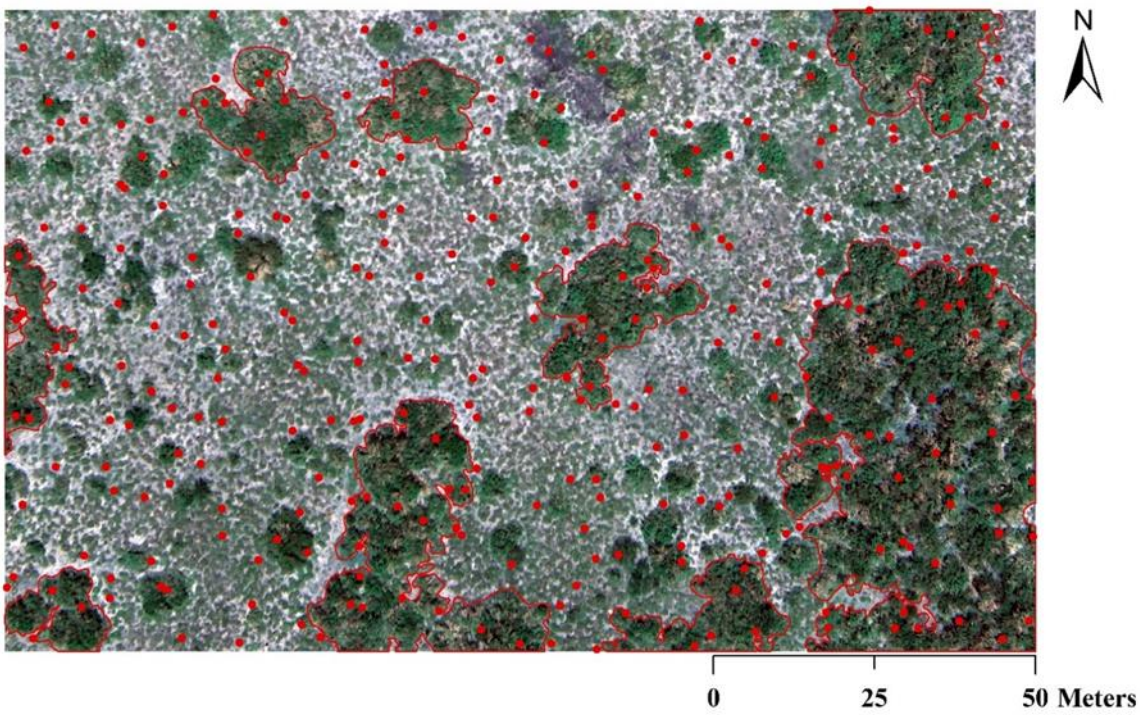

Figure 8.1 Aerial photograph of the 160 × 100 m landscape. Red points indicate locations of the 320 random soil sampling points. Green patches are woody clusters and groves, while light grey areas indicate open grasslands. Canopy edges of groves are highlighted with red lines.

An aliquot of soil that passed through the 2 mm sieve was dried at 65 ˚C for 48 hours, and then pulverized in a centrifugal mill (Angstrom, Inc., Belleville, MI, USA). Collected leaf and fine root tissues were carefully washed, dried, and also pulverized. Total C and total N concentrations of pulverized soil, leaf and fine root tissue samples were determined by dry combustion using a Costech ECS 4010 elemental analyzer (Costech Analytical Technologies Inc., Valencia, CA, USA). Organic C concentration of pulverized soil samples was determined using the same combustion system, but soil samples were pretreated with HCl vapor in a desiccator for 8 hours to remove carbonates

(Harris *et al.* 2001), and dried. Inorganic C concentration of soil samples was calculated by subtracting organic C concentration from total C concentration. The lithium fusion method was used to extract total P from pulverized soil, and from leaf and fine root tissue samples (Lajtha *et al.* 1999). More details can be found in Zhou *et al.* (2018). The P concentration in extracted solutions was determined by using the molybdenum blue colorimetry method (Murphy & Riley 1962) using a Spectronic $20D^{+}$ spectrophotometer (Thermo Fisher Scientific, Inc., Waltham, MA, USA).

Data analyses

C: N, N: P, and C: P ratios were calculated on a mass basis. Datasets that were not following a normal distribution were $\log_{10}$-transformed to improve normality. Variable means of soil C: N, N: P, and C: P ratios for different landscape elements within each depth increment were compared using mixed models which considered spatial autocorrelation as a spatial covariance for adjustment (Littell *et al.* 2006). One-way ANOVA with Student's t test was used to compare leaf and fine root C: N, N: P, and C: P ratios for different plant life forms. A cutoff value of $p < 0.05$ was used to indicate significant differences. All statistical analyses were performed using JMP Pro 12.0 (SAS Institute Inc., Cary, NC, USA).

A sample variogram fitted with a variogram model was constructed to quantify the spatial structure for soil C: N, N: P, and C: P ratios within each depth increment based on 320 random soil samples using R statistical software (R Development Core Team 2014). Ordinary kriging based on parameters from variogram models and values of 320 random soil samples was used for spatial interpolation. Kriged maps of soil C: N, N: P, and C: P

ratios across this landscape and throughout the soil profile were generated accordingly using ArcMap 10.2.2 (ESRI, Redlands, CA, USA). Lacunarity, a scale-dependent measurement of spatial heterogeneity or the "gappiness" of a landscape structure (Plotnick *et al.* 1996), was used to quantify the spatial heterogeneity of soil C: N, N: P, and C: P ratios across this landscape and throughout the soil profile. Lacunarity analyses were performed based on kriged maps using R statistical software. Lacunarity curves, plotted as the natural log transformations of lacunarity values $\Lambda(r)$ against box sizes (r) in meter, were created to visualize the spatial heterogeneity of soil C: N, N: P, and C: P ratios at different spatial scales (i.e. box sizes), with a higher value of lacunarity indicating a more heterogeneous distribution pattern across the landscape.

Correlations between soil C: N, N: P, and C: P ratios, fine root density (kg m^{-3}), soil clay (%), silt (%), pH, and inorganic carbon concentration (g C kg^{-1} soil) across this landscape and throughout the soil profile were assessed using Pearson's correlation coefficients and a modified *t*-test for testing significances. The modified *t*-test adjusts the degrees of freedom based on the extent of spatial autocorrelation in the datasets (Dutilleul *et al.* 1993). Descriptive statistics for fine root density, soil clay, silt, pH and inorganic carbon concentration have been presented elsewhere. Datasets were $\log_{10}$-transformed prior to the analysis of correlations using PASSaGE version 2 (Rosenberg & Anderson 2011).

RESULTS

Plant C: N: P stoichiometry across the landscape

Woody species (both non N_2- and N_2-fixers, hereafter) had lower mean C: N and C: P ratios but higher mean N: P ratios in leaf tissues than grasses, whereas forbs had mean C: N, N: P, and C: P ratios comparable to woody species (Fig. 8.2). Woody species had significantly lower mean C: N and C: P ratios but higher mean N: P ratios in fine root tissues than grasses across this landscape (Fig. 8.2). Overall, mean C: N, N: P, and C: P ratios of leaf tissues were lower than those of fine root tissues for all plant life-forms, especially for the C: P ratio (Fig. 8.2).

Spatial patterns of soil C: N: P stoichiometry

Soil mean C: N, N: P, and C: P ratios all decreased with soil depth, but the decreases in N: P and C: P ratios were considerably larger than those for the C: N ratio (Table 8.1). For example, mean soil C: N ratio decreased from 10.3 in the 0-5 cm depth increment to 8.2 in the 80-120 cm depth increment, whereas the N: P ratio decreased from 9.7 to 3.8 and the C: P ratio decreased from 101.3 to 31.6 (Table 8.1). Variation in soil N: P and C: P ratios across the landscape was generally about 2 to 6 times higher than that for the C: N ratio throughout the entire soil profile, as evidenced by coefficients of variation (CVs) (Table 8.1). When classified by landscape element, groves had significantly higher soil C: N ratios than grasslands throughout the soil profile, except in the 5-15 cm depth increment (Table 8.2). Groves and clusters had significantly higher soil N: P and C: P ratios than grasslands in the 0-5 cm depth increment; however, groves had

significantly lower soil N: P and C: P ratios than both grasslands and clusters throughout the 15-120 cm portion of the soil profile (Table 8.2).

Visual comparison of the classified vegetation map of this landscape and kriged maps of soil C: N ratios at each depth throughout the soil profile revealed that spatial patterns of soil C: N ratios were almost irrelevant to those of vegetation cover (Fig. 8.3a). In contrast, spatial patterns of soil N: P and C: P ratios throughout the soil profile displayed strong resemblance to the spatial distribution of woody patches, except in the 5-15 cm depth increment (Fig. 8.3b and 8.3c). Soil N: P and C: P ratios were the highest at the centers of woody patches, decreased towards the woody patch/grassland boundary, and reached lowest values within the grassland matrix in the 0-5 cm depth increment (Fig. 8.3b and 8.3c). However, these patterns were reversed in deeper portions of the soil profile (15 - 120 cm), with lower soil N: P and C: P ratios underneath groves compared to the remnant grassland matrix (Fig. 8.3b and 8.3c).

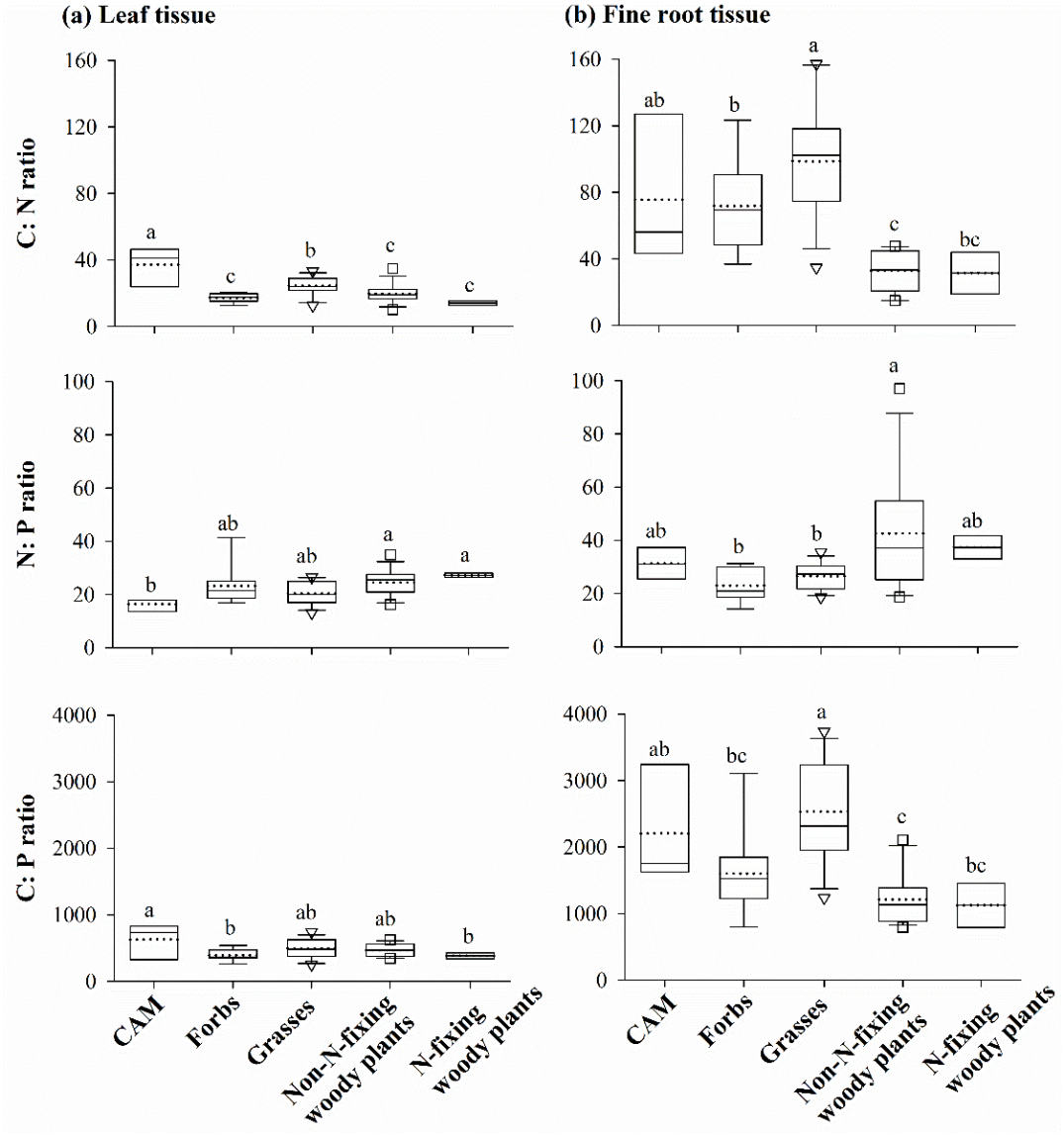

Figure 8.2 C: N, N: P, and C: P ratios of leaf and fine root tissues for different plant life-forms occurring on this 160 m ×100 m landscape. The box plots summarize the distribution of points for each variable of each plant life-form. The central box shows the inter-quartile range, median (horizontal solid line in the box), and mean (horizontal dotted line in the box). Lower and upper error bars indicate 10th and 90th percentiles, and points above and below the error bars are individuals above the 90th or below the 10th percentiles. CAM, crassulacean acid metabolism species, n = 3; Forbs, n = 9; Grasses, n = 13; Non-N-fixing woody species, n = 13; N-fixing woody species, n = 2.

Table 8.1 Descriptive statistics for soil C: N, N: P, and C: P ratios across this 160 m × 100 m landscape throughout the soil profile.

Parameters		Soil depth (cm)					
		0-5	5-15	15-30	30-50	50-80	80-120
C: N ratio							
	Mean	10.34	9.79	10.02	9.67	8.86	8.23
	Median	10.27	9.77	10.00	8.60	8.80	8.31
	Minimum	8.31	8.20	7.83	8.20	8.27	5.79
	Maximum	16.41	11.90	12.64	12.71	10.97	10.71
	CV	0.06	0.06	0.07	0.07	0.06	0.09
	Skewness	2.74	0.54	-0.05	0.87	0.92	-0.18
N: P ratio							
	Mean	9.71	7.48	6.50	5.78	4.77	3.84
	Median	8.48	7.46	6.59	6.02	4.98	3.87
	Minimum	4.45	4.55	2.83	2.75	2.26	1.92
	Maximum	26.88	15.03	9.35	8.52	6.33	6.14
	CV	0.35	0.14	0.16	0.21	0.18	0.14
	Skewness	2.07	1.19	-0.55	-0.32	-0.71	-0.05
C: P ratio							
	Mean	101.31	73.28	65.09	55.72	42.01	31.55
	Median	86.77	72.36	66.39	57.41	42.96	31.54
	Minimum	47.18	39.74	27.36	27.62	22.60	12.33
	Maximum	319.43	161.78	91.52	83.69	59.37	63.70
	CV	0.40	0.16	0.18	0.21	0.16	0.15
	Skewness	2.32	1.57	-0.51	-0.33	-0.41	0.68

Table 8.2 Mean and standard error (SE) of soil C: N, N: P and C: P ratios for different landscape element across this 160 m × 100 m landscape and throughout the soil profile.

Parameter	Landscape element	0-5 cm	5-15 cm	15-30 cm	30-50 cm	50-80 cm	80-120 cm
C: N ratio							
	Grassland	10.23 ± 0.04^{b}	9.70 ± 0.04^{a}	9.93 ± 0.05^{b}	9.47 ± 0.04^{b}	8.65 ± 0.03^{c}	8.09 ± 0.05^{b}
	Cluster	10.62 ± 0.17^{a}	9.88 ± 0.08^{a}	10.23 ± 0.12^{a}	9.97 ± 0.10^{a}	8.99 ± 0.07^{b}	8.26 ± 0.14^{b}
	Grove	10.48 ± 0.07^{a}	9.95 ± 0.06^{a}	10.13 ± 0.08^{ab}	10.02 ± 0.08^{a}	9.31 ± 0.07^{a}	8.58 ± 0.07^{a}
N: P ratio							
	Grassland	7.92 ± 0.07^{b}	7.34 ± 0.05^{b}	6.82 ± 0.05^{a}	6.24 ± 0.07^{a}	5.09 ± 0.04^{a}	3.95 ± 0.03^{a}
	Cluster	12.22 ± 0.51^{a}	8.61 ± 0.22^{a}	6.99 ± 0.14^{a}	6.09 ± 0.16^{a}	5.02 ± 0.12^{a}	4.04 ± 0.09^{a}
	Grove	12.96 ± 0.47^{a}	7.25 ± 0.14^{b}	5.42 ± 0.12^{b}	4.47 ± 0.12^{b}	3.83 ± 0.10^{b}	3.48 ± 0.07^{b}
C: P ratio							
	Grassland	81.08 ± 0.89^{b}	71.20 ± 0.53^{b}	67.76 ± 0.61^{a}	59.02 ± 0.64^{a}	44.03 ± 0.35^{a}	31.90 ± 0.30^{a}
	Cluster	131.32 ± 7.08^{a}	85.19 ± 2.47^{a}	71.49 ± 1.71^{a}	60.42 ± 1.52^{a}	44.98 ± 1.02^{a}	33.49 ± 0.92^{a}
	Grove	136.98 ± 5.51^{a}	72.38 ± 1.57^{b}	55.02 ± 1.35^{b}	44.93 ± 1.30^{b}	35.37 ± 0.80^{b}	29.66 ± 0.56^{b}

Significant differences ($p < 0.05$) between means in landscape element are indicated with different superscript letters. Number of samples: grassland = 200, cluster = 41, and grove = 79.

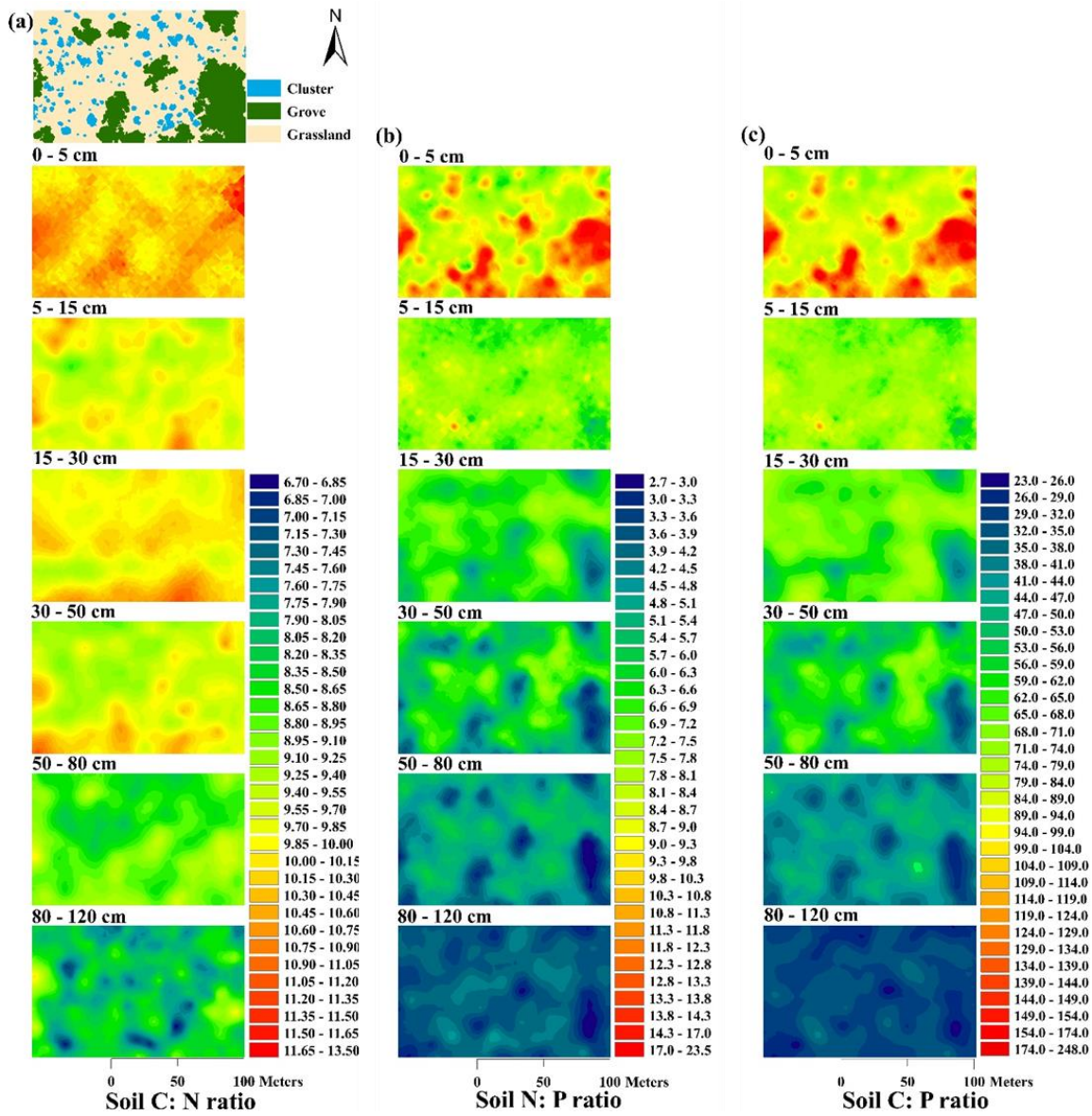

Figure 8.3 Kriged maps of soil C: N (a), N: P (b), and C: P (c) ratios based on 320 random sampling points across this l60 m × 100 m landscape and throughout the soil profile. Note that the scale is different for each elemental ratio.

Lacunarity analyses indicated that spatial heterogeneities of soil C: N ratio for all depth increments (Fig. 8.4a) were remarkably lower than those of soil N: P and C: P ratios (Fig. 8.4b and 8.4c) across this landscape. Additionally, the highest spatial heterogeneity for soil N: P and C: P ratios was observed in the 0-5 cm depth increment (Fig. 8.4b and 8.4c). Results from lacunarity analysis were consistent with variation in C: N, N: P, and C: P ratios as indicated by CVs across this landscape (Table 8.1).

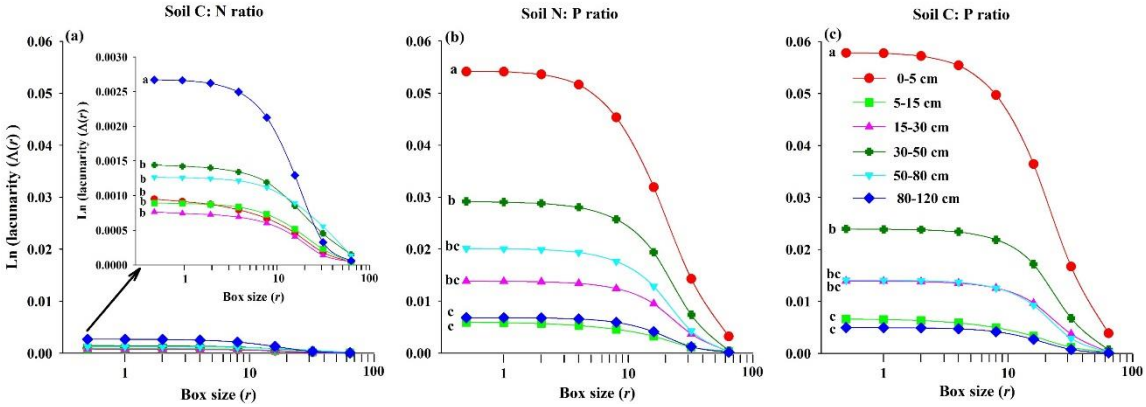

Figure 8.4 Lacunarity curves for soil C: N (a), N: P (b), and C: P (c) ratios across this l60 m × 100 m landscape and throughout the soil profile.

Correlations between soil C-N-P stoichiometry and soil physicochemical factors

Soil N: P ratio was significantly and positively correlated with soil C: P ratio for all depth increments. Soil C: N ratio was significantly and positively correlated with soil N: P ratio in the 0-5 cm depth increment but negatively in the 30-50, 50-80, and 80-120 cm depth increments. Soil C: N ratio was significantly and positively correlated with soil C: P ratio in the 0-5, 5-15, 15-30, and 80-120 cm depth increments but negatively in the

50-80 cm depth increment (Table 8.3). Soil C: N ratio was significantly and positively correlated with fine root density throughout the soil profile except for the 15-30 cm depth increment; soil C: P and N: P ratios were significantly and positively correlated with fine root density in the 0-5 and 5-15 cm depth increments but negatively in the 15-30, 30-50, and 50-80 cm depth increments (Table 8.3). Soil C: N ratio was significantly and negatively correlated with soil clay in the 30-50 and 50-80 cm depth increments and positively correlated with soil *p*H in the 30-50, 50-80, and 80-120 cm depth increments. Soil N: P and C: P ratios were significantly and positively correlated with soil clay in the 30-50, 50-80, and 80-120 cm depth increments and negatively correlated with soil *p*H in the 15-30, 30-50, and 50-80 cm soil depth increments. Soil N: P and C: P ratios were significantly and negatively correlated with soil silt in the 15-30 and 30-50 cm depth increments but positively in the 80-120 cm depth increment. (Table 8.3). Soil C: N ratio was significantly and positively correlated with inorganic carbon in the 0-5, 30-50, 50-80, and 80-120 cm depth increments, but negatively in the 15-30 cm depth increment. Soil N: P and C: P ratios was significantly and positively correlated with inorganic carbon in the 0-5 cm depth increment, but negatively in the 5-15, 15-30, 30-50, and 50-80 cm depth increments (Table 8.3).

Table 8.3 Pearson's correlation coefficients (r) showing relationships between soil C: N, N: P, and C: P ratios, fine root density (FRD), soil clay, silt and pH throughout the soil profile. A modified T-test for correlation was used to test for significance.

Characteristic	Soil N:P	Soil C: P	FRD	Soil clay	Soil silt	Soil pH
0-5 cm						
Soil C: N	0.40***	0.55***	0.17**	0.05	0.01	-0.00
Soil N: P		0.99***	0.73***	0.11	0.21	-0.01
Soil C: P			0.70***	0.11	0.19	-0.01
FRD				0.08	0.19	0.06
Soil clay					0.50*	0.13
Soil silt						0.15*
5-15 cm						
Soil C: N	0.06	0.42***	0.18**	0.04	0.06	0.08
Soil N: P		0.93***	0.18**	-0.03	-0.05	-0.01
Soil C: P			0.23***	-0.01	-0.02	0.02
FRD				0.07	0.36**	0.33***
Soil clay					0.47*	0.14
Soil silt						0.29***
15-30 cm						
Soil C: N	0.03	0.39***	0.12	-0.04	0.15*	0.06
Soil N: P		0.93***	-0.23**	-0.02	-0.37**	-0.46***
Soil C: P			-0.17*	-0.03	-0.28**	-0.40***
FRD				0.03	0.24*	0.32***
Soil clay					0.42*	0.04
Soil silt						0.42***
30-50 cm						
Soil C: N	-0.26***	0.02	0.27***	-0.29***	0.24	0.18*
Soil N: P		0.96***	-0.25***	0.45***	-0.26*	-0.62***
Soil C: P			-0.18**	0.38***	-0.20*	-0.59***
FRD				-0.21**	0.06	0.24**
Soil clay					0.16	-0.24**
Soil silt						0.40***
50-80 cm						
Soil C: N	-0.54***	-0.26***	0.37***	-0.37***	-0.06	0.30***
Soil N: P		0.95***	-0.46***	0.46***	0.02	-0.52***
Soil C: P			-0.39***	0.39***	0.00	-0.49***
FRD				-0.32***	-0.03	0.28***
Soil clay					0.38***	0.05
Soil silt						0.25*
80-120 cm						
Soil C: N	-0.23***	0.34***	0.25***	0.09	0.11	0.29***
Soil N: P		0.84***	-0.22***	0.35***	0.24***	-0.15*
Soil C: P			-0.07	0.39***	0.29***	0.02
FRD				-0.16*	-0.15*	0.16*
Soil clay					0.66***	0.32***
Soil silt						0.16

*, $p < 0.05$; **, $p < 0.01$; ***, $p < 0.001$.

DISCUSSION

Changes in plant C: N: P stoichiometry in response to woody encroachment

Vegetation change from grassland to woodland has dramatically altered plant C: N: P stoichiometry across this landscape (Fig. 8.2). Lower C: N and C: P ratios in leaf and fine root tissues of woody species compared to grasses may be ascribed to the fact that C concentrations of woody species are relatively comparable to those of grasses, while N and P concentrations are much higher in the woody species (unpublished data). There are three potential explanations for this: (1) the dominant tree (i.e. *P. glandulosa*) in woody patches across this landscape is a legume and capable of symbiotic N_2-fixation (Zitzer *et al.* 1996; Boutton & Liao 2010; Soper *et al.* 2015); (2) *P. glandulosa* and other woody species have deeper root systems than herbaceous species (grasses, forbs) that dominate these grasslands (Watts 1993; Boutton *et al.* 1999), allowing them to access deep soil N and P located beyond the reach of other plant species (Zhou *et al.* 2018); and (3) soils beneath N_2-fixers generally have higher phosphatase enzyme activity than non N_2-fixers (Houlton *et al.* 2008; Boutton *et al.* 2009; Blaser *et al.* 2014; Png *et al.* 2017), enabling mineralization of organic P into plant available forms (Kantola 2012). Additional N and P acquired through these mechanisms eventually enrich soils beneath woody plant canopies via litterfall and root turnover (Schlesinger *et al.* 1996). Relatively N- and P-rich soils underneath woody patches compared to grasslands favor higher leaf and root N and P concentrations, thus lower C: N and C: P ratios in woody species (Zechmeister-Boltenstern *et al.* 2015).

Observed higher N: P ratios in leaf and fine root tissues of woody plants than those of grasses suggests soil N is relatively more available than P following woody encroachment. N: P ratios of terrestrial plant species have been extensively studied as indicators of N or P limitation (Koerselman & Meuleman 1996; Güsewell 2004; Han *et al.* 2005; Reich & Oleksyn 2004; Yuan *et al.* 2011). Individual measurements of plant N: P ratios range from approximately 1-100 (Güsewell 2004), but the average for terrestrial plant species is approximately 12.0 -14.0 for leaves (Elser *et al.* 2000; Reich & Oleksyn 2004) and approximately 14.0 – 24.0 for roots depending on root size and status (i.e. live or dead) (Yuan *et al.* 2011). Our N: P ratios for leaves of all collected species are considerably higher than these aforementioned averages (Fig. 8.2), ranging from 16.4 for CAM species to 27.2 for N_2-fixing woody species (Fig. 8.2). It has been proposed that leaf N: P ratios > 16.0 indicate P limitation (Koerselman & Meuleman 1996; Güsewell 2004; Han *et al.* 2005), suggesting that plant species occurring on this landscape are more likely limited by P rather than N.

Soil C: N ratios change little in response to woody encroachment

The significant resorption of N and P during plant organ senescence results in nutrient-depleted litter (Aerts 1996; Güsewell 2004; Lü *et al.* 2012), thus increasing C: N and C: P ratios of litter compared to live tissues (McGroddy *et al.* 2004). For this reason, the C: N: P of live leaf and fine root tissues may not represent those of litter and senesced roots which are the primary sources of soil organic matter. However, microbial decomposition processes tend to retain nutrients more efficiently while consuming a significant amount of C (Moore *et al.* 2011; Manzoni *et al.* 2010 and 2012), thereby

driving C: N: P ratios of litter towards those of soil organic matter and microorganisms (Zechmeister-Boltenstern *et al.* 2015). For example, despite large variation in litter C: N: P stoichiometry (McGroddy *et al.* 2004), a well-constrained mean C: N: P ratio of 72: 6: 1 has been reported for surface soils (0-10 cm) at the global scale (Cleveland & Liptzin 2007). In this subtropical savanna, mean soil C: N: P ratios across this landscape range from 101: 10: 1 in the surface soil to 32: 4: 1 in deeper portions of the profile (Table 8.1). When categorized by landscape elements and compared to soil C: P and N: P ratios, however, the soil C: N ratio varied less among different depth increments (Table 8.1 and 8.2, Fig. 8.4) and also among different landscape elements (Table 8.2), suggesting that responses of soil C: N ratio to woody encroachment throughout the soil profile are more constrained than those of soil C: P and N: P ratios.

The small variation in the depth distribution of soil C: N ratio across this landscape agrees with studies in other savanna ecosystems worldwide (Lilienfein *et al.* 2001; McCulley & Jackson; 2012; Coetsee *et al.* 2013; Dintwe et al; 2015), and with results from regional and global syntheses (Batjes 1996; Tian *et al.* 2010). As soil C and N are biologically mineralized and stabilized together, soil C: N ratio is often used to indicate the degree of decomposition (McGill & Cole 1981; Batjes 1996). The slight decrease in soil C: N ratio throughout the profile is consistent with the fact that soil organic matter stored in deeper portions of the soil profile is older and has experienced a greater degree of microbial decomposition (Boutton *et al.* 1998).

Soils underneath woody patches (both clusters and groves) had slightly higher C: N ratios than those underneath grasslands (Table 8.2). There are two possible

explanations. Firstly, soils underneath woody patches have higher litter and root inputs compared to remnant grasslands (Liu *et al.* 2010; Zhou *et al.* 2017a), potentially leading to a soil organic matter pool comprised largely of plant materials in the early stages of decomposition in the upper portion of the profile (Liao *et al.* 2006). Secondly, litter in wooded areas consists of more biochemically recalcitrant materials (particularly aliphatic biopolymers) which are less suitable as microbial substrates compared to litter in remnant grasslands (Liao *et al.* 2006; Filley *et al.* 2008). This more recalcitrant litter in wooded areas may decompose more slowly and lead to higher soil C: N ratios (McGill & Cole 1981; Batjes 1996).

Despite the small variation in soil C: N ratios across this landscape (Table 8.1 and Fig. 8.4), spatial autocorrelation has been detected for soil C: N ratios throughout the soil profile based on variogram analyses, especially in deep portions of the soil profile (data not shown). However, areas with high C: N ratio presented in these kriged maps were less relevant to the spatial distribution of woody patches, especially in surface soils (0-30 cm) (Fig. 8.3a). Reasons for this discrepancy still remain unknown.

More flexible soil C: P and N: P ratios in response to woody encroachment

Our results indicate that responses of soil C: P and N: P ratios to woody encroachment were very similar (Fig. 8.3b, 8.3c, 8.4b, and 8.4c), as soil C: P and N: P ratios were highly correlated throughout the soil profile ($r > 0.80$, Table 8.3). More importantly, in contrast to the constrained responses of soil C: N ratio to woody encroachment throughout the soil profile, responses of soil C: P and N: P ratios were relatively more flexible. More specifically, spatial heterogeneities of soil C: P and N: P

ratios were substantially higher than those of soil C: N ratios (Fig. 8.4), and decreasing magnitudes in soil C: P and N: P ratios throughout the soil profile were proportionally more dramatic than those of soil C: N ratios (Table 8.1 and 8.2). C: N ratios decreased by approximately 20%, while C: P and N: P ratios decreased by 50-80% from the top to the bottom of the soil profile. Interestingly, soil C: P and N: P ratios were higher under woody patches compared to grasslands in the 0-5 cm depth increment, but this pattern was reversed (i.e., lower ratios under woody patches) in subsurface (15-120 cm) soils (Table 8.2, Fig. 8.3b and 8.3c).

Our observation of increased soil C: P and N: P ratios in surface soils following woody encroachment is consistent with a previous study in this site which reported both soil C: P and N: P ratios increased linearly with stand age of woody patches (0-10 cm, Kantola 2012), but is different from studies in South Africa which showed no changes in either soil C: P or N: P ratios in savannas following the encroachment of the N-fixers *Dichrostachys cinerea* (0-10 cm, Blaser *et al.* 2014) and *Acacia zanzibarica* (0-15 cm, Sitters *et al.* 2013). This discrepancy may be ascribed to the fact that aforementioned savannas in South Africa show no sign of either N or P limitation (Sitters *et al.* 2013; Blaser *et al.* 2014), while our site appears to be P limited based on leaf tissue N: P ratios > 16. This P limitation may lead to a more conservative P use efficiency by increasing P resorption during senescence (Aerts 1996; Güsewell 2004; Lü *et al.* 2012; Zechmeister-Boltenstern *et al.* 2015), resulting in less deposition of P into surface soils where litter is concentrated. In addition, fast growing N_2-fixers usually have a higher P requirement (Treseder & Vitousek 2001; Vitousek *et al.* 2002; Houlton *et al.* 2008) which may be

fulfilled by high rates of phosphatase activity beneath soils of N_2-fixing woody plants (Houlton *et al.* 2008; Blaser *et al.* 2014). Amplified resorption and mineralization due to P limitation in this system may lead to a less proportional accumulation of P than C and N in surface soils following woody encroachment, thereby increasing soil C: P and N: P ratios.

The depth distribution of soil C: P and N: P ratios in savanna ecosystems is less studied compared to that of soil C: N ratio. However, the dramatic decrease in soil C: P and N: P ratios throughout the soil profile in this study (Table 8.1 and 8.2, Fig. 8.3) is consistent with results from a regional study based on 2,384 soil profiles in China (Tian *et al.* 2010) and other studies conducted in a variety of ecosystems (Walker & Adams 1958; Lilienfein *et al.* 2001; Bing *et al.* 2016). The reason for this dramatic decrease may be ascribed to the fact that biologically related soil C and N generally decrease throughout the soil profile more dramatically than soil P which also has a significant geochemical component to its cycle (Walker & Adams 1958; Wood *et al.* 1984; Tian *et al.* 2010; Zhou *et al.* 2018). Interestingly, soil C: P and N: P ratios underneath groves decreased faster than those underneath clusters and grasslands (Table 8.3), creating reversed spatial patterns of soil C: P and N: P ratios in subsurface soils compared to those in surface soils (Fig. 8.3). In this study site, clusters and grasslands occur on soils with a subsurface argillic horizon, whereas groves are present on non-argillic inclusions (Archer 1995; Zhou *et al.* 2017b). Coarse-textured subsurface soils underneath groves may provide less physical protection of soil organic matter in aggregates (Liao *et al.* 2006), thereby enabling more rapid mineralization of soil organic matter (Six *et al.* 2002). Mineralized C and N

eventually leave the system through gaseous emissions (e.g. CO_2, NO, NO_x, N_2O, N_2) and/or leaching (NO_3^-), whereas P can be immobilized by plants and/or microbes or precipitated as calcium phosphates in these alkaline calcareous soils (Carreira *et al.* 2006; Schlesinger & Bernhardt 2013). For this potential reason, subsurface soil C: P and N: P ratios underneath groves were significantly lower than those of clusters and grasslands. This inference is indirectly supported by Pearson's correlation analysis indicating that soil C: P and N: P ratios were significantly and negatively correlated with soil pH and inorganic C concentration in subsurface soils (Table 8.3).

CONCLUSIONS

We found that different plant life-forms (woody vs herbaceous) have distinctive leaf and fine root C: N: P stoichiometry in this subtropical savanna. Correspondingly, the encroachment of *P. glandulosa* and other trees/shrubs has dramatically altered soil C: N: P stoichiometry across this landscape and throughout the soil profile. Differences in soil C: N ratios among different landscape elements and different soil depth increments were relatively small, so their spatial patterns were not strongly affected by vegetation patterns. However, large spatial heterogeneities were found for soil C: P and N: P ratios in both horizontal and vertical planes, creating distinct spatial patterns of soil C: P and N: P ratios that strongly resembled the distribution pattern of woody patches. These contrasting results suggest that responses of soil C: N ratios to woody encroachment may be constrained by the strong biological relationship between C and N in soil organic matter inputs and losses, whereas pool sizes of soil P (and therefore C: P and N: P ratios) can be affected not only by organic matter inputs and losses, but also by geochemical processes

that influence the retention of P in the soil environment. Given that woody encroachment is a globally widespread phenomenon in dryland ecosystems, the complex response of soil C: N: P stoichiometry to woody encroachment observed in this study should be considered in empirical and modeling studies aiming at characterizing soil C, N, and P interactions and variation across multiple spatial scales in dryland ecosystems.

CHAPTER IX

VEGETATION CHANGE ALTERS SOIL PROFILE $\delta^{15}N$ VALUES AT THE LANDSCAPE SCALE*

SYNOPSIS

The assessment of spatial variation in soil $\delta^{15}N$ could provide integrative insights on soil N cycling processes across multiple spatial scales. However, little is known about spatial patterns of $\delta^{15}N$ within soil profiles in arid and semiarid ecosystems, especially those undergoing vegetation change with a distinct shift in dominance and/or functional type. We quantified how changes from grass to woody plant dominance altered spatial patterns of $\delta^{15}N$ throughout a 1.2 m soil profile by collecting 320 spatially-specific soil cores in a 160 m × 100 m subtropical savanna landscape that has undergone encroachment by *Prosopis glandulosa* (an N_2-fixer) during the past century. Leaf $\delta^{15}N$ was comparable among different plant life-forms, while fine roots from woody species had significantly lower $\delta^{15}N$ than herbaceous species across this landscape. Woody encroachment significantly decreased soil $\delta^{15}N$ throughout the entire soil profile, and created horizontal spatial patterns of soil $\delta^{15}N$ that strongly resembled the spatial distribution of woody patches and were evident within each depth increment. The lower soil $\delta^{15}N$ values that characterized areas beneath woody canopies were mostly due to the encroaching woody

* Originally published as: Zhou, Y., Mushinski, R.M., Hyodo, A., Wu, X.B., Boutton, T.W. (2018) Vegetation change alters soil profile $\delta^{15}N$ at the landscape scale. *Soil Biology & Biochemistry*, doi: org/10.1016/j.soilbio.2018.01.012. In press.

species, especially the N_2-fixer *P. glandulosa*, which delivered ^{15}N-depleted organic matter via root turnover throughout the soil profile. Soil $\delta^{15}N$ increased with depth, reached maximum values at intermediate depths, and slightly decreased at greater depths. This vertical pattern may be related to the decrease of ^{15}N-depleted organic matter inputs with depth, and to the presence of a subsurface clay-rich argillic horizon at intermediate depths across this landscape, which may favor the accumulation of ^{15}N-enriched residues. These results indicate that succession from grassland to woodland has altered the spatial variation in soil $\delta^{15}N$ across the landscape and to considerable depth, suggesting significant changes in the relative rates of N-inputs vs. N-losses in this subtropical system after vegetation change.

INTRODUCTION

The stable nitrogen isotope composition ($\delta^{15}N$) of bulk soil, as an integrator of the soil N cycle, reflects the long-term net difference between $\delta^{15}N$ values of N inputs (e.g. fixation, deposition) and those of N outputs (e.g. gaseous losses, leaching) (Högberg 1997; Robinson 2001; Amundson *et al.* 2003; Hobbie & Ouimette 2009; Pardo & Nadelhoffer 2010; Craine *et al.* 2015; Denk *et al.* 2017). As a result, soil $\delta^{15}N$ values can provide integrative insights regarding the behavior of the soil N cycle across a range of spatial and temporal scales.

Soil $\delta^{15}N$ values can vary by as much as 9-10 ‰ within a profile (Hobbie & Ouimette 2009), and generally increase with depth (Bundt *et al.* 2001; Huygens *et al.* 2008; Yang *et al*. 2015). In some cases, maximum soil $\delta^{15}N$ values occur at intermediate soil depths, with lower values both near the soil surface and deeper in the profile

(Bustamante *et al.* 2004; Hobbie & Ouimette, 2009). Several mechanisms have been proposed to explain these vertical patterns of ^{15}N enrichment throughout the soil profile (reviewed in Hobbie & Ouimette 2009), including: (1) accumulation of ^{15}N-encriched microbial residues at depth as a result of transfer of ^{15}N-depleted N to plants by mycorrhizae, especially ectomycorrhizal fungi (Högberg 1997; Lindahl *et al.* 2007; Huygens *et al.* 2008; Hobbie & Ouimette 2009; Hobbie & Högberg 2012; Mayor *et al.* 2015; Denk *et al.* 2017); (2) preferential preservation of ^{15}N-encriched compounds during organic N decomposition (Hobbie & Ouimette 2009); (3) fractionation against ^{15}N during N transformations (e.g. nitrification and denitrification) followed by the subsequent loss of ^{15}N-depleted gases (e.g. NO, N_2O, N_2) produced during those transformations (Nadelhoffer & Fry 1988; Hobbie & Ouimette 2009; Craine *et al.* 2015; Denk *et al*. 2017).

Vegetation can directly affect soil $\delta^{15}N$ through symbiotic N_2-fixation and mycorrhizal associations (Högberg 1997; Craine *et al.* 2015; Mayor *et al.* 2015), or indirectly through the modification of substrate quality/quantity and/or micro-environmental conditions that may influence rates of soil N transformations (Bai *et al.* 2009; Wang *et al.* 2012; Bai *et al.* 2012). For these reasons, when ecosystems undergo disturbances that modify vegetation dominance, primary production, and/or rates of N transformations, soil $\delta^{15}N$ is likely to be altered (Bai *et al.* 2012). These potential modifications of soil $\delta^{15}N$ following vegetation changes represent another complication to the utility of soil $\delta^{15}N$ as a diagnostic tool for inferring prevalent soil N cycling processes under disturbed conditions.

A notable example of a change in vegetation dominance is the geographically widespread phenomenon of woody plant encroachment into grass-dominated ecosystems in arid and semiarid regions, which appears to be caused by livestock overgrazing, reduced fire frequency, rising atmospheric CO_2 concentration, and climate change (Bond & Midgley 2000; Eldridge *et al.* 2011; Archer *et al.* 2017; Stevens *et al*. 2017), all of which have the potential to favor the productivity of C_3 woody plants at the expense of C_4 grasses. Woody plant encroachment is a complex social-ecological issue that has long been of concern to land managers because it has the potential to reduce the productivity of grazing livestock (e.g., cattle, sheep, equines) whose diets are strongly grass-based (Archer *et al.* 2017). In addition, woody encroachment has been shown to have significant impacts on biodiversity, hydrology, and biogeochemistry at ecosystem to global scales (Hibbard *et al.* 2001; Huxman *et al.* 2005; Pacala *et al.* 2007; Ratajczak *et al.* 2012; Ge & Zou, 2013; Anadón *et al.* 2014; Poulter *et al.* 2014).

In the context of soil N cycle, woody plant encroachment has been demonstrated to increase N inputs, intensify rates of soil N cycling processes, and accelerate N losses through leaching and trace gas emissions (Hibbard *et al.* 2001; Martin *et al.* 2003; McCulley *et al.* 2004; Liao *et al.* 2006; McKinley *et al.* 2008; Eldridge *et al.* 2011; Creamer *et al.* 2013; Soper *et al.* 2016). Although many studies have found decreased soil $\delta^{15}N$ after woody plant encroachment (Wheeler *et al.* 2007; Boutton & Liao, 2010; Sitters *et al.* 2013), others have found either no net change (Blaser *et al.* 2014), or even increased soil $\delta^{15}N$ (Bekele & Hudnall 2005; Billings & Richter 2006). Reasons for these discrepancies remain unclear, but may be related to whether or not the encroaching woody

species include plants capable of symbiotic N-fixation, and/or the degree of impact that increased woody plant abundance has on individual soil N processes that vary in the extent of fractionation against ^{15}N. More importantly, most of these studies investigating the impact of woody encroachment on soil $\delta^{15}N$ have focused on surface soils (mostly < 30 cm). However, recent studies have emphasized that woody encroachment can have significant impacts on deep soil biogeochemistry (Chiti *et al*. 2016; Zhou *et al.* 2017a), as encroaching woody species generally have root systems that are distributed more deeply than those of the herbaceous species (Schenk & Jackson 2002). Therefore, there is currently a knowledge gap regarding the direction and magnitude of soil $\delta^{15}N$ changes in deeper portions of the soil profile following disturbance and vegetation change in arid and semiarid ecosystems.

Spatial variations in soil $\delta^{15}N$ could provide integrative insights on the soil N cycle across multiple spatial scales (Craine *et al.* 2009; Pardo & Nadelhoffer 2010; Bai *et al.* 2012; Wang *et al.* 2012; Rascher *et al.* 2012; Ruiz-Navarro *et al.* 2016). Woody plant encroachment into grass-dominated ecosystems is generally associated with the amplification of spatial heterogeneity in soil properties ("islands of fertility", Schlesinger *et al*. 1996), making it more difficult to generalize ecosystem processes based on sampling at small spatial scales and limited sample sizes (Throop & Archer 2008; Liu *et al.* 2011; Zhou *et al.* 2017b). Previous studies have demonstrated the existence of spatial variations in soil $\delta^{15}N$ in arid and semiarid ecosystems and identified driving factors (such as vegetation type, topoedaphic properties, and water availability) responsible for those spatial variations (Bai *et al.* 2012; Wang *et al.* 2013; Ruiz-Navarro *et al.* 2016). However,

these studies were largely confined to surface soils, and it remains unclear how changes in plant life forms and/or functional types in arid and semiarid ecosystems may influence spatial variation in soil $\delta^{15}N$ values in deeper portions of the soil profile.

In this study, we investigated a well-studied subtropical savanna ecosystem that has undergone encroachment by *Prosopis glandulosa* (an N_2-fixing tree legume) and other subordinate tree/shrub species during the past century in southern Texas, USA (Archer *et al.* 1988; Boutton *et al.* 1998). Prior research in this region has documented that woody plant encroachment has altered spatial patterns of soil $\delta^{15}N$ in surface soils (0-15 cm) (Bai *et al.* 2012). To further expand on this work, we collected 320 spatially specific soil cores to a depth of 1.2 m across a 160 m × 100 m landscape in this subtropical savanna to test the following two hypotheses: (1) the deep-rooting characteristics of the encroaching woody species would modify soil $\delta^{15}N$ values to considerable depth within the soil profile; and (2) landscape-scale spatial patterns of soil $\delta^{15}N$ in the horizontal plane would be evident throughout the soil profile and correlated with the distribution patterns of the encroaching woody vegetation.

MATERIALS AND METHODS

Study site

Research was conducted at the Texas A&M AgriLife La Copita Research Area (27˚40′ N, 98˚12′ W; elevation 75-90 m a.s.l.) in Jim Wells County, Texas, USA (Fig. 9.1). The climate is subtropical, with mean annual temperature and precipitation of 22.4 ˚C and 680 mm, respectively. Landscapes consist of well-drained uplands that grade gently (1-3 % slopes) to lower-lying drainage woodlands. Soils on upland portions of the landscape

are sandy loams (Typic and Pachic Argiustolls) with a laterally extensive but discontinuous clay-rich argillic horizon (B_t) which begins 30-50 cm below the surface (Archer, 1995; Zhou *et al*. 2017b).

Multiple lines of evidence (i.e. historical accounts, tree-ring analyses, and coupled $\delta^{13}C$-^{14}C analyses of soil organic matter) have indicated that upland vegetation was once almost exclusively dominated by C_4 grasses, and woody encroachment into C_4 dominated grasslands has occurred during the past century due to overgrazing and reduced fire frequency (Archer *et al.* 1988; Archer 1995; Boutton *et al.* 1998; Archer *et al.* 2001). Current upland vegetation is comprised of discrete woody patches distributed within a remnant C_4 grassland matrix (Archer *et al.* 1988; Archer 1995). Woody patches consist of small shrub clusters (generally < 100 m^2) and large groves (generally > 100 m^2). The formation of woody patches is initiated by the colonization of *Prosopis glandulosa*, an N_2-fixing tree legume (Zitzer *et al.* 1996; Soper *et al.* 2015). Established *P. glandulosa* trees then serve as nurse plants, facilitating the recruitment of other trees/shrubs underneath their canopies to form discrete clusters (Archer *et al*. 1988). The spatial distribution of clusters across this landscape is random and not related to the spatial heterogeneity in subsurface soil texture (Zhou *et al.* 2017b). However, if clusters occur on non-argillic inclusions (i.e. coarse-textured soils), they expand laterally and coalesce to form groves (Archer 1995; Zhou *et al.* 2017b). In the process of occupying the non-argillic inclusions, groves will often merge with clusters that develop on the argillic soils. Therefore, the peripheral areas of groves often occupy soils where the argillic horizon is present. At present, the remnant grassland matrix is dominated by C_4 grasses, but also includes C_3

forbs and a small portion of crassulacean acid metabolism (CAM) species. Groves are dominated by *P. glandulosa* trees with up to 15-20 other tree/shrub species in the understory. Clusters consist of the same woody species as groves, but *P. glandulosa* in clusters are significantly smaller and younger than those in groves (Boutton *et al.* 1998). Grasses and other herbaceous species are extremely rare underneath clusters and groves. Species composition can be found in Appendix A. Based on the plant and soil properties and processes that characterize grasslands, clusters, and groves, each are unique ecosystems that comprise the upland landscape, and we refer to them as landscape elements (Turner *et al.* 2001).

Field sampling and lab analyses

On an upland portion of this study site, a 160 m × 100 m landscape consisting of 10 m × 10 m grid cells was established in January 2002 (Liu et al., 2011) (Fig. 9.1). Each corner of each grid cell was georeferenced using a GPS unit, assigning X, Y coordinates (UTM WGS1984 zone 14N). In each grid cell, two random sampling points were selected in July 2014, yielding 320 sampling points across this landscape (Fig. 9.1). Distances from each sampling point to two georeferenced cell corners were recorded for calculating coordinates of each point. The vegetation of each sampling point was categorized as grassland, cluster or grove based on vegetation type and canopy size of woody patches. At each sampling point, two adjacent soil cores (120 cm deep × 2.8 cm diameter) were collected (PN150 JMC Environmentalist's Subsoil Probe, Clements Associates Inc., Newton, IA, USA) and subdivided into six depth increments (i.e. 0-5, 5-15, 15-30, 30-50, 50-80, and 80-120 cm). A color-infrared aerial photograph of this landscape was acquired

in July 2015 and the normalized difference vegetation index (NDVI) of each sampling point was calculated (Zhou *et al.* 2017a).

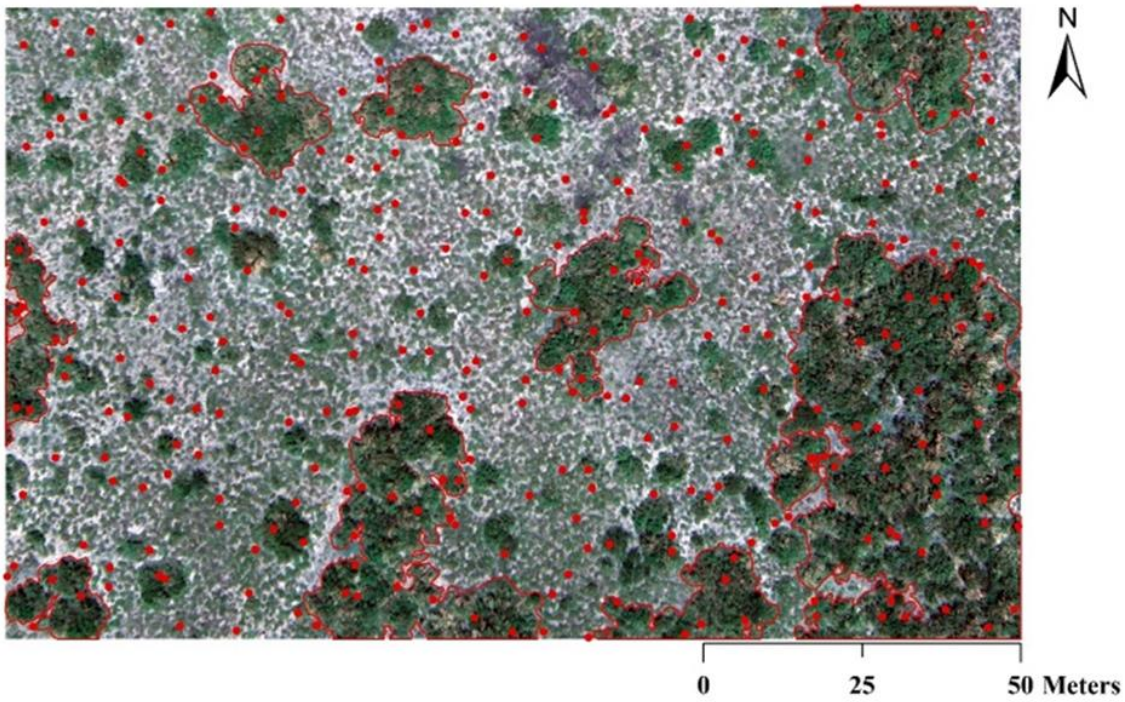

Figure 9.1 Aerial photograph of the 160 × 100 m landscape in a subtropical savanna. Red points indicate 320 random soil sampling points. Green patches are woody clusters and groves, while light grey areas indicate open grasslands. Canopy edges of groves are highlighted with red lines.

Leaf and fine root (< 2 mm) tissues of each plant species occurring on this landscape were collected in September 2016. For each woody species, approximately equal amounts of leaves from three individuals were collected to make a composite sample; then, fine roots were excavated carefully from surface soils (0-15 cm) after confirming their linkages to the selected three individuals and mixed to make a composite

sample. The same sampling method was applied to forbs, grasses, and cacti (CAM species), but more than three individuals/species were sampled in order to meet the mass requirements for elemental and isotopic analyses. Composite leaf and fine root samples were washed carefully, dried, and pulverized in a Mixer Mill MM 400 (Retsch GmbH, Haan, Germany).

Soils within each depth increment from one of the two soil cores were oven-dried at 105°C to determine soil bulk density (no gravel was present in any of the soil samples), and these soils were subsequently used to estimate fine and coarse (> 2 mm) root biomass by washing through sieves. No attempt was made to distinguish between live or dead roots. Retrieved roots were cleaned of soil particles, dried at 65°C, and weighed. In order to analyze $\delta^{15}N$ of fine roots throughout the soil profile, 10 cores were selected from each landscape element (i.e. grassland, cluster, and grove). Fine roots within the selected 10 cores were combined to make a composite fine root sample for each depth increment. This process was repeated three times and three composite fine root samples were made for each landscape element. Composite fine root samples were pulverized in a Mixer Mill MM 400.

Soils within each depth increment from the other soil core were air-dried and then passed through a 2 mm sieve to remove coarse organic matter. An aliquot of sieved soil was used to determine soil texture using the hydrometer method. Another aliquot of sieved soil was dried at 65 ˚C for 48 hours and then pulverized in a centrifugal mill (Angstrom Inc., Belleville, MI, USA). Total N concentrations and $\delta^{15}N$ values of pulverized soils, fine roots extracted from soil cores, and composite leaf and root tissues sampled from

individual plant species were determined using a Costech ECS 4010 elemental analyzer (Costech Analytical Technologies Inc., Valencia, CA, USA) interfaced via a ConFlo IV with a Delta V Advantage isotope ratio mass spectrometer (Thermo Scientific, Bremen, Germany) at the Stable Isotopes for Biosphere Science Laboratory, Department of Ecosystem Science and Management, Texas A&M University. Organic C concentrations of pulverized soil samples were determined in the same way but were treated with HCl vapor in a desiccator to remove carbonates prior to analysis (Harris et al., 2001). Stable N isotopic compositions are reported in the conventional form according to equation (1):

$$\delta^{15}N\ (‰) = \left[\frac{\left(\frac{^{15}N}{^{14}N}\right)_{sample}}{\left(\frac{^{15}N}{^{14}N}\right)_{standard}} - 1\right] \times 1000 \qquad (1)$$

where $(^{15}N/^{14}N)_{sample}$ and $(^{15}N/^{14}N)_{standard}$ are the stable N isotopic ratio of the sample and standard, respectively. The standard is atmospheric N_2 (Mariotti 1983). Precision of duplicate measurements was 0.1 ‰.

Data analyses

All data sets were tested for normality before performing statistical analyses and $\log_{10}$-transformed to improve normality when necessary. Mixed models, which consider spatial autocorrelation as a spatial covariance for adjustment (Littell *et al.* 2006), were used to compare means of measured variables (i.e. NDVI, root biomass, soil total N and $\delta^{15}N$) for different landscape elements within each depth increment.

Across this 160 m × 100 m landscape, groves occur almost exclusively on non-argillic inclusions; however, some groves expand laterally beyond the non-argillic inclusion onto soils where the subsurface argillic horizon is present. In addition, some

non-argillic inclusions within the grassland matrix are still not occupied by groves (Zhou *et al.* 2017b). To address the potential effect of the subsurface argillic horizon on soil $\delta^{15}N$, we subdivided soil cores from both grasslands and groves into those taken where the argillic horizon is present vs. those taken where the argillic horizon is absent using soil diagnostics for the higher categories as outlined in USDA Soil Taxonomy (Soil Survey Staff 1999). More details can be found in Zhou *et al.* (2018). Seventeen out of 200 soil cores from grasslands were taken within non-argillic inclusions, whereas 24 out of 79 soil cores from groves were taken within non-argillic inclusions. All 41 soil cores from clusters were taken where the argillic horizon was present. One-way ANOVA was performed to compare $\delta^{15}N$ values of composited fine root samples and of soil samples from grasslands and groves occurring on non-argillic vs. argillic soils within each depth increment. Post-hoc comparisons of these variables in different landscape elements were conducted with Tukey's test. A cutoff of $p < 0.05$ was used to indicate significant difference. These analyses were performed using JMP Pro 12.0 (SAS Institute Inc., Cary, NC, USA).

Variogram analyses were used to determine the spatial structure of soil total N and $\delta^{15}N$ based on 320 random sampling points across this landscape and throughout the soil profile. A semivariogram is a plot of a series of semivariance values (γ) against the corresponding lag distances (h). The semivariance γ at each h is calculated according to equation (2):

$$\gamma(h) = \frac{1}{2N(h)}\sum_{i=1}^{i=N(h)}[Z(X_i) - Z(X_{i+h})]^2 \qquad (2)$$

where $Z(X_i)$ and $Z(X_{i+h})$ are the values of soil variables at spatial location X_i and X_{i+h} for each depth increment, $N(h)$ is the number of sample pairs with lag distance h. The spherical

model has been selected, as it has been shown to provide an adequate representation of the spatial variability of soil data in dryland ecosystems (Schlesinger *et al.* 1996; Bai *et al.* 2009b). Nugget (C_0), range (A), structure variance (C), sill (C_0 + C), and the ratio of structure variance to sill variance (C/(C_0 + C)) were used to interpret spatial structure. Nugget, the variance at lag distance zero, is due to measurement error and reflects the variability at scales finer than the sampling unit. Range indicates the distance of spatial autocorrelation between data pairs, beyond the range the test variable can be considered spatially independent. The ratio of structure variance to sill variance, representing the proportion of the total variance that is spatially structured, reveals the structure strength. Variogram analyses were conducted using R software (R Development Core Team, 2014). Ordinary kriging was used for spatial interpolation of soil total N and $\delta^{15}N$ values at unsampled locations based on data from 320 sampling points and their spatial structure determined by variogram analysis. Kriged maps of soil total N and $\delta^{15}N$ for each depth increment were generated using ArcMap 10.2.2 (ESRI Inc., Redlands, CA, USA).

A classified vegetation map was delineated from the aerial photograph using ArcMap 10.2.2. To more clearly evaluate variation in soil total N and $\delta^{15}N$ within woody patches vs. grasslands, the distance from each sampling point to the nearest woody patch edge was calculated and correlated with soil total N and $\delta^{15}N$. In this calculation, sampling points located within the grassland matrix were assigned negative distance values. Thus, more negative values indicated that sampling points were farther away from the nearest woody patch edges. In contrast, sampling points located within woody patches were

assigned positive distance values such that larger values indicated sampling points farther away from woody patch edges.

Lacunarity, a scale-dependent measurement of spatial heterogeneity or the "gappiness" of a landscape structure (Plotnick *et al.* 1996), was used to quantify the spatial heterogeneity of soil $\delta^{15}N$ across this landscape and throughout the soil profile. Lacunarity analysis was performed based on kriged maps of soil $\delta^{15}N$ using R software. Briefly, a gliding box of a given size (side length the box, *r*) was first placed at one corner of the kriged map, and the box mass (*S(r)*), the sum of soil $\delta^{15}N$ value of each pixel within the box, was determined. The box was then systematically moved through the kriged map one pixel at a time and the box mas was determined at each location. The lacunarity for box size *r* is calculated according to equation (3):

$$\Lambda\,(r) = \frac{Var(S(r))}{E(Sr)^2} + 1 \qquad (3)$$

where var(*S(r)*) is the variance and E(*S(r)*) is the mean of the box mass (*S(r)*) for a given box size (*r*). The lacunarity curve, a log-log plot of lacunarity *Λ(r)* against box size *r*, was then plotted to quantify spatial heterogeneity of soil $\delta^{15}N$ at different spatial scales for each depth increment, with a higher value of lacunarity indicating a more heterogeneous distribution pattern across the landscape.

The spatial correlations of all measured parameters were assessed using Pearson's correlation coefficients and a modified t-test, which corrects the degrees of freedom based on the extent of spatial autocorrelation in the data (Dutilleul *et al.* 1993). Descriptive statistics for soil parameters (e.g. soil bulk density, soil C: N ratio, and soil texture) across this landscape and throughout the soil profile have been presented elsewhere. Datasets

were log_{10}-transformed prior to the analysis of correlations using PASSaGE version 2 (Rosenberg & Anderson 2011).

RESULTS

Vegetation and soil attributes across this landscape

Grasslands, clusters, and groves covered 62 %, 10 %, and 27 % of this 160 m × 100 m landscape, respectively (Table 9.1). The spatial patterns of the Normalized Difference Vegetation Index (NDVI) across this landscape corresponded closely to the spatial distribution of woody patches; clusters (0.36 ± 0.02) and groves (0.31 ± 0.02) had significantly higher NDVI values than grasslands (0.20 ± 0.003) (Table 9.1).

Woody patches (both clusters and groves, hereafter) had significantly higher fine and total root biomass than grasslands through the soil profile (data not shown). Summed over the entire 1.2 m soil profile, woody patches had 2 times more fine root biomass and 5 times more total root biomass than grasslands (Table 9.1).

Table 9.1 Vegetation attributes across a 160 m × 100 m landscape in a subtropical savanna. Root biomass data is presented for fine and total root biomass throughout the full 120 cm soil profile. Significant differences ($p < 0.05$) between means for landscape elements are indicated with different superscript letters. Values for root biomass and NDVI (normalized difference vegetation index) are mean ± SE. Number of samples: grassland = 200, cluster = 41, and grove = 79.

Landscape element	Vegetation cover		NDVI	Root biomass (Mg ha^{-1})	
	m^2	(%)		Fine roots	Total roots
Grassland	9976	62	0.20 ± 0.00^{b}	10.8 ± 0.19^{b}	12.5 ± 0.40^{b}
Cluster	1649	10	0.36 ± 0.02^{a}	22.9 ± 0.97^{a}	60.0 ± 7.63^{a}
Grove	4375	27	0.31 ± 0.02^{a}	25.6 ± 0.74^{a}	62.1 ± 5.97^{a}

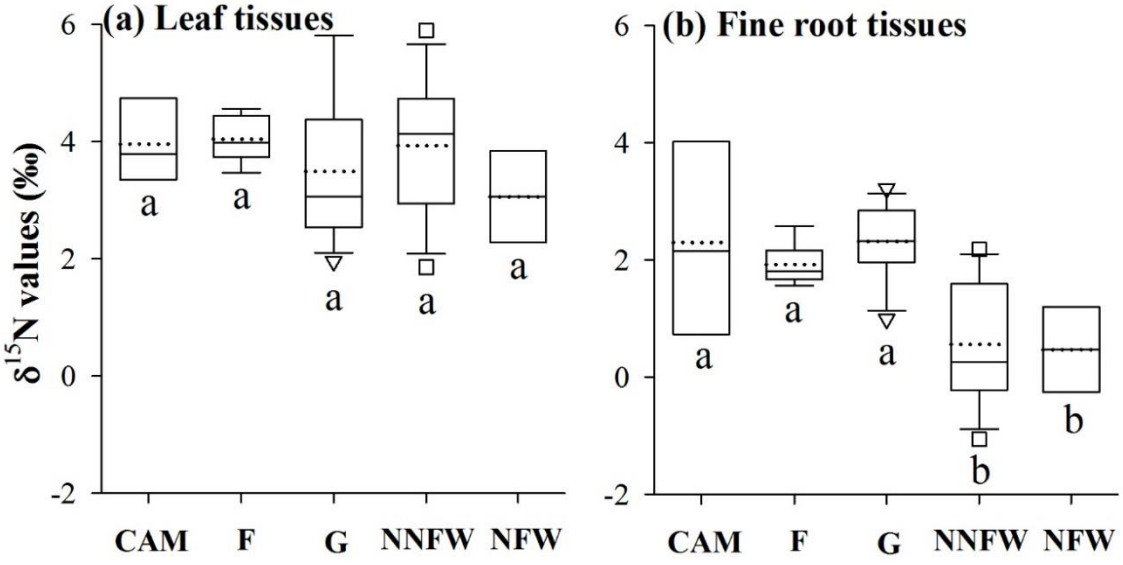

Figure 9.2 $\delta^{15}N$ values (‰) of leaf (a) and fine root (b) tissues for different plant life-forms occurring on this 160 m ×100 m landscape. The box plots summarize the distribution of points for each plant life-form. The central box shows the inter-quartile range, median (horizontal solid line in the box), and mean (horizontal dotted line in the box). Lower and upper error bars indicate 10^{th} and 90^{th} percentiles, and points above and below the error bars are individuals above the 90^{th} or below the 10^{th} percentiles. CAM, crassulacean acid metabolism species, n = 3; F, forbs, n = 9; G, grasses, n = 13; NNFW, non-N_2-fixing woody species, n = 13; NFW, N_2-fixing woody species, n = 2. More details see Appendix A.

Mean $\delta^{15}N$ values of leaf tissues ranged from 3.1 to 4.0 ‰ and were comparable among different plant life-forms (Fig. 9.2). In contrast, mean $\delta^{15}N$ values of fine root tissues ranged from 0.5 to 2.3 ‰ and were significantly lower for woody species (both N_2-fixers and non N_2-fixers) than other plant life-forms (Fig. 9.2). Throughout the entire 1.2 m sampling depth, composite fine root samples from groves had significantly lower $\delta^{15}N$ than fine roots in clusters and grasslands, and $\delta^{15}N$ values of composite fine root

samples from clusters were significantly lower than those from grasslands except in the 50-80 cm depth increment (Fig. 9.3a).

Soil total N decreased continuously with depth throughout the soil profile in all landscape elements (Fig. 9.3b). Soils underneath woody patches had significantly higher total N than those underneath grasslands in upper (0-30 cm) and lower (80-120 cm) soil depth increments but not in the 30-50 and 50-80 cm depth increment (Fig. 9.3b). Spatial patterns of soil total N strongly resembled the spatial distribution of woody patches in the 0-5 and 5-15 cm depth increments; however, the strength of this spatial relationship faded and became more obscure at depths > 15 cm (Fig. 9.4a and b). Soil $\delta^{15}N$ values of grasslands and clusters increased by approximately 2-3 ‰ from the soil surface down to approximately 50 cm, and then decreased slightly in the 80-120 cm increment (Fig. 9.3c). Soils from woody patches had significantly lower $\delta^{15}N$ than those from grasslands in the 0-5 cm depth increment; groves had significantly lower soil $\delta^{15}N$ than both clusters and grasslands below 5 cm of the soil profile; clusters had significantly lower soil $\delta^{15}N$ than grasslands in the 5-15, 15-30, 30-50, and 50-80 cm depth increments (Fig. 9.3c). Soil $\delta^{15}N$ values did not differ between grasslands on argillic soils vs. those on non-argillic inclusions throughout the soil profile (Fig. 9.3d). In contrast, soil $\delta^{15}N$ values under groves on non-argillic inclusions were significantly lower than those where the argillic horizon was present at depths > 30 cm where the argillic horizon begins to occur (Fig. 9.3d).

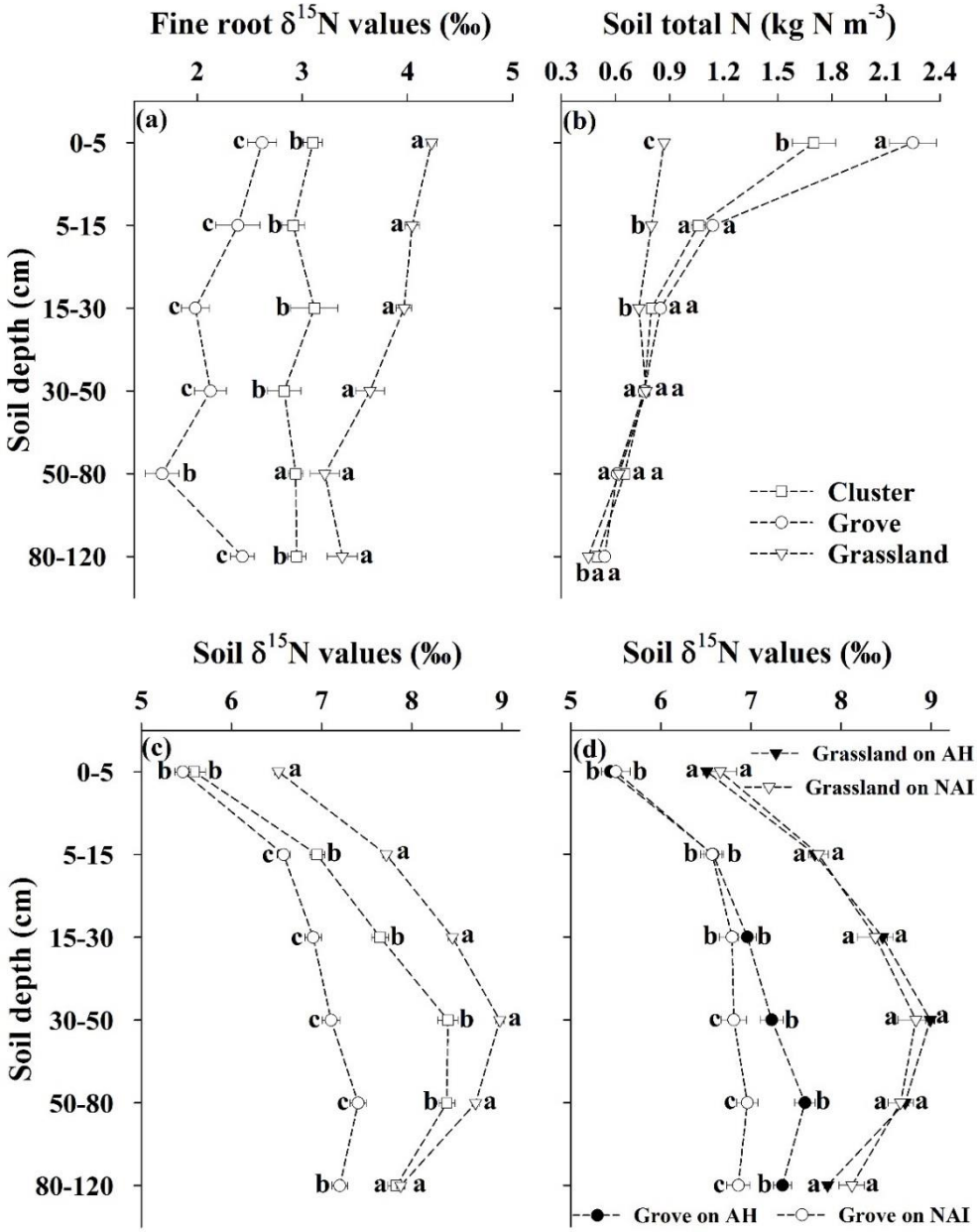

Figure 9.3 $\delta^{15}N$ values (‰) of composited fine root samples (a), soil total N (b) and $\delta^{15}N$ values (‰) (c) of soil samples from grasslands, clusters and groves, and $\delta^{15}N$ values (‰) of soil samples taken from grasslands and groves occurring on argillic horizon (AH) vs. non-argillic inclusions (NAI) (d) throughout the soil profile across this 160 m ×100 m landscape in a subtropical savanna. For composited fine root samples, n = 3 for each landscape element; for soil samples, n = 200 for grasslands, n = 41 for clusters, and n = 79 for groves; for soil samples, n = 183 for grasslands on argillic horizon, n = 17 for grasslands on non-argillic inclusions, n = 55 for groves on argillic horizon, n = 24 for groves on non-argillic inclusions.

Spatial variation of soil $\delta^{15}N$ across the landscape and throughout the soil profile

Both means and medians of soil δ15N increased with depth, reached highest values in the 30-50 cm depth increment and decreased in the last two depth increments across this landscape (Table 9.2). The coefficients of variation for soil $\delta^{15}N$ were higher in the 0-5 cm, 15-30 cm, and 30-50 cm depth increments than in other depth increments (Table 9.2). Variogram analyses indicated that, with spherical models, there were clear distances for spatial autocorrelation in soil $\delta^{15}N$ across this landscape, with ranges from 19.8 m at 80-120 cm to 27.3 m at 0-5 cm in the soil profile (Table 9.3). The strength of spatial structure ($C/(C_0 + C)$) in soil $\delta^{15}N$ also increased with depth, reached the maximum in the 30-50 cm depth increment, and decreased in the two deepest increments (Table 9.3).

Table 9.2 Descriptive statistics of soil $\delta^{15}N$ throughout the soil profile across a 160 m × 100 m landscape in a subtropical savanna.

Soil depth (cm)	Mean	Median	Max.	Min.	S.E.	C.V.	SK	Range
0-5	6.1	6.2	9.2	4.1	0.1	13.7	-0.03	5.2
5-15	7.3	7.4	9.0	4.8	0.0	10.2	-0.05	4.2
15-30	8.0	8.1	9.7	4.5	0.1	11.9	-0.66	5.2
30-50	8.4	8.7	10.3	5.3	0.1	12.6	-0.75	5.0
50-80	8.3	8.5	10.2	6.1	0.1	9.9	-0.50	4.1
80-120	7.7	7.7	9.1	5.7	0.0	9.1	-0.20	3.4

Number of samples: n = 320;

Abbreviations: Max., maximum; Min., minimum; S.E., standard error; C.V., coefficients of variation; SK, skewness.

Table 9.3 Parameters for spherical models fitted to semivariograms of soil $\delta^{15}N$ throughout the soil profile based on 320 random sampling points across a 160 m × 100 m landscape in a subtropical savanna.

Soil depth (cm)	Range (m)	Nugget (C_0)	Sill (C_0+C)	(Sill-Nugget)/Sill C/(C_0+C) (%)	R^2
0-5	27.30	0.21	0.55	61.82	0.46
5-15	22.53	0.09	0.51	82.35	0.49
15-30	25.62	0.12	0.82	85.37	0.62
30-50	25.62	0.08	1.02	92.16	0.71
50-80	22.79	0.11	0.65	83.08	0.62
80-120	19.83	0.14	0.44	68.18	0.45

Maps of soil $\delta^{15}N$ throughout the soil profile derived from ordinary kriging and variogram analyses displayed a strong resemblance to the spatial distribution of woody patches (Fig. 9.4a and c). This is consistent with significant correlations between soil $\delta^{15}N$ and NDVI throughout the soil profile (Table 9.4). Soil $\delta^{15}N$ values were lowest near the central portions of woody patches, increased towards the edges, and reached the highest values in the remnant grassland matrix (Fig. 9.4a and c). This spatial trend observed visually in the kriged maps was statistically supported by significantly negative correlations between soil $\delta^{15}N$ and distance from each sampling point to the nearest woody patch edges throughout the soil profile (Fig. 9.5). Although these spatial patterns were strong in every soil depth increment, they were especially evident at intermediate depths (e.g. 30-50 cm). Lacunarity analyses indicated that soil $\delta^{15}N$ in the 0-5, 5-15, and 30-50 cm depth increment was more heterogeneous than in other depth increments (Fig. 9.6), corresponding well with results from coefficients of variation (Table 9.2).

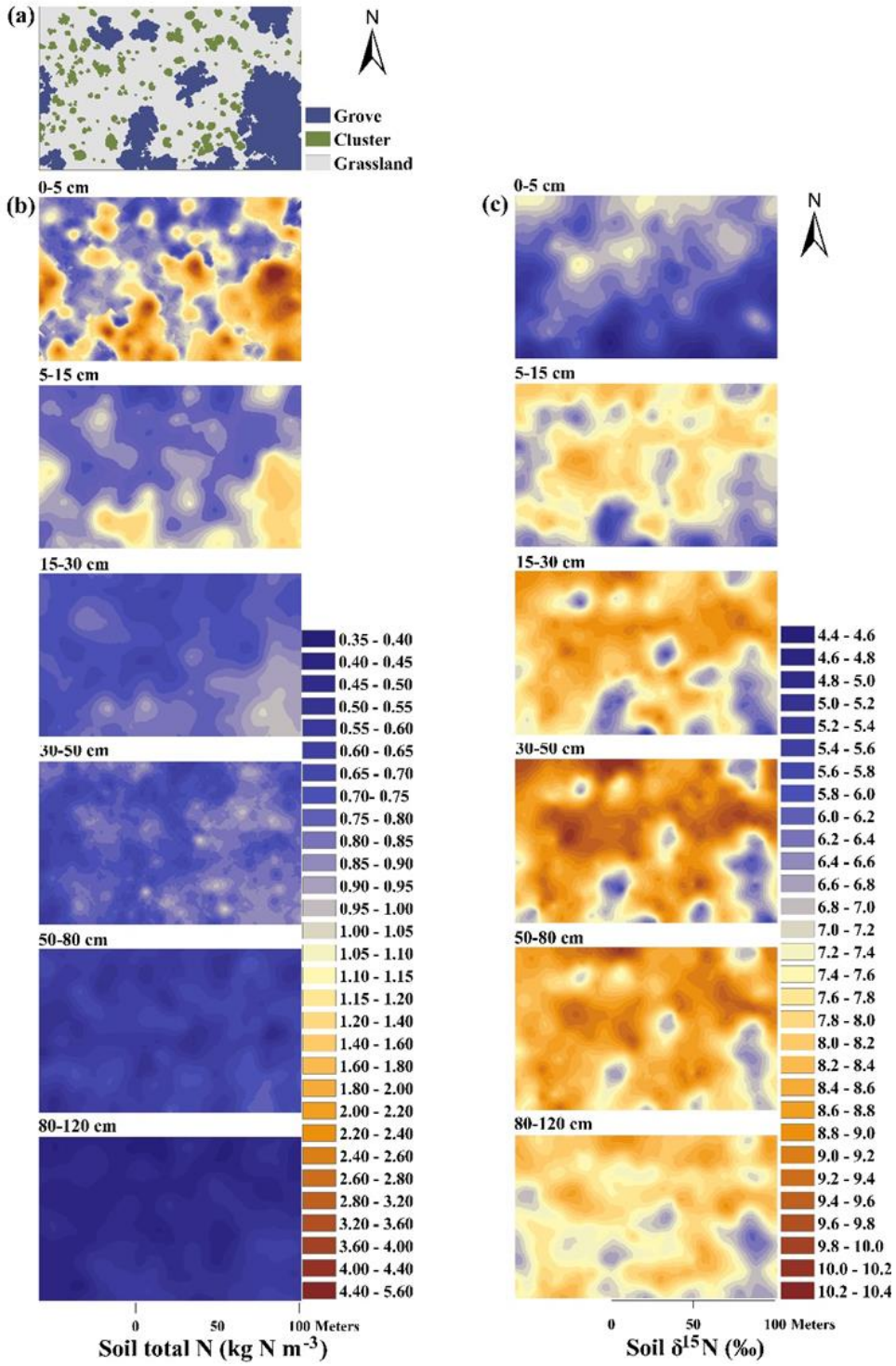

Figure 9.4 The classified vegetation map for this 160 m ×100 m landscape (a) and kriged maps of soil total N (kg N m^{-3}) (b) and soil $\delta^{15}N$ values (‰) (c) throughout the soil profile based on 320 randomly located sampling points in a subtropical savanna.

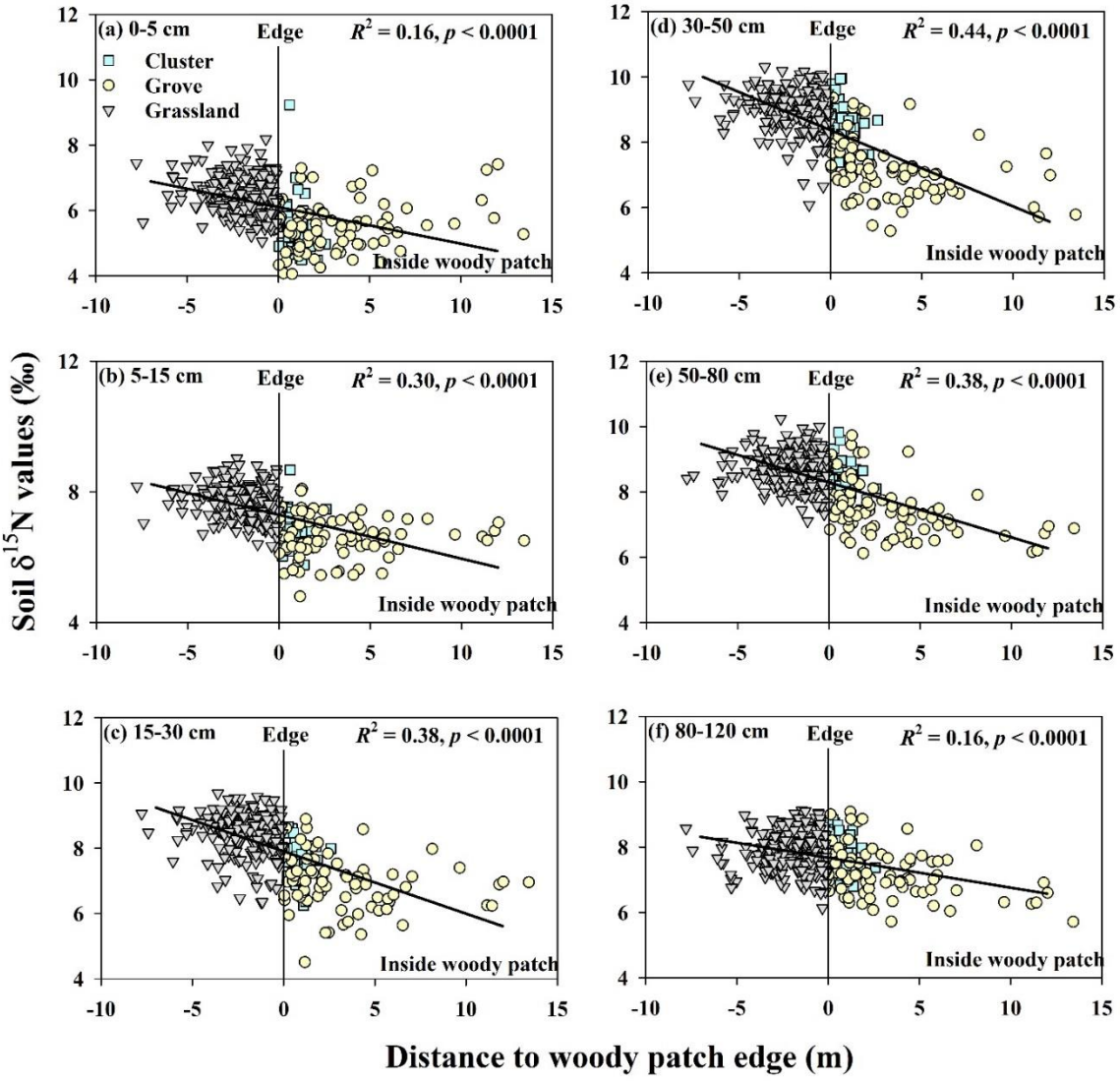

Figure 9.5 Relationships between soil δ^{15}N value (‰) and distance of each sampling point to the nearest woody patch edge (m) throughout the soil profile. Positive distances indicate that sampling points are within woody patches, whereas negative values indicate that sampling points are within the grassland matrix.

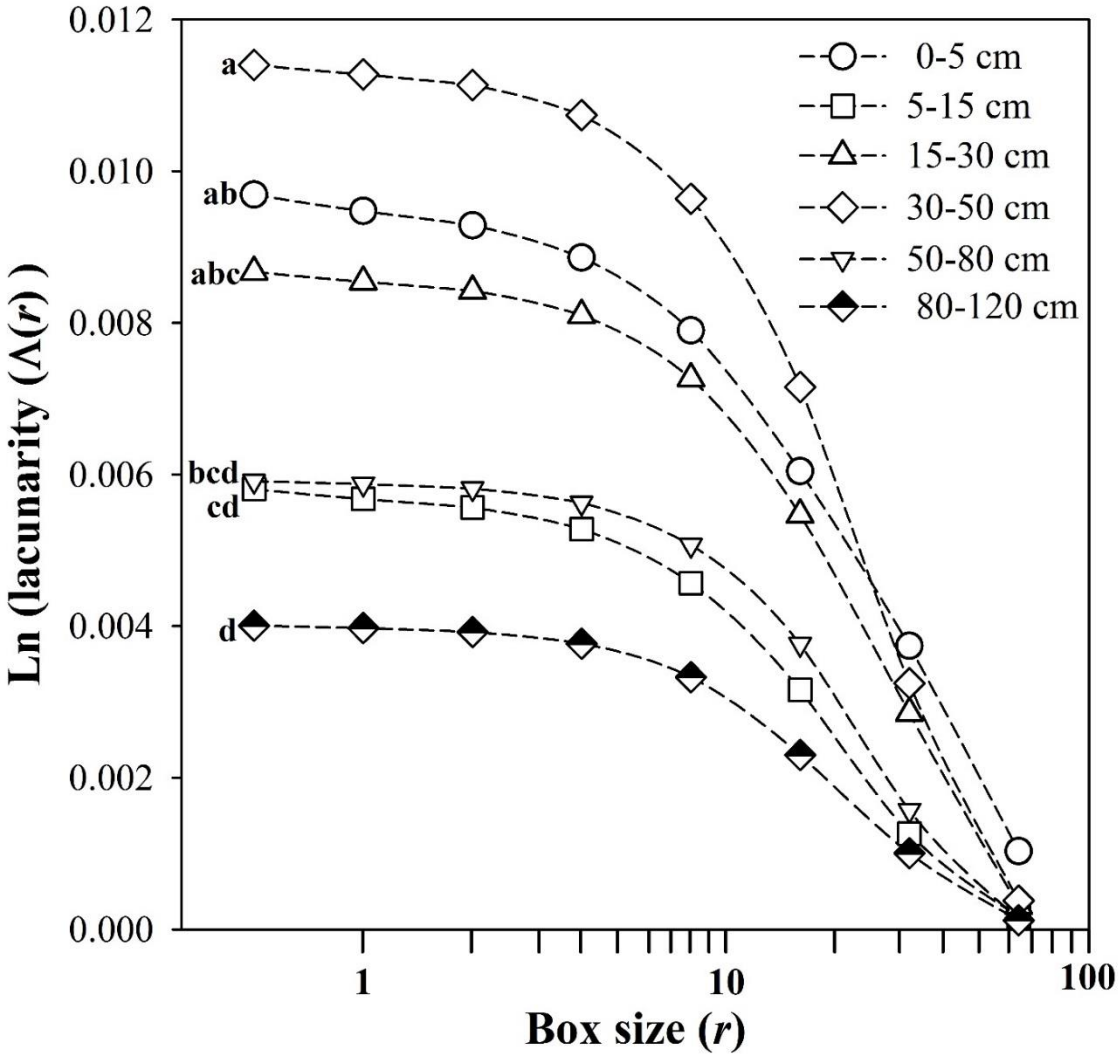

Figure 9.6 Lacunarity curves along the soil profile based on kriged maps of soil $\delta^{15}N$ values (‰). Significant differences ($p < 0.05$) between different depth increments were tested based on one-way ANOVA and indicated with different letters.

Soil $\delta^{15}N$ was significantly and negatively correlated with fine root biomass but positively with soil bulk density across this landscape throughout the entire soil profile (Table 9.4). Soil $\delta^{15}N$ was significantly and negatively correlated with soil C: N ratio throughout the soil profile except in the 15-30 cm depth increment (Table 9.4). Soil $\delta^{15}N$ was significantly and negatively correlated with soil total N throughout the soil profile except in the 30-50 and 50-80 cm depth increments where soil $\delta^{15}N$ was significantly and positively correlated with soil clay content (Table 9.4).

Table 9.4 Correlations between soil $\delta^{15}N$ (‰) and vegetation/soil attributes across a 160 m × 100 m landscape and throughout the soil profile. Vegetation/soil attributes includes NDVI, fine root biomass (FRB) (g m^{-2}), total N (TN) (kg N m^{-3}), C: N ratio, soil bulk density (SBD) (g cm^{-3}), and soil clay content (%). The correlations were calculated using a modified t-test which adjusts the degrees of freedom based on the extent of spatial autocorrelation in the data (Dutilleul et al. 1993).

Depth (cm)	NDVI	FRB	TN	C:N	SBD	Clay
0-5	-0.33***	-0.53***	-0.63***	-0.44***	0.59***	-0.30
5-15	-0.34***	-0.61***	-0.64***	-0.26***	0.52***	-0.08
15-30	-0.34***	-0.56***	-0.44***	-0.10	0.28***	0.02
30-50	-0.34***	-0.43***	0.11	-0.43***	0.24**	0.37***
50-80	-0.25***	-0.52***	0.15	-0.53***	0.44***	0.31***
80-120	-0.14*	-0.35***	-0.30***	-0.51***	0.38***	0.03

*, $p < 0.05$; **, $p < 0.01$; ***, $p < 0.001$

DISCUSSION

Globally widespread woody encroachment has dramatically altered the structure and function of grassland and savanna ecosystems (Eldridge *et al.* 2011), with the potential to profoundly influence soil biogeochemical cycling (Hibbard *et al.* 2001). The spatially

explicit approach of our study enabled us to assess the impact of the encroachment of *P. glandulosa* and other woody species into this subtropical savanna on spatial variation of soil $\delta^{15}N$ in both horizontal and vertical planes. Consistent with our first hypothesis, we found that woody encroachment into areas that were once grassland decreased soil $\delta^{15}N$ significantly throughout the entire 1.2 m soil profile (Fig. 9.3c). In addition, we found that spatial patterns of soil $\delta^{15}N$ displayed strong resemblance to the spatial distribution of woody patches, and this spatial relationship was evident throughout the entire soil profile (Fig. 4a and c), supporting our second hypothesis.

Spatial variation of soil $\delta^{15}N$ in the horizontal plane

Overall, the vegetation shift from grass to woody plant dominance, which altered the amount of root biomass that delivers ^{15}N-delepleted organic matter to soils through root turnover (Table 9.1, Fig. 9.2 and 9.3a), is likely to be the mechanism responsible for the observed spatial variation in soil $\delta^{15}N$ in the horizontal plane, as spatial patterns of soil $\delta^{15}N$ throughout the soil profile resembled the spatial distribution of woody patches (Fig. 9.4a and 9.4c) and soil $\delta^{15}N$ was significantly and positively correlated with NDVI but negatively with fine root biomass (Table 9.4). In arid and semiarid ecosystems, trees/shrubs tend to have lower $\delta^{15}N$ than herbaceous species (Bustamante *et al.* 2004; Bai *et al.* 2009; Boutton & Liao, 2010; Sitters *et al.* 2013; Blaser *et al.* 2014; Soper *et al.* 2015). This is especially true for trees/shrubs with the capability of fixing N symbiotically as the $\delta^{15}N$ value of biologically fixed N generally approximates 0 ‰ (Hobbie & Ouimette 2009; Denk *et al.* 2017), which is substantially lower than the $\delta^{15}N$ value of soils from which non N_2-fixing herbaceous species derive their N. Although $\delta^{15}N$ in leaf tissue was

comparable between woody and herbaceous species across this landscape (Fig. 9.2a), fine root tissues from woody species were generally 2 ‰ lower in $\delta^{15}N$ than those from herbaceous species (Fig. 9.2b and 9.3a). Since root residues and exudates are the primary source for soil organic matter (Rasse *et al.* 2005; Schmidt *et al.* 2011; Clemmensen *et al*. 2013) and woody patches have 2 times more fine root biomass and 5 times more total root biomass than grasslands throughout the entire soil profile (Table 9.1) (Zhou *et al*. 2017a), increased inputs of organic N derived from woody roots with lower $\delta^{15}N$ results in lower soil $\delta^{15}N$ in areas encroached by woody plants (Fig. 9.3a). These changes in soil $\delta^{15}N$ driven by the establishment of woody patches in areas that were once grassland create strong spatial structures in soil $\delta^{15}N$ (Table 9.3) and corresponding spatial patterns in soil $\delta^{15}N$ across this landscape and throughout the soil profile (Fig. 4c).

Observed declines in soil $\delta^{15}N$ following woody legume encroachment in this study are consistent with findings in other studies (Wheeler *et al.* 2007; Boutton & Liao 2010; Bai *et al.* 2012; Sitters *et al.* 2013), although these prior studies investigated surface soils only. For example, proliferation of *Acacia zanzibarica* (an N_2-fixing tree) in a humid Tanzanian savanna decreased soil $\delta^{15}N$ in the 0-15 cm depth increment while simultaneously increasing total N within the same interval (Sitters *et al.* 2013). However, some other studies have reported that soil $\delta^{15}N$ remains unchanged or actually increases after woody encroachment (Bekele & Hudnall 2005; Billings & Richter 2006; Blaser *et al.* 2014). For example, Blaser *et al.* (2014) reported that the encroachment of *Dichrostachys cinerea* (an N_2-fixing shrub) in a mesic savanna in Zambia did not change soil $\delta^{15}N$ (0-10 cm); and, Bekele & Hudnall (2005) found that the proliferation of

Juniperus virginiana (a non N_2-fixing tree) in a calcareous prairie actually increased soil $\delta^{15}N$ (0-10 cm). Despite this inconsistency in direction of soil $\delta^{15}N$ change following vegetation change, it is interesting to note that, in all of these studies, the encroaching woody species all had lower $\delta^{15}N$ in leaf and/or root tissues than the plants in the herbaceous communities they were invading. This suggests that the $\delta^{15}N$ values of the organic matter inputs are not the sole determinants of soil $\delta^{15}N$ following woody encroachment, and that other biotic or abiotic factors affected by encroachment may be modifying the rates and magnitudes of key soil N transformations that fractionate N isotopes and that could therefore offset or obscure the $\delta^{15}N$ values of N inputs from litterfall and root turnover.

Apart from the addition of ^{15}N depleted organic matter derived from woody species, spatial patterns of soil $\delta^{15}N$ are also affected by the net outcome of spatial variation in the extent of fractionation against ^{15}N during soil N cycling processes across the landscape. For example, although soil $\delta^{15}N$ in wooded areas was significantly lower than in herbaceous areas in the 0-5 cm depth increment (Fig. 9.3a), visual assessment of the classified vegetation map (Fig. 9.4a) and the kriged map of soil $\delta^{15}N$ in the 0-5 cm depth increment (Fig. 9.4c) reveals other subtleties, such as (1) soils under some woody patches were more enriched in ^{15}N than under others; (2) soils under some woody patches had $\delta^{15}N$ similar to those within the grassland matrix; and (3) there were ^{15}N-enriched hotspots inside some woody patches. Previous studies at this site have demonstrated that woody plant encroachment has significantly magnified the pool size of soil microbial N (McCulley *et al.* 2004a; Liao & Boutton 2008), soil enzyme activities for organic N

decomposition (Creamer *et al.* 2013), and accelerated the rates of other soil N transformations (e.g., ammonification, nitrification) (Hibbard *et al.* 2001; McCulley *et al.* 2004) that can lead to N losses from surface soils. Most soil N transformation processes fractionate strongly against ^{15}N (Hobbie & Ouimette 2009; Denk *et al.* 2017). For example, $\delta^{15}N$ values of gaseous N lost from nitrification, denitrification, and ammonia volatilization are highly ^{15}N-depleted (ranging from - 64.0 ‰ to -10.0 ‰, reviewed in Denk *et al.* 2017). Thus, woody plant encroachment may exert different degrees of control on these soil N transformation processes for a variety of reasons, such as woody patch sizes, microclimatic conditions, substrate concentrations, topoedaphic properties, and bioturbation (Liao *et al.* 2006; Liu *et al.* 2011; Bai *et al.* 2012), leading to these discrepancies in surface soil $\delta^{15}N$ between and inside woody patches across this landscape (Fig. 9.4a and 9.4c).

Spatial variation of soil $\delta^{15}N$ in the vertical plane

For all landscape elements, soil $\delta^{15}N$ values were relatively low in the uppermost portions of the profile, and then increased continuously to approximately 50 cm (Fig. 9.3c, 9.4c, and Table 9.2). This is consistent with other studies in a variety of ecosystems (e.g. Nadelhoffer & Fry 1988; Högberg 1997; Bustamante *et al.* 2004; Hobbie & Ouimette, 2009). Low $\delta^{15}N$ values in the upper profile results from the fact that $\delta^{15}N$ values of leaves (3-4 ‰) and fine roots (2-4 ‰) are lower than those of soils (Fig. 9.2, 9.3a and 9.3c); thus, deposition of relatively ^{15}N-depleted litter and roots to soils would decrease $\delta^{15}N$ values of the soil N pool. In addition, organic matter inputs from litterfall and root turnover are largely concentrated in the uppermost portion of the soil profile, and decrease

exponentially with soil depth (Jackson *et al.* 1996). Consequently, the influence of ^{15}N-depeleted litterfall and root turnover on soil δ^{15}N values decreases with depth.

Soil δ^{15}N reached maximum values between 50 and 80 cm in all landscape elements, and then declined slightly at depths ≥ 80 cm (Fig. 9.4c, 9.5 and Table 9.2). This vertical pattern was especially evident in clusters and grasslands, but was less evident in groves (Fig. 9.4c). These patterns resulted in the highest spatial heterogeneity of soil δ^{15}N in the 30-50 cm depth compared to all other depth increments, as revealed by lacunarity analyses (Fig. 9.6).

What mechanism(s) might account for the different δ^{15}N depth distributions between groves vs. grasslands and clusters? Hobbie & Ouimette (2009) proposed that production of ^{15}N-depleted N_2O and N_2 during denitrification at intermediate depths could be a plausible mechanism causing ^{15}N enrichment at intermediate depths relative to shallower and greater depths. Since all soil cores from (n = 41) clusters and the majority of soil cores (183 out of 200 cores) from grasslands included an argillic horizon beginning around the 30-50 cm depth, it is possible that the presence/absence of this clay-rich horizon is somehow related to the vertical patterns of soil δ^{15}N values in this landscape. Higher clay content in the argillic horizon beneath grasslands and clusters would be conducive to greater moisture retention and lower oxygen availability following rainfall events (Maag & Vinther, 1996; Bouwman *et al.* 2002; Van der Salm *et al.* 2007; Zhu *et al.* 2012), thereby favoring the loss of ^{15}N-depleted N_2O and N_2 via denitrification, and the accumulation of ^{15}N-enriched residual soil N in this portion of the soil profile.

In contrast, the absence of the clay-rich argillic horizon in groves would likely be conducive to more rapid drainage of water through the soil profile, minimizing the potential for the development of anaerobic conditions and N-losses via denitrification, thereby resulting in the lower soil $\delta^{15}N$ values that we observe in groves vs. clusters and grasslands. Interestingly, where groves have expanded beyond the boundaries of the non-argillic inclusions onto areas where the argillic horizon is present, their $\delta^{15}N$ depth distribution patterns becomes more similar to those of clusters and grasslands (Fig. 9.3d), suggesting further that the presence/absence of the argillic horizon exerts an effect on N-cycling processes that influence soil $\delta^{15}N$.

However, this argument is unable to account for the fact that grasslands occurring on non-argillic inclusions that have not yet been colonized by woody plants have soil $\delta^{15}N$ depth distributions patterns that are not significantly different from grasslands growing on soils where the argillic horizon is present (Fig. 3d). This suggests that there may be important plant attributes (e.g., plant tissue chemistry, root distribution patterns) that interact with the presence/absence of the argillic horizon to influence depth distribution patterns of soil $\delta^{15}N$ values. Further studies are needed to explore how changes in soil texture throughout the soil profile interact with vegetation change to affect soil N cycling processes that ultimately lead to these discrepancies in vertical patterns of soil $\delta^{15}N$ among different landscape elements across this landscape.

CONCLUSIONS

Our results indicate that the establishment of woody patches dominated by N_2-fixing trees in areas that were once grassland has had a dramatic impact on landscape-

scale spatial patterns of soil $\delta^{15}N$ throughout the upper 1.2 m of the soil profile. An increasing amount of ^{15}N-depleted inputs derived from encroaching woody species differentiated soil $\delta^{15}N$ in wooded areas from that in herbaceous areas, creating spatial patterns of $\delta^{15}N$ throughout the soil profile that resembled the spatial distribution of woody patches. While soil $\delta^{15}N$ in grasslands and clusters increased with depth to maximum values at 30-50 cm, and then decreased slightly in the 80-120 cm increment, the soil $\delta^{15}N$ values in groves increased with depth throughout the entire profile. The exact mechanisms shaping this discrepancy remain unknown, but may related to the presence (under grasslands and clusters) or absence (under groves) of a subsurface argillic horizon that could interact with vegetation change to drive the vertical patterns of soil $\delta^{15}N$. Our results also highlight the benefits of spatially-specific deep soil sampling for the study of soil $\delta^{15}N$ in arid and semiarid ecosystems. Further studies aimed at improving our understanding of the mechanisms and controls over spatial variations in soil $\delta^{15}N$ will enhance our ability to apply $\delta^{15}N$ as a tool for inferring soil N dynamics across multiple spatial scales. Since woody plant encroachment is a geographically widespread phenomenon in dryland regions which cover 41% of Earth's land surface (Reynolds *et al.* 2007; Stevens *et al.* 2017), this land cover change has the potential to significantly alter patterns of soil $\delta^{15}N$ at regional to global scales. Ultimately, a better characterization of global patterns of soil $\delta^{15}N$ values may facilitate our ability to predict changes in N cycling processes that can influence global biogeochemistry and the climate system (Craine *et al.* 2015).

CHAPTER X

SUMMARY AND CONCLUSIONS

SUMMARY

Woody plant encroachment and its corresponding effects on soil biogeochemical cycling were assessed in a 160 m × 100 m subtropical savanna landscape in the Rio Grande Plains of Texas, USA. Results from soil $\delta^{13}C$ throughout the soil profile indicated that this landscape was once primarily dominated by C_4 grasses. When this information was considered in conjunction with previous radiocarbon measurements on SOC at this site, it was clear that this area was invaded by woody plants during the past century. Currently, this landscape is experiencing a dramatic vegetation change, characterized by (1) an increasing abundance of C_3 forbs within the remnant grassland matrix and (2) ongoing formation and expansion of woody patches across this landscape. The purpose of this study was to characterize the spatial heterogeneity of soil biogeochemical properties that has developed in response to woody encroachment in this subtropical savanna.

The encroachment of woody plants is initiated by the colonization of *Prosopis glandulosa,* a N_2-fixing tree legume. Established *P. glandulosa* trees then serve as nurse plants, facilitating the recruitment of other woody species underneath their canopies to form discrete clusters (< 100 m^2). The location of discrete clusters across this landscape is random. However, the soils across this landscape have non-argillic inclusions (i.e. patches with coarser-textured soils) embedded within an otherwise continuous clay-rich argillic horizon. These subsurface non-argillic inclusions tend to favor the growth and

persistence of woody plants by enabling root penetration deeper into the profile, providing greater access to water and nutrients that are less accessible on those portions of the landscape where the argillic horizon is present. If discrete clusters occur within these non-argillic inclusions, they expand rapidly and eventually coalescence to form large groves (> 100 m^2). Thus, the location of these non-argillic inclusions across this landscape regulates the distribution of grove vegetation and structures the evolution of this landscape.

Woody encroachment into grasslands has dramatically altered soil carbon (C), nitrogen (N), and phosphorus (P) storage and dynamics across this landscape and along the entire soil profile. Increased soil organic C (SOC), total N (TN), and total P (TP) accumulations following woody encroachment were observed to considerable depth (i.e., 1.2 m), albeit at reduced magnitudes in deeper portions of the soil profile. Overall, woody clusters and groves accumulated 12.87 and 18.67 Mg C ha^{-1} more SOC, 1.04 and 1.52 Mg N ha^{-1} more TN, and 0.10 and 0.53 Mg P ha^{-1} more TP, compared to grasslands to a depth of 1.2 m. However, SOC and TN were strongly coupled with respect to increasing magnitudes throughout the soil profile following woody encroachment, while TP increased slower than SOC and TN in surface soils but faster in subsurface soils. The slower accumulation of soil TP compared to SOC and TN in surface soils might be attributed to the fact that this system is limited by P, which in turn causes: (1) lower deposition of P to surface soils from plant residues compared to N, and (2) more efficient use of P through the active cycling of soil organic P pools. In contrast, the more rapid accrual of TP in subsurface soils may be a function of the high pH values and abundant

$CaCO_3$ found in deeper portions of the profile that favor the formation of insoluble Ca phosphates.

Woody encroachment significantly altered patterns of spatial heterogeneity of SOC and TN to a depth of 5 cm, with marginal effect at 5-15 cm, and no significant impact on soils below 15 cm. However, woody encroachment significantly altered patterns of spatial heterogeneity of TP throughout the entire soil profile, albeit at reduced magnitudes in deeper portions of the soil profile. Spatial patterns of TP were different from those of SOC and TN, especially in subsurface soils (15-120 cm). These discrepant responses of SOC, TN, and TP to woody encroachment at the landscape scale highlight that the relative importance of biotic vs. abiotic mechanisms controlling C and N vs. P accumulation following vegetation change may vary with depth in the profile.

As woody plants have distinctive leaf and fine root C-N-P stoichiometry compared to grasses, woody encroachment into grasslands has corresponding effects on soil C-N-P stoichiometry. Variations of soil C: N ratio across this landscape and throughout the soil profile were remarkably smaller than those of soil N: P and C: P ratios. Therefore, spatial patterns of soil C: N ratios throughout the profile were not influenced by vegetation cover. In contrast, spatial patterns of soil N: P and C: P ratios displayed a strong resemblance to that of vegetation cover throughout the soil profile. Soil N: P and C: P ratios were highest in the centers of woody patches, decreased towards the canopy edges of woody patches, and reached lowest values within the grassland matrix in surface soils (0-5 cm); however, these patterns were reversed in subsurface soils (15-120 cm). These contrasting results indicated complex responses of soil C: N: P stoichiometry to vegetation change from

grassland to woodland, suggesting that changes in soil C: N ratio following woody encroachment were more constrained while soil N: P and C: P ratios were more flexible.

Since woody species have lower fine root $\delta^{15}N$ than herbaceous species across this landscape, woody encroachment significantly decreased soil $\delta^{15}N$ throughout the entire soil profile. Spatial patterns of soil $\delta^{15}N$ throughout the soil profile displayed a strong resemblance to the spatial distribution of woody patches across this landscape, with soil $\delta^{15}N$ being the lowest at the centers of woody patches, increasing towards canopy edges, and reaching highest values within the remnant grassland matrix. Meanwhile, soil $\delta^{15}N$ increased with depth, reached maximum values in the 30-50 cm depth increment, and then decreased slightly at greater depths. Such vertical patterns might be related to the presence of the subsurface argillic horizon across this landscape which may favor more rapid N transformation rates and higher preferential ^{14}N losses. Results indicated that succession from grassland to woodland altered spatial variation in soil $\delta^{15}N$ across the landscape and to considerable depth, suggesting significant changes in the relative rates of N-inputs vs. N-losses in this system. We suggest that the lower soil $\delta^{15}N$ values that characterize areas beneath woody canopies are due to N-fixation by *P. glandulosa*, which delivers ^{15}N-depleted organic matter via root turnover to subcanopy soils.

CONCLUSIONS

The geographically widespread occurrence of woody plant encroachment into grasslands has the potential to influence soil biogeochemical cycling across multiple spatial scales. However, most previous studies conducted at the ecosystem level, have not been based on spatially explicit sampling regimes, and have been confined to surface soils

and overlooked the effects of deep-rooting woody species on deep soil properties and processes. As one of the first studies of its kind, this dissertation explored the impact of woody plant encroachment into grassland on spatial variation of soil C, N, and P storage and dynamics in both horizontal and vertical planes by taking spatially-specific soil cores to a depth of 1.2 m across a 160 m × 100 m landscape that has undergone encroachment by *P. glandulosa* and other subtropical trees/shrubs during the past century in southern Texas, USA. Overall, this dissertation has demonstrated that vegetation change from grassland to woodland has dramatic impacts on several aspects of ecosystem function in this subtropical savanna, including landscape-scale accumulations of soil C, N, and P throughout the upper 1.2 m of the profile. This dissertation has potentially far-reaching implications on both empirical and modelling studies aiming at improving our understanding for the particular mechanisms underlying the ecological consequences of woody encroachment in arid and semiarid ecosystems.

As atmospheric CO_2 concentrations continue to increase exponentially, C sequestration has become a particularly important ecosystem service. Woody encroachment into grasslands has been identified as a significant contributor to C sequestration at regional to continental scales in the terrestrial C budget. This study further supported the perspective that many dryland ecosystems function as carbon sinks in response to woody encroachment. In addition, this research demonstrated that substantial SOC sequestration occurred even in deeper portions of the soil profile (i.e., depths approaching 1.2 m) following woody encroachment. As previous estimates of changes in C storage following woody encroachment were based largely on data from surface soils,

attention will now need to focus more on quantifying deep C sequestration after vegetation change. Given the geographic extent of woody encroachment on a global scale, this undocumented deep soil C sequestration suggested this vegetation change may play a more significant role in regional and global C sequestration than previously thought.

Increased soil C storage in this landscape is accompanied by a significant increase in soil N. Although this landscape does not appear to be N-limited because both soil N and C increase proportionally and the encroaching *P. glandulosa* is able to bring extra N to this system by fixing N symbiotically, larger N concentrations and pool sizes in the soil environment could have profound impacts on many ecosystem processes. Increased soil N could improve the quantity of organic C stored within this subtropical savanna. However, increased soil N may also contribute substantially to the acidification of soils, the release of the potent greenhouse gas N_2O, and the loss of other soil nutrients, such as calcium and potassium. In addition, increased soil N may reduce the ability of plants to efficiently use N, leading to the loss of plant diversity and soil. Further investigation is needed to study the consequences of increased soil N on ecosystem processes after vegetation change, especially the belowground processes.

On the other hand, the fact that N: P ratios for plant leaf tissues are greater than 16 implies that P is limiting for plant growth in this system. In addition, soil P does not increase proportionally with increases in soil C and N, further implying that P is limiting. As encroaching woody plants with deep rooting systems continuously uplift P from deeper portions of the soil profile and deposit it in the upper soil layers, how will increases in this element influence ecosystem processes and the future dynamics of this landscape? The

continuous increase in surface soil P in this P limited system may benefit the growth of *P. glandulosa* as the process of N-fixation requires a significant amount of P supply. The growth of *P. glandulosa* could provide more favorable environment for the colonization and establishment other woody species, potentially leading the expansion of woody patches. Although the distribution of woody vegetation has been largely explained by topoedaphic heterogeneity of this landscape, attention will be now need to shift to explore how soil nutrients may regulate vegetation dynamics individually or interactively with other factors.

It is well recognized that the availability of soil nutrient could regulate the exchange of CO_2 between terrestrial ecosystems and the atmosphere, potentially imposing strong controls on climate-carbon cycling feedbacks. For this reason, N cycles have been well represented in coupled climate-carbon cycling models and P cycles have been proposed to be incorporated into these models. As N and P cycles are regulated by different biogeochemical factors, and P cycles may respond differently to environmental change compared to N cycles. For example, in this dissertation, we found that soil P increased slower than soil N in surface soils but faster in subsurface soils in response to woody encroachment. This suggest that, from a modelling perspective, P cycles could not be simply captured as the way used to represent N cycles in climate-carbon cycling models. Continued improvements in our understanding of P cycles and their interactions with C and N cycles in terrestrial ecosystems will enhance our ability to represent P cycles in coupled climate-carbon cycling models.

Overall, this dissertation quantifies how landscape-scape spatial patterns of soil C, N, and P change differently throughout the soil profile after grasslands have been invaded by woody plants, highlighting the importance of considering spatial heterogeneity of soil properties in both horizontal and vertical planes in dryland ecosystems consisting of divergent plant life forms. As the relative importance of biotic vs. abiotic mechanisms controlling C and N vs. P accumulation following woody encroachment in this subtropical savanna vary with depth in the profile, future research efforts should place greater emphasis on exploring and understanding deep soil biogeochemical dynamics in response to vegetation change.

REFERENCES

Achat, D.L., Augusto, L., Gallet-Budynek, A., & Loustau, D. (2016) Future challenges in coupled C-N-P cycle models for terrestrial ecosystems under global change: a review. *Biogeochemistry*, **131**, 173-202.

Aerts, R. (1996) Nutrient resorption from senescing leaves of perennials: are there general patterns? *Journal of Ecology*, **84**, 597-608.

Aerts, R., & Chapin, F.S. (1999) The mineral nutrition of wild plants revisited: A re-evaluation of processes and patterns. *Advances in Ecological Research*, **30**, 1-67.

Amundson, R., Austin, A.T., Schuur, E.A.G., Yoo, K., Matzek, V., Kendall, C., Uebersax, A., Brenner, D., & Baisden, W.T. (2003) Global patterns of the isotopic composition of soil and plant nitrogen. *Global Biogeochemical Cycles*, **17**, 1031. https://doi.org/10.1029/2002GB001903.

Anadón, J.D., Sala, O.E., Turner, B.L. & Bennett, E.M. (2014) Effect of woody-plant encroachment on livestock production in North and South America. *Proceedings of the National Academy of Sciences*, **111**, 12948-12953.

Archer, S. (1995) Tree-grass dynamics in a *Prosopis*-thornscrub savanna parkland: reconstructing the past and predicting the future. *Ecoscience*, **2**, 83-99.

Archer, S. R. (2010) Rangeland conservation and shrub encroachment: New perspectives on an old problem. In J. du Toit, R. Kock, & J. Deutsch (Eds.), Wild rangelands: Conserving wildlife while maintaining livestock in semi-arid ecosystems (pp. 53–97). Oxford, UK: Wiley-Blackwell.

Archer, S.R., Boutton, T.W. & Hibbard, K. (2001) Trees in grasslands: Biogeochemical consequences of woody plant expansion. IN: *Global Biogeochemical Cycles in the Climate System*, pp. 115-137, Schulze, E.D., Harrison, S.P., Heimann, M., Holland, E.A., Lloyd, J., Prentice, I.C., & Schimel, D. Eds. Academic Press, San Diego.

Archer, S., Scifres, C., Bassham, C.R., & Maggio, R. (1988) Autogenic succession in a subtropical savanna: conversion of grassland to thorn woodland. *Ecological Monographs*, **58**, 111-127.

Archer, S., & Smeins, F.E. (1991) *Ecosystem-level processes*. Grazing management: an ecological perspective. Timber Press, Portland, OR, 109-139.

Arora, V.K., & Boer, G.J. (2003) A representation of variable root distribution in dynamic vegetation models. *Earth Interactions*, **7**, 1-19.

Arshad, M.A. (1982) Influence of the termite *Macrotermes michaelseni* (Sjöst) on soil fertility and vegetation in a semi-arid savannah ecosystem. *Agro-ecosystems*, **8**, 47-58

Augustine, D.J., Derner, J.D., Milchunas, D., Blumenthal, D., & Porensky, L.M. (2017) Grazing moderates increases in C_3 grass abundance over seven decades across a soil texture gradient in shortgrass steppe. *Journal of Vegetation Science*, **28**, 562-572.

Bai, E., Boutton, T.W., Liu, F., Wu, X.B., & Archer, S.R. (2012) Spatial patterns of soil $\delta^{13}C$ reveal grassland-to-woodland successional processes. *Organic Geochemistry*, **42**, 1512-1518.

Bai, E., Boutton, T.W., Wu, X.B., Liu, F., & Archer, S.R. (2009) Landscape-scale vegetation dynamics inferred from spatial patterns of soil $\delta^{13}C$ in a subtropical savanna parkland. *Journal of Geophysical Research: Biogeosciences*, **114**, G01019, doi:10.1029/2008JG000839.

Bai, E., Boutton, T.W., Liu, F., Wu, X.B., & Archer, S.R. (2013) ^{15}N isoscapes in a subtropical savanna parkland: spatial-temporal perspectives. *Ecosphere*, **4**, 1-17.

Bai, E., Boutton, T.W., Liu, F., Wu, X.B., Archer, S.R., & Hallmark, C.T. (2008) Spatial variation of $\delta^{15}N$ of woody plants along a topoedaphic gradient in a subtropical savanna. *Oecologia*, **159**, 493-503.

Bailey, R.G. (1996) *Ecosystem Geography*, Springer, New York.

Bardgett, R.D., & Wardle, D.A. (2010) *Aboveground-belowground linkages: biotic interactions, ecosystem processes, and global change*. New York, NY: Oxford University Press.

Barger, N.N., Archer, S.R., Campbell, J.L., Huang, C., Morton, J.A., & Knapp, A.K. (2011) Woody plant proliferation in North American drylands: A synthesis of impacts on ecosystem carbon balance. *Journal of Geophysical Research: Biogeosciences*, **116**, G00K07, doi:10.1029/2010JG001506.

Batjes, N.H. (1996) Total carbon and nitrogen in the soils of the world. *European Journal of Soil Science*, **47**, 151-163.

Beale, C.M., Lennon, J.J., Yearsley, J.M., Brewer, M.J., & Elston, D.A. (2010) Regression analysis of spatial data. *Ecology Letters*, **13**, 246-264.

Bekele, A., & Hudnall, W.H. (2005) Response of soil $\delta^{15}N$ and nutrients to eastern red cedar (*Juniperus virginiana*) encroachment into a relict calcareous prairie. *Plant and Soil*, **271**, 143-155.

Biedenbender, S.H., McClaran, M.P., Quade, J., & Weltz, M.A. (2004) Landscape patterns of vegetation change indicated by soil carbon isotope composition. *Geoderma*, **119**, 69-83.

Biggs, T.H., Quade, J., & Webb, R.H. (2002) $\delta^{13}C$ values of soil organic matter in semiarid grassland with mesquite (*Prosopis*) encroachment in southeastern Arizona. *Geoderma*, **110**, 109-130.

Billings, S.A., & Richter, D.D. (2006) Changes in stable isotopic signatures of soil nitrogen and carbon during 40 years of forest development. *Oecologia*, **148**, 325-333.

Bing, H., Wu, Y., Zhou, J., Sun, H., Luo, J., Wang, J., & Yu, D. (2016) Stoichiometric variation of carbon, nitrogen, and phosphorus in soils and its implication for nutrient limitation in alpine ecosystem of Eastern Tibetan Plateau. *Journal of Soils and Sediments*, **16**, 405-416.

Blaser, W.J., Shanungu, G.K., Edwards, P.J., & Olde Venterink, H. (2014) Woody encroachment reduces nutrient limitation and promotes soil carbon sequestration. *Ecology and Evolution*, **4**, 1423-1438.

Bonachela, J.A., Pringle, R.M., Sheffer, E., Coverdale, T.C., Guyton, J.A., Caylor, K.K., Levin, S.A., & Tarnita, C.E. (2015) Termite mounds can increase the robustness of dryland ecosystems to climatic change. *Science*, **347**, 651-655.

Bond, W.J., & Midgley, G.F. (2000) A proposed CO_2-controlled mechanism of woody plant invasion in grasslands and savannas. *Global Change Biology*, **6**, 865–869.

Bond, W.J., Midgley, G.F., Woodward, F.I., Hoffman, M.T., & Cowling, R.M. (2003) What controls South African vegetation—climate or fire? *South African Journal of Botany*, **69**, 79-91.

Boström, B., Comstedt, D., & Ekblad, A. (2007) Isotope fractionation and ^{13}C enrichment in soil profiles during the decomposition of soil organic matter. *Oecologia*, **153**, 89-98.

Boutton, T.W. (1996) Stable carbon isotope ratios of soil organic matter and their use as indicators of vegetation and climate change. In: *Mass Spectrometry of Soils* (eds Boutton, T.W., Yamasaki, S.), pp. 47–82. Marcel Dekker Inc., New York

Boutton, T.W., Archer, S.R., & Midwood, A.J. (1999) Stable isotopes in ecosystem science: structure, function and dynamics of a subtropical savanna. *Rapid Communications in Mass Spectrometry*, **13**, 1263-1277.

Boutton, T.W., Archer, S.R., Midwood, A.J., Zitzer, S.F., & Bol, R. (1998) $\delta^{13}C$ values of soil organic carbon and their use in documenting vegetation change in a subtropical savanna ecosystem. *Geoderma*, **82**, 5-41.

Boutton, T.W., Kantola, I.B., Stott, D.E., Balthrop, S.L., Tribble, J.E., & Filley, T.R. (2009a) Soil phosphatase activity and plant available phosphorus increase following grassland invasion by N-fixing tree legumes. *Eos Transactions of the American Geophysical Union* **90**, 52: B21B-0338.

Boutton, T.W., Liao, J.D., Filley, T.R., & Archer, S.R. (2009b) Belowground carbon storage and dynamics accompanying woody plant encroachment in a subtropical savanna. IN: *Soil Carbon Sequestration and the Greenhouse Effect*, 2nd ed., pp. 181-205, Lal R. & Follett R., Eds. Soil Science Society of America, Madison, WI.

Boutton, T.W., & Liao, J.D. (2010) Changes in soil nitrogen storage and $\delta^{15}N$ with woody plant encroachment in a subtropical savanna parkland landscape. *Journal of Geophysical Research: Biogeosciences*, **115**, G03019, doi:10.1029/2009JG001184.

Bouwman, A.F., Boumans, L.J.M., & Batjes, N.H. (2002) Emissions of N_2O and NO from fertilized fields: Summary of available measurement data. *Global Biogeochemical Cycles*, **16**, 1058, doi:10.1029/2001GB001811, 2002.

Brunelle, A., Minckley, T.A., Delgadillo, J., & Blissett, S. (2014) A long-term perspective on woody plant encroachment in the desert southwest, New Mexico, USA. *Journal of Vegetation Science*, **25**, 829-838.

Brown, J.R., & Archer, S. (1990) Water relations of a perennial grass and seedling vs adult woody plants in a subtropical savanna, Texas. *Oikos*, **57**, 366-374.

Bundt, M., Jäggi, M., Blaser, P., Siegwolf, R., & Hagedorn, F. (2001) Carbon and nitrogen dynamics in preferential flow paths and matrix of a forest soil. *Soil Science Society of America Journal*, **65**, 1529-1538.

Buitenwerf, R., Bond, W.J., Stevens, N., & Trollope, W.S.W. (2012) Increased tree densities in South African savannas: > 50 years of data suggests CO_2 as a driver. *Global Change Biology*, **18**, 675-684.

Bustamante, M.M.C., Martinelli, L.A., Silva, D.A., Camargo, P.B., Klink, C.A., Domingues, T.F., & Santos, R.V. (2004) ^{15}N natural abundance in woody plants and soils of central Brazilian savannas (cerrado). *Ecological Applications*, **14**, 200-213.

Caldwell, M.M., Manwaring, J.H., & Durham, S.L. (1996) Species interactions at the level of fine roots in the field: influence of soil nutrient heterogeneity and plant size. *Oecologia*, **106**, 440-447.

Carreira, J.A., Vinegla, B., & Lajtha, K. (2006) Secondary $CaCO_3$ and precipitation of P-Ca compounds control the retention of soil P in arid ecosystems. *Journal of Arid Environments*, **64**, 460-473.

Chiti, T., Mihindou, V., Jeffery, K.J., Malhi, Y., De Oliveira, F. L., White, L.J., & Valentini, R. (2017) Impact of woody encroachment on soil organic carbon storage in the Lopé National Park, Gabon. *Biotropica*, **49**, 9-13.

Clemmensen, K.E., Bahr, A., Ovaskainen, O., Dahlberg, A., Ekblad, A., Wallander, H., Stenlid, J., Finlay, R.D., Wardle, D.A., & Lindahl, B.D. (2013) Roots and associated fungi drive long-term carbon sequestration in boreal forest. *Science*, **339**, 1615-1618.

Cleveland, C.C., & Liptzin, D. (2007) C: N: P stoichiometry in soil: is there a "Redfield ratio" for the microbial biomass? *Biogeochemistry*, **85**, 235-252.

Cleveland, C.C., Townsend, A.R., & Schmidt, S.K. (2002) Phosphorus limitation of microbial processes in moist tropical forests: evidence from short-term laboratory incubations and field studies. *Ecosystems*, **5**, 680-691.

Coetsee, C., Gray, E.F., Wakeling, J., Wigley, B.J., & Bond, W.J. (2013) Low gains in ecosystem carbon with woody plant encroachment in a South African savanna. *Journal of Tropical Ecology*, **29**, 49-60.

Craine, J.M., Ballantyne, F., Peel, M., Zambatis, N., Morrow, C., & Stock, W.D. (2009) Grazing and landscape controls on nitrogen availability across 330 South African savanna sites. *Austral Ecology*, **34**, 731-740.

Craine, J.M., Brookshire, E.N.J., Cramer, M.D., Hasselquist, N.J., Koba, K., Marin-Spiotta, E., & Wang, L. (2015) Ecological interpretations of nitrogen isotope ratios of terrestrial plants and soils. *Plant and Soil*, **396**, 1-26.

Craine, J.M., Elmore, A.J., Aidar, M.P. *et al.* (2009) Global patterns of foliar nitrogen isotopes and their relationships with climate, mycorrhizal fungi, foliar nutrient concentrations, and nitrogen availability. *New Phytologist*, **183**, 980-992.

Creamer, C.A., Filley, T.R., Boutton, T.W., Oleynik, S., & Kantola, I.B. (2011) Controls on soil carbon accumulation during woody plant encroachment: evidence from physical fractionation, soil respiration, and $\delta^{13}C$ of respired CO_2. *Soil Biology and Biochemistry*, **43**, 1678-1687.

Creamer, C.A., Filley, T.R., & Boutton, T.W. (2013) Long-term incubations of size and density separated soil fractions to inform soil organic carbon decay dynamics. *Soil Biology and Biochemistry*, **57**, 496-503.

Dalle, G., Maass, B.L., & Isselstein, J. (2006) Encroachment of woody plants and its impact on pastoral livestock production in the Borana lowlands, southern Oromia, Ethiopia. *African Journal of Ecology*, **44**, 237-246.

Daryanto, S., Eldridge, D.J., & Throop, H.L. (2013a) Managing semi-arid woodlands for carbon storage: grazing and shrub effects on above-and belowground carbon. *Agriculture, Ecosystems & Environment*, **169**, 1-11.

Daryanto, S., Eldridge, D.J., & Wang, L. (2013b) Ploughing and grazing alter the spatial patterning of surface soils in a shrub-encroached woodland. *Geoderma*, **200**, 67-76.

Dean, C., Kirkpatrick, J.B., Harper, R.J., & Eldridge, D.J. (2015) Optimising carbon sequestration in arid and semiarid rangelands. *Ecological Engineering*, **74**, 148-163.

Delgado-Baquerizo, M., Maestre, F.T., Gallardo, A. *et al.* (2013) Decoupling of soil nutrient cycles as a function of aridity in global drylands. *Nature*, **502**, 672-676.

DeMalach, N., Zaady, E., Weiner, J., & Kadmon, R. (2016) Size asymmetry of resource competition and the structure of plant communities. *Journal of Ecology*, **104**, 899-910.

Denk, T.R., Mohn, J., Decock, C., Lewicka-Szczebak, D., Harris, E., Butterbach-Bahl, K., Kiese, R., & Wolf, B. *et al.* (2017) The nitrogen cycle: A review of isotope effects and isotope modeling approaches. *Soil Biology and Biochemistry*, **105**, 121-137.

Devine, A.P., McDonald, R.A., Quaife, T., & Maclean, I.M. (2017). Determinants of woody encroachment and cover in African savannas. *Oecologia*, **183**, 939-951.

Dijkstra, F.A., Pendall, E., Morgan, J.A., Blumenthal, D.M., Carrillo, Y., LeCain, D.R., Follett, R.F., & Williams, D. G. (2012) Climate change alters stoichiometry of phosphorus and nitrogen in a semiarid grassland. *New Phytologist*, **196**, 807-815.

Diniz-Filho, J.A.F., Bini, L.M., & Hawkins, B.A. (2003) Spatial autocorrelation and red herrings in geographical ecology. *Global Ecology and Biogeography*, **12**, 53-64.

Dintwe, K., Okin, G.S., D'Odorico, P., Hrast, T., Mladenov, N., Handorean, A., Bhattachan, A., & Caylor, K.K. (2015) Soil organic C and total N pools in the Kalahari: potential impacts of climate change on C sequestration in savannas. *Plant and Soil*, **396**, 27-44.

Don, A., Schumacher, J., & Freibauer, A. (2011) Impact of tropical land-use change on soil organic carbon stocks-a meta-analysis. *Global Change Biology*, **17**, 1658-1670.

Dumig, A., Schad, P., Rumpel, C., Dignac, M.F., Kögel-Knabner, I. (2008). *Araucaria* forest expansion on grassland in the southern Brazilian highlands as revealed by ^{14}C and $\delta^{13}C$ studies. *Geoderma*, **145**, 143-157.

Dungait, J.A., Hopkins, D.W., Gregory, A.S., & Whitmore, A.P. (2012) Soil organic matter turnover is governed by accessibility not recalcitrance. *Global Change Biology*, **18**, 1781-1796.

Dutilleul, P., Clifford, P., Richardson, S., & Hemon, D. (1993) Modifying the t test for assessing the correlation between two spatial processes. *Biometrics*, **49**, 305-314.

Dzurec, R.S., Boutton, T.W., Caldwell, M.M., & Smith, B.N. (1985) Carbon isotope ratios of soil organic matter and their use in assessing community composition changes in Curlew Valley, Utah. *Oecologia*, **66**, 17-24.

Ehleringer J.R., Buchmann N. & Flanagan L.B. (2000) Carbon isotope ratios in belowground carbon cycle processes. *Ecological Applications*, **10**, 412-422.

Eldridge, D.J., Bowker, M.A., Maestre, F., Roger, E., Reynolds, J., & Whitford, W.G. (2011) Impacts of shrub encroachment on ecosystem structure and functioning: Towards a global synthesis. *Ecology Letters*, **14**, 709-722.

Eldridge, D., Codina, S.S. (2014) Are shrubs really a sign of declining ecosystem function? Disentangling the myths and truths of woody encroachment in Australia. *Australian Journal of Botany*, **62**, 594-608.

Elser, J., & Bennett, E. (2011) Phosphorus cycle: A broken biogeochemical cycle. *Nature*, **478**, 29-31.

Elser, J.J., Fagan, W.F., Kerkhoff, A.J., Swenson, N.G., & Enquist, B.J. (2010) Biological stoichiometry of plant production: metabolism, scaling and ecological response to global change. *New Phytologist*, **186**, 593-608.

Ettema, C.H., & Wardle, D.A. (2002) Spatial soil ecology. *Trends in Ecology & Evolution*, **17**, 177-183.

February, E. C., & Higgins, S. I. (2010) The distribution of tree and grass roots in savannas in relation to soil nitrogen and water. *South African Journal of Botany*, **76**, 517-523.

Filley, T.R., Boutton, T.W., Liao, J.D., Jastrow, J.D., & Gamblin, D.E. (2008) Chemical changes to nonaggregated particulate soil organic matter following grassland-to-woodland transition in a subtropical savanna. *Journal of Geophysical Research: Biogeosciences*, **113**, G03009, doi: 10.1029/2007JG000564

Finzi, A.C., Austin, A.T., Cleland, E.E., Frey, S.D., Houlton, B.Z. & Wallenstein, M. D. (2011) Responses and feedbacks of coupled biogeochemical cycles to climate change: examples from terrestrial ecosystems. *Frontiers in Ecology and the Environment*, **9**, 61-67.

Fontaine, S., Barot, S., Barré, P., Bdioui, N., Mary, B., & Rumpel, C. (2007) Stability of organic carbon in deep soil layers controlled by fresh carbon supply. *Nature*, **450**, 277-280.

Freier, K. P., Glaser, B., & Zech, W. (2010) Mathematical modeling of soil carbon turnover in natural *Podocarpus* forest and *Eucalyptus* plantation in Ethiopia using compound specific $\delta^{13}C$ analysis. *Global Change Biology*, **16**, 1487-1502.

Ge, J., & Zou, C. (2013) Impacts of woody plant encroachment on regional climate in the southern Great Plains of the United States. *Journal of Geophysical Research: Atmospheres*, **118**, 9093-9104.

Geesing, D., Felker, P., & Bingham, R.L. (2000) Influence of mesquite (*Prosopis glandulosa*) on soil nitrogen and carbon development: Implications for global carbon sequestration. *Journal of Arid Environments*, **46**, 157-180.

Gill, R.A., & Jackson, R.B. (2000) Global patterns of root turnover for terrestrial ecosystems. *New Phytologist*, **147**, 13-31.

González-Roglich, M., Swenson, J.J., Jobbágy, E.G., & Jackson, R.B. (2014) Shifting carbon pools along a plant cover gradient in woody encroached savannas of central Argentina. *Forest Ecology and Management*, **331**, 71-78.

Grace, J.B. (2006) Structural equation modeling and natural systems. Cambridge University Press.

Guo, L.B., & Gifford, R.M. (2002) Soil carbon stocks and land use change: a meta analysis. *Global Change Biology*, **8**, 345-360.

Güsewell, S. (2004) N: P ratios in terrestrial plants: variation and functional significance. *New Phytologist*, **164**, 243-266.

Haase, P. (1995) Spatial pattern analysis in ecology based on Ripley's K-function: Introduction and methods of edge correction. *Journal of Vegetation Science*, **6**, 575-582.

Hamerlynck, E.P., McAuliffe, J.R., & Smith, S.D. (2000) Effects of surface and sub-surface soil horizons on the seasonal performance of *Larrea tridentata* (creosotebush). *Functional Ecology*, **14**, 596-606.

Han, W., Fang, J., Guo, D., & Zhang, Y. (2005) Leaf nitrogen and phosphorus stoichiometry across 753 terrestrial plant species in China. *New Phytologist*, **168**, 377-385.

Harris, D., Horwáth, W.R., & van Kessel, C. (2001) Acid fumigation of soils to remove carbonates prior to total organic carbon or carbon-13 isotopic analysis. *Soil Science Society of America Journal*, **65**, 1853-1856.

Hessen, D.O., Ågren, G.I., Anderson, T.R., Elser, J.J., & de Ruiter, P.C. (2004) Carbon sequestration in ecosystems: the role of stoichiometry. *Ecology*, **85**, 1179-1192.

Hendrick, R.L., & Pregitzer, K.S. (1996) Temporal and depth-related patterns of fine root dynamics in northern hardwood forests. *Journal of Ecology*, **84**,167-176.

Hibbard, K.A., Archer, S., Schimel, D.S., & Valentine, D.W. (2001) Biogeochemical changes accompanying woody plant encroachment in a subtropical savanna. *Ecology*, **82**, 1999-2011.

Hibbard, K.A., Schimel, D.S., Archer, S., Ojima, D.S., & Parton, W. (2003) Grassland to woodland transitions: integrating changes in landscape structure and biogeochemistry. *Ecological Applications*, **13**, 911-926.

Higgins, S.I., Bond, W.J., & Trollope, W.S. (2000) Fire, resprouting and variability: a recipe for grass–tree coexistence in savanna. *Journal of Ecology*, **88**, 213-229.

Hipondoka, M.H.T., & Versfeld, W.D. (2006) Root system of Terminalia sericea shrubs across rainfall gradient in a semi-arid environment of Etosha National Park, Namibia. *Ecological Indicators*, **6**, 516-524.

Hobbie, E.A., & Högberg, P. (2012) Nitrogen isotopes link mycorrhizal fungi and plants to nitrogen dynamics. *New Phytologist*, **196**, 367-382.

Hobbie, E.A., & Ouimette, A.P. (2009) Controls of nitrogen isotope patterns in soil profiles. *Biogeochemistry*, **95**, 355-371.

Hobbie, S.E., & Vitousek, P.M. (2000) Nutrient limitation of decomposition in Hawaiian forests. *Ecology*, **81**, 1867-1877.

Hodge, A. (2004) The plastic plant: root responses to heterogeneous supplies of nutrients. *New Phytologist*, **162**, 9-24.

Högberg, P. (1997) Tansley Review No. 95 ^{15}N natural abundance in soil-plant systems. *New Phytologist*, **137**, 179-203.

Holdo, R.M. (2013) Revisiting the two-layer hypothesis: coexistence of alternative functional rooting strategies in savannas. *PLoS ONE*, **8**, e69625, doi:10.1371 /journal.pone.0069625.

Houghton, R.A., & Hackler, J.L. (2000) Changes in terrestrial carbon storage in the United States. 1: The roles of agriculture and forestry. *Global Ecology and Biogeography*, **9**, 125-144.

Houghton, R.A., Hackler, J.L., & Lawrence, K.T. (1999) The US carbon budget: Contributions from land-use change. *Science*, **285**, 574-578.

Houlton, B.Z., Sigman, D.M., Schuur, E.A., & Hedin, L.O. (2007) A climate-driven switch in plant nitrogen acquisition within tropical forest communities. *Proceedings of the National Academy of Sciences*, **104**, 8902-8906.

Houlton, B. Z., Wang, Y.P., Vitousek, P.M., & Field, C.B. (2008) A unifying framework for dinitrogen fixation in the terrestrial biosphere. *Nature*, **454**, 327-330.

Hughes, R.F., Archer, S.R., Asner, G.P., Wessman, C.A., McMurtry, C., Nelson, J., & Ansley, R.J. (2006) Changes in aboveground primary production and carbon and nitrogen pools accompanying woody plant encroachment in a temperate savanna. *Global Change Biology*, **12**, 1733-1747.

Huxman, T.E., Wilcox, B.P., Breshears, D.D., Scott, R.L., Snyder, K.A., Small, E.E., Hultine, K., Pockman, W.T., & Jackson, R.B. (2005) Ecohydrological implications of woody plant encroachment. *Ecology*, **86**, 308-319.

Huygens, D., Denef, K., Vandeweyer, R., Godoy, R., Van Cleemput, O., & Boeckx, P. (2008). Do nitrogen isotope patterns reflect microbial colonization of soil organic matter fractions? *Biology and Fertility of Soils*, **44**, 955-964.

IPCC (2006) Generic methodologies applicable to multiple land-use categories. In: 2006 IPCC Guidelines for National Greenhouse Gas Inventories. Volume 4. Agriculture, Forestry and Other Land Use (eds Eggleston, H.S., Buendia, L., Miwa, K., Ngara, T., Tanabe, K.), pp. 2.1–2.59. IGES, Japan.

Ippolito, J.A., Blecker, S.W., Freeman, C.L., McCulley, R.L., Blair, J.M., & Kelly, E.F. (2010) Phosphorus biogeochemistry across a precipitation gradient in grasslands of central North America. *Journal of Arid Environments*, **74**, 954-961.

Israel, D.W. (1987) Investigation of the role of phosphorus in symbiotic dinitrogen fixation. *Plant Physiology*, **84**, 835-840.

Jackson, R.B., Banner, J.L., Jobbagy, E.G., Pockman, W.T., & Wall, D.H. (2002) Ecosystem carbon loss with woody plant invasion of grasslands. *Nature*, **418**, 23-626.

Jackson, R.B., & Caldwell, M.M. (1993) Geostatistical patterns of soil heterogeneity around individual perennial plants. *Journal of Ecology*, **81**, 683-692.

Jackson, R.B., Canadell, J., Ehleringer, J.R., Mooney, H.A., Sala, O.E., & Schulze, E.D. (1996) A global analysis of root distributions for terrestrial biomes. *Oecologia*, **108**, 389-411.

Jiao, F., Shi, X.R., Han, F.P., & Yuan, Z.Y. (2016) Increasing aridity, temperature and soil pH induce soil C-N-P imbalance in grasslands. *Scientific Reports*, **6**, 19601, doi: 10.1038/srep19601

Jobbágy, E.G., & Jackson, R.B. (2000) The vertical distribution of soil organic carbon and its relation to climate and vegetation. *Ecological Applications*, **10**, 423-436.

Jobbágy, E.G., & Jackson, R.B. (2001) The distribution of soil nutrients with depth: global patterns and the imprint of plants. *Biogeochemistry*, **53**, 51-77.

Joslin, J.D., Gaudinski, J.B., Torn, M.S., Riley, W.J., & Hanson, P.J. (2006) Fine-root turnover patterns and their relationship to root diameter and soil depth in a ^{14}C-labeled hardwood forest. *New Phytologist*, **172**, 523-535.

Kambatuku, J. R., Cramer, M. D., & Ward, D. (2013) Overlap in soil water sources of savanna woody seedlings and grasses. *Ecohydrology*, **6**, 464-473.

Kantola, I.B. (2012) Biogeochemistry of woody plant invasion: phosphorus cycling and microbial community composition. Ph.D. Dissertation, Texas A&M University, College Station, Texas, USA

Kautz, T., Amelung, W., Ewert, F. *et al.* (2013) Nutrient acquisition from arable subsoils in temperate climates: A review. *Soil Biology and Biochemistry*, **57**, 1003-1022.

King, A.W., Dilling, L., Zimmerman, G.P., Fairman, D.M., Houghton, R.A., Marland, G., Rose, A.Z., & Wilbanks, T.J. (2007) Executive Summary. In: *The First State of the Carbon Cycle Report (SOCCR): The North American Carbon Budget and Implications for the Global Carbon Cycle*. A Report by the U.S. Climate Change Science Program and the Subcommittee on Global Change Research [King, A.W., Dilling, L., Zimmerman, G.P., Fairman, D.M., Houghton, R.A., Marland, G., Rose, A.Z., Wilbanks, T.J. (eds.)]. National Oceanic and Atmospheric Administration, National Climatic Data Center, Asheville, NC, USA, pp, 1-14

Koerselman, W., & Meuleman, A.F. (1996) The vegetation N: P ratio: a new tool to detect the nature of nutrient limitation. *Journal of Applied Ecology*, **33**, 1441-1450.

Konaté, S., Le Roux, X., Tessier, D., & Lepage, M. (1999) Influence of large termitaria on soil characteristics, soil water regime, and tree leaf shedding pattern in a West African savanna. *Plant and Soil*, **206**, 47-60.

Koteen, L.E., Raz-Yaseef, N., & Baldocchi, D.D. (2015) Spatial heterogeneity of fine root biomass and soil carbon in a California oak savanna illuminates plant functional strategy across periods of high and low resource supply. *Ecohydrology*, **8**, 294-308.

Krull, E., Bray, S., Harms, B., Baxter, N., Bol, R., & Farquhar, G. (2007) Development of a stable isotope index to assess decadal-scale vegetation change and application to woodlands of the Burdekin catchment, Australia. *Global Change Biology*, **13**, 1455-1468.

Kulmatiski, A., & Beard, K.H. (2013) Woody plant encroachment facilitated by increased precipitation intensity. *Nature Climate Change*, **3**, 833-837.

Laio, F., D'Odorico, P., & Ridolfi, L. (2006) An analytical model to relate the vertical root distribution to climate and soil properties. *Geophysical Research Letters*, **33**, L18401, doi: 10.1029/2006GL027331

Lajtha, K., Driscoll, C.T., Jarrell, W.M., & Elliott, E.T. (1999) Soil phosphorus: characterization and total element analysis, in: Roberts, G .P., Coleman, D. C., Bledsoe, C.S. & Sollins, P. (Eds.), *Standard Soil Methods for Long-Term Ecological Research*, Oxford University Press, New York, 1999, pp. 115-142.

Lal, R. (2004) Carbon sequestration in dryland ecosystems. *Environmental Management*, **33**, 528-544.

Lambers, H., Shane, M.W., Cramer, M.D., Pearse, S.J. & Veneklaas, E.J. (2006) Root structure and functioning for efficient acquisition of phosphorus: Matching morphological and physiological traits. *Annals of Botany*, **98**, 693–713.

Li, H., Shen, H., Chen, L., Liu, T., Hu, H., Zhao, X., Zhou, L., Zhang, P., & Fang, J. (2016a) Effects of shrub encroachment on soil organic carbon in global grasslands. *Scientific Reports*, **6**, doi:10.1038/srep28974.

Li, C., Zhao, L., Sun, P., Zhao, F., Kang, D., Yang, G., Han, X., Feng, Y., & Ren, G. (2016b) Deep soil C, N, and P stocks and stoichiometry in response to land use patterns in the loess hilly region of China. *PloS ONE*, **11**, e0159075, doi:10.1371/journal.pone.0159075.

Liao, J.D., & Boutton, T.W. (2008) Soil microbial biomass response to woody plant invasion of grassland. *Soil Biology and Biochemistry*, **40**, 1207–1216.

Liao, J.D., Boutton, T.W., & Jastrow, J.D. (2006) Storage and dynamics of carbon and nitrogen in soil physical fractions following woody plant invasion of grassland. *Soil Biology and Biochemistry*, **38**, 3184-3196.

Lilienfein, J., Wilcke, W., Thomas, R., Vilela, L., do Carmo Lima, S., & Zech, W. (2001) Effects of *Pinus caribaea* forests on the C, N, P, and S status of Brazilian savanna Oxisols. *Forest Ecology and Management*, **147**, 171-182.

Lindahl, B.D., Ihrmark, K., Boberg, J., Trumbore, S.E., Högberg, P., Stenlid, J., & Finlay, R.D. (2007) Spatial separation of litter decomposition and mycorrhizal nitrogen uptake in a boreal forest. *New Phytologist*, **173**, 611-620.

Littell, R.C., Milliken, G.A., Stroup, W.W., Wolfinger, R.D., & Schabenberger, O. (2006) *SAS* for *mixed models*. SAS Institute Inc., Cary, NC, USA.

Liu, F., Wu, X., Bai, E., Boutton, T.W., & Archer, S.R. (2011) Quantifying soil organic carbon in complex landscapes: an example of grassland undergoing encroachment of woody plants. *Global Change Biology*, 17, 1119-1129.

Liu, F., Wu, X., Bai, E., Boutton, T.W., & Archer, S.R. (2010) Spatial scaling of ecosystem C and N in a subtropical savanna landscape. *Global Change Biology*, **16**, 2213-2223.

Lobry de Bruyn, L.A., & Conacher, A.J. (1990) The role of termites and ants in soil modification-a review. *Soil Research*, **28**, 55-93.

Loiola, P.P., Carvalho, G.H., & Batalha, M.A. (2016) Disentangling the roles of resource availability and disturbance in fine and coarse root biomass in savanna. *Austral Ecology*, **41**, 255-262.

Loomis, L.E. (1989) Influence of heterogeneous subsoil development on vegetation patterns in a subtropical savanna parkland, Texas. Ph.D. Dissertation, Texas A&M University, College Station, Texas, USA.

Ludovici, K.H. (2004) Tree roots and their interaction with soil. In: Burley J, Evans J, Youngquist JA (eds) Encyclopedia of forest sciences. Elsevier, Oxford, pp 1195-1201.

Lü, X.T., Freschet, G.T., Flynn, D.F., & Han, X.G. (2012) Plasticity in leaf and stem nutrient resorption proficiency potentially reinforces plant–soil feedbacks and microscale heterogeneity in a semi-arid grassland. *Journal of Ecology*, **100**, 144-150.

Maag, M., & Vinther, F.P. (1996) Nitrous oxide emission by nitrification and denitrification in different soil types and at different soil moisture contents and temperatures. *Applied Soil Ecology*, **4**, 5-14.

Maestre, F. T., Bowker, M. A., Puche, M. D. *et al.* (2009) Shrub encroachment can reverse desertification in semi-arid Mediterranean grasslands. *Ecology Letters*, **12**, 930-941.

Mahowald, N., Jickells, T.D., Baker, A.R. *et al.* (2008) Global distribution of atmospheric phosphorus sources, concentrations and deposition rates, and anthropogenic impacts. *Global Biogeochemical Cycles*, **22**, GB4026, doi: 10.1029/2008GB003240.

Manzoni, S., Taylor, P., Richter, A., Porporato, A., & Ågren, G.I. (2012) Environmental and stoichiometric controls on microbial carbon-use efficiency in soils. *New Phytologist*, **196**, 79-91.

Manzoni, S., Trofymow, J.A., Jackson, R.B., & Porporato, A. (2010) Stoichiometric controls on carbon, nitrogen, and phosphorus dynamics in decomposing litter. *Ecological Monographs*, **80**, 89-106.

Matamala, R., Gonzalez-Meler, M.A., Jastrow, J.D., Norby, R.J., & Schlesinger, W.H. (2003) Impacts of fine root turnover on forest NPP and soil C sequestration potential. *Science*, **302**, 1385-1387.

Martin, R.E., Asner, G.P., Ansley, R.J., & Mosier, A.R. (2003) Effects of woody vegetation encroachment on soil nitrogen oxide emissions in a temperate savanna. *Ecological Applications*, **13**, 897-910.

Mayor, J., Bahram, M., Henkel, T., Buegger, F., Pritsch, K., & Tedersoo, L. (2015) Ectomycorrhizal impacts on plant nitrogen nutrition: emerging isotopic patterns, latitudinal variation and hidden mechanisms. *Ecology Letters*, **18**, 96-107.

Macinnis-Ng, C.M.O., Fuentes, S., O'Grady, A.P., Palmer, A.R., Taylor, D., Whitley, R.J., Yunusa, I., Zeppel, M.J.B, & Eamus, D. (2010). Root biomass distribution and soil properties of an open woodland on a duplex soil. *Plant and Soil*, **327**, 377-388.

McAuliffe, J.R. (1994) Landscape evolution, soil formation, and ecological patterns and processes in Sonoran Desert bajadas. *Ecology Monographs*, **64**, 111-148.

McClaran, M.P., Moore-Kucera, J., Martens, D.A., van Haren, J., & Marsh, S.E. (2008) Soil carbon and nitrogen in relation to shrub size and death in a semi-arid grassland. *Geoderma*, **145**, 60-68.

McCulley, R.L., Archer, S.R., Boutton, T.W., Hons, F.M., & Zuberer, D.A. (2004a) Soil respiration and nutrient cycling in wooded communities developing in grassland. *Ecology*, **85**, 2804-2817.

McCulley, R.L., Jobbagy, E.G., Pockman, W.T. & Jackson, R.B. (2004b) Nutrient uptake as a contributing explanation for deep rooting in arid and semi-arid ecosystems. *Oecologia*, **141**, 620-628.

McCulley, R.L., & Jackson, R.B. (2012) Conversion of tallgrass prairie to woodland: consequences for carbon and nitrogen cycling. *The American Midland Naturalist*, **167**, 307-321.

McGill, W.B., & Cole, C.V. (1981) Comparative aspects of cycling of organic C, N, S and P through soil organic matter. *Geoderma*, **26**, 267-286.

McGroddy, M.E., Daufresne, T., & Hedin, L.O. (2004) Scaling of C: N: P stoichiometry in forests worldwide: Implications of terrestrial redfield-type ratios. *Ecology*, **85**, 2390-2401.

McKinley, D.C., Norriss, M.D., Blair, J.M., & Johnson, L.C. (2008) Altered ecosystem processes as a consequence of Juniperus virginiana L. encroachment into North American tallgrass prairie. In: Van Auken, O.W. (Ed.), Western North American Juniperus Communities: a Dynamic Vegetation Type. Springer, New York, pp. 170–187.

Midwood, A.J., Boutton, T.W., Archer, S.R., Watts, & S.E. (1998) Water use by woody plants on contrasting soils in a savanna parkland: Assessment with δ^2H and $\delta^{18}O$. *Plant and Soil*, **205**, 13-24.

Miller, G.R., Chen, X., Rubin, Y., Ma, S., & Baldocchi, D.D. (2010) Groundwater uptake by woody vegetation in a semiarid oak savanna. *Water Resources Research*, **46**, W10503, doi:10.1029/2009WR008902.

Mobley, M.L., Lajtha, K., Kramer, M.G., Bacon, A.R., Heine, P.R., & Richter, D.D. (2015) Surficial gains and subsoil losses of soil carbon and nitrogen during secondary forest development. *Global Change Biology*, **21**, 986-996.

Moore, T.R., Trofymow, J.A., Prescott, C.E., Titus, B.D., & CIDET Working Group. (2011) Nature and nurture in the dynamics of C, N and P during litter decomposition in Canadian forests. *Plant and Soil*, **339**, 163-175.

Morgan, J.A., Milchunas, D.G., LeCain, D.R., West, M., & Mosier, A.R. (2007). Carbon dioxide enrichment alters plant community structure and accelerates shrub growth in the shortgrass steppe. *Proceedings of the National Academy of Sciences*, **104**, 14724-14729.

Mudrak, E.L., Schafer, J.L., Fuentes-Ramirez, A., Holzapfel, C., & Moloney, K.A. (2014) Predictive modeling of spatial patterns of soil nutrients related to fertility islands. *Landscape Ecology*, **29**, 491-505.

Murphy, J., & Riley, J.P. (1962) A modified single solution method for the determination of phosphate in natural waters. *Analytica Chimica Acta*, **27**, 31-36.

Nadelhoffer, K.J., & Fry, B. (1988) Controls on natural nitrogen-15 and carbon-13 abundances in forest soil organic matter. *Soil Science Society of America Journal*, **52**, 1633-1640.

Niklas, K.J., & Cobb, E.D. (2005) N, P, and C stoichiometry of *Eranthis hyemalis* (Ranunculaceae) and the allometry of plant growth. *American Journal of Botany*, **92**, 1256-1263.

Nippert, J.B., & Holdo, R.M. (2015) Challenging the maximum rooting depth paradigm in grasslands and savannas. *Functional Ecology*, **29**, 739-745.

NRCS (1979) Soil survey of Jim Wells County, Texas. Natural Resource Conservation Service, United States Department of Agriculture, Washington, DC.

O'Donnell, F.C., Caylor, K.K., Bhattachan, A., Dintwe, K., D'Odorico, P., & Okin, G.S. (2015) A quantitative description of the interspecies diversity of belowground structure in savanna woody plants. *Ecosphere*, **6**, 1-15.

Oelofse, M., Birch-Thomsen, T., Magid, J., de Neergaard, A., van Deventer, R., Bruun, S., & Hill, T. (2016) The impact of black wattle encroachment of indigenous grasslands on soil carbon, Eastern Cape, South Africa. *Biological Invasions*, **18**, 445-456.

Olde Venterink, H. (2011) Legumes have a higher root phosphatase activity than other forbs, particularly under low inorganic P and N supply. *Plant and Soil*, **347**, 137–146.

Oliveira, R. S., Bezerra, L., Davidson, E. A., Pinto, F., Klink, C. A., Nepstad, D. C., & Moreira, A. (2005) Deep root function in soil water dynamics in cerrado savannas of central Brazil. *Functional Ecology*, **19**, 574-581.

Pacala, S.W., Hurtt, G.C., Baker, D. *et al.* (2001) Consistent land-and atmosphere-based US carbon sink estimates. *Science*, **292**, 2316-2320.

Pardo, L.H. & Nadelhoffer, K.J. (2010) Using nitrogen isotope ratios to assess terrestrial ecosystems at regional and global scales. Isoscapes: Understanding movement, pattern, and process on earth through isotope mapping (eds West, J.B., Bowen, G.J., Dawson T.E., & Tu K.P.), pp. 221–249. Springer, London.

Pellegrini, A.F., Hoffmann, W.A., & Franco, A.C. (2014) Carbon accumulation and nitrogen pool recovery during transitions from savanna to forest in central Brazil. *Ecology*, **95**, 342-352.

Peñuelas, J., Sardans, J., Rivas-ubach, A., & Janssens, I.A. (2012) The human-induced imbalance between C, N and P in Earth's life system. *Global Change Biology*, **18**, 3-6.

Plante, P.M., Rivest, D., Vézina, A., & Vanasse, A. (2014) Root distribution of different mature tree species growing on contrasting textured soils in temperate windbreaks. *Plant and Soil*, **380**, 429-439.

Plotnick, R.E., Gardner, R.H., Hargrove, W.W., Prestegaard, K., & Perlmutter, M. (1996) Lacunarity analysis: a general technique for the analysis of spatial patterns. *Physical Review E*, **53**, 5461-5468.

Png, G.K., Turner, B.L., Albornoz, F.E., Hayes, P.E., Lambers, H., & Laliberté, E. (2017) Greater root phosphatase activity in nitrogen-fixing rhizobial but not actinorhizal plants with declining phosphorus availability. *Journal of Ecology*, **105**, 1246-1255.

Poulter, B., Frank, D., Ciais, P. *et al.* (2014) Contribution of semi-arid ecosystems to interannual variability of the global carbon cycle. *Nature*, **509**, 600-603.

Pregitzer, K.S. (2002) Fine roots of trees–a new perspective. *New Phytologist*, **154**, 267-270

Price, J.N., & Morgan, J.W. (2008) Woody plant encroachment reduces species richness of herb-rich woodlands in southern Australia. *Austral Ecology*, **33**, 278-289.

Pringle, R.M., Doak, D.F., Brody, A.K., Jocqué, R., & Palmer, T.M. (2010) Spatial pattern enhances ecosystem functioning in an African savanna. *PLoS Biology*, **8**, e1000377. doi:10.1371/journal.pbio.1000377.

Puttock, A., Dungait, J.A., Bol, R., Dixon, E.R., Macleod, C.J., & Brazier, R.E. (2012) Stable carbon isotope analysis of fluvial sediment fluxes over two contrasting C_4-C_3 semi-arid vegetation transitions. *Rapid Communications in Mass Spectrometry*, **26**, 2386-2392.

R Development Core Team (2014) R: A Language and Environment for Statistical Computing. Vienna, Austria: R Foundation for Statistical Computing.

Rajaniemi, T.K. (2003) Evidence for size asymmetry of belowground competition. *Basic Applied Ecology*, **4**, 239-247.

Rascher, K.G., Hellmann, C., Máguas, C., & Werner, C. (2012) Community scale ^{15}N isoscapes: tracing the spatial impact of an exotic N_2-fixing invader. *Ecology Letters*, **15**, 484-491.

Rasse, D.P., Rumpel, C., & Dignac, M.F. (2005) Is soil carbon mostly root carbon? Mechanisms for a specific stabilisation. *Plant and Soil*, **269**, 341-356.

Ratajczak, Z., Nippert, J.B., & Collins, S.L. (2012) Woody encroachment decreases diversity across North American grasslands and savannas. *Ecology*, **93**, 697-703.

Redfield, A.C. (1958) The biological control of chemical factors in the environment. *American Scientist*, **46**, 205-221.

Reed, S.C., Townsend, A.R., Davidson, E.A., & Cleveland, C.C. (2012) Stoichiometric patterns in foliar nutrient resorption across multiple scales. *New Phytologist*, **196**, 173-180.

Reed, S.C., Yang, X., & Thornton, P.E. (2015) Incorporating phosphorus cycling into global modeling efforts: a worthwhile, tractable endeavor. *New Phytologist*, **208**, 324-329.

Reich, P.B., & Oleksyn, J. (2004) Global patterns of plant leaf N and P in relation to temperature and latitude. *Proceedings of the National Academy of Sciences*, **101**, 11001-11006.

Reich, P.B., Walters, M.B., & Ellsworth, D.S. (1997) From tropics to tundra: global convergence in plant functioning. *Proceedings of the National Academy of Sciences*, **94**, 13730-13734.

Reynolds, J. F., Smith, D.M.S. Lambin, E.F. *et al.* (2007) Global desertification: building a science for dryland development. *Science*, **316**, 847-851.

Ripley, B.D. (1981) Spatial Statistics. John Wiley & Sons, Inc., USA.

Robinson, D. (2001) $\delta^{15}N$ as an integrator of the nitrogen cycle. *Trends in Ecology & Evolution*, **16**, 153-162.

Rosenberg, M.S., & Anderson, C.D. (2011) PASSaGE: pattern analysis, spatial statistics and geographic exegesis. Version 2. *Methods in Ecology and Evolution*, **2**, 229-232.

Ruiz-Navarro, A., Barberá, G. G., Albaladejo, J., & Querejeta, J.I. (2016) Plant $\delta^{15}N$ reflects the high landscape-scale heterogeneity of soil fertility and vegetation productivity in a Mediterranean semiarid ecosystem. *New Phytologist*, **212**, 1030-1043.

Rumpel, C., & Kögel-Knabner, I. (2011) Deep soil organic matter-a key but poorly understood component of terrestrial C cycle. *Plant and Soil*, **338**, 143-158.

Saiz, G., Bird, M.I., Wurster, C., Quesada, C.A., Ascough, P., Domingues, T., Schrodt, F., Schwarz, M., Feldpausch, T.R., Veenendaal, E., Djagbletey, G., Jacobsen, G., Hien, F., Compaore, H., Diallo, A., & Lloyd, J. (2015) The influence of C_3 and C_4 vegetation on soil organic matter dynamics in contrasting semi-natural tropical ecosystems. *Biogeosciences*, **12**, 5041–5059.

Salomé, C., Nunan, N., Pouteau, V., Lerch, T.Z., & Chenu, C. (2010) Carbon dynamics in topsoil and in subsoil may be controlled by different regulatory mechanisms. *Global Change Biology*, **16**, 416-426.

Sankaran, M., Augustine, D.J., & Ratnam, J. (2013) Native ungulates of diverse body sizes collectively regulate long-term woody plant demography and structure of a semi-arid savanna. *Journal of Ecology*, **101**, 1389-1399.

Sankaran, M., Hanan, N.P., Scholes, R.J. *et al.* (2005) Determinants of woody cover in African savannas. *Nature*, **438**, 846-849.

Sankaran, M., Ratnam, J., & Hanan, N.P. (2004) Tree-grass coexistence in savannas revisited–insights from an examination of assumptions and mechanisms invoked in existing models. *Ecology Letters*, **7**, 480-490.

Sanaiotti, T.M., Martinelli, L.A., Victoria, R.L., Trumbore, S.E., Camargo, P.B. (2002) Past vegetation changes in Amazon savannas determined using carbon isotopes of soil organic matter. *Biotropica*, **34**, 2–16.

Sardans, J., & Peñuelas, J. (2014) Hydraulic redistribution by plants and nutrient stoichiometry: Shifts under global change. *Ecohydrology*, **7**, 1-20.

Sardans, J., Rivas-Ubach, A., & Peñuelas, J. (2012) The C: N: P stoichiometry of organisms and ecosystems in a changing world: a review and perspectives. *Perspectives in Plant Ecology, Evolution and Systematics*, **14**, 33-47.

Scheiter, S., Higgins, S.I., Beringer, & J., Hutley, L.B. (2015) Climate change and long-term fire management impacts on Australian savannas. *New Phytologist*, **205**, 1211-1226.

Schenk, H.J. (2006) Root competition: beyond resource depletion. *Journal of Ecology*, **94**, 725-739.

Schenk, H. J., & Jackson, R.B. (2002) Rooting depths, lateral root spreads and below-ground/above-ground allometries of plants in water-limited ecosystems. *Journal of Ecology*, **90**, 480-494.

Schenk, H.J., & Jackson, R.B. (2005) Mapping the global distribution of deep roots in relation to climate and soil characteristics. *Geoderma*, **126**, 129-140.

Schlesinger, W.H., & Bernhardt, E.S. (2013) *Biogeochemistry: an analysis of global change*. Springer, Netherlands

Schlesinger, W.H., Raikes, J.A., Hartley, A.E., & Cross, A.F. (1996) On the spatial pattern of soil nutrients in desert ecosystems. *Ecology*, **77**, 364-374

Schmidt, M.W., Torn, M.S., Abiven, S. *et al.* (2011) Persistence of soil organic matter as an ecosystem property. *Nature*, **478**, 49-56.

Scholes, R.J., & Archer, S.R. (1997) Tree-grass interactions in savannas. *Annual Review of Ecology, Evolution, and Systematics*, **28**, 517-544.

Schwinning, S., & Weiner, J. (1998) Mechanisms determining the degree of size asymmetry in competition among plants. *Oecologia*, **113**, 447-455.

Scifres, C.J., & Koerth, B.H. (1987) Climate, soils, and vegetation of the La Copita Research Area. Texas Agricultural Experiment Station MP-1626. Texas A&M University System, College Station.

Selmants, P.C., & Hart, S.C. (2010) Phosphorus and soil development: does the Walker and Syers model apply to semiarid ecosystems? *Ecology*, **91**, 474-484.

Sheldrick, B.H., & Wang, C. (1993) Particle size distribution. Carter, M.R. (Ed.), Soil Sampling and Methods of Analysis, Canadian Society of Soil Science, Lewis Publishers, Ann Arbor, MI (1993), pp. 499–511

Sileshi, G.W., Arshad, M.A., Konaté, S., & Nkunika, P.O. (2010) Termite-induced heterogeneity in African savanna vegetation: mechanisms and patterns. *Journal of Vegetation Science*, **21**, 923-937.

Silver, W.L., & Miya, R.K. (2001) Global patterns in root decomposition: comparisons of climate and litter quality effects. *Oecologia*, **129**, 407-419.

Sistla, S.A., & Schimel, J.P. (2012) Stoichiometric flexibility as a regulator of carbon and nutrient cycling in terrestrial ecosystems under change. *New Phytologist*, **196**, 68-78.

Sitters, J., Edwards, P.J., & Venterink, H.O. (2013) Increases of soil C, N, and P pools along an *Acacia* tree density gradient and their effects on trees and grasses. *Ecosystems*, **16**, 347-357.

Six, J., Conant, R.T., Paul, E.A., & Paustian, K. (2002) Stabilization mechanisms of soil organic matter: implications for C-saturation of soils. *Plant and Soil*, **241**, 155-176.

Soil Survey Staff. (1999) Soil taxonomy: a basic system of soil classification for making and interpreting soil surveys. Second edition. Natural Resources Conservation Service, U.S. Department of Agriculture, Washington, D.C., USA.

Soper, F.M., & Sparks, J.P. (2017) Estimating ecosystem nitrogen addition by a leguminous tree: a mass balance approach using a woody encroachment chronosequence. *Ecosystems*, **20**, 1164-1178.

Soper, F.M., Boutton, T.W., Groffman, P.M., & Sparks, J.P. (2016) Nitrogen trace gas fluxes from a semiarid subtropical savanna under woody legume encroachment. *Global Biogeochemical Cycles*, **30**, 614-628.

Soper, F.M., Boutton, T.W., & Sparks, J.P. (2015) Investigating patterns of symbiotic nitrogen fixation during vegetation change from grassland to woodland using fine scale $\delta^{15}N$ measurements. *Plant, Cell & Environment*, **38**, 89-100.

Springsteen, A., Loya, W., Liebig, M., & Hendrickson, J. (2010) Soil carbon and nitrogen across a chronosequence of woody plant expansion in North Dakota. *Plant and Soil*, **328**, 369-379.

Sterner, R.W., & Elser, J.J. (2002) Ecological stoichiometry: the biology of elements from molecules to the biosphere. Princeton University Press, Princeton, NJ, USA.

Stevens, N., Lehmann, C.E., Murphy, B.P., & Durigan, G. (2017) Savanna woody encroachment is widespread across three continents. *Global Change Biology*, **23**, 235-244.

Stoker, R.L. (1997) Object-oriented, spatially explicit simulation model of vegetation dynamics in a south Texas savanna. Ph.D. Dissertation, Texas A&M University, College Station, Texas, USA.

Stokes, C.J. (1999) Woody plant dynamics in a south Texas savanna: pattern and process, Ph.D. Dissertation, Texas A&M University, College Station, Texas, USA.

Strong, W.L., & La Roi, G.H. (1985). Root density-soil relationships in selected boreal forests of central Alberta, Canada. *Forest Ecology and Management*, **12**, 233-251.

Sudmeyer, R.A., Speijers, J., & Nicholas, B.D. (2004) Root distribution of *Pinus pinaster*, *P. radiata*, *Eucalyptus globulus* and *E. kochii* and associated soil chemistry in agricultural land adjacent to tree lines. *Tree physiology*, **24**, 1333-1346.

Sun, Y., Peng, S., Goll, D.S., Ciais, P., Guenet, B., Guimberteau, M., Hinsinger, P., Janssens, I.A., Peñuelas, J., Piao, S., Poulter, B., Violette, A., Yang, X., Yin, Y., & Zeng, H. (2017) Diagnosing phosphorus limitations in natural terrestrial ecosystems in carbon cycle models. *Earth's Future*, **5**, 730-749.

Throop, H.L., & Archer, S.R. (2008) Shrub (*Prosopis velutina*) encroachment in a semidesert grassland: spatial-temporal changes in soil organic carbon and nitrogen pools. *Global Change Biology*, **14**, 2420–2431.

Tian, H., Chen, G., Zhang, C., Melillo, J.M., & Hall, C.A. (2010) Pattern and variation of C: N: P ratios in China's soils: a synthesis of observational data. *Biogeochemistry*, **98**, 139-151.

Treseder, K.K., & Vitousek, P.M. (2001) Effects of soil nutrient availability on investment in acquisition of N and P in Hawaiian rain forests. *Ecology*, **82**, 946-954.

Turnbull, L., Brazier, R.E., Wainwright, J., Dixon, L., & Bol, R. (2008) Use of carbon isotope analysis to understand semi-arid erosion dynamics and long-term semi-arid land degradation. *Rapid Communications in Mass Spectrometry*, **22**, 1697-1702.

Turner, B.L., Clark, W.C., Kates, R.W., Richards, J.F., Mathews, J.T., & Meyer, W.B. (1990) The Earth as transformed by human action: global and regional changes in the biosphere over the past 300 years. Cambridge: Cambridge University Press.

Turner, J.S., Marais, E., Vinte, M., Mudengi, A., & Park, W.L. (2006) Termites, water and soils. *Agricola*, **16**, 40–45.

Turner, M.G., Gardner, R.H., & O'neill, R.V. (2001) Landscape ecology in theory and practice (Vol. 401). New York: Springer.

Van Auken, O.W. (2000) Shrub invasions of North American semiarid grasslands. *Annual Review of Ecology, Evolution, and Systematics*, **31**, 197-215.

Van Auken, O.W. (2009) Causes and consequences of woody plant encroachment into western North American grasslands. *Journal of Environmental Management*, **90**, 2931-2942.

Van der Salm, C., Dolfing, J., Heinen, M., & Velthof, G.L. (2007) Estimation of nitrogen losses via denitrification from a heavy clay soil under grass. *Agriculture, Ecosystems & Environment*, **119**, 311-319.

van Kessel, C., Farrell, R.E., & Pennock, D.J. (1994) Carbon-13 and nitrogen-15 natural abundance in crop residues and soil organic matter. *Soil Science Society of America Journal*, **58**, 382-389.

Victoria, R.L., Fernandes, F., Martinelli, L.A., Cássia Piccolo, M., Camargo, P.B., & Trumbore, S. (1995) Past vegetation changes in the Brazilian Pantanal arboreal–grassy savanna ecotone by using carbon isotopes in the soil organic matter. *Global Change Biology*, **1**, 165-171.

Vitousek, P.M. (2004) *Nutrient cycling and limitation: Hawai'i as a model system*. Princeton University Press, Princeton, NJ, USA.

Vitousek, P.M., Cassman, K., Cleveland, C., Crews, T., Field, C.B., Grimm, N.B., Howarth, R.W., Marino, R., Martinelli, L., Rastetter, E.B., Sprent, J.I.(2002) Towards an ecological understanding of biological nitrogen fixation. *Biogeochemistry*, **57**, 1-45.

Vitousek, P.M., Porder, S., Houlton, B.Z., & Chadwick. O.A. (2010) Terrestrial phosphorus limitation: mechanisms, implications, and nitrogen-phosphorus interactions. *Ecological Applications*, **20**, 5-15.

Volder, A., Briske, D.D., & Tjoelker, M.G. (2013) Climate warming and precipitation redistribution modify tree–grass interactions and tree species establishment in a warm-temperate savanna. *Global Change Biology*, **19**, 843-857.

Walter, H. (1971) *Ecology of Tropical and Subtropical Vegetation*. Oliver and Boyd, Edinburgh, UK.

Walker, T.W., & Adams, A.F.R. (1958) Studies on soil organic matter: I. Influence of phosphorus content of parent materials on accumulations of carbon, nitrogen, sulfur, and organic phosphorus in grassland soils. *Soil Science*, **85**, 307-318.

Walker T.W., & Syers, J.K. (1976) The fate of phosphorus during pedogenesis. *Geoderma*, **15**, 1-19.

Wang, L., Okin, G. S., D'Odorico, P., Caylor, K.K., & Macko, S.A. (2013) Ecosystem-scale spatial heterogeneity of stable isotopes of soil nitrogen in African savannas. *Landscape Ecology*, **28**, 685-698.

Wang, Y., Amundson, R., Trumbore, S. (1996) Radiocarbon dating of soil organic matter. *Quaternary Research*, **45**, 282-288.

Warren, J.M., Hanson, P.J., Iversen, C.M., Kumar, J., Walker, A.P., & Wullschleger, S.D. (2015) Root structural and functional dynamics in terrestrial biosphere models–evaluation and recommendations. *New Phytologist*, **205**, 59-78.

Watts, S.E. (1993) Rooting patterns of co-occurring woody plants on contrasting soils in a subtropical savanna. M.S. Thesis, Texas A&M University, College Station, TX, USA.

Wheeler, C.W., Archer, S.R., Asner, G.P., & McMurtry, C.R. (2007) Climatic/edaphic controls on soil carbon/nitrogen response to shrub encroachment in desert grassland. *Ecological Applications*, **17**, 1911-1928.

Wigley, B.J., Bond, W.J., & Hoffman, M. (2010) Thicket expansion in a South African savanna under divergent land use: local vs. global drivers? *Global Change Biology*, **16**, 964-976.

Whittaker, R.H., Gilbert, L.E., & Connell, J.H. (1979). Analysis of two-phase pattern in a mesquite grassland, Texas. *Journal of Ecology*, **67**, 935-952.

Wood, T., Bormann, F.H., & Voigt, G. K. (1984) Phosphorus cycling in a northern hardwood forest: biological and chemical control. *Science*, **223**, 391-393.

Wu, X.B., & Archer, S.R. (2005) Scale-dependent influence of topography-based hydrologic features on patterns of woody plant encroachment in savanna landscapes. *Landscape Ecology*, **20**, 733-742.

Wynn, J.G., & Bird, M.I. (2007) C_4-derived soil organic carbon decomposes faster than its C_3 counterpart in mixed C_3/C_4 soils. *Global Change Biology*, **13**, 2206-2217.

Xiao, C., Janssens, I.A., Zhou, Y., Su, J., Liang, Y., & Guenet, B. (2015) Strong stoichiometric resilience after litter manipulation experiments; a case study in a Chinese grassland. *Biogeosciences*, **12**, 757-767.

Yang, W., Cheng, H., Hao, F., Ouyang, W., Liu, S., & Lin, C. (2012) The influence of land-use change on the forms of phosphorus in soil profiles from the Sanjiang Plain of China. *Geoderma*, **189**, 207-214.

Yang, X., Post, W.M., Thornton, P.E., & Jain, A. (2013) The distribution of soil phosphorus for global biogeochemical modeling. *Biogeosciences*, **10**, 2525–2537.

Yang, X., Thornton, P.E., Ricciuto, D. M., & Hoffman, F.M. (2016a) Phosphorus feedbacks constraining tropical ecosystem responses to changes in atmospheric CO_2 and climate. *Geophysical Research Letters*, **43**, 7205-7214.

Yang, Y., Donohue, R.J., & McVicar, T.R. (2016b) Global estimation of effective plant rooting depth: Implications for hydrological modeling. *Water Resources Research*, **52**, 8260–8276.

Yang, Y., & Luo, Y. (2011) Carbon: nitrogen stoichiometry in forest ecosystems during stand development. *Global Ecology and Biogeography*, **20**, 354-361.

Yang, Y., Siegwolf, R.T., & Körner, C. (2015) Species specific and environment induced variation of $\delta^{13}C$ and $\delta^{15}N$ in alpine plants. *Frontiers in Plant Science*, **6**, 423, doi: 10.3389/fpls.2015.00423

Yuan, Z.Y., Chen, H.Y., & Reich, P.B. (2011) Global-scale latitudinal patterns of plant fine-root nitrogen and phosphorus. *Nature Communications*, **2**, 344, doi: 10.1038/ncomms1346.

Yue, K., Fornara, D.A., Yang, W. Peng, Y., Li, Z., Wu, F., & Peng, C. (2017) Effects of three global change drivers on terrestrial C: N: P stoichiometry: a global synthesis. *Global Change Biology*, **23**, 2450–2463.

Zhang, H.Y., Yu, Q., Lü, X.T., Trumbore, S.E., Yang, J.J., & Han, X.G. (2016) Impacts of leguminous shrub encroachment on neighboring grasses include transfer of fixed nitrogen. *Oecologia*, **180**, 1213–1222.

Zechmeister-Boltenstern, S., Keiblinger, K.M., Mooshammer, M., Peñuelas, J., Richter, A., Sardans, J., & Wanek, W. (2015) The application of ecological stoichiometry to plant-microbial-soil organic matter transformations. *Ecological Monographs*, **85**, 133-155.

Zhou, Y., Boutton, T.W. & Wu, X.B. (2017a) Soil carbon response to woody plant encroachment: Importance of spatial heterogeneity and deep soil storage. *Journal of Ecology*, **105**, 1738-1749.

Zhou, Y., Boutton, T.W., Wu, X.B., & Yang, C. (2017b) Spatial heterogeneity of subsurface soil texture drives landscape-scale patterns of woody patches in a subtropical savanna. *Landscape Ecology*, **32**, 915-929.

Zhou, Y., Boutton, T.W., & Wu, X.B. (2018) Woody plant encroachment amplifies spatial heterogeneity of soil phosphorus to considerable depth. *Ecology*, **99**, 136-147.

Zhu, X., Burger, M., Doane, T.A., & Horwath, W.R. (2013) Ammonia oxidation pathways and nitrifier denitrification are significant sources of N_2O and NO under low oxygen availability. *Proceedings of the National Academy of Sciences*, **110**, 6328-6333.

Zitzer, S.F., Archer, S.R., & Boutton, T.W. (1996) Spatial variability in the potential for symbiotic N2-fixation by woody plants in a subtropical savanna ecosystem. *Journal of Applied Ecology*, **33**, 1125-1136.

Zou, C.B., Barnes, P.W., Archer, S., & McMurtry, C.R. (2005) Soil moisture redistribution as a mechanism of facilitation in savanna tree-shrub clusters. *Oecologia*, **145**, 32-40.

APPENDIX A

A list of plant species across this 160 m × 100 m landscape in a subtropical savanna ecosystem and C, N, and P concentrations (%), $\delta^{13}C$ and $\delta^{15}N$ values (‰) of leaf and fine root tissues for each species. Number of Non N_2-fixing woody species = 13, N_2-fixing woody species = 2, forbs = 9, grasses = 13, and CAM species = 3.

Species name	Leaf tissue					Fine root tissue				
	C conc. (g/kg)	N conc. (g/kg)	P conc. (g/kg)	$\delta^{13}C$ value (‰)	$\delta^{15}N$ value (‰)	C conc. (g/kg)	N conc. (g/kg)	P conc. (g/kg)	$\delta^{13}C$ value (‰)	$\delta^{15}N$ value (‰)
Non N_2-fixing woody species										
Bernardia myricifolia	426.2	30.0	1.14	-27.1	4.58	491.5	19.0	0.62	-26.1	-0.12
Celtis pallida	406.9	39.9	1.14	-30.9	5.9	467.2	30.9	0.32	-30.0	1.98
Condalia hookeri	456.5	20.1	0.78	-30.4	2.43	472.8	23.8	0.54	-28.5	0.25
Diospyros texana	513.4	23.1	0.82	-29.0	3.15	477.3	11.7	0.37	-25.9	1.14
Foresteria angustifolia	480.0	21.9	0.86	-29.5	4.61	482.2	10.1	0.54	-26.5	-0.63
Karwinskia humboldtiana	471.4	28.8	1.01	-28.7	2.74	484.6	10.5	0.53	-27.0	1.62
Lycium berlandieri	492.2	21.0	1.02	-28.1	4.59	491.9	10.6	0.43	-27.1	1.56
Mahonia trifoliolata	501.6	14.4	0.89	-26.2	3.41	522.3	15.6	0.42	-25.7	-0.23
Schaefferia cuneifolia	437.0	25.3	1.18	-29.5	4.86	475.7	31.8	0.43	-27.5	0.78
Zanthoxylum fagara	483.3	25.9	1.22	-28.7	5.31	488.5	22.5	0.56	-27.9	-0.22
Coleogyne ramosissima	521.1	26.1	1.06	-28.2	1.86	535.2	16.3	0.28	-27.5	-1.06
Salvia ballotiflora	480.1	25.2	1.40	-30.2	3.53	522.9	12.0	0.46	-27.6	2.18
Acacia greggii	510.1	30.2	1.12	-28.7	4.13	486.0	12.0	0.23	-26.4	0.01
N_2-fixing woody species										
Acacia schaffneri	513.1	33.5	1.20	-29.9	2.28	502.4	11.4	0.34	-28.3	1.2
Prosopis glandulosa	510.4	40.0	1.52	-27.8	3.84	506.9	26.7	0.64	-25.6	-0.26
Forbs										
Croton texensis	461.9	30.4	1.42	-29.6	4.35	484.8	4.8	0.16	-27.8	2.25

Wedelia texana	418.7	26.0	1.16	-29.8	4.23	500.0	7.6	0.26	-27.6	2.58
Aphanostephus riddellii	450.2	23.2	1.21	-30.7	3.69	490.4	9.1	0.38	-27.9	1.8
Ambrosia confertiflora	475.9	31.1	1.84	-29.5	3.78	490.8	13.3	0.43	-27.5	1.92
Parthenium hysterophorus	390.8	30.7	0.74	-30.0	4.56	481.3	6.6	0.31	-28.3	1.7
Palafoxia callosa	455.6	22.3	0.84	-28.6	3.79	493.6	4.0	0.28	-27.5	1.81
Amphiachyris amoena	493.7	26.5	1.36	-28.6	4.54	497.7	6.2	0.33	-27.5	1.56
Thymophylla pentachaeta	429.6	21.3	1.18	-28.9	3.47	486.2	7.0	0.37	-27.9	1.64
Xanthisma texanum	485.0	27.5	1.16	-29.3	3.99	507.5	11.8	0.64	-26.9	2.07
Grasses										
Tridens albescens	427.5	17.9	0.68	-13.9	3.32	516.2	8.2	0.28	-14.4	2.37
Setaria texana	442.4	35.2	1.76	-13.0	6.17	479.7	13.8	0.39	-12.7	1.35
Bothriochloa ischaemum	447.8	14.6	0.93	-11.6	4.02	466.2	3.0	0.13	-12.4	2.79
Aristida purpurea	463.3	13.9	1.06	-12.4	2.41	482.5	4.0	0.13	-12.5	1.69
Cenchrus ciliaris	426.5	24.8	1.45	-11.8	5.28	489.7	6.4	0.23	-12.2	2.32
Heteropogon contortus	444.9	15.2	0.70	-12.5	2.67	455.9	2.9	0.14	-11.6	0.99
Chloris cucullata	469.1	18.2	0.76	-14.4	4.73	508.5	4.7	0.18	-12.7	3.01
Eragrostis secundiflora	464.5	16.8	0.80	-12.3	3.00	501.7	4.9	0.15	-12.4	2.91
Paspalum setaceum	427.6	17.8	0.93	-12.5	3.4	486.9	6.5	0.31	-11.2	3.22
Sporobolus neglectus	442.3	20.2	1.19	-13.8	1.96	515.3	4.7	0.25	-12.5	2.24
Bouteloua rigidiseta	430.5	15.0	0.58	-14.3	2.32	497.8	4.3	0.16	-13.8	2.23
Bouteloua trifida	438.3	20.4	1.15	-14.2	3.06	475.6	6.4	0.23	-13.3	2.79
Panicum hallii	442.3	20.0	0.77	-13.0	3.05	501.9	5.5	0.22	-13.2	2.24
CAM species										
Opuntia engelmannii	338.8	7.3	0.41	-13.6	4.74	461.7	8.2	0.26	-12.8	4.02
Cylindropuntia leptocaulis	388.1	9.4	0.53	-13.9	3.35	499.7	11.5	0.31	-14.2	0.73
Yucca treculeana	445.9	18.6	1.37	-14.8	3.79	508.9	4.0	0.16	-13.2	2.15

APPENDIX B

VITA

Education

- B.S., Ecology, Northeast Normal University, 2006-2010
- M.S., Ecology, Institute of Botany, the Chinese Academy of Sciences, 2010-2013
- Ph.D., Ecosystem Science and Management, Texas A&M University, 2013-2018

Selected Awards & Research Grants

- 2017-18 Tom Slick Graduate Research Fellowship, Texas A&M University
- 2017 ESSM Outstanding Graduate Student Award-Ph.D., Texas A&M University
- 2016-18 Doctoral Dissertation Improvement Grant, National Science Foundation
- 2015 The Exploration Fund Grant, Explorers Club
- 2015 Howard McCarley Student Research Award, Southwestern Association of Naturalists
- 2013-17 Sid Kyle Graduate Merit Assistantship, Texas A&M University
- 2013 Excellence Fellowship, Texas A&M University

Selected Publications

- **Zhou, Y.**, Boutton, T.W., Wu, X.B. (2018) Soil phosphorus does not keep pace with soil carbon and nitrogen accumulation following woody encroachment. *Global Change Biology*, doi: 10.1111/gcb.14048
- **Zhou, Y.**, Mushinski, R.M., Hyodo, A., Wu, X.B., & Boutton, T.W. (2018) Vegetation change alters soil profile $\delta^{15}N$ at the landscape scale. *Soil Biology & Biochemistry*, doi: 10.1016/j.soilbio.2018.01.012
- **Zhou, Y.**, Boutton, T.W., Wu, X.B., Wright, C., & Dion, A. (2018) Rooting strategies in a subtropical savanna: a landscape-scale three-dimensional assessment. *Oecologia*, doi: 10.1007/s00442-018-4083-9.
- **Zhou, Y.**, Boutton, T.W., & Wu, X.B. (2018) Woody plant encroachment amplifies spatial heterogeneity of soil phosphorus to considerable depth. *Ecology*, **99**, 136–147.
- **Zhou, Y.**, Boutton, T.W., & Wu, X.B. (2017) Soil carbon response to woody plant encroachment: importance of spatial heterogeneity and deep soil storage. *Journal of Ecology*, **105**, 1738-1749.
- **Zhou, Y.**, Boutton, T.W., Wu, X.B., & Yang, C. (2017) Spatial heterogeneity of subsurface soil texture drives landscape-scale patterns of woody patches in a subtropical savanna. *Landscape Ecology*, **32**, 915-929.
- **Zhou, Y.**, Clark, M., Su, J., & Xiao, C. (2015) Litter decomposition and soil microbial community composition in three Korean pine (*Pinus koraiensis*) forests along an altitudinal gradient. *Plant and Soil*, **386**, 171-183.
- **Zhou, Y.**, Su, J., Janssens, I.A., Zhou, G., & Xiao, C. (2014) Fine root and litterfall dynamics of three Korean pine (*Pinus koraiensis*) forests along an altitudinal gradient. *Plant and Soil*, **374**, 19-32.